May 2021

Part I: Development of Small-Molecule-Based Probes for the Vitamin D Receptor; Part II: Development of a Scalable Manufacturing Process for Orcein Dye

Tania Roseann Mutchie
University of Wisconsin-Milwaukee

PART I: DEVELOPMENT OF SMALL-MOLECULE-BASED PROBES FOR THE VITAMIN D RECEPTOR

PART II: DEVELOPMENT OF A SCALABLE MANUFACTURING PROCESS FOR ORCEIN DYE

by

Tania R. Mutchie

A Dissertation Submitted in

Partial Fulfillment of the

Requirements for the Degree of

Doctor of Philosophy

in Chemistry

at

The University of Wisconsin – Milwaukee

May 2021

ABSTRACT

PART I: DEVELOPMENT OF SMALL-MOLECULE-BASED PROBES FOR THE VITAMIN D RECEPTOR

PART II: DEVELOPMENT OF A SCALABLE MANUFACTURING PROCESS FOR ORCEIN DYE

by

Tania R. Mutchie

The University of Wisconsin – Milwaukee, 2021

Under the Supervision of Professor Alexander Arnold

PART I:

The vitamin D receptor (VDR) is a ligand-dependent transcription factor and member of the nuclear hormone receptor superfamily.[1] VDR is expressed in the epithelia of endocrine organs, digestive system, bronchi, kidneys, and thymus, as well as being present in leukocytes and bone cells.[2] Cell proliferation, cell differentiation, and immunomodulation, along with calcium and phosphate homeostasis, are all processes regulated by the receptor.[3-6] Within the cell, VDR can be membrane-bound or located in the nucleus.[7-8] Nuclear localization of VDR transpires following the binding of vitamin D metabolites, the most active of which is 1α,25-dihydroxyvitamin D_3 (calcitriol). Within the nucleus, interactions with coregulators and DNA occur to induce gene transcription.[9-12] Universal tool compounds to further elucidate the expression and localization of VDR are currently unavailable. Therefore, development of a novel ligand that can easily be traced *in vitro* and *in vivo* is necessary to further probe the complete role VDR plays within the cell.

Intrinsically fluorescent VDR ligands containing a coumarin scaffold were designed to mirror the structures of known VDR agonists. Understanding of the binding requirements for VDR ligand-binding pocket (VDR-LBP) affinity, in combination with molecular modeling using VDR crystal structures, has provided a foundation for rational compound design. Ten coumarin-containing ligands targeting VDR were synthesized to maintain an emission signal in the visible light range. Additionally, evaluation of the synthetic ligands in a luciferase-based transcription assay indicated their agonist and/or antagonistic properties towards VDR. Toxicity of the synthetic ligands under the transfected conditions is also reported.

The development of a tight-binding, intrinsically fluorescent VDR ligand will not only provide a means to further investigate direct receptor-ligand interactions, but also allows for the development of a new *in vitro*, high-throughput screening assay that targets the VDR-LBP. Furthermore, and unlike immunohistochemistry, the use of an intrinsically fluorescent ligand *in vivo* could enable the physiological distribution of VDR to be determined in live cells and whole animals.

PART II:

Orcein dye was used as a cheap fabric dye during the Middle Ages, but was repurposed as a histochemical stain near the end of the 19th century.[13-14] Orcein dye can be used today to visualize altered stromal material, elastic and connective tissues, collagen, basement membrane, chromosomes, hepatitis B surface antigens, copper-associated protein, and hepatocellular carcinoma.[14] Traditionally, orsellinic acid depsides were extracted from *Roccella*,

Lecanora, and *Varialaria* lichens, which subsequently underwent hydrolysis, decarboxylation, and treatment with either urine or ammonia and air to produce the red-violet dye.[13] In present day, direct production occurs from synthetic orcinol.[15] A mixture of chemical structures results during the current manufacturing process, with batch to batch variation leading to inconsistent biological tissue staining.[14]

Isolation of the eight major chemical structures from orcein dye occurred in the 1950s[16-17], but it remains unclear which compound structures, or combination thereof, are responsible for staining. Isolated synthesis of the specific chemical components within orcein dye will aid in determining the structures responsible for optimal staining. Furthermore, isolated synthesis will provide consistency between product batches and diminish the variation currently observed during biological staining. Herein, the development of a scalable manufacturing process for α-hydroxy orcein, one of the major components of orcein dye, is described.

References

1.   Mangelsdorf, D. J.; Thummel, C.; Beato, M.; Herrlich, P.; Schütz, G.; Umesono, K.; Blumberg, B.; Kastner, P.; Mark, M.; Chambon, P., The nuclear receptor superfamily: the second decade. *Cell* **1995,** *83* (6), 835.
2.   Wang, Y.; Zhu, J.; DeLuca, H. F., Where is the vitamin D receptor? *Archives of biochemistry and biophysics* **2012,** *523* (1), 123-133.
3.   Pinette, K. V.; Yee, Y. K.; Amegadzie, B. Y.; Nagpal, S., Vitamin D receptor as a drug discovery target. *Mini reviews in medicinal chemistry* **2003,** *3* (3), 193-204.
4.   Pike, J. W.; Meyer, M. B.; Lee, S.-M.; Onal, M.; Benkusky, N. A., The vitamin D receptor: contemporary genomic approaches reveal new basic and translational insights. *The Journal of Clinical Investigation* **2017,** *127* (4), 1146-1154.
5.   Colston, K.; Colston, M. J.; Feldman, D., 1,25-dihydroxyvitamin D_3 and malignant melanoma: the presence of receptors and inhibition of cell growth in culture. *Endocrinology* **1981,** *108* (3), 1083-1086.

6.   Miyaura, C.; Abe, E.; Kuribayashi, T.; Tanaka, H.; Konno, K.; Nishii, Y.; Suda, T., 1α,25-Dihydroxyvitamin D_3 induces differentiation of human myeloid leukemia cells. *Biochemical and biophysical research communications* **1981,** *102* (3), 937-943.

7.   Huhtakangas, J. A.; Olivera, C. J.; Bishop, J. E.; Zanello, L. P.; Norman, A. W., The vitamin D receptor is present in caveolae-enriched plasma membranes and binds 1α,25(OH)$_2$-vitamin D_3 *in vivo* and *in vitro. Molecular Endocrinology* **2004,** *18* (11), 2660-2671.

8.   Haussler, M. R.; Jurutka, P.; Hsieh, J.-C.; Thompson, P.; Selznick, S.; Haussler, C.; Whitfield, G. K., New understanding of the molecular mechanism of receptor-mediated genomic actions of the vitamin D hormone. *Bone* **1995,** *17* (2), S33-S38.

9.   Tsai, H. C.; Norman, A. W., Studies on Calciferol Metabolism: VIII. Evidence for a cytoplasmic receptor for 1,25-dihydroxy-vitamin D_3 in the intestinal mucosa. *Journal of Biological Chemistry* **1973,** *248* (17), 5967-5975.

10.   Brumbaugh, P. F.; Haussler, M. R., Nuclear and cytoplasmic receptors for 1,25-dihydroxycholecalciferol in intestinal mucosa. *Biochemical and biophysical research communications* **1973,** *51* (1), 74-80.

11.   Brumbaugh, P.; Haussler, M. R., Specific binding of 1α,25-dihydroxycholecalciferol to nuclear components of chick intestine. *Journal of Biological Chemistry* **1975,** *250* (4), 1588-1594.

12.   Brumbaugh, P. F.; Hughes, M. R.; Haussler, M. R., Cytoplasmic and nuclear binding components for 1α,25-dihydroxyvitamin D_3 in chick parathyroid glands. *Proceedings of the National Academy of Sciences* **1975,** *72* (12), 4871-4875.

13.   Beecken, H.; Gottschalk, E.; v Gizycki, U.; Krämer, H.; Maassen, D.; Matthies, H.; Musso, H.; Rathjen, C.; Zdhorszky, U., Orcein and litmus. *Biotechnic & histochemistry* **2003,** *78* (6), 289-302.

14.   Henwood, A., Current applications of orcein in histochemistry. A brief review with some new observations concerning influence of dye batch variation and aging of dye solutions on staining. *Biotechnic & histochemistry* **2003,** *78* (6), 303-308.

15.   Kirkpatrick, P., Use of orcein in detecting hepatitis B antigen in paraffin sections of liver. *Journal of clinical pathology* **1982,** *35* (4), 430-433.

16.   Musso, H., Die Trennung des Orceins in seine Komponenten (II Mitteil. Über Orceinfarbstoffe). *Chemische Berichte* **1956,** *89* (7), 1659-1673.

17.   Musso, H.; Beecken, H., Über Orceinfarbstoffe, VI. Die Konstitution von α-,β-und γ-Amino-Orcein. *Chemische Berichte* **1957,** *90* (10), 2190-2196.

TABLE OF CONTENTS

LIST OF FIGURES

LIST OF SCHEMES

LIST OF ABBREVIATIONS

ACN: Acetonitrile

AF: Activation function

AIBN: Azobisisobutyronitrile

B(OMe)$_3$: Trimethyl borate

CeCl$_3$: Cerium(III) chloride

CHCl$_3$: Chloroform

CSA: Camphorsulfonic acid

CTE: C-terminal extension

CuSO$_4$: Copper(II) sulfate

DBD: DNA-binding domain

DCM: Dichloromethane

DIBAL-H: Diisobutylaluminum hydride

DMF: Dimethylformamide

ER: Estrogen receptor

Et$_2$O: Diethyl ether

EtOAc: Ethyl acetate

EtOH: Ethanol

HCl: Hydrochloric acid

Hex: Hexanes

H$_2$O: Water

H$_2$SO$_4$: Sulfuric acid

HPLC: High performance liquid chromatography

HRE: Hormone response element

K$_2$CO$_3$: Potassium carbonate

KHCO$_3$: Potassium bicarbonate

KSAc: Potassium thioacetate

LBD: Ligand-binding domain

LBP: Ligand-binding pocket

LiAlH$_4$: Lithium aluminum hydride

LiOH: Lithium hydroxide

MeI: Iodomethane

MeMgBr: Methyl magnesium bromide

MeOH: Methanol

MgSO$_4$: Magnesium sulfate

MOE: Molecular Operating Environment

MTBE: Methyl *tert*-butyl ether

NaBH$_4$: Sodium borohydride

NaOH: Sodium hydroxide

NBS: N-Bromosuccinimide

n-BuLi: n-Butyllithium

NH$_4$Ac: Ammonium acetate

NH$_4$Cl: Ammonium chloride

NMP: N-Methyl-2-pyrrolidone

NMR: Nuclear magnetic resonance

NR: Nuclear receptor

Pd$_2$(dba)$_3$: Tris(dibenzylideneacetone)dipalladium(0)

Pd(PPh$_3$)$_4$: Tetrakis(triphenylphosphine)palladium(0)

PTSA: *p*-Toluenesulfonic acid

RBF: Round-bottom flask

TEA: Triethylamine

TES-Cl: Triethylsilyl chloride

TES-OTf: Triethylsilyl triflate

THC: Tetrahydrochrysene

THF: Tetrahydrofuran

TLC: Thin layer chromatography

UV: Ultraviolet

VDR: Vitamin D receptor

VDRE: Vitamin D response element

ACKNOWLEDGEMENTS

There are many individuals to whom I am very appreciative of for their support during my time as a graduate student. Firstly, thank you to my doctoral advisor, Professor Alexander Arnold, for providing me with guidance throughout my research projects and graduate studies. I am grateful for the many techniques and skills I have been able to experience and learn while being a member of his research group, all of which have made me a better scientist.

I would also like to express gratitude to my committee members, Drs. James Cook, Terry Moore, Alan Schwabacher, Nicholas Silvaggi, and Douglas Stafford, for contributing both insights and advice to my research project as it progressed.

Thank you to all the friends I have made in the Department of Chemistry & Biochemistry at UW-Milwaukee. I am very appreciative of all the conversations had and time spent together that have made my experience in graduate school an enjoyable one. A special thank you to Trevor Melkonian for providing encouragement and keeping matters light-hearted when my research would reach a standstill.

For supporting graduate research within the Department of Chemistry & Biochemistry at UW-Milwaukee, thank you to the late Professor George Sosnovsky. It was an honor to receive the Sosnovsky Award for Excellence in Graduate Research during my final year of graduate school.

Last but certainly not least, thank you to my wonderful family. They are the reason I have made it to this point in my education in the first place, and to whom I always strive to bring pride. My parents, Mark and Renae Mutchie, are my primary examples of hard-working individuals. They

have consistently encouraged me to set high goals for myself and have been the ones there to help me achieve them. An additional thank you goes out to my sister, Julia Mutchie. I greatly appreciate her emotional support as we embarked through our respective graduate programs together and am glad to have her as my go-to distraction from work. Finally, recognition goes out to my Sophie girl for the many hours she spent sitting by my side and at my feet as I studied.

PART I: DEVELOPMENT OF SMALL-MOLECULE-BASED PROBES FOR THE VITAMIN D RECEPTOR

Chapter One: An overview of the vitamin D receptor

1.1 The vitamin D receptor: an important pharmaceutical target

Extensive studies on the structure and function of the vitamin D receptor (VDR) have occurred since its isolation in the late 1960s.[1] The activity of VDR was quickly associated with calcium and phosphate homeostasis, as well as bone maintenance, when VDR was discovered to be highly expressed in cells of the bone, intestine, kidney, and parathyroid gland.[2-3] Existence of VDR in other cell types was later uncovered, suggesting a more intricate purpose for the receptor beyond mineral ion regulation.[4] VDR is now known to be expressed in the epithelia of endocrine organs, digestive system, bronchi, kidneys, and thymus, as well as being present in leukocytes and bone cells.[5] Within the cell, VDR can be located in the nucleus or can be membrane-bound.[6-7] Nuclear localization of cytoplasmic VDR was first observed in the 1970s[8-11], a process that was indicative of hormone receptors. Continued work on the characterization of VDR, followed by its cloning in 1987[12] and crystallization in 2000[13], established VDR as a member of the nuclear hormone receptor superfamily.[14]

VDR is a ligand-dependent transcription factor that regulates cell proliferation[15], cell differentiation[16], and immunomodulation[2]. Since gene expression is tightly regulated, VDR transcriptional activity has the ability to affect reproduction, development, inflammation, and general metabolic processes.[17-18] Additionally, calcium and phosphate are highly abundant in all

tissues. Therefore, the involvement of VDR in maintaining a physiological equilibrium for these minerals is highly important. An imbalance in calcium or phosphate can disrupt normal biological functions and affect nearly any organ system.[19-20] Immense progress has been made over the last fifty years to understand the complex role VDR has in biological systems. The connection VDR has to a variety of cellular processes makes it an important pharmaceutical target in treating metabolic disorders[21-22], skin diseases[23-24], cancer[25-26], autoimmune diseases[27], and cardiovascular diseases[28].

1.2   Nuclear receptor homology

Nuclear receptors (NRs) form one of the largest families of transcription factors, placing VDR alongside the receptors for thyroid (TR) and steroid hormones (i.e. estrogen receptor (ER), androgen receptor (AR), etc.), retinoic acid receptors (RARs), and peroxisome proliferator-activated receptors (PPARs), amongst others.[29] Activation of NRs occurs upon ligand binding, which induces a conformational change within the receptor. Dissociation of corepressors and the recruitment of coactivators allow for the initiation of gene transcription. The binding of NRs to DNA can occur as a homodimer, a heterodimer with the retinoid X receptor (RXR), or in some cases, as a monomer.[30] VDR is able to homodimerize, or heterodimerize with RXR, though heterodimerization is the primary form of DNA binding for VDR. (Figure 1) Each receptor complex recognizes specific hormone response elements (HREs) on the promoter region of DNA, which affects transcription through the recruitment of coregulators, components of the transcription initiation complex, or RNA polymerase II.[31]
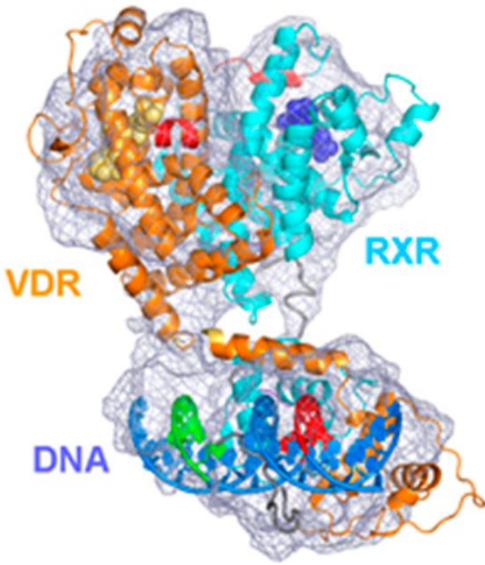
Figure 1. Molecular model of the full RXR/VDR/DNA complex, resulting from a cryo-electron microscopy map with fitted VDR and RXR crystal structures. (Image adopted from Orlov, et al. 2012)

Crystal structures for several NRs have been solved, revealing structural similarities within the NR superfamily that influence the receptor's function.[32] The shared homology between NRs includes multiple domains necessary for gene transcription. Members of the NR family contain the following regions: an amino-terminus (region A/B), a DNA-binding domain (DBD) (region C), a hinge region (region D), and a ligand-binding domain (LBD) (region E).[29, 32-33] (Figure 2) Some NRs also contain a poorly understood terminal region (region F) at the carboxyl-terminus, though region F is absent in VDR.

The amino-terminus region (region A/B) has the weakest evolutionary conservation and is the most variable domain between NRs in regard to both size and sequence.[34] Generally, this region of steroid receptors is much longer than that of non-steroid receptors.[31] The A/B region of NRs are found to be either unfolded or only partially folded when in their native state, so elucidating the complete function of this domain has remained challenging.[35] It is known that the A/B region is targeted for post-translational modifications that regulate transcription, however.[36] Additionally, a known component of the A/B region is activation function 1 (AF-1), which contributes to ligand-independent activation of the receptor.[29] AF-1 can interact with various coregulators, as well as work in tandem with a second activation function (AF-2) found in the carboxyl-terminus.[17, 36]

4
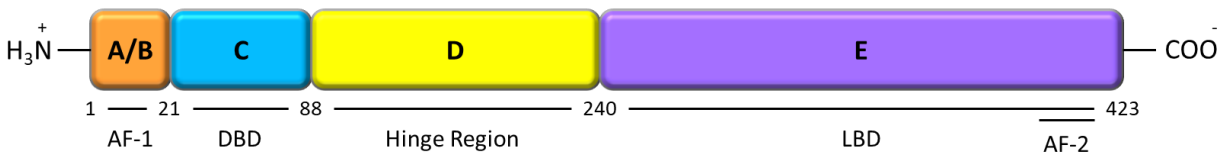
Figure 2. VDR (rat) domains and activation functions. Rat VDR is a 423-amino acid peptide, while human VDR is a 427-amino acid peptide. (DeLuca, et al. 2004)

The DBD (region C) in NRs is highly conserved and composed of 60-70 amino acid residues. Within the DBD, there are two subdomains that each contain a zinc finger.[36] (Figure 3) Eight conserved cysteines in the DBD organize into these two zinc-fingers, with four cysteine residues coordinating each zinc ion in a tetrahedral manner.[37] The two zinc fingers fold together to form a compact, α-helical 'reading domain' used for specific DNA sequence recognition.[29, 38] The first subdomain interacts with genomic response elements in the DNA major groove, while the second subdomain makes non-specific contacts with the DNA backbone and contributes to DBD dimerization with other proteins.[36] Some NRs, including VDR, also contain a variable C-terminal extension (CTE) in the DBD that interacts with specific base sequences in the DNA minor groove. The CTE helps to further stabilize the DBD-DNA binding interaction, and may also participate in protein-protein interactions within the homodimer or heterodimer.[31, 36] The HRE dictates which NR will bind, and is commonly composed of two hexameric sequences that are structured in direct, inverted, or everted repeat sequences. The base arrangement and variance in space between hexameric sequences largely determines NR binding.[39] For example, most VDR response elements (VDREs) are arranged as direct repeat sequences that are separated by three base pairs.[40] Steroid receptors typically favor 5'-AGAACA-3' motifs while non-steroid receptors, as well as the ER, prefer binding at 5'-AGGTCA-3' sequences.[31]
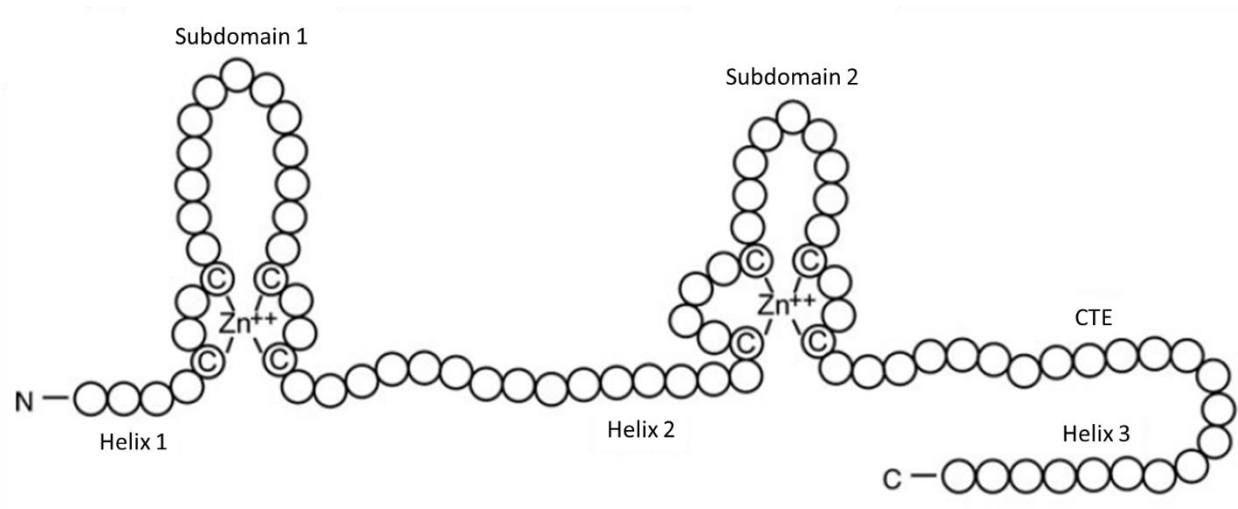
Figure 3. Simplified representation of NR DBDs with zinc finger subdomains and CTE region. (Image adapted from Weikum, et al. 2018)

The hinge region (region D) is traditionally known as a flexible, linker region between the DBD and LBD domains. It is a poorly conserved region between NRs, but a highly conserved sequence in different VDR species. Shaffer, et al. displayed that a short deletion of five amino acids from the C-terminal end of the VDR hinge region reduces transcriptional activation by more than half, suggesting that the length of the hinge region is important for proper functioning of the receptor.[40] While the N-terminal end of the VDR hinge region contains residues that are necessary for dimerization[41], the C-terminal end of the hinge region appears to function as a sequence-independent linker to ensure proper binding geometry between the DBD and LBD for coregulator interactions.[40]

Located at the carboxyl-terminus is the conserved ligand-binding domain (LBD) (region E). The LBD is less conserved than the DBD, but still maintains similarities between NRs while serving as a multifunctional region.[42] This region operates as a transcriptional regulatory domain that binds ligands, mediates dimerization, and directly interacts with coregulator proteins.[36, 43] The top-half of the LBD which contains helices H1, H4, H5, and H7-10, is the most similar between

NRs, whereas the lower-half containing the ligand-binding pocket (LBP) has more variety.[44] A three-layered, antiparallel helical 'sandwich' forms the LBD of NRs. NRs contain twelve conserved α-helices and a conserved β-turn between helix 5 and helix 6.[29, 32] The LBP that arises from NR-LBD folding is primarily a hydrophobic cavity for which specific contacts with ligands can be made. Diversity in the lower LBP region is what provides distinction in NR ligand recognition. Additionally, a highly structured, ligand-dependent second activation function (AF-2) is present in the LBD region of NRs. AF-2 is a major interface for both heterodimerization with RXR and coregulators.[45] Upon ligand-binding in the NR-LBP, a major conformational change occurs in which helix 11 repositions itself to align with helix 10. Associated with the repositioning of helix 11 is the 'mouse-trap' intramolecular folding mechanism of helix 12, the α-helix nearest to the carboxyl-terminus.[46] Helix 12 closes the LBP while releasing the Ω-loop, which is located between helix 2 and helix 3, to flip underneath helix 6.[45] The sealing of the LBP by helix 12 further stabilizes the active conformation of the bound ligand. (Figure 4) Furthermore, the movement of helix 12 is crucial for AF-2 transcriptional activity because its repositioning provides the surface for coactivator interactions.[32]
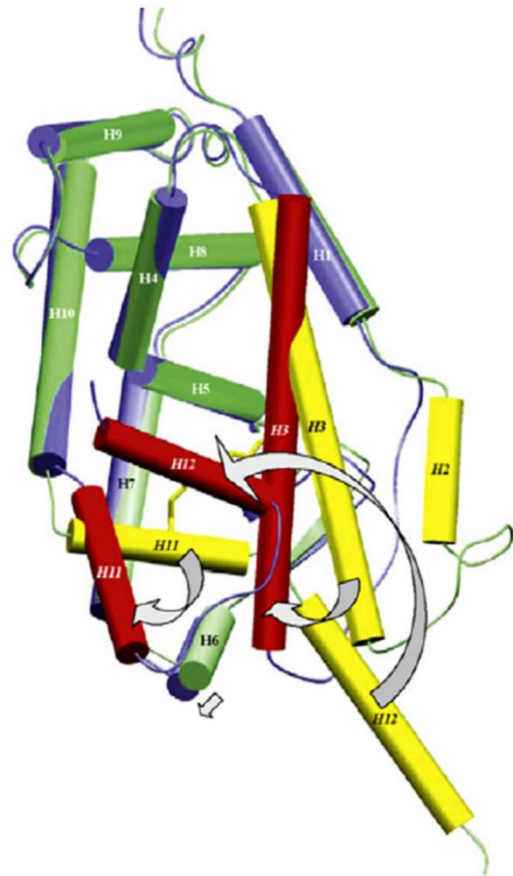
Figure 4. NR ligand-induced conformational change displayed in the RXRα-LBD. Primary conformational changes are observed in helices 3, 11, and 12 (yellow to red). The unliganded receptor is shown in yellow and green, while the liganded receptor is shown in red and blue. (Figure adapted from Rochel and Moras, 2011)

1.3   The vitamin D receptor – ligand binding pocket

As a member of the NR superfamily, VDR mediates its genomic response through ligand-receptor complexation.[47] Vitamin D itself does not bind VDR at physiological concentrations, but undergoes metabolism to its most active form, 1α,25-dihydroxyvitamin D_3 (calcitriol). (Figure 5) This discovery was made in 1961 when Chalk and Kodicek discovered that ^{14}C-labeled vitamin D_2 underwent 'destruction' when incubated in rat serum.[48] Subsequent studies around the 1970s began identifying vitamin D metabolites and reported the hydroxylation of vitamin D, which results in the tight-binding VDR ligand.[49-51] VDR is one of only 11 NRs that has a K_d value below 1 nM for its specific ligand.[46]
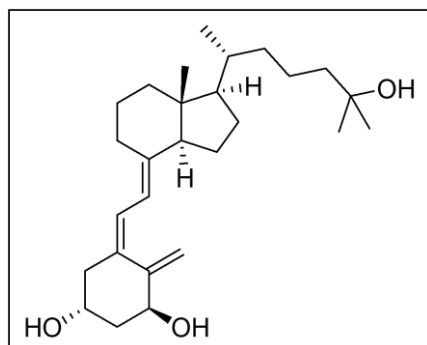
Figure 5. Chemical structure of calcitriol.

Rochel, et al. successfully crystallized the VDR-LBD complexed with calcitriol in 2000.[13] The crystallization of holo-VDR displayed the contacts made between the receptor and calcitriol while in the active form, which improved the evaluation of ligand-induced VDR function. An intricate network of stabilizing residues was uncovered in activated VDR that involves contribution from the hydroxyl functional groups on calcitriol. The LBP of VDR is primarily lined with hydrophobic residues but contains key polar residues to interact with the C1, C3, and C25 hydroxyls on calcitriol for receptor-ligand complex stabilization. Calcitriol orients itself in the VDR-LBP with the A-ring at the carboxyl-terminus of helix 5, and the 25-OH near helices 7 and 11.[45] (Figure 6A) Two hydrogen-bond interactions from Ser237 on helix 3 and Arg274 on helix 5 interact with the 1α-OH group, while the 3β-OH group hydrogen-bonds with

8

Ser278 on helix 5 and Tyr143 in the loop between helices 1 and 2. The A-ring sits in a chair

conformation with 1α-OH in the equatorial position and 3β-OH in the axial position.[52] Deep

inside the VDR-LBP are His305 and His 397, which are located on the loop between helices 6

and 7, and on helix 11, respectively. These two histidine residues form hydrogen-bonding

contacts with the 25-OH, leaving the ligand in an extended conformation.[45] An additional

structural insight gained upon receptor crystallization includes the non-planar geometry in the

conjugated triene, which causes a curved shape of the ligand when it is in the active

conformation.[13] (Figure 6B)
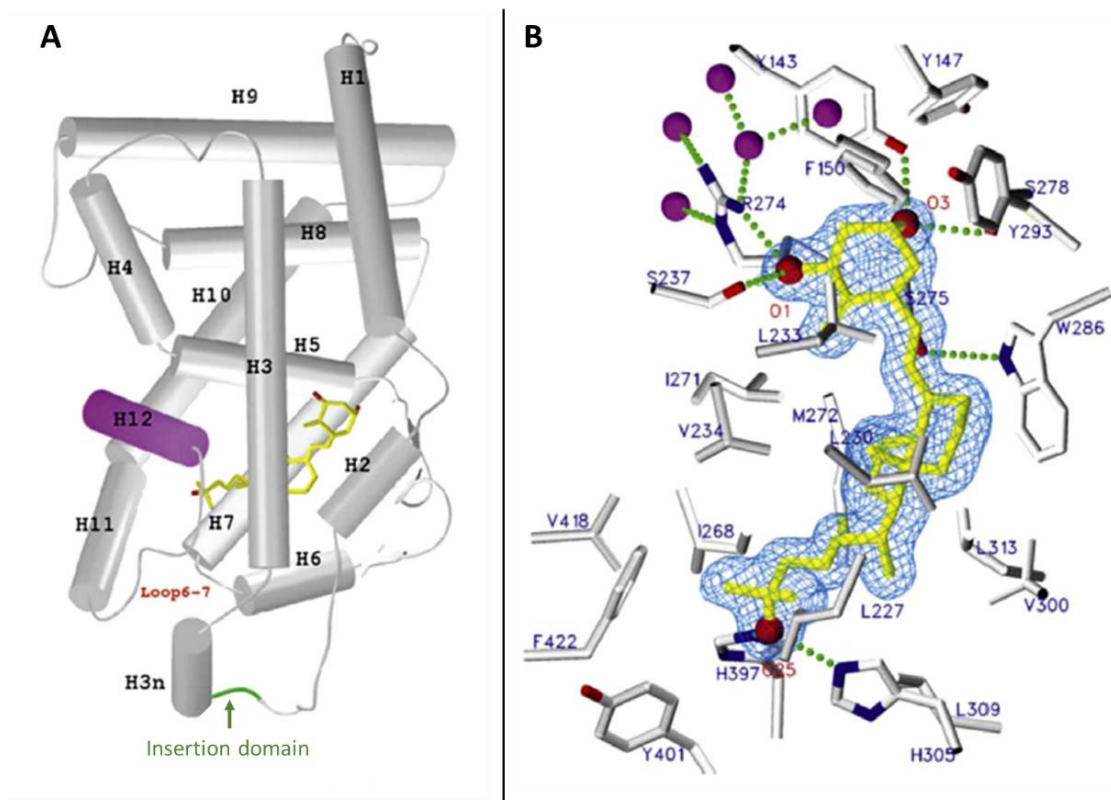
Figure 6. A) Overall fold of hVDR-LBD with calcitriol depicted in yellow. An insertion domain unique to VDR is shown in green. B) Calcitriol in the hVDR-LBP; hydroxyl groups are indicated by red spheres, hydrogen-bonds as green dotted lines, and water molecules as purple spheres. (Images adapted from Rochel and Moras, 2011)

As discussed in section 1.1, VDR exhibits regulatory control over cell proliferation and differentiation, as well as calcium homeostasis. Contrary to the original hypothesis that a separate membrane receptor was responsible for the rapid responses produced by calcitriol[53], experiments using VDR knock-out mice proved that VDR was necessary for the occurrence of calcitriol-mediated rapid responses in osteoblasts.[54] The ability of calcitriol to elicit both genomic and rapid responses within VDR is thought to be due to potential flexibility of the ligand within the receptor. The VDR-LBP has a large volume (697 Å^3) that is only 56% occupied by calcitriol.[45] Therefore, genomic and rapid responses may arise from different ligand conformations when receptor-bound.

6-s-*trans* conformation   6-s-*cis* conformation
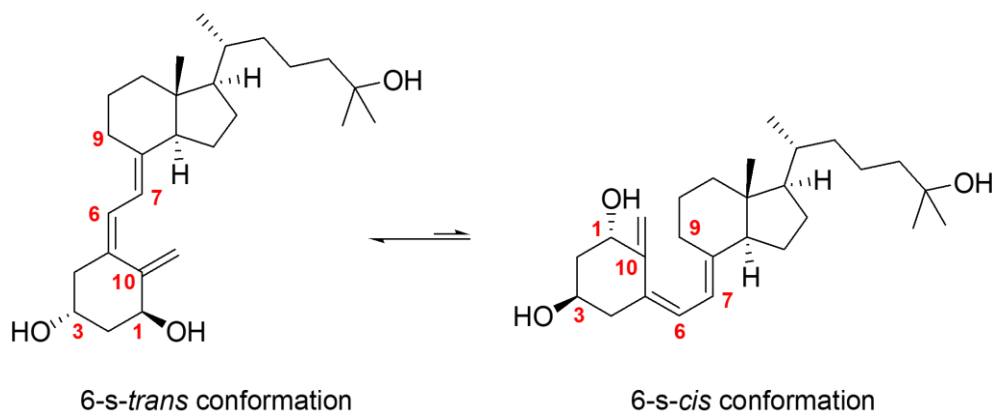
Figure 7. Rotation around C6-C7 bond in calcitriol that allows for different conformations of the secosteroidal structure.

Norman, et al. highlighted the possible rotation around the C6-C7 bond in calcitriol, due to the broken C9-C10 bond that would form the B-ring in a traditional steroid scaffold.[55] (Figure 7) Calcitriol derivatives locked in either the *cis* or *trans* conformation were used to evaluate transcaltachia, the rapid stimulation of intestinal calcium absorption. It was revealed that the *cis*-conformation derivatives were able to effectively induce transcaltachia, while the *trans*-conformation derivatives did not. Menegaz, et al. then observed that one of the *cis*-derivatives,
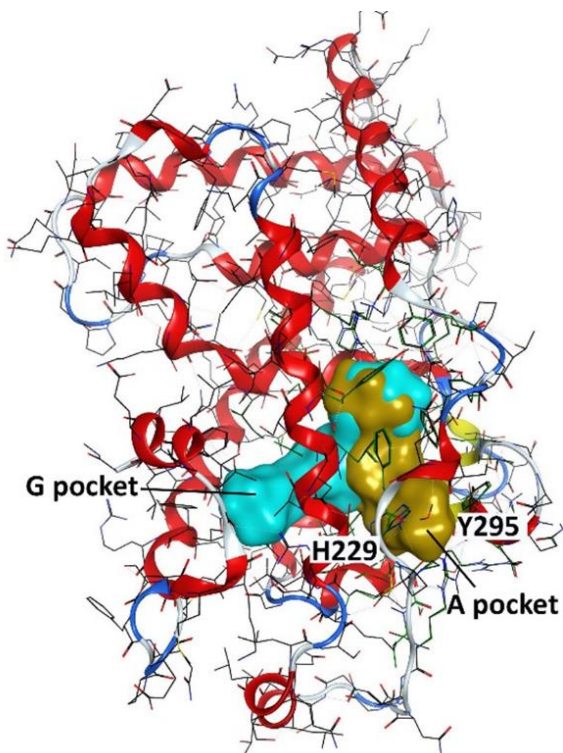
Figure 8. VDR-LBD (PDB: 1DB1) with genomic pocket (cyan) and alternative pocket (gold). (Figure adopted from Mutchie, et al. 2019)

$1\alpha,25(OH)_2$ lumisterol D_3 (JN), was able to stimulate chlorine ion channels in Sertoli cells more effectively than calcitriol, while being a weak inhibitor to the VDR–calcitriol interaction.[56] The ability for calcitriol to adopt the 6-s-*cis* or 6-s-*trans* conformation may account for the rapid responses it elicits when bound to VDR, in addition to its known genomic functions. In fact, molecular modeling of $1\alpha,25(OH)_2$ lumisterol D_3 (JN) revealed an alternative 'A-pocket' within the VDR-LBP that partially overlaps with the genomic LBP.[57] (Figure 8) The higher-energy 6-s-*cis* conformation of calcitriol was able to bind in this A-pocket, providing a possible explanation for the non-genomic responses produced by calcitriol-bound VDR.[58]

1.4 Evaluation of vitamin D analogs

One of the most important qualities of vitamin D is its natural ability to regulate multiple physiological processes. The potential of synthetic small-molecules to partially reproduce or inhibit the activity of calcitriol establishes the VDR-LBD as an important domain for pharmaceutical targeting.[44] A major, yet complicated, goal in vitamin D-related research has involved preparing ligands in an effort to separate the multiple functions mediated by the VDR-

calcitriol complex.[59-60] Hypercalcemia, increasing bone resorption, and soft tissue calcification limit the use of natural vitamin D in clinical applications.[13] Developing calcitriol derivatives with improved biological profiles may lead to new therapeutic treatments for hyperproliferative diseases.[60] In fact, a number of commercialized VDR ligands have already been developed including the psoriasis treatments calcipotriol (Dovonex®) and tacalcitol (Curatoderm®), secondary hyperparathyroidism treatments paricalcitol (Zemplar®) and doxercalciferol (Hectorol®), and the osteoporosis treatment eldecalcitol (Edirol®).[61]

Various derivatives of calcitriol have been studied to gain further insight into the structural features needed for suitable VDR binding. As mentioned in section 1.3, calcitriol ($1\alpha,25(OH)_2D_3$) is the vitamin D metabolite with the highest affinity for VDR. The formation of calcitriol occurs from two sequential hydroxylation steps from vitamin D_3: an initial hydroxylation on C25 that transpires primarily in the liver, followed by a C1 hydroxylation in the kidney.[62-63] The metabolite following C25-hydroxylation is known as calcifediol ($25OHD_3$), which is the major circulating form of vitamin D_3 present in the blood.[55, 64] (Figure 9)

In 1975, Procsal, et al. performed a competitive binding assay of calcifediol and other vitamin D_3 analogs against tritium-labeled calcitriol in chick intestinal chromatin.[65] The lack of the 1α-OH functional group inherent to calcifediol showed only 1/900 VDR binding affinity relative to calcitriol. Alfacalcidiol, which lacks the 25-OH functional group (Figure 9), also displayed 1/900 VDR binding affinity relative to calcitriol. Conversely, loss of the 3β-OH from the calcitriol scaffold retained 1/8 the binding affinity of calcitriol. The hydrocarbon scaffold with a singular hydroxyl present in the 1α-position maintained 1/5000 binding affinity, but the sole 3β-OH analog lost all ability to compete with calcitriol for VDR. The findings reported by Procsal, et al.

indicate that the polar 1α-OH and 25-OH substituents are significantly more important that the 3β-OH functional group to promote VDR binding.
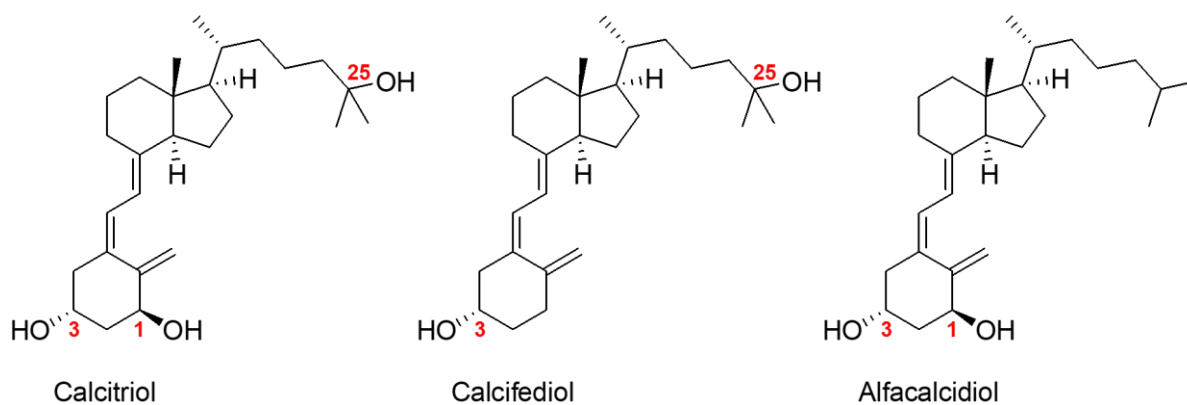
Figure 9. Chemical structures of calcitriol, calcifediol, and alfacalcidiol with numbered hydroxyl positions (red).

In addition to the necessary presence of a hydroxyl substituent in the C1 position for effective VDR binding, the stereochemistry of the 1α-OH group is also highly important to retain VDR affinity. In 1993, Norman, et al. evaluated the stereochemistry of the hydroxyl substituents on the A-ring of calcitriol in an *in vitro* binding assay to chick intestinal VDR.[66] Inversion of the 3β-OH to the 3α-OH epimer retained 24% VDR affinity relative to calcitriol; however, epimerization of the 1α-OH to the 1β-OH analog reduced the VDR affinity to 0.2%. The conclusion that the interaction of the 1α-OH substituent is more influential than the 3-OH regarding VDR binding is further supported by this study.

Calcitriol contains a triene within its hydrocarbon scaffold. Two of the alkenes, between C5-C6 and C7-C8, link the A-ring to the fused C,D-ring system, while the third alkene is a substituent at position C10 on the A-ring. The conjugated triene in the natural metabolite has a 5(Z),7(E) configuration. (Figure 10) In 1980, Wecksler and Norman analyzed the C5-C6 *trans*-isomer of calcitriol in a competitive binding assay against tritium-labeled calcitriol in chick intestinal VDR.

It was determined that the 5(E),7(E)-isomer had 13% affinity for VDR relative to calcitriol.[67] Following in 1994, VanAlstyne, et al. synthesized the 5(Z),7(Z)-isomer and 5(E),7(Z)-isomer of calcitriol. The 5(Z),5(Z) derivative maintained only 0.82% affinity for VDR, whereas the 5(E),7(Z) had 1.6% VDR affinity relative to calcitriol in the same assay.[68] Therefore, the geometry and positioning of the fused C,D-ring system relative to the A-ring is important for suitable binding in the VDR-LBP.
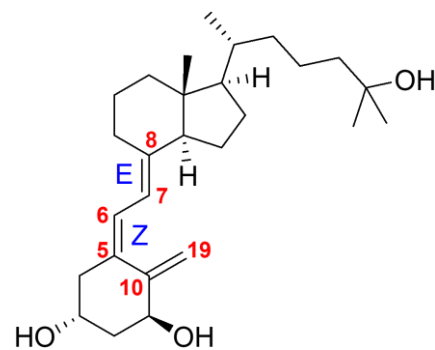
Figure 10. Chemical structure of calcitriol with triene numbering (red) and 5(Z),7(E) conformation (blue) labels.
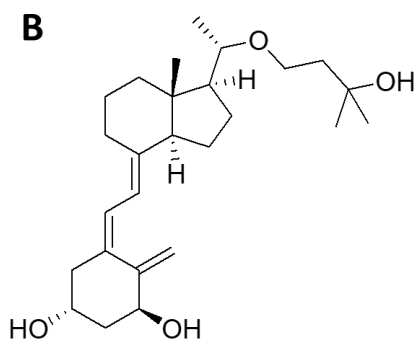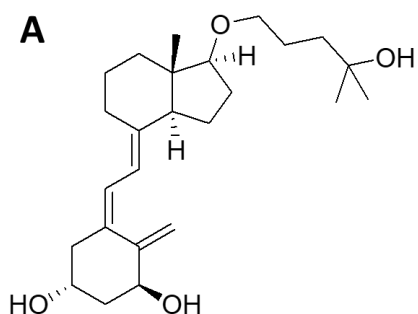
Figure 11. A) Chemical structure of the 20-oxa-21-norvitamin D_3 analog; B) Chemical structure of the 22-oxavitamin D_3 analog.

Hydrophobicity within the center of VDR ligands is also important for good binding to VDR, due to the largely lipophilic VDR-LBP. In 1986, researchers at New Drug Research Laboratories, Chugai Pharmaceutical Co. sought to develop an analog of calcitriol that was able to induce differentiation of myeloid leukemia cells without altering mineral homeostasis. By replacing the C20 carbon with an oxygen atom (with loss of the C21 methyl), it was discovered that the 20-oxa-21-norvitamin D_3 analog (Figure 11A) was as effective as calcitriol in differentiating human myeloid leukemia (HL-60) cells *in vitro* and had no effect on bone calcium mobilization in rats. The affinity for VDR was only 1/1000 that of calcitriol, however.[69] Moving the ether linkage to the C22 position, and therefore retention of the C21

14

methyl (Figure 11B), found that differentiation of HL-60 cells was 10-fold higher than differentiation induced by calcitriol. Similarly, no effect on bone calcium mobilization was observed in rats for the 22-oxavitamin D_3 analog. The binding affinity was reported to be 1/14 that of calcitriol.[70] While the presence of an ether linkage in the aliphatic chain was able to influence differentiation and regulatory effects, the added polarity also negatively impacted VDR affinity.

More than 3,000 synthetic analogues of calcitriol have been developed for VDR that retain the secosteroidal scaffold.[71] Generally, it can be concluded that structural changes to the hydrophobic core of calcitriol can still result in high affinity ligands for VDR. Positioning of the hydroxyl functionalities to conserve hydrogen-bonding interactions with polar residues in the VDR-LBP are particularly important. In fact, non-secosteroidal ligands have been developed as agonists for VDR that maintain a similar conformation to calcitriol in the VDR-LBP. Boehm, et al. synthesized non-secosteroidal ligands with a structurally distinct *bis*-phenyl scaffold.[72] One racemic analog, LG190178 (Figure 12), was found to activate VDR in HEPG2 cells using a transcription assay with an EC_{50} of 40 nM. A competitive binding assay with tritium-labeled calcitriol showed the racemic mixture of LG190178 to have 0.3% affinity to VDR relative to calcitriol. Crystallization of YR301, the 2(S),2'(R)-isomer of LG190178, revealed that the two ethyl substituents on the quaternary carbon center aligned well with the fused C,D-ring system of VDR-bound calcitriol.[73] YR301 was determined to be the most active isomer of the LG190178 racemates, with a 28.3% affinity for VDR compared to calcitriol.[74]
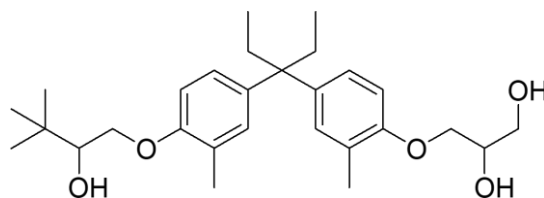
Figure 12. Chemical structure of LG190178.

Beyond the many synthetic ligands developed as agonists for mediating VDR genomic activity, synthetic antagonists have also displayed high affinity for VDR. In 1999, Miura, et al. reported the first series of VDR antagonists containing a lactone-ring.[75] (Figure 13) The antagonists were derivatives from the natural occurring vitamin D metabolite, (23S,25R)-1α,25(OH)$_2$D$_3$-26,23-lactone, which was first isolated in 1981.[76] Compared to calcitriol, TEI-9647 had 10% affinity for VDR in HL-60 cells, while TEI-9648, the C23 epimer, maintained 8% VDR affinity.[75] Further research using MALDI-TOF MS confirmed that the unsaturated esters underwent a conjugate addition reaction with cysteine residues in the CTE region of the human VDR ligand pocket.[77]

(23S,25R)-1α,25-(OH)$_2$D$_3$-26,23-lactone   TEI-9647   TEI-9648
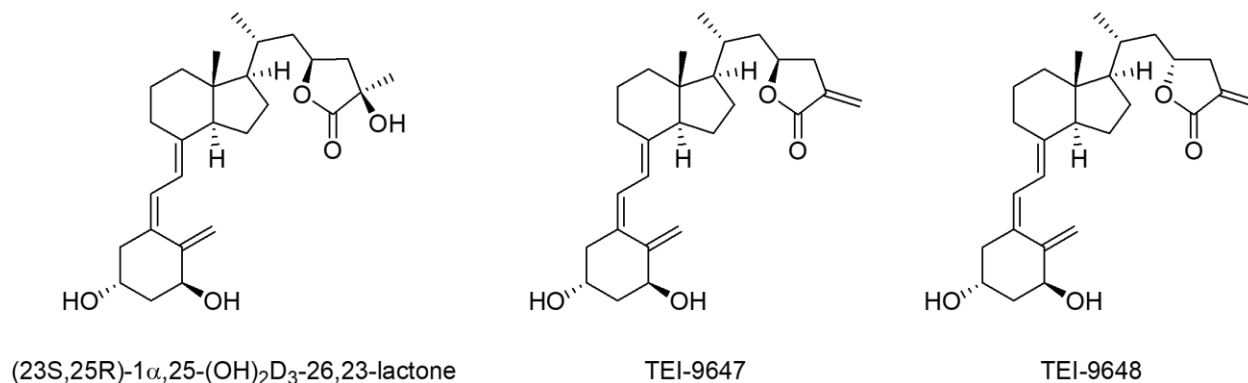
Figure 13. Vitamin D analogs containing a lactone-ring.

Agonism and antagonism of hormone analogs are closely related processes.[78] Incorrect stabilization of helix 12 prevents coactivator interaction with the AF-2 domain in the VDR-LBD. Synthetic compounds, ZK159222 and ZK168281 (Figure 14), act to displace helix 12 in this manner. Both ZK159222 and ZK168281 are poor inducers of VDR transcription, but reduce calcitriol-meditated transcription.[79]
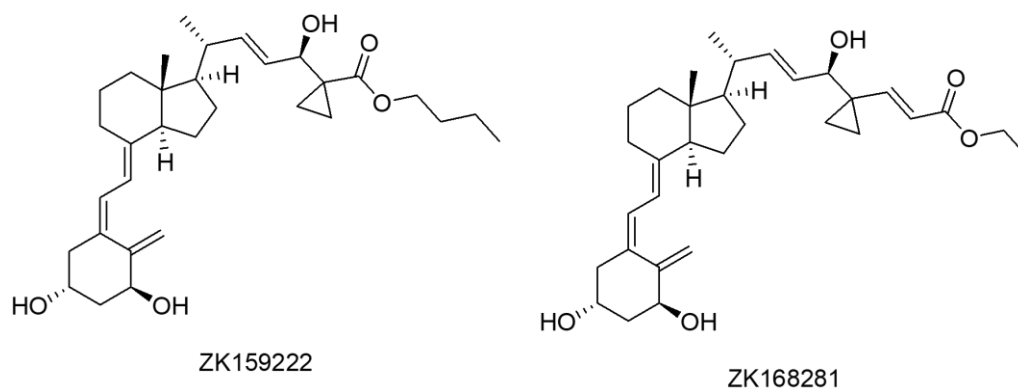
Figure 14. Chemical structure of VDR antagonists, ZK159222 and ZK168281.

Significant advancements in understanding the role of VDR have occurred since its isolation over 50 years ago. A great deal of this knowledge arises from evaluating the impact ligand structural changes have on VDR-mediated biological responses. In order to further clarify the complete activity transpiring within the LBP, and to understand the diverse pharmacological effects ligands have on VDR, a method to monitor ligand-receptor complexation in real-time must be established. The development of an intrinsically fluorescent ligand for this purpose would probe direct ligand-receptor interactions, as well as provide a noninvasive means to trace cellular VDR distribution and localization.

References

1.   Haussler, M. R.; Norman, A. W., Chromosomal receptor for a vitamin D metabolite. *Proceedings of the National Academy of Sciences* **1969,** *62* (1), 155-162.
2.   Pinette, K. V.; Yee, Y. K.; Amegadzie, B. Y.; Nagpal, S., Vitamin D receptor as a drug discovery target. *Mini reviews in medicinal chemistry* **2003,** *3* (3), 193-204.
3.   Pike, J. W.; Meyer, M. B.; Lee, S.-M.; Onal, M.; Benkusky, N. A., The vitamin D receptor: contemporary genomic approaches reveal new basic and translational insights. *The Journal of Clinical Investigation* **2017,** *127* (4), 1146-1154.
4.   Pike, J. W.; Goozé, L. L.; Haussler, M. R., Biochemical evidence for 1,25-dihydroxyvitamin D receptor macromolecules in parathyroid, pancreatic, pituitary, and placental tissues. *Life sciences* **1980,** *26* (5), 407-414.

5.   Wang, Y.; Zhu, J.; DeLuca, H. F., Where is the vitamin D receptor? *Archives of biochemistry and biophysics* **2012,** *523* (1), 123-133.

6.   Huhtakangas, J. A.; Olivera, C. J.; Bishop, J. E.; Zanello, L. P.; Norman, A. W., The vitamin D receptor is present in caveolae-enriched plasma membranes and binds $1\alpha,25(OH)_2$-vitamin D_3 *in vivo* and *in vitro*. *Molecular Endocrinology* **2004,** *18* (11), 2660-2671.

7.   Haussler, M. R.; Jurutka, P.; Hsieh, J.-C.; Thompson, P.; Selznick, S.; Haussler, C.; Whitfield, G. K., New understanding of the molecular mechanism of receptor-mediated genomic actions of the vitamin D hormone. *Bone* **1995,** *17* (2), S33-S38.

8.   Tsai, H. C.; Norman, A. W., Studies on Calciferol Metabolism: VIII. EVIDENCE FOR A CYTOPLASMIC RECEPTOR FOR 1,25-DIHYDROXY-VITAMIN D_3 IN THE INTESTINAL MUCOSA. *Journal of Biological Chemistry* **1973,** *248* (17), 5967-5975.

9.   Brumbaugh, P. F.; Haussler, M. R., Nuclear and cytoplasmic receptors for 1,25-dihydroxycholecalciferol in intestinal mucosa. *Biochemical and biophysical research communications* **1973,** *51* (1), 74-80.

10.   Brumbaugh, P.; Haussler, M. R., Specific binding of $1\alpha,25$-dihydroxycholecalciferol to nuclear components of chick intestine. *Journal of Biological Chemistry* **1975,** *250* (4), 1588-1594.

11.   Brumbaugh, P. F.; Hughes, M. R.; Haussler, M. R., Cytoplasmic and nuclear binding components for $1\alpha,25$-dihydroxyvitamin D_3 in chick parathyroid glands. *Proceedings of the National Academy of Sciences* **1975,** *72* (12), 4871-4875.

12.   McDonnell, D. P.; Mangelsdorf, D. J.; Pike, J. W.; Haussler, M. R.; O'Malley, B. W., Molecular cloning of complementary DNA encoding the avian receptor for vitamin D. *Science* **1987,** *235* (4793), 1214-1217.

13.   Rochel, N.; Wurtz, J.; Mitschler, A.; Klaholz, B.; Moras, D., The crystal structure of the nuclear receptor for vitamin D bound to its natural ligand. *Molecular cell* **2000,** *5* (1), 173-179.

14.   Mangelsdorf, D. J.; Thummel, C.; Beato, M.; Herrlich, P.; Schütz, G.; Umesono, K.; Blumberg, B.; Kastner, P.; Mark, M.; Chambon, P., The nuclear receptor superfamily: the second decade. *Cell* **1995,** *83* (6), 835.

15.   Colston, K.; Colston, M. J.; Feldman, D., 1,25-dihydroxyvitamin D_3 and malignant melanoma: the presence of receptors and inhibition of cell growth in culture. *Endocrinology* **1981,** *108* (3), 1083-1086.

16.   Miyaura, C.; Abe, E.; Kuribayashi, T.; Tanaka, H.; Konno, K.; Nishii, Y.; Suda, T., $1\alpha,25$-Dihydroxyvitamin D_3 induces differentiation of human myeloid leukemia cells. *Biochemical and biophysical research communications* **1981,** *102* (3), 937-943.

17.   Shao, D.; Lazar, M. A., Modulating nuclear receptor function: may the phos be with you. *The Journal of clinical investigation* **1999,** *103* (12), 1617-1618.

18.   Carlberg, C.; Seuter, S., A genomic perspective on vitamin D signaling. *Anticancer research* **2009,** *29* (9), 3485-3493.

19.   Carmeliet, G.; Van Cromphaut, S.; Daci, E.; Maes, C.; Bouillon, R., Disorders of calcium homeostasis. *Best Practice & Research Clinical Endocrinology & Metabolism* **2003,** *17* (4), 529-546.

20.   Hansen, K. E.; Drezner, M. K., Clinical Disorders of Phosphate Homeostasis. In *Vitamin D*, Elsevier: 2011; pp 1155-1186.

21.   Al-Badr, W.; Martin, K. J., Vitamin D and kidney disease. *Clinical Journal of the American Society of Nephrology* **2008,** *3* (5), 1555-1560.

22.   Santoro, D.; Caccamo, D.; Gagliostro, G.; Ientile, R.; Benvenga, S.; Bellinghieri, G.; Savica, V., Vitamin D metabolism and activity as well as genetic variants of the vitamin D receptor (VDR) in chronic kidney disease patients. *Journal of Nephrology* **2013,** *26* (4), 636-644.

23.   MacLaughlin, J.; Gange, W.; Taylor, D.; Smith, E.; Holick, M., Cultured psoriatic fibroblasts from involved and uninvolved sites have a partial but not absolute resistance to the proliferation-inhibition activity of 1,25-dihydroxyvitamin D$_3$. *Proceedings of the National Academy of Sciences* **1985,** *82* (16), 5409-5412.

24.   Reichrath, J.; Zouboulis, C. C.; Vogt, T.; Holick, M. F., Targeting the vitamin D endocrine system (VDES) for the management of inflammatory and malignant skin diseases: An historical view and outlook. *Reviews in Endocrine and Metabolic Disorders* **2016,** *17* (3), 405-417.

25.   Skowronski, R. J.; Peehl, D. M.; Feldman, D., Vitamin D and prostate cancer: 1,25 dihydroxyvitamin D3 receptors and actions in human prostate cancer cell lines. *Endocrinology* **1993,** *132* (5), 1952-1960.

26.   Wada, K.; Tanaka, H.; Maeda, K.; Inoue, T.; Noda, E.; Amano, R.; Kubo, N.; Muguruma, K.; Yamada, N.; Yashiro, M., Vitamin D receptor expression is associated with colon cancer in ulcerative colitis. *Oncology reports* **2009,** *22* (5), 1021-1025.

27.   Adorini, L.; Penna, G., Control of autoimmune diseases by the vitamin D endocrine system. *Nature clinical practice Rheumatology* **2008,** *4* (8), 404-412.

28.   Judd, S.; Tangpricha, V., Vitamin D deficiency and risk for cardiovascular disease. *Circulation* **2008,** *117* (4), 503.

29.   Aranda, A.; Pascual, A., Nuclear hormone receptors and gene expression. *Physiological reviews* **2001,** *81* (3), 1269-1304.

30.   Olefsky, J. M., Nuclear receptor minireview series. *Journal of biological chemistry* **2001,** *276* (40), 36863-36864.

31.   Helsen, C.; Claessens, F., Looking at nuclear receptors from a new angle. *Molecular and cellular endocrinology* **2014,** *382* (1), 97-106.

32.   Moras, D.; Gronemeyer, H., The nuclear receptor ligand-binding domain: structure and function. *Current opinion in cell biology* **1998,** *10* (3), 384-391.

33.   Mutchie, T. R.; Olivia, B. Y.; Di Milo, E. S.; Arnold, L. A., Alternative binding sites at the vitamin D receptor and their ligands. *Molecular and cellular endocrinology* **2019,** *485*, 1-8.

34.   Laudet, V.; Gronemeyer, H., *The nuclear receptor factsbook*. Gulf Professional Publishing: 2002.

35.   Kumar, R.; Thompson, E. B., Transactivation functions of the N-terminal domains of nuclear hormone receptors: protein folding and coactivator interactions. *Molecular Endocrinology* **2003,** *17* (1), 1-10.

36.   Weikum, E. R.; Liu, X.; Ortlund, E. A., The nuclear receptor superfamily: A structural perspective. *Protein Science* **2018,** *27* (11), 1876-1892.

37.   Beato, M., Transcriptional control by nuclear receptors. *The FASEB Journal* **1991,** *5* (7), 2044-2051.

38.   Lin, R.; White, J. H., The pleiotropic actions of vitamin D. *Bioessays* **2004,** *26* (1), 21-28.

39.   Kurokawa, R.; Yu, V.; Näär, A.; Kyakumoto, S.; Han, Z.; Silverman, S.; Rosenfeld, M.; Glass, C., Differential orientations of the DNA-binding domain and carboxy-terminal

dimerization interface regulate binding site selection by nuclear receptor heterodimers. *Genes & development* **1993,** *7* (7b), 1423-1435.

40.   Shaffer, P. L.; McDonnell, D. P.; Gewirth, D. T., Characterization of transcriptional activation and DNA-binding functions in the hinge region of the vitamin D receptor. *Biochemistry* **2005,** *44* (7), 2678-2685.

41.   Quack, M.; Szafranski, K.; Carlberg, C.; Rouvinen, J., The role of the T-box for the function of the vitamin D receptor on different types of response elements. *Nucleic acids research* **1998,** *26* (23), 5372-5378.

42.   Jehan, F.; DeLuca, H. F., Cloning and characterization of the mouse vitamin D receptor promoter. *Proceedings of the National Academy of Sciences* **1997,** *94* (19), 10138-10143.

43.   Dimitrov, V.; Salehi-Tabar, R.; An, B.-S.; White, J. H., Non-classical mechanisms of transcriptional regulation by the vitamin D receptor: insights into calcium homeostasis, immune system regulation and cancer chemoprevention. *The Journal of steroid biochemistry and molecular biology* **2014,** *144*, 74-80.

44.   Bourguet, W.; Germain, P.; Gronemeyer, H., Nuclear receptor ligand-binding domains: three-dimensional structures, molecular interactions and pharmacological implications. *Trends in pharmacological sciences* **2000,** *21* (10), 381-388.

45.   Rochel, N.; Moras, D., Structural basis for ligand activity in VDR. In *Vitamin D*, Elsevier: 2011; pp 171-191.

46.   Carlberg, C., Ligand-mediated conformational changes of the VDR are required for gene transactivation. *The Journal of steroid biochemistry and molecular biology* **2004,** *89*, 227-232.

47.   Norman, A. W., Vitamin D receptor: new assignments for an already busy receptor. *Endocrinology* **2006,** *147* (12), 5542-5548.

48.   Chalk, K. J.; Kodicek, E., The association of 14C-labelled vitamin D2 with rat serum proteins. *Biochem. J.* **1961,** *79*, 1-7.

49.   Blunt, J.; DeLuca, H.; Schnoes, H., 25-Hydroxycholecalciferol. A biologically active metabolite of vitamin D_3. *Biochemistry* **1968,** *7* (10), 3317-3322.

50.   Blunt, J.; DeLuca, H. F., The synthesis of 25-hydroxycholecalciferol. A biologically active metabolite of vitamin D_3. *Biochemistry* **1969,** *8* (2), 671-675.

51.   Holick, M.; Schnoes, H.; DeLuca, H.; Gray, R.; Boyle, I.; Suda, T., Isolation and identification of 24,25-dihydroxycholecalciferol, a metabolite of vitamin D_3 made in the kidney. *Biochemistry* **1972,** *11* (23), 4251-4255.

52.   Bouillon, R.; Okamura, W. H.; Norman, A. W., Structure-function relationships in the vitamin D endocrine system. *Endocrine reviews* **1995,** *16* (2), 200-257.

53.   Nemere, I.; Dormanen, M. C.; Hammond, M. W.; Okamura, W. H.; Norman, A. W., Identification of a specific binding protein for 1α,25-dihydroxyvitamin D_3 in basal-lateral membranes of chick intestinal epithelium and relationship to transcaltachia. *Journal of Biological Chemistry* **1994,** *269* (38), 23750-23756.

54.   Zanello, L. P.; Norman, A. W., Rapid modulation of osteoblast ion channel responses by 1α,25$(OH)_2$-vitamin D_3 requires the presence of a functional vitamin D nuclear receptor. *Proceedings of the National Academy of Sciences* **2004,** *101* (6), 1589-1594.

55.   Norman, A. W.; Song, X.; Zanello, L.; Bula, C.; Okamura, W. H., Rapid and genomic biological responses are mediated by different shapes of the agonist steroid hormone, 1α,25$(OH)_2$vitamin D_3. *Steroids* **1999,** *64* (1-2), 120-128.

56.	Menegaz, D.; Barrientos-Duran, A.; Kline, A.; Silva, F. R.; Norman, A. W.; Mizwicki, M. T.; Zanello, L. P., 1α,25(OH)$_2$-Vitamin D$_3$ stimulation of secretion via chloride channel activation in Sertoli cells. *The Journal of steroid biochemistry and molecular biology* **2010,** *119* (3-5), 127-134.

57.	Mizwicki, M. T.; Keidel, D.; Bula, C. M.; Bishop, J. E.; Zanello, L. P.; Wurtz, J.-M.; Moras, D.; Norman, A. W., Identification of an alternative ligand-binding pocket in the nuclear vitamin D receptor and its functional importance in 1α,25(OH)$_2$-vitamin D$_3$ signaling. *Proceedings of the National Academy of Sciences* **2004,** *101* (35), 12876-12881.

58.	Mizwicki, M. T.; Menegaz, D.; Yaghmaei, S.; Henry, H. L.; Norman, A. W., A molecular description of ligand binding to the two overlapping binding pockets of the nuclear vitamin D receptor (VDR): structure-function implications. *The Journal of steroid biochemistry and molecular biology* **2010,** *121* (1-2), 98-105.

59.	DeLuca, H. F., Overview of general physiologic features and functions of vitamin D. *The American journal of clinical nutrition* **2004,** *80* (6), 1689S-1696S.

60.	Carlberg, C.; Mouriño, A., New vitamin D receptor ligands. *Expert opinion on therapeutic patents* **2003,** *13* (6), 761-772.

61.	Leyssens, C.; Verlinden, L.; Verstuyf, A., The future of vitamin D analogs. *Frontiers in physiology* **2014,** *5*, 122.

62.	DeLuca, H. F.; Schnoes, H. K., Vitamin D: recent advances. *Annual review of biochemistry* **1983,** *52* (1), 411-439.

63.	Monkawa, T.; Yoshida, T.; Wakino, S.; Shinki, T.; Anazawa, H.; Deluca, H. F.; Suda, T.; Hayashi, M.; Saruta, T., Molecular cloning of cDNA and genomic DNA for human 25-hydroxyvitamin D31α-hydroxylase. *Biochemical and biophysical research communications* **1997,** *239* (2), 527-533.

64.	Blunt, J. W.; DeLuca, H. F.; Schnoes, H. K., 25-hydroxycholecalciferol. A biologically active metabolite of vitamin D3. *Biochemistry* **1968,** *7* (10), 3317-22.

65.	Procsal, D.; Okamura, W.; Norman, A., Structural requirements for the interaction of 1α,25-(OH) $_2$-vitiamin D$_3$ with its chick interestinal receptor system. *Journal of Biological Chemistry* **1975,** *250* (21), 8382-8388.

66.	Norman, A.; Bouillon, R.; Farach-Carson, M.; Bishop, J.; Zhou, L.-X.; Nemere, I.; Zhao, J.; Muralidharan, K.; Okamura, W., Demonstration that 1 beta, 25-dihydroxyvitamin D3 is an antagonist of the nongenomic but not genomic biological responses and biological profile of the three A-ring diastereomers of 1 alpha, 25-dihydroxyvitamin D3. *Journal of Biological Chemistry* **1993,** *268* (27), 20022-20030.

67.	Wecksler, W. R.; Norman, A. W., Studies on the mode of action of calciferol XXV. 1α,25-dihydroxy-5,6-trans-vitamin D$_3$, the 5E-isomer of 1α,25-dihydroxyvitamin D$_3$. *Steroids* **1980,** *35* (4), 419-425.

68.	VanAlstyne, E. M.; Norman, A. W.; Okamura, W. H., 7,8-Cis Geometric Isomers of the Steroid Hormone 1α,25-Dihydroxyvitamin D$_3$. *Journal of the American Chemical Society* **1994,** *116* (14), 6207-6216.

69.	Kubodera, N.; Miyamoto, K.; Ochi, K.; Matsunaga, I., Synthetic studies of vitamin D analogues. VII. Synthesis of 20-oxa-21-norvitamin D$_3$ analogues. *Chemical and pharmaceutical bulletin* **1986,** *34* (5), 2286-2289.

70.   Murayama, E.; Miyamoto, K.; Kubodera, N.; Mori, T.; Matsunaga, I., Synthetic studies of vitamin D_3 analogues. VIII. Synthesis of 22-oxavitamin D_3 analogues. *Chemical and pharmaceutical bulletin* **1986,** *34* (10), 4410-4413.

71.   Carlberg, C.; Molnár, F., Current status of vitamin D signaling and its therapeutic applications. *Current topics in medicinal chemistry* **2012,** *12* (6), 528-547.

72.   Boehm, M. F.; Fitzgerald, P.; Zou, A.; Elgort, M. G.; Bischoff, E. D.; Mere, L.; Mais, D. E.; Bissonnette, R. P.; Heyman, R. A.; Nadzan, A. M.; Reichman, M.; Allegretto, E. A., Novel nonsecosteroidal vitamin D mimics exert VDR-modulating activities with less calcium mobilization than 1,25-dihydroxyvitamin D_3. *Chemistry & biology* **1999,** *6* (5), 265-275.

73.   Kakuda, S.; Okada, K.; Eguchi, H.; Takenouchi, K.; Hakamata, W.; Kurihara, M.; Takimoto-Kamimura, M., Structure of the ligand-binding domain of rat VDR in complex with the nonsecosteroidal vitamin D_3 analogue YR301. *Acta Crystallographica Section F: Structural Biology and Crystallization Communications* **2008,** *64* (11), 970-973.

74.   Hakamata, W.; Sato, Y.; Okuda, H.; Honzawa, S.; Saito, N.; Kishimoto, S.; Yamashita, A.; Sugiura, T.; Kittaka, A.; Kurihara, M., (2S,2'R)-analogue of LG190178 is a major active isomer. *Bioorganic & medicinal chemistry letters* **2008,** *18* (1), 120-123.

75.   Miura, D.; Manabe, K.; Ozono, K.; Saito, M.; Gao, Q.; Norman, A. W.; Ishizuka, S., Antagonistic action of novel 1α,25-dihydroxyvitamin D_3-26,23-lactone analogs on differentiation of human leukemia cells (HL-60) induced by 1α,25-dihydroxyvitamin D_3. *Journal of Biological Chemistry* **1999,** *274* (23), 16392-16399.

76.   Ishizuka, S.; Yamaguchi, H.; Yamada, S.; Nakayama, K.; Takayama, H., Stereochemistry of 25-hydroxyvitamin D_3—26,23-lactone and 1α,25—dihydroxyvitamin D_3—26,23-lactone in rat serum. *FEBS letters* **1981,** *134* (2), 207-211.

77.   Kakuda, S.; Ishizuka, S.; Eguchi, H.; Mizwicki, M. T.; Norman, A. W.; Takimoto-Kamimura, M., Structural basis of the histidine-mediated vitamin D receptor agonistic and antagonistic mechanisms of (23S)-25-dehydro-1α-hydroxyvitamin D_3-26,23-lactone. *Acta Crystallographica Section D: Biological Crystallography* **2010,** *66* (8), 918-926.

78.   Herdick, M.; Steinmeyer, A.; Carlberg, C., Carboxylic ester antagonists of 1α,25-dihydroxyvitamin D_3 show cell-specific actions. *Chemistry & biology* **2000,** *7* (11), 885-894.

79.   Bury, Y.; Steinmeyer, A.; Carlberg, C., Structure activity relationship of carboxylic ester antagonists of the vitamin D_3 receptor. *Molecular pharmacology* **2000,** *58* (5), 1067-1074.

Chapter Two: Design of an intrinsically fluorescent VDR ligand

2.1   Fluorescence detection in biological systems

Many creative approaches for analyzing receptor-ligand interactions have furthered our

knowledge about the complexity of intertwined cellular processes. Assessment of receptor

function is often completed through indirect measurements or extraction assays, which leaves

room for ambiguity in understanding the complete function of the receptor in its natural

environment.[1] Direct measurement assays that utilize fluorescence imaging could uncover

information that is currently missed with existing imaging techniques. Fluorescence signaling

has the ability to produce strong signals at low concentrations; therefore, compound activation

can be exploited over compound accumulation.[2] Furthermore, fluorescence-based assays can

be a fast, simple, and highly sensitive way to analyze biological targets in a nondestructive

manner.[3] As a result, this noninvasive method of imaging is being widely used for detecting

both protein-protein and ligand-protein pharmaceutical targets.[4] A distinct shift in the

fluorescent properties of a chemical probe upon binding or interacting with a biological target

permits real-time observations to occur both *in vitro* and *in vivo*.[5] Therefore, rational design of

small-molecule fluorescent probes have the potential to directly monitor the activity of specific

protein targets in living cells.[6] Visualization of complex processes by fluorescence may be the

answer to revealing new avenues for future pharmaceutical discovery and development.

2.2   Intrinsically fluorescent small-molecule probes

Various methods exist that utilize fluorescence to monitor molecular movement and observe

target distribution, including labeling small-molecule ligands, tagging protein targets, and

reaction-based fluorophore activation.[7-8] While each of these approaches to biological imaging

possesses benefits and limitations in their applications, we are particularly interested in the use

of small-molecule fluorescence to develop a novel and efficient *in vitro* assay for the VDR-LBP.

Fluorophores with long emission wavelengths are available for the extrinsic labeling of small-

molecules, such as BODIPY-labeled calcitriol.[9-10] Emission wavelengths in the visible light-range

allow background autofluorescence to be avoided, simplifying imaging and removing the need

for specialized equipment.[11] Extrinsic labels often result in large attached fluorophores that are

the same size or even larger than the ligand itself though. The presence of these extrinsic labels

may dramatically impact the physical and chemical properties of the cellular environment being

monitored, affecting the interpretation of monitored events.[12]
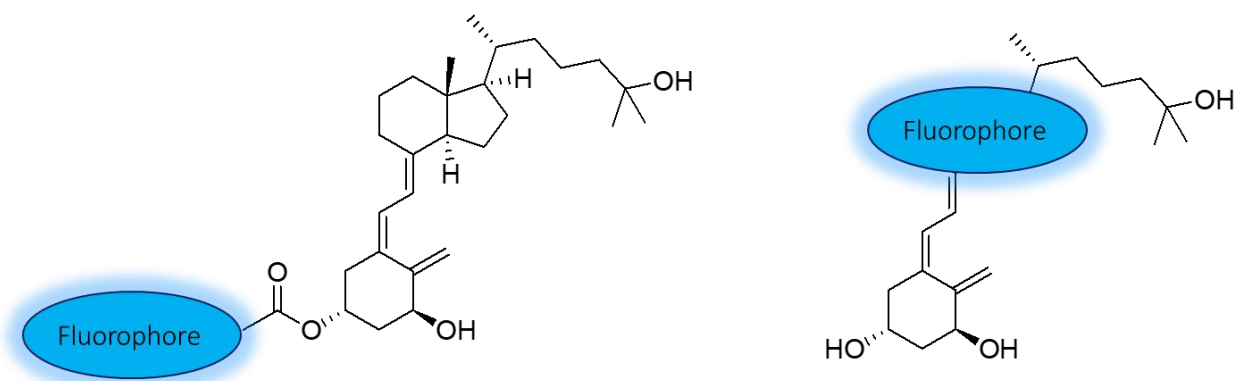
Figure 15. Extrinsic fluorescence from fluorophore-labeled calcitriol (left) and intrinsic fluorescence from fluorophore-incorporated calcitriol (right).

Direct incorporation of a fluorophore or conjugated π-system into the ligand design creates an

inherently photo-excitable compound capable of cellular mapping, while minimizing

disturbances to the natural cellular process.[13] Designing a ligand to be intrinsically fluorescent

provides a more accurate representation of the traditional biological process relative to an

extrinsically-tagged ligand. (Figure 15)

A majority of biological fluorophores were discovered empirically, but novel approaches to

develop fluorophores for targeted purposes are increasingly common. A series of studies during

the 1980s led by John Katzenellenbogen sought to make use of a fluorescent estrogen ligand

that was suitable for visualizing nuclear ERs.[14-18] Extrinsically-tagged ER ligands were generally

reported as having low ER affinity with high non-specific binding. Therefore, the development

of an intrinsically fluorescent ligands began in the 1990s.[19] A major challenge faced while

designing an intrinsically fluorescent ligand was maintaining sufficient fluorescence for cellular

visualization while ensuring a high affinity for the ER was maintained. Hwang, et al. began

developing a series of substituted 5,6,11,12-tetrahydrochrysenes (THCs) in an attempt to fulfill

both spectral and binding requirements.[19] In particular, a 5,11-diethyl-substituted
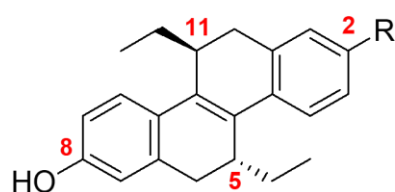
Figure 16. Intrinsically fluorescent ER ligand with a THC scaffold. Substituted positions numbered in red.

tetrahydrochrysene (THC) scaffold displayed high ER affinity, with the 2,8-diol analog surpassing the estradiol affinity for ER.[20] (Figure 16) While the 2,8-diol had a maximum emission wavelength of only 382 nm in ethanol, placing an electron-withdrawing group in the 2-position considerably improved the

spectral properties. For example, the electron donor-acceptor system created by substituting

the 2-hydroxyl functionality for a 2-acetyl shifted the maximum emission wavelength to 525 nm

in ethanol. The 2-acetyl analog also maintained 40% affinity for ER relative to estradiol. These

THC compounds are reportedly the first fluorescent ligands where fluorescence from a

receptor-bound ligand can be observed due to their sensitivity to solvent polarity.[20]

More recently, Yang, et al. synthesized coumarin-based analogs

as fluorescent probes for the ER.[4] One compound (3e) (Figure

17) was reported to display ERα antagonist activity in a

luciferase-reporter assay with an IC_{50} value of 12 nM.
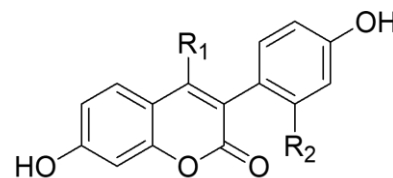
Additionally, 3e was described to be equipotent to 4-

hydroxytamoxifen in reducing hormone-dependent cancer cell

3c: R_1 = Me, R_2 = Me
3e: R_1 = Et, R_2 = F

Figure 17. Intrinsically fluorescent ER ligand with a coumarin scaffold.

proliferation in MCF-7 cells. The maximum emission wavelength of 3e was 406 nm in methanol,

which shifted to 457 nm in an aqueous buffer solution. Compound 3e was observed in real-time

to cross the cell membrane and localize in ER-(+) MCF-7 cells. Another derivative, compound 3c,

exhibited ERβ agonist activity in a luciferase-reporter assay with an EC_{50} value of 11 nM, though

the spectral data for 3c was not reported nor was it evaluated *in vitro*. Nonetheless, coumarin

fluorophores have promising potential as ligand scaffolds for NR imaging and as therapeutic

treatments.

Coumarin-based fluorescent ligands have been synthesized for GPCRs as well. De la Fuente

Revenga, et al. substituted the indole present in the natural melatonin neurohormone for a
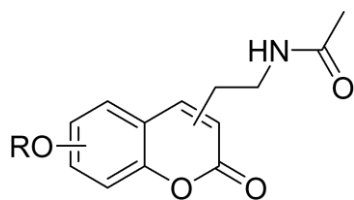
Figure 18. Intrinsically fluorescent MT ligand with a coumarin scaffold.

coumarin fluorophore.[21] (Figure 18) Coumarin analog (3), having

the amide linkage at position 4 and a methoxy functional group at

position 6, had the highest affinity for both melatonin receptors,

MT_1 and MT_2. When competing with 2-[^{125}I]-iodomelatonin,

compound 3 had a K_i value of 13 nM for MT_1 and a K_i value of 3.4

nM for MT_2. Additionally, compound 3 was observed to be a potent agonist with an EC_{50} value

of 117.8 nM in *Xenopus laevis* melanophores. Though no cellular imaging experiments were

described, a maximum emission wavelength of 435 nm in phosphate buffer for compound 3

was reported.

Another approach toward developing a fluorescing melatonin neurohormone was fusing a

BODIPY fluorophore with the natural melatonin scaffold.[22] Thireau, et al. synthesized four

indole-based BODIPY ligands (Figure 19) and reported the maximum emission wavelength

ranging from 493-616 nm in DMSO. All four ligands had good affinity for the MT_1 and MT_2

receptors in the nanomolar range when in competition with 2-[^{125}I]-iodomelatonin as well.

Compound I displayed the highest affinity for both MT_1 and MT_2, with K_i values of 32 nM and 10

nM, respectively. Compound II was more selective toward MT_2, while compound III had a

higher selectivity for MT_1 during the binding assay. Melatonin receptors have a very low level of

expression despite being linked to a number of biological processes. Thus, BODIPY fluorophores

may also provide promising scaffolds for intrinsically fluorescent ligands.

I: R_1 = Me, R_2 = H, R_3 = Me
II: R_1 = Me, R_2 = Et, R_3 = Me

III

IV

Figure 19. Fluorescent MT receptor ligands.
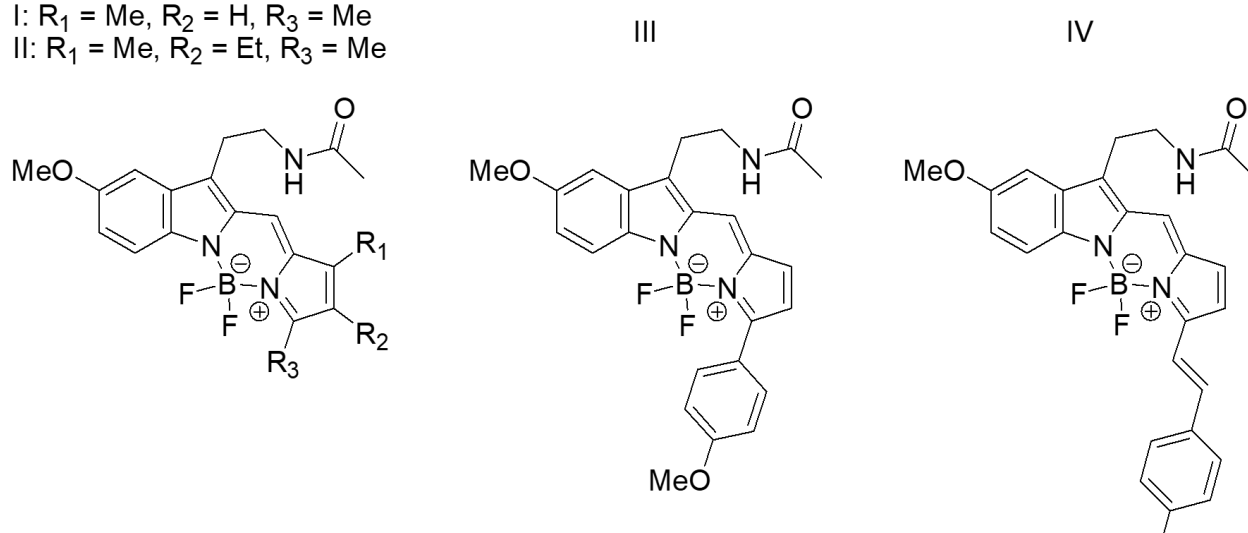
While a number of intrinsically fluorescent ligands have been developed and continue to be explored for their imaging properties, an intrinsically fluorescent ligand comparable to the ones described above does not currently exist for VDR.

2.3   Rational design of intrinsically fluorescent VDR ligands

A coumarin scaffold is an appealing fluorophore for developing an intrinsically fluorescent ligand due to its small molecular weight, biocompatibility, sensitivity to polarity changes, and strong yet stable fluorescence emission.[5, 23] Coumarins are among the oldest and most easily synthesized fluorophores that are commonly used for both *in vitro* and *in vivo* imaging and diagnostics.[24-25]
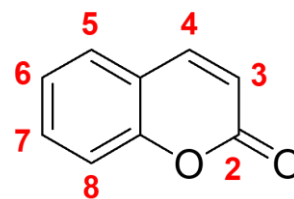
Figure 20. Chemical structure of coumarin with numbering (red).

In fact, the commercially available Alexa 350 and Alexa 430 dyes are based on a coumarin scaffold.[26] Structurally consisting of a fused α-pyrone and benzene ring, the core coumarin structure contains a cyclic ester functionality and a rigid 3,4-alkene locked in the *cis*-conformation. (Figure 20) While unsubstituted coumarins display little to no fluorescence, suitable emission in the visible light range can arise from properly substituting coumarins to create a push-pull effect though the structure.[27-28] Strong fluorescence emission and good photostability is also largely attributed to the rigidity of the coumarin structure.[23]

2.3.1 Design of the series A scaffold

Maintaining a high affinity for the VDR-LBP is central to our intrinsically fluorescent ligand design. Therefore, the initial compound design incorporating a coumarin fluorophore was based off the secosteroidal structure of calcitriol. As mentioned in section 1.3, calcitriol is the vitamin D metabolite with the highest affinity for VDR. It was hypothesized that mirroring the structure of calcitriol would allow a synthetic analog to retain good affinity for VDR. Calcitriol contains a fused two-ring structure (C and D rings), as does the coumarin structure. Thus, we substituted the C and D rings in calcitriol for the unsaturated coumarin fluorophore. (Figure 21)
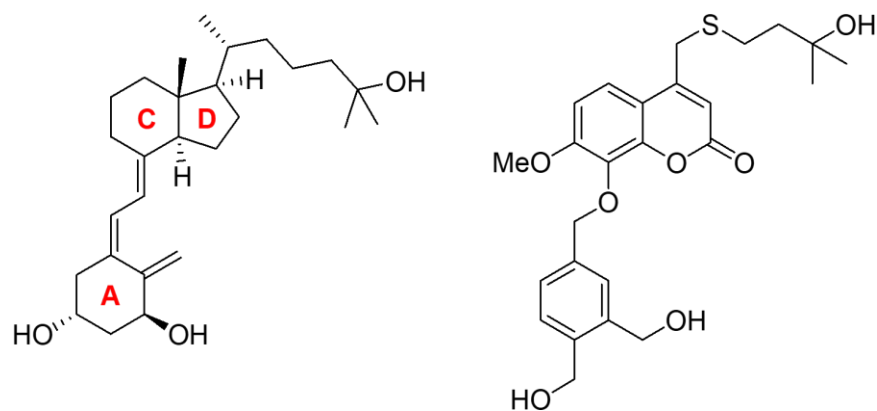
Figure 21. Chemical structure of calcitriol with ring labels in red (left)
and the initial synthetic ligand, TM-II-21 (right).

The tertiary alcohol was planned as an attachment at position 4 with a thioether linkage for ease of synthesis. Additionally, a 1,2-benzenedimethanol source was used to replace the A-ring in calcitriol. This particular diol source has been used in non-steroidal synthetic VDR agonists[29], and thus is capable of making appropriate contacts within the VDR-LBP for receptor activation. Although calcitriol naturally contains a diene that connects the A and C rings, the unsaturation inherent to the coumarin structure prohibits an alkene attachment at position 8 that would mimic the C7=C8 bond in calcitriol. An ether linkage was incorporated into the compound

29

design for connecting the pseudo 'A' and 'C' rings in our synthetic ligand. Furthermore, a

methoxy substituent is present in position 7 to promote suitable emission properties for

cellular imaging. Molecular modeling of this initial compound (TM-II-21) in the calcitriol-VDR

crystal structure (PDB: 1DB1) displayed that the synthetic analog was able to orient similarly to

the natural ligand following induced-fit refinement. (Figure 22)
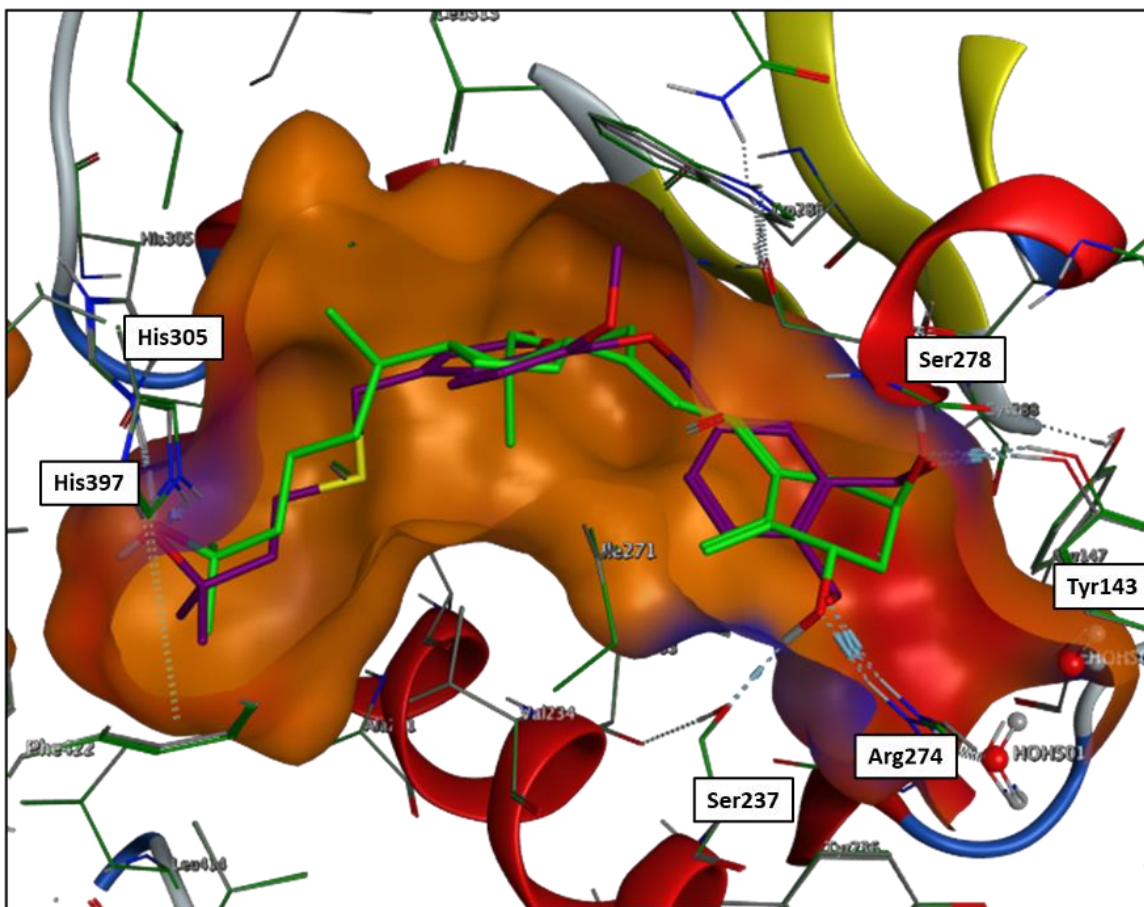
Figure 22. Molecular modeling of TM-II-21 (purple) in the calcitriol (green) crystal structure.
[PDB 1DB1] The displayed pose made hydrogen bonding contacts with His305, His397, Tyr143,
and Arg274.

2.3.2 Design of the series B scaffold

The series B scaffold design continued to utilize a 4,7,8-substituted coumarin as our

fluorophore source, maintaining the methoxy substituent in position 7. Relative to the series A

scaffold, however, the orientation of the coumarin was flipped to attach the tertiary alcohol in

position 8 and the diol source in position 4. To streamline the compound synthesis (further

discussed in chapter 3), a thioglycerol substituent was utilized as the diol source instead of the

1,2-benezenedimethanol that was used in the series A scaffold. A glycerol moiety is present in

the non-secosteroidal VDR agonist, LG190178, and thus is capable of maintaining necessary

hydrogen bonds with polar residues near the VDR-LBP opening. The shorter length of the thioglycerol substituent relative to the 1,2-benezenedimethanol moiety required a lengthened alkyl chain for the tertiary alcohol to reach the His305 and His397 residues deep in the VDR-LBP. (Figure 23)
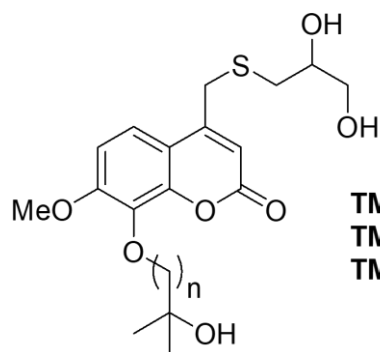
TM-III-20: n = 3
TM-II-72: n = 4
TM-III-31: n = 5

Figure 23. Chemical structure of the series B scaffold.

One promising conformation of TM-II-72 in the YR301-VDR crystal structure (PDB: 2ZFX)

displayed potential π-stacking interactions between C5=C6 on the coumarin and Trp282.

Furthermore, a water molecule was able to create a hydrogen-bonding network between

Tyr143, Ser274 and a hydroxyl on the thioglycerol substituent, while the thioether sulfur

maintained a hydrogen bond with Cys284. (Figure 24)
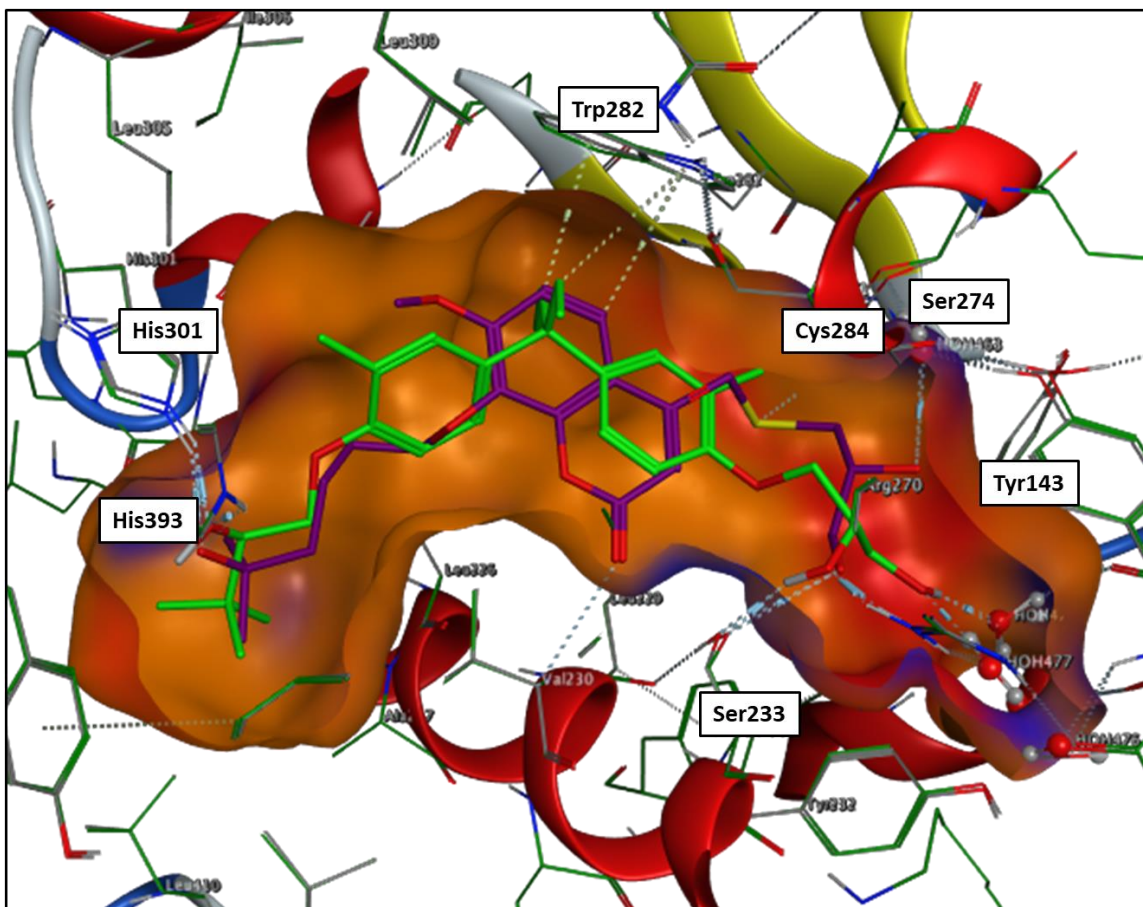
Figure 24. Molecular modeling of TM-II-72 (purple) in the YR301 (green) crystal structure. [PDB 2ZFX] The displayed pose made hydrogen bonding contacts with His301, His393, Ser233, Tyr143, Ser274, and Cys284.

2.3.3 Design of the series C scaffold

Concurrent with the design of the series B scaffold, a series C

scaffold was conceived as a potential intrinsically fluorescent

ligand for VDR. The series C scaffold utilized a 4,7-substituted

coumarin where a thioglycerol substituent was maintained in

position 4 and an ether linkage to the tertiary alcohol source

was located at position 7. (Figure 25) The 4,7-substitution gives
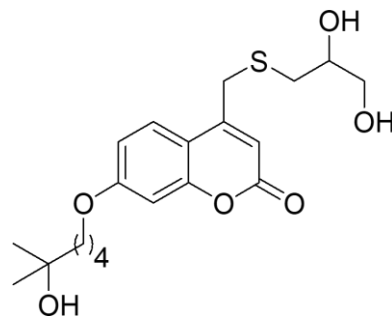
Figure 25. Chemical structure of the series B scaffold (TM-II-88).

the compound a natural 'bend' when in an extended conformation, similar to the active

conformation known VDR agonists have in the LBP.

While maintaining hydrogen bonding contacts with both His301, His393, and Ser233 in the

YR301-VDR crystal structure, TM-II-88 was also able to create a hydrogen bonding network with

a water molecule, Tyr143, and Ser274. Furthermore, the thioether sulfur made hydrogen

bonding contact with Ser271 while the coumarin carbonyl had a hydrogen bonding interaction

with Cys284. (Figure 26)
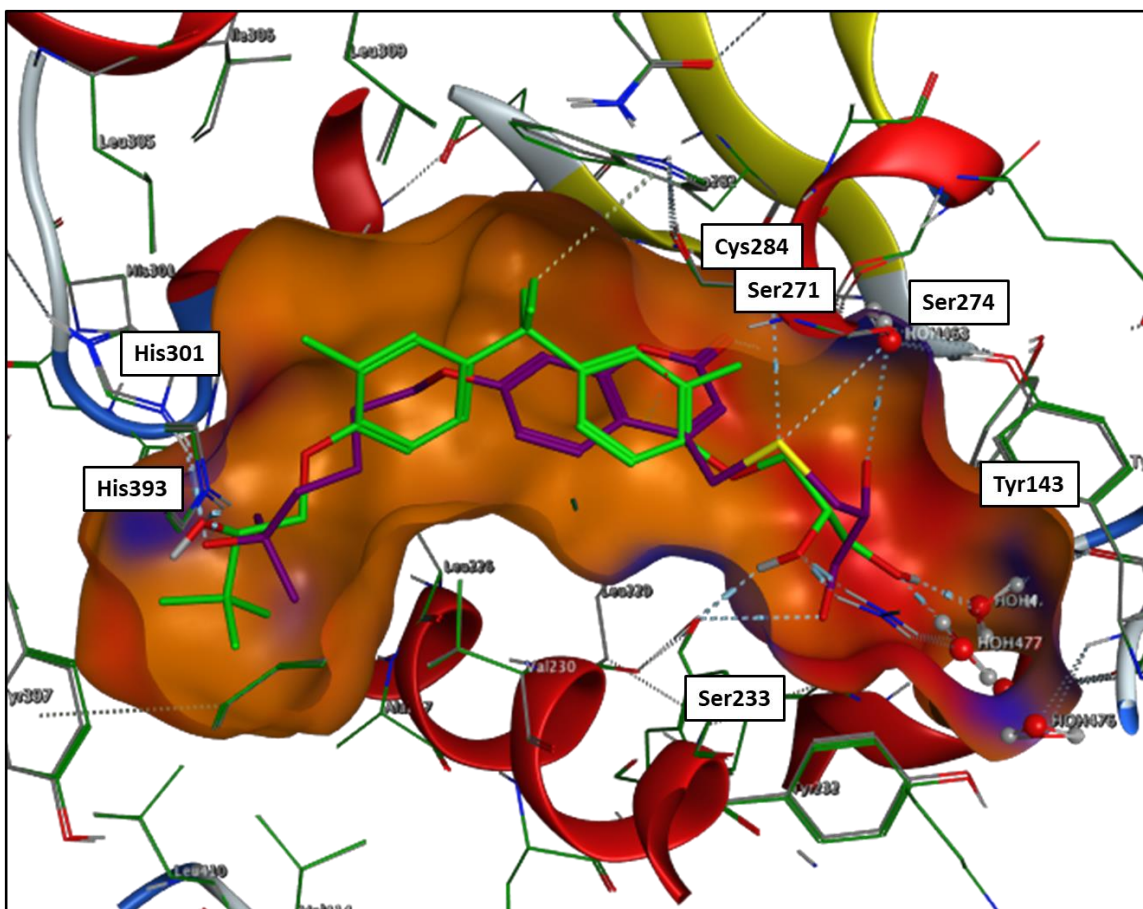
Figure 26. Molecular modeling of TM-II-88 (purple) in the YR301 (green) crystal structure. [PDB 2ZFX] The displayed pose made hydrogen bonding contacts with His301, His393, Ser233, Tyr143, Ser274, Ser271, and Cys284.

2.3.4 Design of the series D scaffold

Design of the series D scaffold intended for the coumarin fluorophore to be kept near the

opening of the VDR-LBP. Since the VDR-LBP is primarily lined with hydrophobic residues, a long

alkyl chain was attached at position 7 to reach the two histidine residues while a substituent

capable of hydrogen bonding was located in position 3. (Figure 27) Simple, deconstructed

calcitriol analogs that have highly flexible structures have shown to induce moderate VDR

activity.[30-32] Furthermore, the 3,7-substitution pattern in coumarins can

have excellent emission properties upon creating a push-pull system

through the fluorophore. Therefore, the first conceived series D
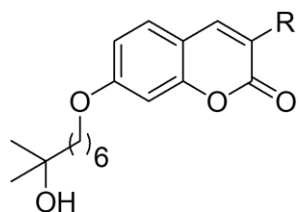
Figure 27. General chemical structure of the series D scaffold.

compound (TM-III-91) contained a carboxylic acid substituent in

position 3.

An intriguing pose displayed by TM-III-91 in the calcitriol-VDR crystal structure showed an

interaction between Arg274 and the carboxylate oxygen, while the carbonyl oxygen maintained

a hydrogen bonding interaction with Tyr143. The cyclic carbonyl in the coumarin fluorophore

also formed a hydrogen bond with Cys288. (Figure 28)
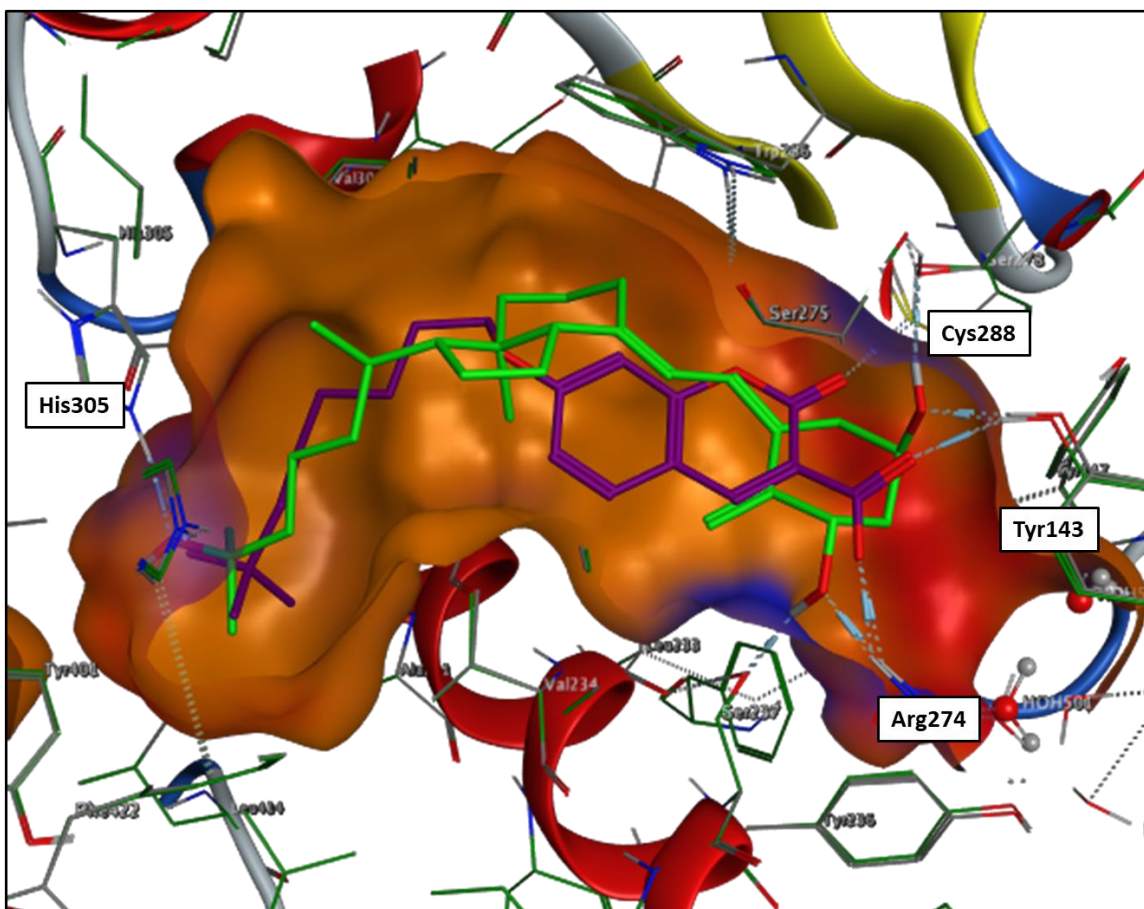
Figure 28. Molecular modeling of TM-III-91 (purple) in the calcitriol (green) crystal structure. [PDB 1DB1] The displayed pose made hydrogen bonding contacts with His305, Tyr143, Arg274, and Cys288.

A secondary alcohol in position 3 (TM-IV-18) resulted in a hydrogen bond contact between the hydroxy and Tyr143 while the cyclic carbonyl oxygen interacted with Arg274, indicating that a flipped orientation of the fluorophore can still make contacts with polar residues near the LBP opening. (Figure 29)
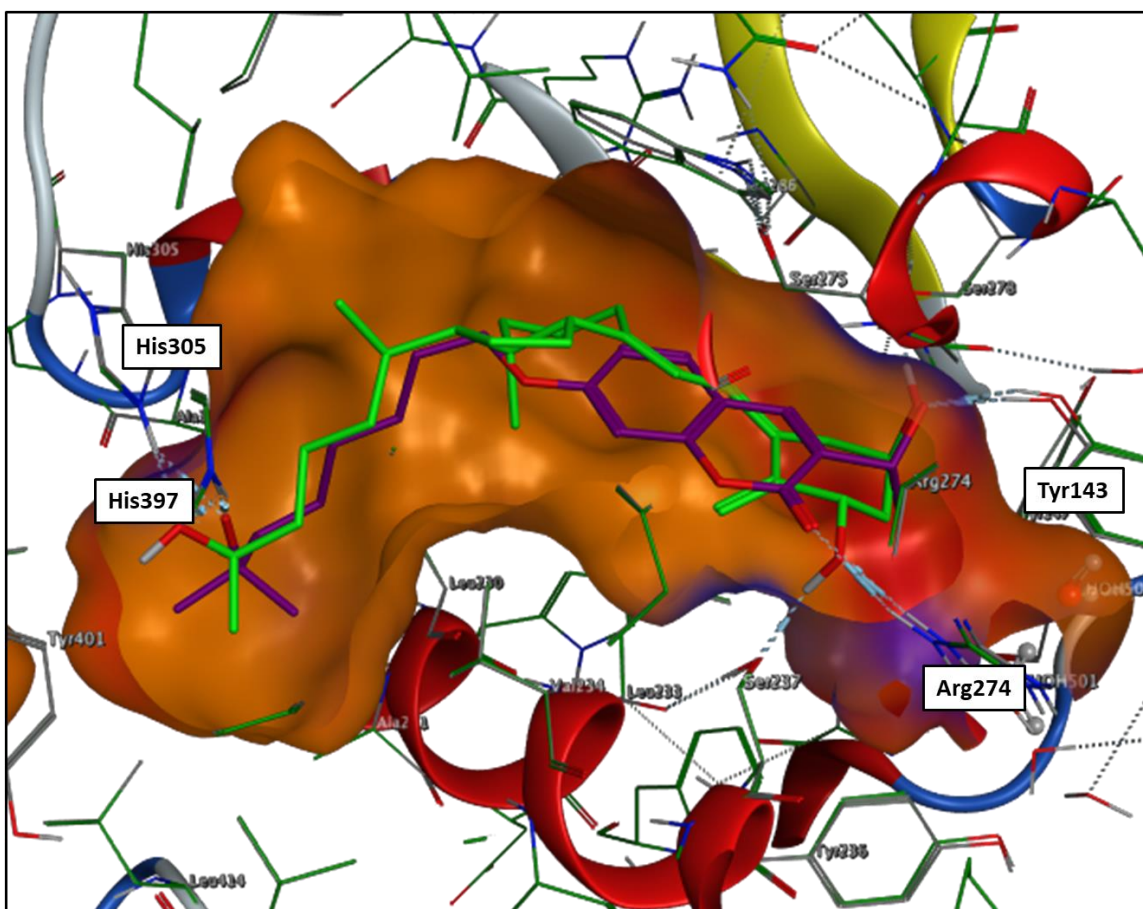
Figure 29. Molecular modeling of TM-IV-18 (purple) in the calcitriol (green) crystal structure. [PDB 1DB1] The displayed pose made hydrogen bonding contacts with His305, His397, Tyr143, and Arg274.

In the YR301-VDR crystal structure, a nitrile substituent in position 3 (TM-IV-16) was able to create a hydrogen bond contact to Arg270 through a water molecule, while the cyclic carbonyl also interacted with Arg270. (Figure 30) Therefore, other electron-withdrawing groups that can contribute to the push-pull effect through the fluorophore may be tolerated within the VDR-LBP.
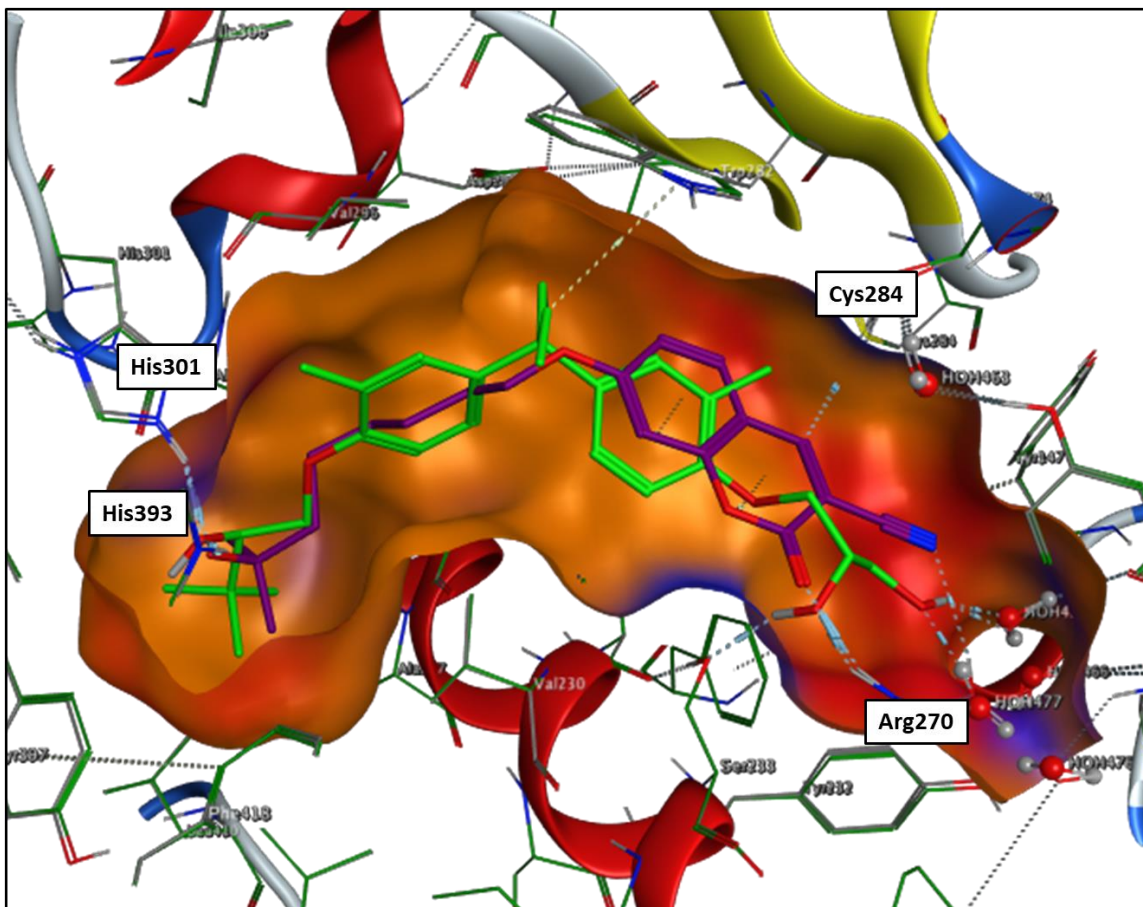
Figure 30. Molecular modeling of TM-IV-16 (purple) in the YR301 (green) crystal structure. [PDB 2ZFX] The displayed pose made hydrogen bonding contacts with His301, His393, and Arg270.

2.3.5 Cysteine click reaction

Modeling of the series D compounds often highlighted an interaction between Cys288 and the

C4 position on the coumarin fluorophore. (Figure 31) Coumarins inherently contain a cyclic α,β-

unsaturated ester, and many of our modeled ligands contained substituents in position 3 that

also presented α,β-unsaturation with the C3=C4 alkene. If properly aligned, a Michael addition

could hypothetically occur at the C4 position.

In 1987, researchers at the University of Leiden described a conjugate addition between

hydrogen sulfide and a divinyl ketone, with one of the alkenes being the C3=C4 alkene of the

coumarin ring system.[33] Analysis of incomplete reaction mixtures by ^{1}H-NMR revealed that the

first addition occurs at the C4 position when at reflux in an ethanol-dioxane mixture.

Interestingly, under the reported reaction conditions, spontaneous dehydrogenation occurred

following the conjugate addition to retain the unsaturation between positions 3 and 4.

Conversely, Tamam, et al. reported C3-C4 saturation following the Michael addition between

ethyl thioglycolate and 2-cyano-3-(coumarin-3-yl) crotononitrile.[34] Thus, at elevated

temperatures, thiolate conjugate additions are possible at the C4 position. Reacting β-mercaptoethanol and 7-hydroxy-2-oxo-*2H*-chromene-3-carboxylic acid ethyl ester in a methanol-water mixture while in the presence of lithium hydroxide did not result in a conjugate addition for us at ambient temperatures, though.
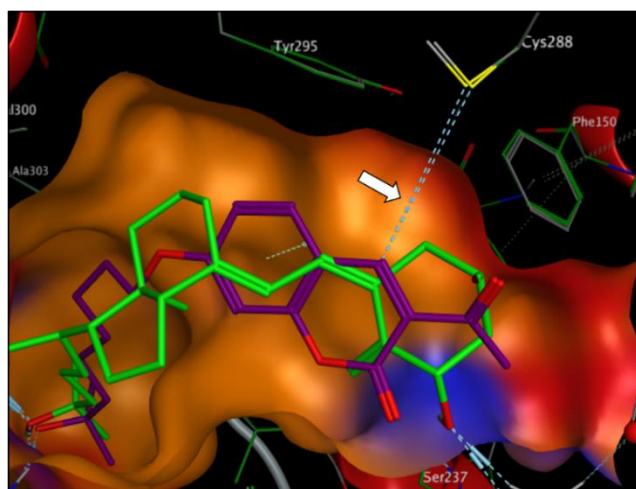
Figure 31. Cys288 interaction with the C4 position of TM-IV-6 in the calcitriol-VDR crystal structure. [PDB: 1DB1]

References

1.   Dubach, J.; Vinegoni, C.; Mazitschek, R.; Feruglio, P. F.; Cameron, L.; Weissleder, R., In vivo imaging of specific drug–target binding at subcellular resolution. *Nature communications* **2014,** *5* (1), 1-9.

2.   Terai, T.; Nagano, T., Small-molecule fluorophores and fluorescent probes for bioimaging. *Pflügers Archiv-European Journal of Physiology* **2013,** *465* (3), 347-359.

3.   Fang, X.; Zheng, Y.; Duan, Y.; Liu, Y.; Zhong, W., Recent advances in design of fluorescence-based assays for high-throughput screening. *Analytical chemistry* **2018,** *91* (1), 482-504.

4.   Yang, L.; Hu, Z.; Luo, J.; Tang, C.; Zhang, S.; Ning, W.; Dong, C.; Huang, J.; Liu, X.; Zhou, H.-B., Dual functional small molecule fluorescent probes for image-guided estrogen receptor-specific targeting coupled potent antiproliferative potency for breast cancer therapy. *Bioorganic & medicinal chemistry* **2017,** *25* (13), 3531-3539.

5.   Signore, G.; Nifosi, R.; Albertazzi, L.; Storti, B.; Bizzarri, R., Polarity-sensitive coumarins tailored to live cell imaging. *Journal of the American Chemical Society* **2010,** *132* (4), 1276-1288.

6.   Akchurin, I. O.; Yakhutina, A. I.; Bochkov, A. Y.; Solovjova, N. P.; Traven, V. F., Synthesis of novel push-pull fluorescent dyes–7-(diethylamino) furo [3, 2-c] coumarin and 7-(diethylamino) thieno [3, 2-c] coumarin derivatives. *Heterocyclic Communications* **2018,** *24* (2), 85-91.

7.   Johnson, I., Fluorescent probes for living cells. *The Histochemical Journal* **1998,** *30* (3), 123-140.

8.   Chan, J.; Dodani, S. C.; Chang, C. J., Reaction-based small-molecule fluorescent probes for chemoselective bioimaging. *Nature chemistry* **2012,** *4* (12), 973-984.

9.   Barsony, J.; Renyi, I.; Mckoy, W.; Kang, H. C.; Haugland, R. P.; Smith, C. L., Development of a biologically active fluorescent-labeled calcitriol and its use to study hormone binding to the vitamin D receptor. *Analytical biochemistry* **1995,** *229* (1), 68-79.

10.   Barsony, J.; Renyi, I.; McKoy, W., Subcellular distribution of normal and mutant vitamin D receptors in living cells: Studies with a novel fluorescent ligand. *Journal of Biological Chemistry* **1997,** *272* (9), 5774-5782.

11.   Modzel, M.; Solanko, K.; Szomek, M.; Hansen, S.; Dupont, A.; Nåbo, L.; Kongsted, J.; Wüstner, D., Live-cell imaging of new polyene sterols for improved analysis of intracellular cholesterol transport. *Journal of microscopy* **2018,** *271* (1), 36-48.

12.   Fechner, P.; Bleher, O.; Ewald, M.; Freudenberger, K.; Furin, D.; Hilbig, U.; Kolarov, F.; Krieg, K.; Leidner, L.; Markovic, G., Size does matter! Label-free detection of small molecule–protein interaction. *Analytical and bioanalytical chemistry* **2014,** *406* (17), 4033-4051.

13.   Garcia, L.; Lazzaretti, M.; Diguet, A.; Mussi, F.; Bisceglie, F.; Xie, J.; Pelosi, G.; Buschini, A.; Baigl, D.; Policar, C., An intrinsically fluorescent glycoligand for direct imaging of ligand trafficking in artificial and living cell systems. *New Journal of Chemistry* **2013,** *37* (10), 3030-3034.

14.   Martin, P. M.; Magdelenat, H. P.; Benyahia, B.; Rigaud, O.; Katzenellenbogen, J. A., New approach for visualizing estrogen receptors in target cells using inherently fluorescent ligands and image intensification. *Cancer research* **1983,** *43* (10), 4956-4965.

15.	Katzenellenbogen, J. A.; Carlson, K. E.; Bindal, R. D.; Neeley, R. L.; Martin, P. M.; Magdelenat, H. P., Fluorescence-based assay of estrogen receptor using 12-oxo-9(11)-dehydroestradiol-17β. *Analytical biochemistry* **1986,** *159* (2), 336-348.

16.	Fevig, T. L.; Lloyd, J. E.; Zablocki, J. A.; Katzenellenbogen, J. A., Preparation, receptor binding, and fluorescence properties of hexestrol-fluorophore conjugates: evaluation of site of attachment, fluorophore structure, and fluorophore-ligand spacing. *Journal of medicinal chemistry* **1987,** *30* (1), 156-165.

17.	Anstead, G. M.; Altenbach, R. J.; Wilson, S. R.; Katzenellenbogen, J. A., 2,3-Diarylindenes and 2,3-diarylindenones: synthesis, molecular structure, photochemistry, estrogen receptor binding affinity, and comparisons with related triarylethylenes. *Journal of medicinal chemistry* **1988,** *31* (7), 1316-1326.

18.	Carlson, K. E.; Coppey, M.; Magdelenat, H.; Katzenellenbogen, J. A., Receptor binding of NBD-labeled fluorescent estrogens and progestins in whole cells and cell-free preparations. *Journal of steroid biochemistry* **1989,** *32* (3), 345-355.

19.	Hwang, K. J.; O'Neil, J. P.; Katzenellenbogen, J. A., 5,6,11,12-Tetrahydrochrysenes: synthesis of rigid stilbene systems designed to be fluorescent ligands for the estrogen receptor. *The Journal of Organic Chemistry* **1992,** *57* (4), 1262-1271.

20.	Hwang, K. J.; Carlson, K. E.; Anstead, G. M.; Katzenellenbogen, J. A., Donor-acceptor tetrahydrochrysenes, inherently fluorescent, high-affinity ligands for the estrogen receptor: binding and fluorescence characteristics and fluorometric assay of receptor. *Biochemistry* **1992,** *31* (46), 11536-11545.

21.	de la Fuente Revenga, M.; Herrera-Arozamena, C.; Fernández-Sáez, N.; Barco, G.; García-Orue, I.; Sugden, D.; Rivara, S.; Rodríguez-Franco, M. I., New coumarin-based fluorescent melatonin ligands. Design, synthesis and pharmacological characterization. *European journal of medicinal chemistry* **2015,** *103*, 370-373.

22.	Thireau, J.; Marteaux, J.; Delagrange, P.; Lefoulon, F.; Dufourny, L.; Guillaumet, G.; Suzenet, F., Original design of fluorescent ligands by fusing BODIPY and melatonin neurohormone. *ACS medicinal chemistry letters* **2014,** *5* (2), 158-161.

23.	Cao, D.; Liu, Z.; Verwilst, P.; Koo, S.; Jangjili, P.; Kim, J. S.; Lin, W., Coumarin-based small-molecule fluorescent chemosensors. *Chemical reviews* **2019,** *119* (18), 10403-10519.

24.	Fu, Y.; Finney, N. S., Small-molecule fluorescent probes and their design. *RSC advances* **2018,** *8* (51), 29051-29061.

25.	Meimetis, L. G.; Carlson, J. C.; Giedt, R. J.; Kohler, R. H.; Weissleder, R., Ultrafluorogenic coumarin–tetrazine probes for real-time biological imaging. *Angewandte Chemie* **2014,** *126* (29), 7661-7664.

26.	Panchuk-Voloshina, N.; Haugland, R. P.; Bishop-Stewart, J.; Bhalgat, M. K.; Millard, P. J.; Mao, F.; Leung, W.-Y.; Haugland, R. P., Alexa dyes, a series of new fluorescent dyes that yield exceptionally bright, photostable conjugates. *Journal of Histochemistry & Cytochemistry* **1999,** *47* (9), 1179-1188.

27.	Li, H.; Cai, L.; Chen, Z., Coumarin-derived fluorescent chemosensors. *Advances in chemical sensors* **2012,** *1*, 121-150.

28.	Kim, J. H.; Sumranjit, J.; Kang, H. J.; Chung, S. J., Discovery of coumarin derivatives as fluorescence acceptors for intrinsic fluorescence resonance energy transfer of proteins. *Molecular BioSystems* **2014,** *10* (1), 30-33.

29.   Perakyla, M.; Malinen, M.; Herzig, K.-H.; Carlberg, C., Gene regulatory potential of nonsteroidal vitamin D receptor ligands. *Molecular endocrinology* **2005,** *19* (8), 2060-2073.

30.   Kutner, A.; Zhao, H.; Fitak, H.; Wilson, S., Synthesis of Retiferol RAD1 and RAD2, the Lead Representatives of a New Class of des-CD Analogs of Cholecalciferol. *Bioorganic Chemistry* **1995,** *23* (1), 22-32.

31.   Stayrook, K. R.; Carson, M. W.; Ma, Y. L.; Dodge, J. A., Non-secosteroidal ligands and modulators. In *Vitamin D*, Elsevier: 2011; pp 1497-1508.

32.   Fujii, S.; Masuno, H.; Taoda, Y.; Kano, A.; Wongmayura, A.; Nakabayashi, M.; Ito, N.; Shimizu, M.; Kawachi, E.; Hirano, T., Boron cluster-based development of potent nonsecosteroidal vitamin D receptor ligands: direct observation of hydrophobic interaction between protein surface and carborane. *Journal of the American Chemical Society* **2011,** *133* (51), 20933-20941.

33.   van den Goorbergh, J.; Van der Steeg, M.; van der Gen, A., Synthesis of new hetero-annulated coumarins: 2, 3-dihydro-4-oxothiapyrano [2, 3-c]-benzopyran-2-ones, 4-oxothiapyrano [2, 3-c]-1-benzopyran-2-ones and 2-oxo-3, 4-dihydrobenzopyrano [4, 3-b]-4-piperidones. *Synthesis* **1987,** *1987* (03), 314-317.

34.   Tamam, G.; Bakeer, H.; Abdel-Motelab, R.; Arafa, W., Synthesis and Some Reactions of Coumarin-3-yl Crotononitrile Derivatives. *Journal of the Chinese Chemical Society* **2005,** *52* (6), 1191-1199.

Chapter Three: Synthesis of novel VDR ligands

3.1　Series A scaffold

The synthetic route towards the initial ligand, TM-II-21, was achieved through the coupling of

three individual components: an aliphatic thiol bearing a protected tertiary alcohol (A), a tri-

substituted coumarin core (B), and a benzyl bromide moiety containing a protected diol

functionality (C). (Figure 1)
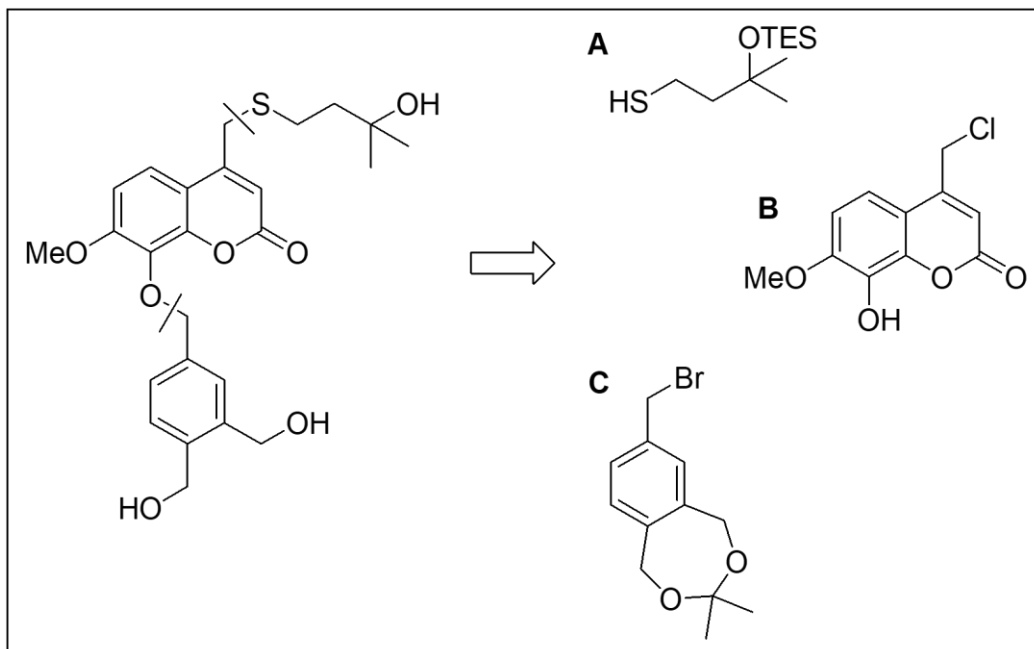
Figure 32. Retrosynthesis of the series A scaffold.

Compound A (Figure 32) was synthesized in three steps, beginning with a Michael addition

between potassium thioacetate and methyl vinyl ketone to form the initial thioester (1).

(Scheme 1) The Michael addition is a well-understood reaction in which a nucleophile acts on

the β-position of an α,β-unsaturated ketone. Following the conjugate addition, protonation allows for formation of the keto-enol tautomer. The ketone tautomer is generally favored over the enol due to the relative stability of the C=O double bond over the C=C double bond. Using the conditions described by Coster and De Voss[1], our reaction between potassium thioacetate and methyl vinyl ketone resulted in a 95% yield of compound 1. (Scheme 1)
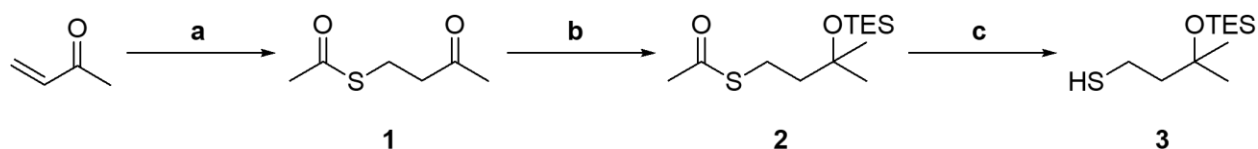
Scheme 1. Synthesis towards compound 3: a) KSAc, Py, AcOH, DCM; 0°C, 1 h; 25°C, 12 h; b) 1. MeMgBr, Et$_2$O; -78°C, 30 min; 0°C, 4 h; 2. TES-OTf, 2,6-lutidine; -78°C, 30 min; 25°C, 12 h; c) LiAlH$_4$, Et$_2$O; -78°C, 30 min; 25°C, 1.5 h.

A Grignard reaction between 1.5 equivalents of methyl magnesium bromide (MeMgBr) and compound 1 at -78 °C resulted in the formation of a tertiary alcohol functionality. The presence of the lone pair of sulfur makes the adjacent sp2 carbon less electrophilic than a ketone carbonyl carbon and is therefore less prone to nucleophilic attack by the Grignard reagent. The selective reactivity of MeMgBr with the ketone carbonyl over the thioester carbonyl in compound 1 was confirmed during this reaction. Following C-C bond formation, the alcohol oxygen atom is deprotonated as an alkoxide magnesium bromide salt until undergoing an acidic workup. Protection of the tertiary alcohol was necessary to prevent elimination of the alcohol in future synthetic steps; therefore, an *in situ* silyl protection of the newly formed alcohol was attempted to eliminate a separate synthetic step. Triethylsilyl group was chosen as the protecting group. Since the tertiary alcohol is more sterically hindered, a more reactive silyl triflate was used instead of the corresponding silyl chloride.[2-3] Additionally, a silyl group with minimal steric bulk was desired to ensure steric factors did not prevent O-Si bond formation

from occurring. Complete conversion from the ketone to the alcohol, and subsequently conversion of the alcohol to the silyl ether was observable by TLC (Figure 33). Purification of the silyl ether was difficult to achieve by column chromatography because a silyl
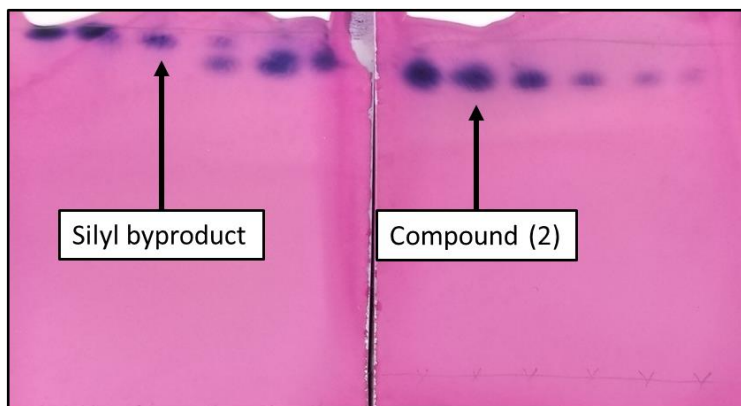
Figure 33. Fractions from compound 2 purification by column chromatography, using EtOAc/Hex (gradient to 5:95 EtOAc:Hex). TLC ran 5% EtOAc in Hex and is visualized using the *p*-anisaldehyde stain.

byproduct formed following the work-up exhibited a similar retention time. Purification by column chromatography was tedious and required multiple repetitions. Therefore, the crude material was routinely used in the following synthetic steps. Distillation of compound 2 was not attempted but may be worthwhile for future ease of purification.

The final step in Scheme 1 was deacylation of the thioester to produce the thiol. Lithium aluminum hydride (LiAlH$_4$) is a commonly used reducing agent in organic synthesis that is able to generate compound 3 (Scheme 1). The reaction begins with a nucleophilic hydride from LiAlH$_4$ attacking the electrophilic carbonyl carbon in compound 2. This prompts the π-electrons between the C=O to localize on the oxygen atom, forming a tetrahedral metal alkoxide complex intermediate. Reformation of the carbonyl cleaves the sulfur-carbon bond, and subsequent protonation during the work-up resulted in the desired compound in 94% yield.
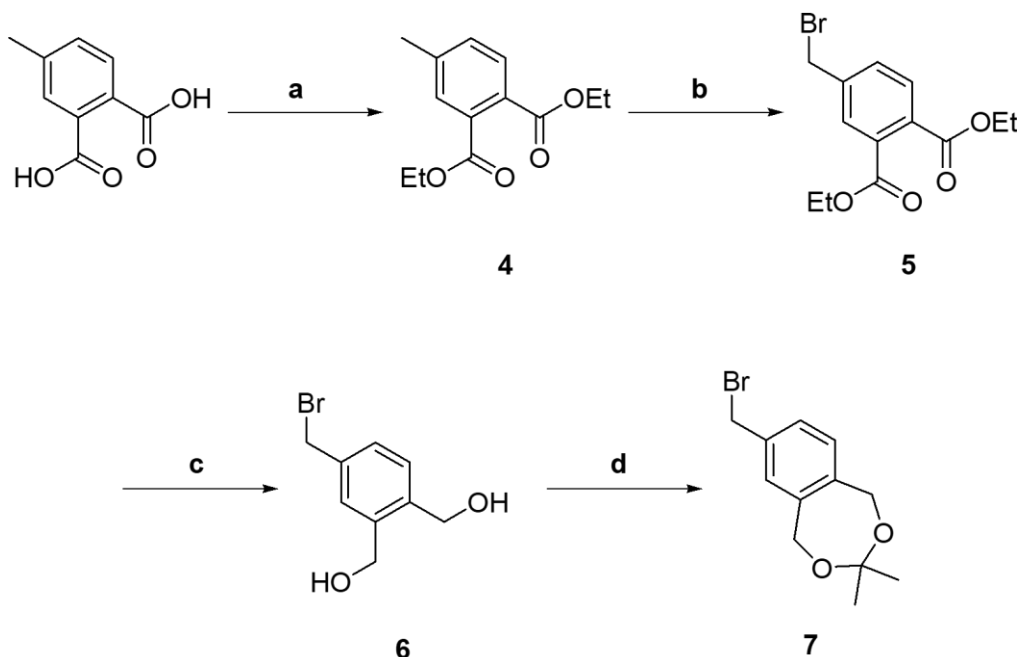
Scheme 2. Synthesis towards compound 7: a) H_2SO_4, EtOH; Reflux, 18 h; b) NBS, AIBN, CCl_4; Reflux, 8 h; c) DIBAL-H, DCM; -61°C, 10 h; d) PTSA, Acetone; 25°C, 2 h.

Compound C (Figure 32) was synthesized from commercially available 4-methylphthalic acid over four steps. The first step performed was a Fisher esterification with ethanol to yield compound 4 (Scheme 2). Sulfuric acid behaves as a catalyst by protonating the carbonyl oxygen and increasing the electrophilicity of the carbonyl carbon. Ethanol is then sufficiently nucleophilic to attack the carbonyl carbon, pushing the C=O π-electrons onto the oxygen atom. A proton transfer to the hydroxyl group forms a good-leaving hydronium ion. Therefore, water is formed as a byproduct of the reaction upon reformation of the carbonyl. An equilibrium exists between the acid and ester functional groups during the Fisher esterification. Utilizing an excess of alcohol solvent and removing water from the reaction are two methods employed to push the equilibrium towards the ester product. While a yield of 92% was able to be achieved when forming compound 4, the mono-esterified compound was a consistent byproduct in the reaction. Complete conversion to the diethyl ester was inconsistent; likely due to over-

protonation of the solvent when attempting to scale the reaction. An excess of sulfuric acid in the reaction begins to hinder progression of the reaction, as protonation of the solvent diminishes the nucleophilicity of the alcohol. Further optimization to the amount of acid catalyst employed during the reaction will likely improve the consistency and yield of compound 4 formation.

Bromination of the benzylic position on compound 4 provides a convenient means for coupling the final diol to the coumarin core, since benzyl halogens are relatively good leaving groups. The Wohl-Ziegler bromination was used prior to ester reduction to ensure bromination occurs solely on the 4-methyl group, as an additional two benzylic positions would have the potential to react following reduction. Upon radical initiation using azobisisobutyronitrile (AIBN), appearance of a burnt orange color indicated the presence of molecular bromine. (Figure 34) Compound 5 was able to be collected in 40% yield. (Scheme 2) A major impurity arising from the Wohl-Ziegler bromination is the dibrominated product. After monobromination occurs, two benzylic hydrogens are still present. Under these reaction conditions, the dibrominated product
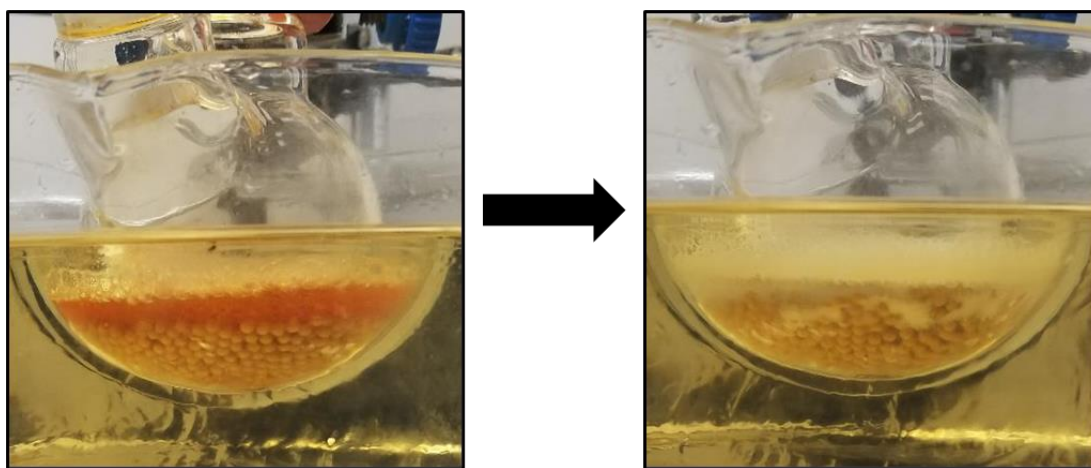
Figure 34. Radical initiation with AIBN. Reaction begins clear (not pictured), followed by formation of molecular bromine upon reaction initiation (left), and color disappearance within a few minutes (right).
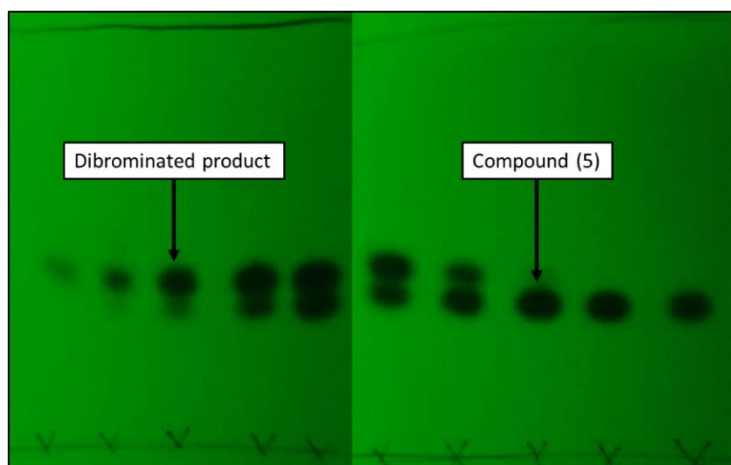
Figure 35. Fractions from compound 5 purification by column chromatography, using Et$_2$O/Hex (gradient to 30:70 Et$_2$O:Hex). TLC ran 20% Et$_2$O in Hex and is visualized under UV light (254 nm).

was able to form, even when using only one equivalent of NBS. The presence of the dibrominated product made the purification of compound 5 by column chromatography tedious, as the retention times between the monobrominated and dibrominated species maintained similarity during various solvent and gradient adjustments. (Figure 35)

In forming compound 6, the ester functional groups on compound 5 were reduced to primary alcohols using diisobutylaluminum hydride (DIBAL-H) (Scheme 2). DIBAL-H acts as an electrophilic reducing agent that reduces esters to either aldehydes or alcohols, dependent upon the reaction conditions and number of equivalents used. Therefore, we utilized an excess of DIBAL-H (8 equivalents) to ensure reduction of both ester functional groups to alcohols. Nucleophilic reducing agents, such as LiAlH$_4$, were unsuitable for our reaction since the nucleophilic hydride would be able to displace the newly-installed benzyl bromide.[4] Compound 6 was able to be formed under these reaction conditions; however, the process was difficult. Performing this reaction at -78°C took a minimum of 12 hours before full conversion was observed by TLC. It is necessary for the reaction to run below -70°C to cease reactivity at the aldehyde, but higher temperatures should be tolerated for alcohol formation. Performing this reaction at 0°C allowed for full conversion from compound 5 in two hours, but I was unable to

confirm the formation of compound 6 by NMR during this trial. In an attempt to decrease the reaction time while successfully forming the desired product, the reaction was performed at -61°C. After 10 hours at -61°C, full conversion from compound 5 was visible by TLC. Isolation of the diol was another challenge encountered. Large emulsions were present during the work-up, even after stirring the crude mixture in 1.0 M HCl for one hour prior to extraction. Additionally, a 1.0 M solution of Rochelle salt and 1.0 M solution of citric acid was utilized in an attempt to disrupt the aluminum complex, and brine washes were used to promote extraction of compound 6 in ethyl acetate. The large work-up emulsions are likely a major contributing factor to the low yields observed during this reaction. Increased stir times in an acidic aqueous solution following reaction quenching may be beneficial in efficient extraction of compound 6 into an organic solvent. Additionally, it has been reported that DIBAL-H was able to successfully reduce ester functional groups to the alcohol in the presence of a benzylic bromide at above-zero temperatures.[5] Insufficient isolation of compound 6 following DIBAL-H reduction at 0°C is suspected to play a role as to why identification by NMR was unsuccessful. Further optimization to this procedure should allow for increased yields of compound 6 to be obtained.

Protection of the diol using an acetonide ring was the final step in synthesizing compound C. (Figure 32) The cyclic ketal formation occurs between acetone and the benzene dimethanol portion of compound 6 in the presence of an acid catalyst, such as *p*-toluenesulfonic acid. Conversion to compound 7 was visible by TLC after two hours at 25°C. Following purification by column chromatography, compound 7 was able to be isolated in 73% yield.

Synthesis of compound B (Figure 32) can be completed in one step by following the Pechmann condensation reaction mechanism, one of the most well-known reactions for coumarin

synthesis.[6] From commercially available 3-methoxycatechol and 4-chloroethyl acetoacetate, compound 8 was synthesized in neat sulfuric acid in two hours (Scheme 3). Sulfuric acid catalyzes the transesterification of the ethyl ester on 4-chloroethyl acetoacetate with the phenol, as well as enolization 4-chloroethyl acetoacetate. A cascade of electron rearrangements, beginning with the lone pair of electrons on the phenolic oxygen, prompts a Michael addition to occur between a pair of π-electrons from aromatic ring and the β-position of the α,β-unsaturated carbonyl, resulting in the formation of a six-membered ring. Rearomatization and subsequent electron rearrangement forms the final coumarin while losing water as a byproduct. Precipitation of compound 8 was achieved by pouring the acidic reaction mixture over ice water. Subsequent filtration and recrystallization in ethanol allowed for large batches of compound 8 to be easily purified in high yield.

The coupling between compounds 7 and 8 was performed following the Williamson ether synthesis. Potassium carbonate was used to deprotonate the phenol on compound 8, which successively acted as a nucleophile in the SN2 substitution of benzylic bromide compound 7. The resulting compound 9 was synthesized in 37% yield (Scheme 3). Compound 3 was coupled with compound 9 through another SN2 reaction. Triethylamine was used to deprotonate the thiol 3, which then behaved as a nucleophile to substitute the benzyl chloride in position 4 on the coumarin scaffold. Compound 10 was synthesized in 76% yield (Scheme 3).
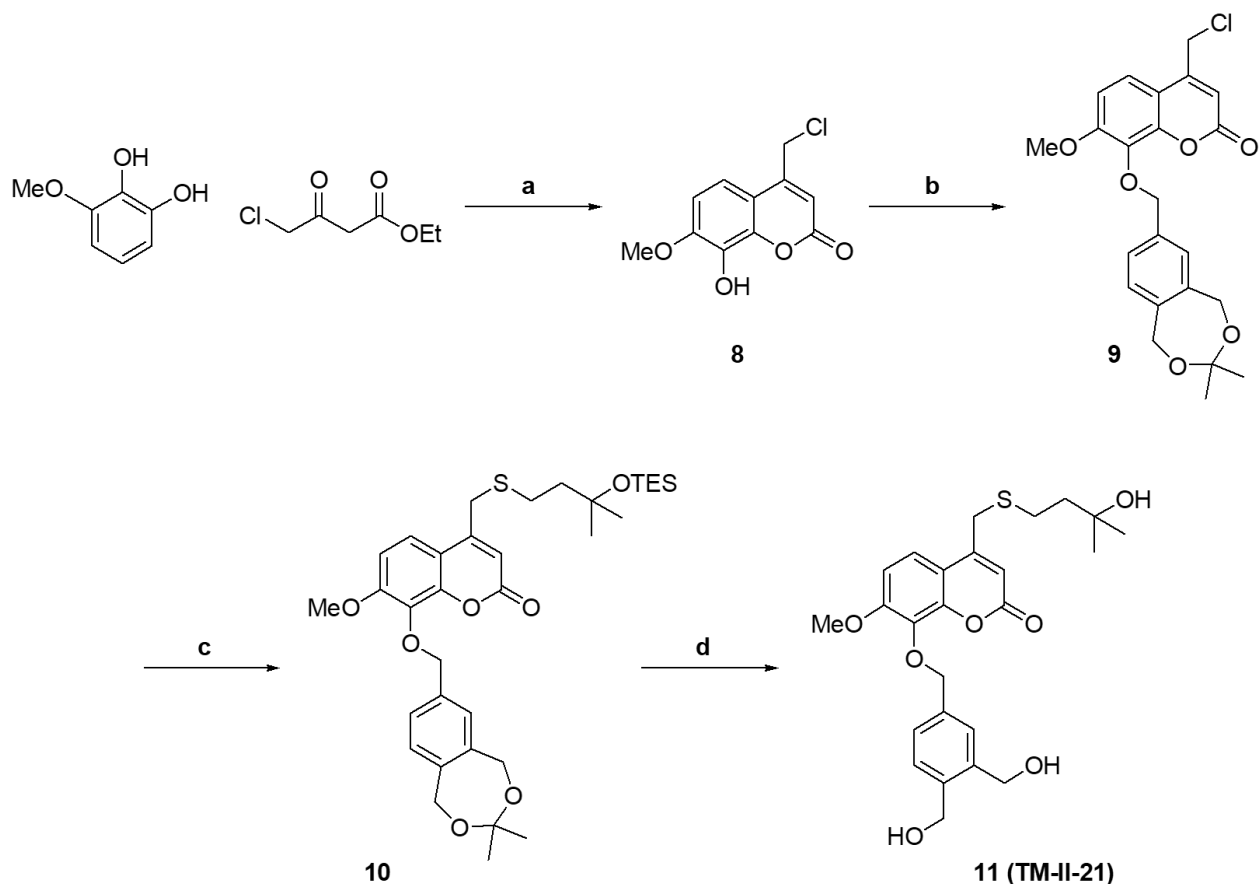
Scheme 3. Synthesis towards compound 11 (TM-II-21): a) H_2SO_4; 25°C, 2 h; b) Compound 7 (scheme 2), K_2CO_3, ACN; 50°C, 8 h; 25°C, 13 h; c) Compound 3 (scheme 1), TEA, DMF; 25°C, 18 h; d) CSA, MeOH; 0°C, 4 h.

The final reaction towards TM-II-21 was simultaneous silyl and acetonide deprotection. A catalytic amount of camphor sulfonic acid (CSA) in methanol removed both protecting groups within four hours at 0°C. Deprotection of the silyl ether occurs as the oxygen atom becomes protonated, resulting in a good leaving group. A polar protic solvent, such as methanol, acts as a nucleophile to displace the existing O-Si bond. Deprotection of the acetonide ring also begins with protonation of an ether oxygen. As a lone pair of electrons on the adjacent carbon forms a carbonyl, the ring breaks and releases the free alcohol functionality. A molecule of methanol can then attack the carbonyl and repeat the described process, releasing the second alcohol functionality. Compound 11 (TM-II-21) was synthesized in 49% yield, though decreasing the

amount of CSA in future trials would likely improve the reaction yield. Elimination of the

tertiary alcohol on TM-II-21 is possible under acidic conditions and may have contributed to the

loss of the final product.

3.2 Series B and C scaffolds

Other derivatives were generated by varying the compound length on 4-thioglycerol

substituted coumarins. The corresponding bromides were synthesized in two steps and used in

the SN2 coupling reaction, rather than the thiol that was previously present in compound A

(Figure 32). Attachment of compound D was planned as an ether linkage off of the phenolic

position in compound E as the phenol would be nucleophilic enough to substitute an alkyl

bromide. (Figure 36)
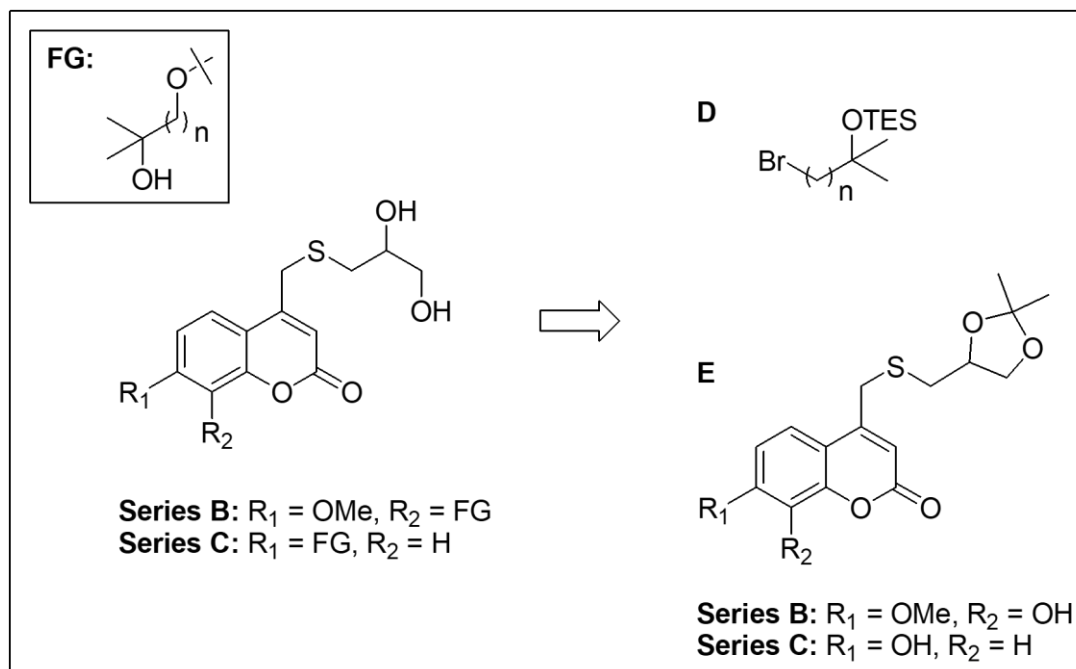
Figure 36. Retrosynthesis of the series B and C scaffolds.

52

Varying lengths of compound D were synthesized in two steps. Commercially available methyl 4-bromobutyrate, methyl 5-bromovalerate, and methyl 6-bromohexanoate underwent a Grignard reaction with MeMgBr, followed by a silyl protection using triethylsilyl chloride (TES-Cl) (Scheme 4). The Grignard reaction for compounds 12, 21, and 25 followed reaction conditions from a previously reported procedure[7], while utilizing the same mechanism described for compound 2 (Scheme 1). Two equivalents of MeMgBr are essential to yield the tertiary alcohol from the ester functional group, however.

n = 3, 4, 5

12: n = 4
21: n = 3
25: n = 5

13: n = 4
22: n = 3
26: n = 5
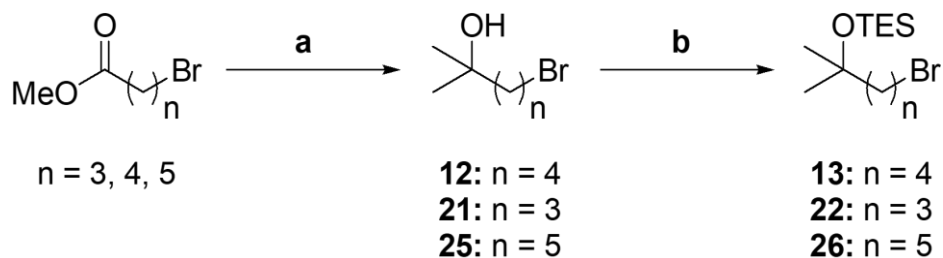
Scheme 4. Synthesis towards compounds 13, 22, and 26: a) MeMgBr, Et$_2$O; 0°C, 30 min; 25°C, 4 h; b) TES-Cl, 2,6-lutidine, DCM; 0°C, 30 min; 25°C, 18 h.

Unlike the protection to form compound 2, an *in situ* reaction to synthesize compounds 13, 22, and 26 was not performed following the Grignard reaction. Compound 2 was protected using
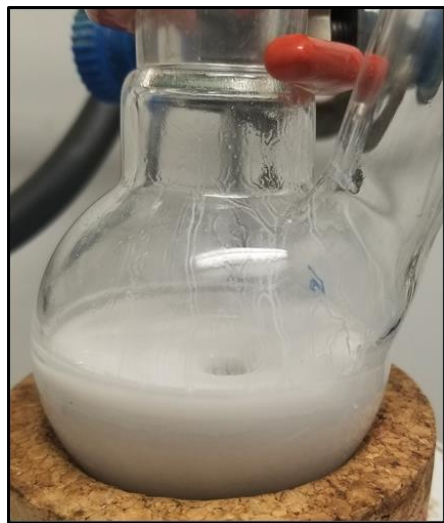
Figure 37. Grignard reaction on methyl 5-bromovalerate.

TES-OTf, while compounds 12, 21, and 25 were protected using TES-Cl, which was readily available in our laboratory. Alcohol protection did not sufficiently occur with TES-Cl when the magnesium salt was present during the *in situ* reaction trial (Figure 37). Work-up and isolation of the alcohol was necessary prior to silyl protection. Tertiary alcohol protection using TES-Cl was completed at 0°C rather than -78°C when using TES-OTf. The yields for compounds

53

13, 22, and 26 ranged from 60-86%, and therefore were slightly lower than the yield for compound 2 when TES-OTf was used.

Similar to TM-II-21, the series B scaffold continued to use a thioether linkage at position 4 on the coumarin ring. However, the series B scaffold utilized the thioether as a connection to a diol rather than the tertiary alcohol (Figure 36). Due to the difficulties associated with the synthesis of compound B (Figure 32; Scheme 2), the diol was exchanged for commercially available α-thioglycerol, which also decreased the number of separate synthesis steps needed to complete the final ligand structures.

Substitution of the benzylic chloride 8 was achieved by the thiolate generated by deprotonating the thiol with potassium carbonate. Selective substitution by the sulfur in α-thioglycerol occurred due to the higher nucleophilicity inherent to thiols over alcohols. After refluxing for four hours in acetonitrile, full conversion from compound 8 was visible by TLC. The triol resulting from α-thioglycerol coupling with compound 8 yields a highly polar compound. A difficult isolation of this compound using standard work-up techniques was anticipated, therefore, immediate protection of the diol was performed to simplify purification. A solvent exchange from acetonitrile to acetone was done *in vacuo*, and *p*-toluenesulfonic acid was added to the crude suspension to create an acidic solution. A five-membered acetonide ring was formed using the same reaction mechanism described during the synthesis of compound 7 (Scheme 2). Purification by column chromatography provided compound 14 in 82% yield.

The series C scaffold shared the thioglycerol diol at position 4 on the coumarin ring; however, the ether attachment to the tertiary alcohol was located at position 7. This positioning in the

series C scaffold eliminated the methoxy functional group at position 7 that was present in the series B scaffold. Position 8 in series C was unfunctionalized, only having a hydrogen present. (Figure 5)

Compound 17 (Scheme 5) was synthesized by the Pechmann condensation previously described for compound 8. Resorcinol replaced 3-methoxycatechol in the reaction with ethyl 4-chloroacetoacetate and sulfuric acid to yield compound 17. Previously, recrystallization was used to easily purify compound 8; however, recrystallization of compound 17 was unsuccessful, despite literature reports claiming purification by this method. Recrystallization was attempted in ethanol, methanol, toluene, chloroform, acetonitrile, and water without success, despite ensuring a neutral pH of the crude solid prior to recrystallization. White product crystals were observed to form at the top of a glass vial when attempting to recrystallize from a 50:50 ethanol:water solution following overnight organic solvent evaporation (Figure 38). However, purification on a larger scale using the 50:50 ethanol: water solution was unsuccessful. Resorcinol has an unsubstituted position in both positions ortho to the phenolic position, so regioisomers can be formed during the reaction. Potential byproducts resulting from the reaction with resorcinol may have interfered with the recrystallization. Nonetheless, the crude solid precipitated from the reaction to synthesize compound 17 was thoroughly washed with water and dried on the vacuum filter prior to its use in the successive substitution and protection reactions that were described for
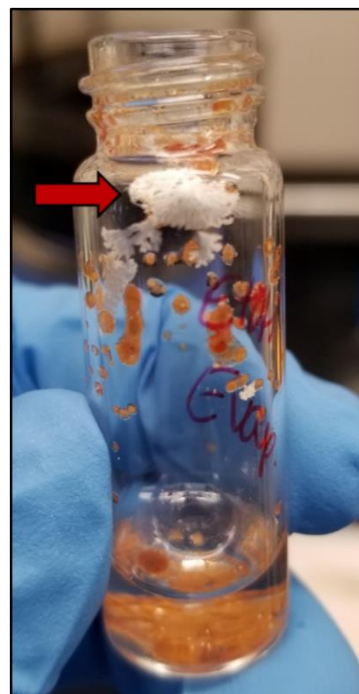
Figure 38. Recrystallization trial of compound 17 in 50:50 EtOH:Water. Product crystal formation following overnight solvent evaporation (red arrow).

compound 14 (Scheme 5). Compound 18 was successfully isolated in 30% yield following

chromatographic purification. Further purification of compound 17 could increase the yield of

compound 18.

3-Methoxycatechol: R_1 = OMe, R_2 = OH
Resorcinol: R_1 = OH, R_2 = H

8: R_1 = OMe, R_2 = OH
17: R_1 = OH, R_2 = H

14: R_1 = OMe, R_2 = OH
18: R_1 = OH, R_2 = H

FG:

15: R_1 = OMe, R_2 = FG (n = 4, R_3 = H)
19: R_1 = FG (n = 4, R_3 = TES), R_2 = H
23: R_1 = OMe, R_2 = FG (n = 3, R_3 = TES)
27: R_1 = OMe, R_2 = FG (n = 5, R_3 = H)

16 (TM-II-72): R_1 = OMe, R_2 = FG (n = 4, R_3 = H)
19 (TM-II-88): R_1 = FG (n = 4, R_3 = H), R_2 = H
24 (TM-III-20): R_1 = OMe, R_2 = FG (n = 3, R_3 = H)
28 (TM-III-31): R_1 = OMe, R_2 = FG (n = 5, R_3 = H)
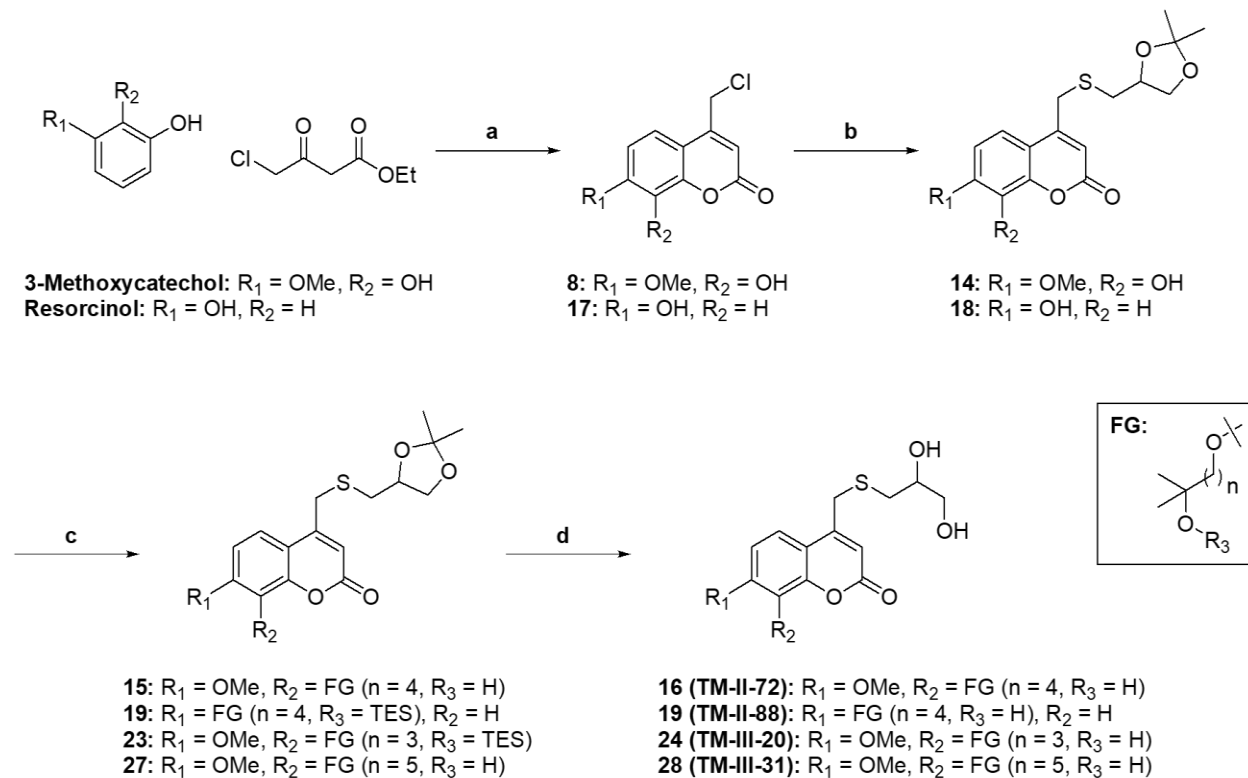
Scheme 5. Synthesis towards compounds 16 (TM-II-72), 22 (TM-III-20), and 26 (TM-III-31): a) 1. α-thioglycerol, K_2CO_3, ACN; Reflux, 4 h; 2. PTSA, Acetone; 25°C, 22 h; b) Compound 13, 22, or 26 (scheme 4), K_2CO_3, ACN; Reflux, 18 h; c) HCl, MeOH; 25°C, 4-8 h.

The Williamson ether synthesis was employed for separate coupling of compounds 13, 22, and

26 to compound 14, along with compound 13 to both compounds 14 and 18. It was essential

for this reaction to occur following the α-thioglycerol coupling. Elevated temperatures were

needed to substitute the aliphatic bromides with the coumarin hydroxyl group, but also allowed

for dimerization to occur when the benzylic chloride functionality was present in position 4.

While bromides are better leaving groups than chlorides, a benzylic position is more reactive

than an aliphatic position. Therefore, due to the positioning of the benzylic chloride in

compound 8, α-thioglycerol substitution needed to occur prior to the aliphatic bromide coupling.

Compounds 15, 19, 23, and 27 were all synthesized, isolated, and purified following the same protocol; however, loss of the silyl protecting group occurred following column chromatography in compounds 15 and 27. Silica is known to be a weakly acidic metal oxide[8] and is able to degrade certain compounds during purification. Since silyl groups are commonly deprotected under acidic conditions, it is thought that silyl deprotection occurred during column purification for compounds 15 and 27. Compound elution was routinely done the same day crude samples were loaded onto the column; however, the time each product spent in contact with the silica was variable. Even for the compounds that remained protected with the silyl group, a portion of the final yield was lost to the deprotected tertiary alcohol product. It is unlikely that degradation of the silyl protecting group occurred prior to the reaction, as the Williamson ether synthesis was completed shortly after silyl protection of the aliphatic bromides. Additionally, coupling trials attempted with the deprotected alcohol were unsuccessful, resulting in intramolecular cyclization between the tertiary alcohol and the aliphatic bromide. Deprotection during the coupling reaction would have been visible by TLC when monitoring the reaction progress. Formation of compound 19 also used compound 13 while yielding the silyl-protected product, contrasting from the results in synthesizing compound 15. Each of these observations support the hypothesis that column purification may be responsible for cleaving the silyl protecting group. The addition of a weak base, such as triethylamine, to the mobile phase during column purification may aid in consistent elution of the silyl-protected products.

The final step in synthesizing TM-II-72, TM-II-88, TM-III-20, and TM-III-31 was simultaneous deprotection of the silyl protecting group and acetonide ring. Therefore, the deprotection of the tertiary alcohol during column purification for compounds 15 and 27 did not affect our plan for the overall synthetic route. The deprotection of the acetonide ring was most effectively completed in 0.01 M HCl in MeOH, though 0.05 M HCl in MeOH was also tolerated, with complete conversion taking between four and eight hours. Successful purification was achieved using reverse-phase (C18) column chromatography in methanol and water. A gradient from 100% water up to 100% methanol allowed for salt impurities to elute in water, and the final compounds to elute between 40-60% methanol in water.
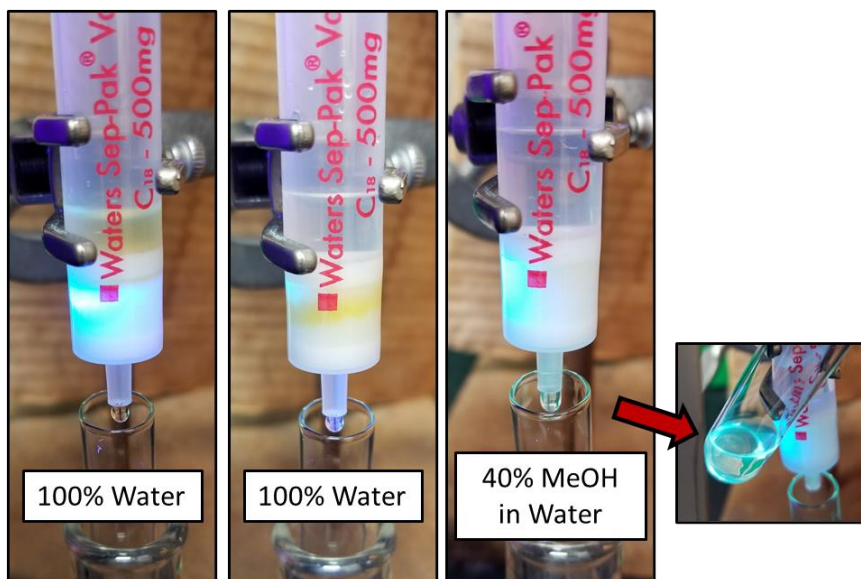
Figure 39. Purification of TM-III-20 using reverse-phase column chromatography. Under UV light (360 nm), impurities are visualized eluding in 100% water. TM-III-20 began to elude in 40:60 MeOH:Water; and exhibited a blue-green fluorescent color.

3.3   Series D scaffold

The series D scaffold explored substitution the coumarin core with a long aliphatic chain bearing a tertiary alcohol in position 7, with different hydrogen-bonding functional groups directly attached to the coumarin scaffold. Synthesis of the aliphatic carbon chain containing

the tertiary alcohol and a bromide functional group followed the same approach as the

syntheses of compounds 13, 22, and 26 (scheme 4), but substituted the use of TES-Cl for TES-

OTf during the silyl protection. Compounds 29 was synthesized following the Grignard reaction

from commercially available ethyl 7-bromoheptanoate in 99% yield. Following, compound 30

was protected using a triethylsilyl group in 87% yield.
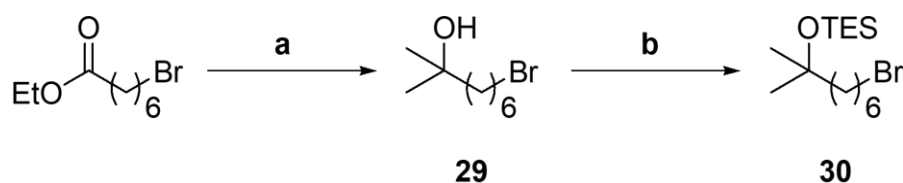
Scheme 6. Synthesis towards compounds 29 and 30: a) MeMgBr, Et$_2$O;
0°C, 30 min; 25°C, 4 h; b) TES-OTf, 2,6-lutidine, DCM; -78°C, 30 min; 25°C,
18 h.

The Knoevenagel condensation was employed for synthesis of all series D coumarin scaffolds.

For compound 31, the Knoevenagel condensation occurred by reacting 2,4-

dihydroxybenzaldehyde with diethyl malonate in the presence of piperidine. The same reaction

conditions were used in the synthesis of compound 35, substituting ethyl acetoacetate for

diethyl malonate. Piperidine acts as a base in the removal of an α-hydrogen from either diethyl

malonate or ethyl acetoacetate, which in turn creates a nucleophile capable of attacking the

carbonyl of 2,4-dihydroxybenzaldehyde. Subsequent protonation of the benzylic alkoxide leads

to the loss of a molecule of water and alkene formation. Additionally, deprotonation of the

ortho-phenol allows for nucleophilic attack of the free carbonyl. The resulting intramolecular

cyclization pushes the carbonyl π-electrons onto the carbonyl oxygen atom. Reformation of the

carbonyl forms the final coumarin product while ethanol is lost as a byproduct. This reaction

was done solvent-free, causing the reaction mixture to become extremely viscous as the

reaction proceeds, leading to difficulty with stirring. However, the viscosity of the reaction

59
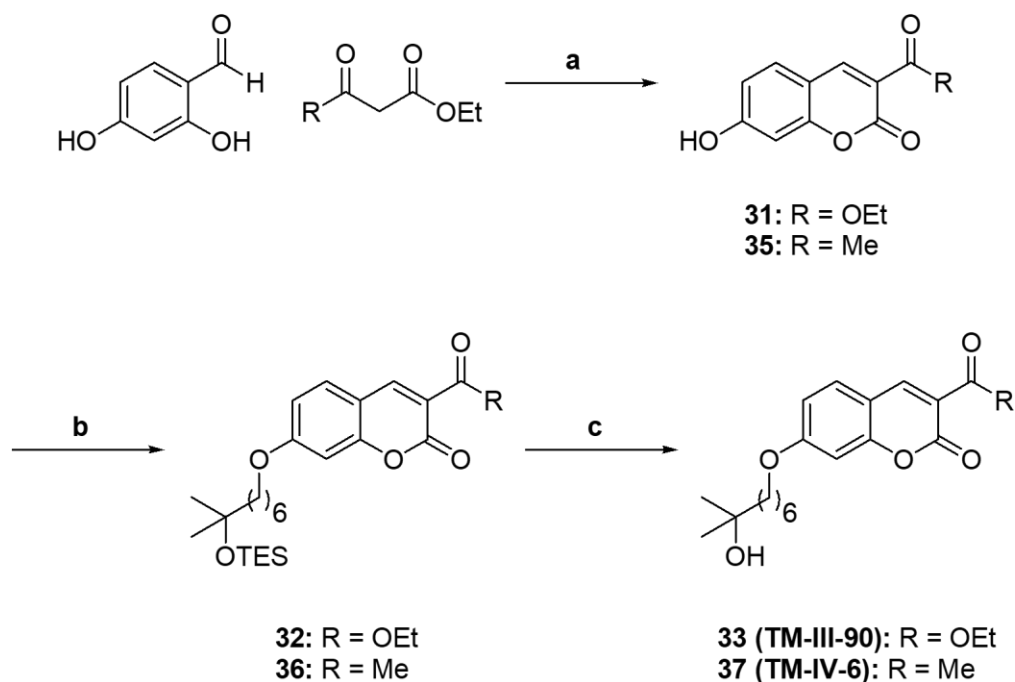
Scheme 7. Synthesis towards compounds 33 and 37: a) Piperidine; 25°C, 1 h; b) Compound 30 (scheme 6), K_2CO_3, ACN; Reflux, 18-72 h; c) HCl, MeOH (compound 33) or EtOH (compound 37), THF; 25°C, 1-3 h.

mixture did not hinder either reaction from going to completion. Conveniently, recrystallization of compounds 31 and 35 in anhydrous ethanol allowed for simple purification. In order to achieve successful recrystallization, the reaction mixture needed to be poured over acidic ice water. The reverse addition led to the encapsulation of piperidine within the crude product and led to unsuccessful recrystallization in ethanol. Additionally, thorough washing of the crude solid until the filtrate was clear was necessary for successful recrystallization. The filtrate commonly reaches a neutral pH while maintaining a yellowed color; however, recrystallization at this stage was unsuccessful. Isolation of the final crystals may require two filtrations, as a sticky, red precipitate also formed during the recrystallization process (Figure 40).

The Williamson ether synthesis between compounds 30 and 31, as well as compounds 30 and 35, followed the previously described procedures. Refluxing compound 30 with the respective coumarin in ACN, in the presence of potassium carbonate, led to the formation of the silyl protected compounds 32 and 36 in 54% yield and 42% yield, respectively.

Figure 40. Recrystallization of compound 31 (off-white crystals) on the vacuum filter with a sticky, red precipitate byproduct.

The following silyl deprotection was achieved in 0.01 M HCl in EtOH/THF for TM-III-90 and 0.01 M HCl in MeOH/THF for TM-IV-6. Ethanol was used in the deprotection of compound 32 to avoid any potential transesterification. TM-III-90 was purified in 91% yield following column chromatography, and TM-IV-6 was purified in 78% yield.

TM-III-90 was further hydrolyzed, yielding a carboxylic acid at the position 3 (Scheme 8). Lithium hydroxide was used for this reaction since it is weaker than the other alkali metal hydroxides. However, the ester hydrolysis still appeared to form many byproducts by TLC as the reaction proceeded. A convenient and environmentally-friendly Knoevenagel condensation that affords the carboxylic acid has been reported.[9] This strategy would allow the challenges of ester hydrolysis to be avoided. However, we observed a competing reaction during the Williamson ether synthesis with the carboxylic acid acting as a nucleophile. This was previously observed by other reports, which yielded esters from alkylating the acid, in addition to product mixtures of the ester and ether from alkylating the phenol.[10] Reverse-phase column chromatography using methanol and water was attempted for TM-III-91, but significant contamination of the final product by TM-III-90 was observed. Rather than repeating the column purification, an acid-base

33 (TM-III-90)   **34 (TM-III-91)**
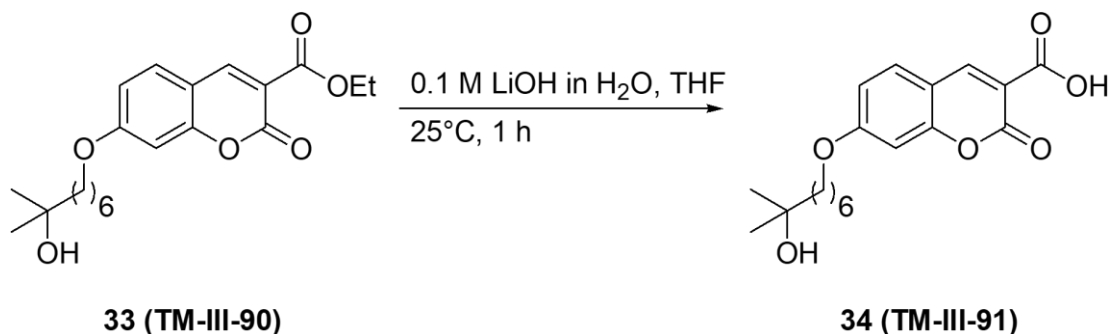
Scheme 8. Ester hydrolysis conditions used to form TM-III-91.

extraction was used to separate TM-III-90 from TM-III-91. While under basic conditions, TM-III-90 was discarded with organic dichloromethane washes. Acidification of the aqueous layer then allowed for TM-III-91 to be extracted in chloroform. Further optimization to the ester hydrolysis procedure is needed to improve the yield of TM-III-91, which was isolated in 45% yield.

Reduction of α,β-unsaturated ketones with sodium borohydride in methanol, while in the presence of cerium(III) chloride, has been shown to yield the allylic alcohol products.[11] Reduction of TM-IV-6 to the secondary alcohol, TM-IV-18, was accomplished following the Luche reduction mechanism, maintaining the cyclic alkene in the aromatic coumarin system. (Scheme 9)

37 (TM-IV-6)   **38 (TM-IV-18)**
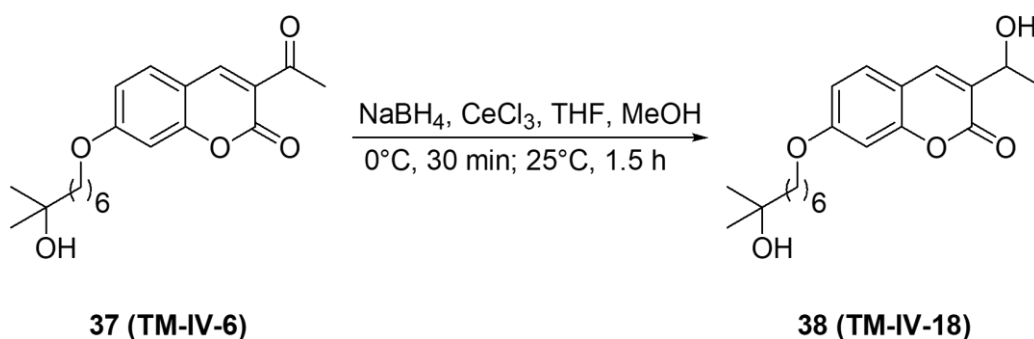
Scheme 9. Luche reduction conditions used to form TM-IV-18.

The Luche reduction utilizes a polar protic solvent (i.e. methanol) to create a complex with cerium(III) chloride, which in turn, increases the acidity of the environment.[12] Additionally, methanol reacts with sodium borohydride to form more reactive alkoxyborohydrides, evolving

62

hydrogen gas in the process. Sodium borohydride increases in hardness as hydrides are substituted by alkoxy groups.[12] Under these conditions, the addition to α,β-unsaturated ketones favorably occurs at the carbonyl carbon. Ketones are hard Lewis bases that increase in electrophilicity when in the presence of the cerium salt complex, while alkenes are softer Lewis bases.[13] According to hard and soft acids and bases (HSAB) theory, hard acids preferentially react with hard bases. Therefore, the 1,2-addition is favored over the 1,4-addition during the Luche reduction. TM-IV-18 was synthesized following this protocol in 63% yield.

The final series D scaffold synthesized included a nitrile group present in position 3. Compound 39 (scheme 10) was synthesized by the Knoevenagel condensation, following a procedure reported by Wang, et al.[14] In water, 2,4-dihydroxybenzyaldehyde reacted with malononitrile while in the presence of ammonium acetate. The coumarin forms at room temperature over the course of four hours and precipitates out to form a viscous solution as the reaction progresses (Figure 41). The solid imine product was filtered and dried. Following, hydrolysis to

39

40   **41 (TM-IV-16)**
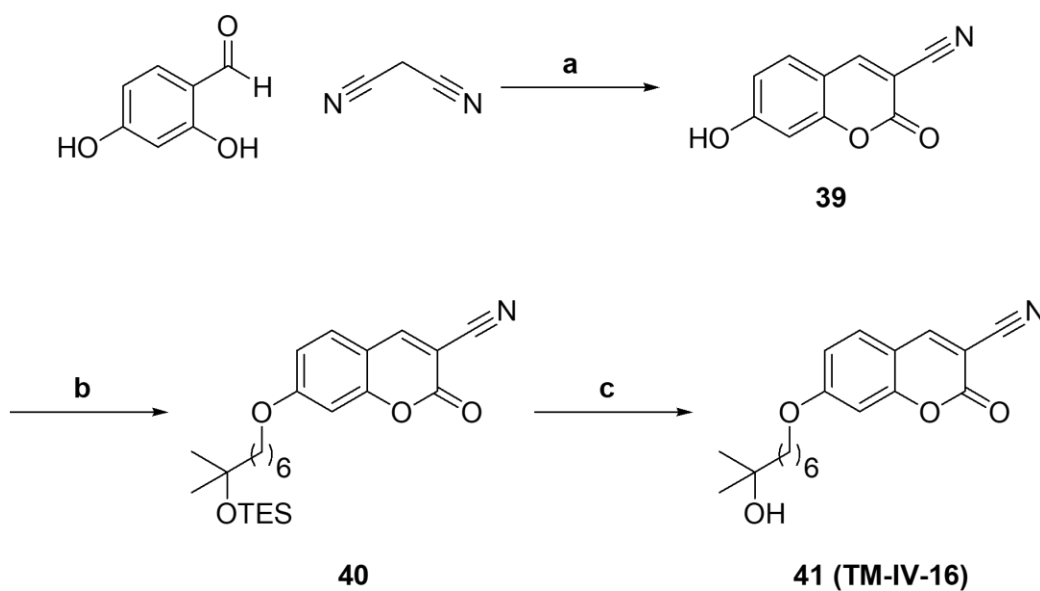
Scheme 10. Synthesis towards TM-IV-16: a) 1. NH$_4$Ac, H$_2$O; 25°C, 4 h; 2. HCl, H$_2$O; 75°C, 1 h; b) Compound 30 (scheme 6), K$_2$CO$_3$, ACN; Reflux, 18 h; c) HCl, MeOH; 25°C, 1 h.

the coumarin was achieved by heating the solid in 3.0 M HCl solution at 75°C for one hour. Subsequent filtration and recrystallization in ethanol yielded compound 39 in 44% yield. The yield for compound 39 can likely be increased
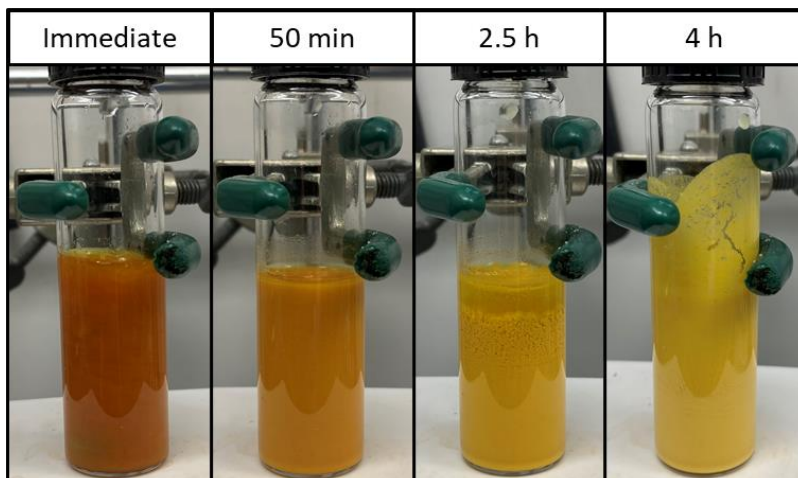
Figure 41. Knoevenagel condensation with 2,4-dihydroxybenzaldehyde and malononitrile in aqueous NH$_4$Ac solution.

during the purification stage, as the ethanol recrystallization was more challenging than the recrystallizations for compounds 31 or 35. A light and fluffy red powder was characteristic of compound 39, which seemed to maintain a degree of solubility in the recrystallization solvent.

The final steps towards TM-IV-16 followed the previously discussed Williamson ether synthesis with compound 30, followed by silyl deprotection in 0.01 M HCl in MeOH/THF. Compound 40 was purified in 68% yield, and TM-IV-16 in 99% yield.

3.4 Compound characterizations

All reactions were performed under a nitrogen atmosphere unless otherwise noted. Reaction

temperatures refer to the surrounding bath temperatures, or an oil bath held under the same

reaction conditions in the case of reactions run in tandem on the carousel. Reactions were

monitored by TLC using POLYGRAM SIL G UV254 plates (Macherey-Nagel, 805023).

Visualization was performed with UV light and cerium molybdate general stain followed by

heating. NMR spectra were recorded on a Bruker Advance 500 MHz instrument with

compounds dissolved in the specified deuterated solvent. HRMS analysis was completed on the

Shimadzu IT-TOF instrument.

3.4.1 TM-II-21 and intermediate compound characterizations
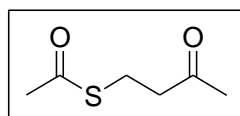
Synthesis of thioacetic acid *S*-(3-oxo-butyl) ester (1): Potassium

thioacetate (12.339 g, 108 mmol) was dissolved in dry DCM (50 mL) and

cooled to 0°C in an RBF. Pyridine (11.6 mL, 143 mmol) was added slowly, followed by the

addition of AcOH (6.2 mL, 108 mmol). The solution was stirred for 1 hour at 0°C before methyl

vinyl ketone (5.8 mL, 71.5 mmol) was added. The solution was allowed to gradually reach 25°C

overnight. The reaction was diluted in Et_2O and washed with 1.0 M HCl (30 mL), 10% $CuSO_4$

solution (90 mL), saturated $KHCO_3$ (60 mL), and brine (60 mL). The organic layers were collected

and dried over $MgSO_4$, filtered, and concentrated to dryness. Thioacetic acid S-(3-oxo-butyl)

ester (1) was collected as a yellow oil at 95% yield and was not subjected to any further

purification. ^{1}H NMR (500 MHz, CDCl$_3$) δ 3.06 (t, J = 6.8 Hz, 2H), 2.78 (t, J = 6.8 Hz, 2H), 2.32 (s, 3H), 2.16 (s, 3H). ^{13}C NMR (126 MHz, CDCl$_3$) δ 206.36, 195.92, 43.28, 30.51, 29.86, 22.94.
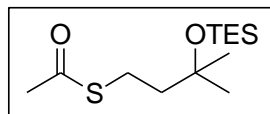
Synthesis of thioacetic acid *S*-(3-methyl-3-triethylsilanyloxy-butyl) ester (2): Compound 1 (4 g, 27.4 mmol) was dissolved in dry Et$_2$O (40 mL) and cooled to -78°C in an RBF. MeMgBr, 3.0 M in Et$_2$O (13. 5 mL, 40.5 mmol) was added dropwise to the RBF, which proceeded to react for 4 hours at 0°C. The reaction was then cooled to -78°C. A dropwise addition of 2,6-lutidine (5 mL, 42.9 mmol) followed by TES-triflate (12.5 mL, 55.3 mmol) was added at -78°C. The reaction gradually reached 25°C overnight and was then quenched with 20% NH$_4$Cl solution (pH = 7, 40 mL). The product was washed with 10% CuSO$_4$ solution (60 mL) and brine (40 mL). The organic layers were collected, dried over MgSO4, filtered, and concentrated to dryness. Thioacetic acid S-(3-methyl-3-triethylsilanyloxy-butyl) ester (2) was collected as a pale-yellow oil and was used without further purification. ^{1}H NMR (500 MHz, CDCl$_3$) δ 2.95 – 2.90 (m, 2H), 2.29 (s, 3H), 1.69 – 1.63 (m, 2H), 1.23 (s, 6H), 0.94 (t, J = 8.0 Hz, 9H), 0.57 (q, J = 8.0 Hz, 6H). ^{13}C NMR (126 MHz, CDCl$_3$) δ 195.80, 72.91, 44.63, 30.46, 29.68, 24.49, 7.02, 6.68.
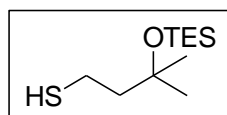
Synthesis of 3-methyl-3-triethylsilanyloxy-butane-1-thiol (3): Dry Et$_2$O (10 mL) was cooled to -78°C in an RBF and LiAlH$_4$, 2.0 M in THF (1.1 mL, 2.2 mmol) was added at -78°C and stirred for 10 minutes. Compound 2 (300 mg, 1.08 mmol) was added dropwise to the reaction flask at -78°C and reacted for 1.5 h while gradually warming up to 25°C. After full conversion was observed by TLC, the reaction was quenched with the dropwise addition 20% NH$_4$Cl solution (pH = 7, 40 mL) until bubbling of the solution ceased. The crude product was extracted in DCM (40 mL) and washed with water (40 mL). The organic

layers were collected, dried over MgSO$_4$, filtered, and concentrated to dryness. 3-Methyl-3-triethylsilanyloxy-butane-1-thiol (3) was collected as a pale-yellow oil at 94% yield. No further purification was performed. ^{1}H NMR (500 MHz, CDCl$_3$) δ 2.62 – 2.56 (m, 2H), 1.77 – 1.72 (m, 2H), 1.21 (s, 6H), 0.94 (t, J = 8.0 Hz, 9H), 0.57 (q, J = 7.9 Hz, 6H). ^{13}C NMR (126 MHz, CDCl$_3$) δ 73.01, 50.02, 29.80, 19.80, 7.07, 6.71.
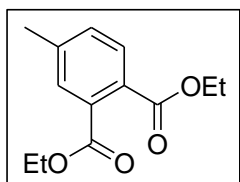
Synthesis of 4-methyl-phthalic acid diethyl ester (4): 4-Methylphthalic acid (3.1 g, 17.2 mmol), dry EtOH (150 mL), and 3Å sieves were combined in an RBF, followed by a dropwise addition of H$_2$SO$_4$ (1.0 mL). The reaction flask was refluxed without stirring for two hours or until conversion was observed by TLC. Excess EtOH was distilled off and the crude product was redissolved in EtOAc. The solution was washed with 20% NH$_4$Cl solution (pH = 7, 100 mL) before collecting the organic layer, which was subsequently dried over MgSO$_4$, filtered, and concentrated to dryness. The crude product was purified by column chromatography using EtOAc/Hex (gradient up to 30:70 EtOAc:Hex). 4-Methyl-phthalic acid diethyl ester (4) was collected as a clear to pale-yellow oil at 92% yield. ^{1}H NMR (500 MHz, CDCl$_3$) δ 7.64 (d, J = 7.9 Hz, 1H), 7.44 (s, 1H), 7.28 (d, J = 7.5 Hz, 1H), 4.33 (dq, J = 9.4, 7.1 Hz, 4H), 2.37 (s, 3H), 1.33 (td, J = 7.2, 4.8 Hz, 6H). ^{13}C NMR (126 MHz, CDCl$_3$) δ 168.14, 167.24, 141.82, 132.97, 131.22, 129.16, 129.10, 128.70, 61.51, 61.35, 21.23, 14.08, 14.05. *m/z* calculated for C$_{13}$H$_{16}$O$_4$ 237.1121 [M+H]$^+$, found 237.1093.
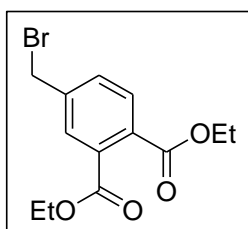
Synthesis of 4-bromomethyl-phthalic acid diethyl ester (5): Compound 4 (980 mg, 4.15 mmol), CCl$_4$ (20 mL), and 3Å sieves were added to an RBF. In one portion, NBS (915 mg, 5.14 mmol) was added to the stirring reaction mixture, followed immediately by the addition of AIBN (24.5 mg, 149 μmol). The reaction flask

was brought to reflux for 8 hours or until full conversion was observed by TLC. Excess CCl_4 was

distilled off and the crude solid was redissolved in Et_2O (50 mL). The crude product was washed

with 20% NH_4Cl solution (pH = 7, 60 mL) and brine (40 mL). The organic layer was collected,

dried over $MgSO_4$, filtered, and concentrated to dryness. The crude product was purified by

column chromatography using Et_2O/Hex (gradient to 30:70 Et_2O:Hex). 4-Bromomethyl-phthalic

acid diethyl ester (5) was collected as a clear oil at 40% yield. ^{1}H NMR (500 MHz, $CDCl_3$) δ 7.73

(d, J = 1.6 Hz, 1H), 7.70 (d, J = 7.9 Hz, 1H), 7.55 (dd, J = 7.9, 1.7 Hz, 1H), 4.48 (s, 2H), 4.37 (qd, J =

7.1, 5.4 Hz, 4H), 1.37 (dd, J = 13.1, 7.0 Hz, 6H). ^{13}C NMR (126 MHz, $CDCl_3$) δ 167.12, 167.07,

140.97, 132.87, 131.94, 131.41, 129.50, 129.36, 61.84, 61.76, 31.40, 14.08. m/z calculated for

$C_{13}H_{15}BrO_4$ 315.0226 $[M+H]^+$, found 315.0206.
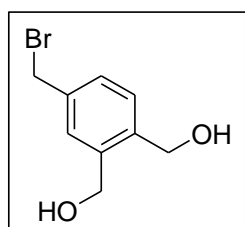
Synthesis of (5-bromomethyl-2-hydroxymethyl-phenyl)-methanol (6):

In an RBF containing 3Å sieves, DIBAL-H, 1.0 M in heptane (8 mL, 8 mmol) was added and cooled to -61°C. Compound 5 (312 mg, 990 µmol) was

dissolved in dry DCM (3 mL) and added to the reaction flask in a dropwise manner. The solution

was held at -61°C and reacted for 10 hours or until full conversion was observed by TLC. The

reaction was quenched with cold water and slowly poured over a mixture of ice and 1.0 M HCl

(100 mL). The mixture was stirred in the acidic aqueous solution for 1 hour before extracting

the product in EtOAc (200 mL). The organic layer was washed with 1.0 M Rochelle salt (50 mL),

1.0 M citric acid solution (50 mL), and brine (50 mL). The organic layer was subsequently

collected, dried over $MgSO_4$, filtered, and concentrated to dryness. (5-Bromomethyl-2-

hydroxymethyl-phenyl)-methanol was collected as an off-white powder at 49% yield and used

without further purification. ^{1}H NMR (500 MHz, MeOD) δ 7.50 (d, J = 1.7 Hz, 1H), 7.41 (d, J = 7.9

Hz, 1H), 7.35 (dd, *J* = 7.8, 1.9 Hz, 1H), 4.71 (d, *J* = 3.1 Hz, 4H), 4.59 (s, 2H). ^{13}C NMR (126 MHz,

MeOD) δ 139.43, 139.07, 137.55, 128.35, 128.01, 127.82, 61.19, 61.12, 45.32, 32.49.
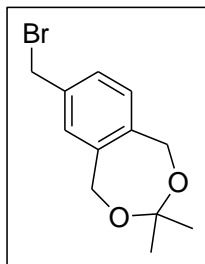
Synthesis of 2-Bromomethyl-7,7-dimethyl-5*H*,9*H*-6,8-dioxa-

benzocycloheptene (7): Compound 6 (289 mg, 1.25 mmol), dry acetone (20

mL), and 3Å sieves were added to an RBF. A catalytic amount of PTSA was

added to the reaction flask, and the mixture was stirred for 2 hours or until

complete conversion was observed by TLC. Excess acetone was removed *in vacuo*, and the

product was redissolved in DCM (20 mL). The organic layer was washed with water (30 mL),

dried with MgSO₄, filtered, and concentrated to dryness. The crude product was purified by

column chromatography using EtOAc/Hex (gradient up to 15:85 EtOAc:Hex). 2-Bromomethyl-

7,7-dimethyl-5H,9H-6,8-dioxa-benzocycloheptene was collected as a clear oil at 73% yield. [1]H

NMR (500 MHz, CDCl₃) δ 7.22 (dd, *J* = 7.8, 1.7 Hz, 1H), 7.12 (s, 1H), 7.07 (d, *J* = 7.9 Hz, 1H), 4.87

(d, *J* = 5.0 Hz, 4H), 4.48 (s, 2H), 1.53 (s, 6H). ^{13}C NMR (126 MHz, CDCl₃) δ 138.91, 138.67, 136.26,

127.36, 126.85, 126.64, 102.29, 64.70, 64.68, 33.16, 23.77.
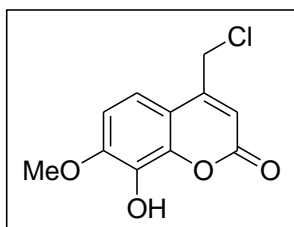
Synthesis of 4-Chloromethyl-8-hydroxy-7-methoxy-chromen-2-one

(8): Neat H₂SO₄ (5.0 mL) was charged to an RBF (flask 1) and cooled to

0°C. In a separate RBF (flask 2), 3-methoxycatechol (2 mL, 18.1 mmol)

and ethyl 4-chloroacetoacetate (2.6 mL, 19.3 mmol) were combined. Flask 2 was added to flask

1 in a dropwise manner at 0°C. The ice bath was removed, and the reaction gradually warmed

up over the course of 2 hours. The reaction mixture was then carefully poured over ice water,

forming a solid precipitate. The precipitate was filtered and rinsed with water until the filtrate

pH was neutral (pH = 6). The crude product was left to dry on the vacuum filter overnight. The

dry solid was recrystallized in EtOH to yield 4-chloromethyl-8-hydroxy-7-methoxy-chromen-2-one as white to light tan crystals at 86% yield. ^{1}H NMR (500 MHz, CDCl$_3$) δ 7.22 (d, J = 8.8 Hz, 1H), 6.93 (d, J = 8.8 Hz, 1H), 6.47 (s, 1H), 5.75 (s, 1H), 4.65 (d, J = 0.7 Hz, 2H), 4.03 (s, 3H). ^{13}C NMR (126 MHz, CDCl$_3$) δ 159.68, 149.85, 149.67, 142.02, 133.23, 115.08, 113.21, 111.84, 107.62, 56.59, 41.33. *m/z* calculated for C$_{11}$H$_9$ClO$_4$ 241.0262 [M+H]$^+$, found 241.0233.
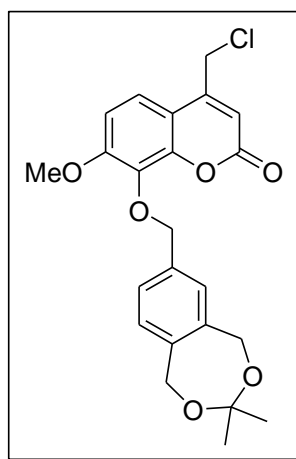
Synthesis of 4-Chloromethyl-8-(7,7-dimethyl-5,9-dihydro-6,8-dioxa-benzocyclohepten-2-ylmethoxy)-7-methoxy-chromen-2-one (9): Compound 7 (147 mg, 542 µmol), compound 8 (135 mg, 561 µmol), dry ACN (5 mL), and 3Å sieves were charged to an RBF. In one portion, K$_2$CO$_3$ (151 mg, 1.09 mmol) was added to the reaction flask. The mixture was stirred overnight at 25°C, at which point conversion was observed by TLC. The reaction was quenched with 20% NH$_4$Cl solution (pH = 7, 5 mL) and the product was extracted in EtOAc (20 mL). The organic layer was washed with brine (20 mL), was subsequently collected, dried over MgSO$_4$, filtered, and concentrated to dryness. The crude product was purified by column chromatography using EtOAc/Hex (gradient up to 70:30 EtOAc:Hex). 4-Chloromethyl-8-(7,7-dimethyl-5,9-dihydro-6,8-dioxa-benzocyclohepten-2-ylmethoxy)-7-methoxy-chromen-2-one was collected as an off-white powder at 37% yield. ^{1}H NMR (500 MHz, CDCl$_3$) δ 7.34 (dd, J = 8.0, 4.4 Hz, 2H), 7.29 (s, 1H), 7.06 (d, J = 7.7 Hz, 1H), 6.90 (d, J = 9.0 Hz, 1H), 6.41 (s, 1H), 5.14 (s, 2H), 4.86 (d, J = 15.5 Hz, 4H), 4.61 (s, 2H), 3.94 (s, 3H), 1.51 (s, 6H). ^{13}C NMR (126 MHz, CDCl$_3$) δ 159.96, 155.94, 149.59, 148.26, 138.27, 138.17, 135.44, 135.16, 126.81, 126.30, 126.10, 119.33, 113.05, 111.93, 108.40, 102.17, 75.13, 64.92, 64.76, 56.38, 41.39, 23.82. *m/z* calculated for C$_{23}$H$_{23}$ClO$_6$ 453.1075 [M+Na]$^+$, found 453.1085.

70
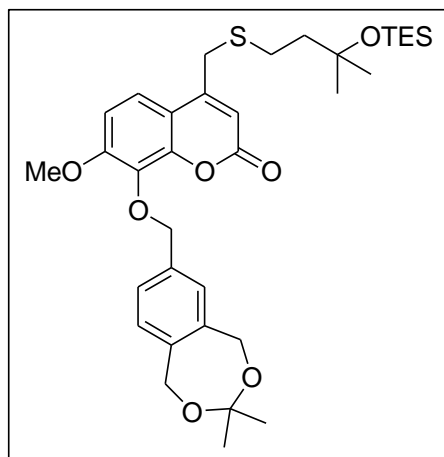
Synthesis of 8-(7,7-Dimethyl-5,9-dihydro-6,8-dioxa-benzocyclohepten-2-ylmethoxy)-7-methoxy-4-(3-methyl-3-triethylsilanyloxy-butylsulfanylmethyl)-chromen-2-one (10): Compound 3 (32.2 µL) and compound 9 (45.4 mg, 105 µmol) were charged to an RBF and dissolved in dry DMF (2 mL). TEA (22.2 µL, 158 µmol) was then added to the RBF, and the reaction stirred for 20 hours at 25°C. The reaction solution was diluted with brine (15 mL) and the crude product was extracted in DCM (30 mL). The organic layers were collected, dried over $MgSO_4$, filtered, and concentrated to dryness. The crude product was purified by column chromatography using EtOAc/Hex (gradient to 40:60 EtOAc:Hex). 8-(7,7-Dimethyl-5,9-dihydro-6,8-dioxa-benzocyclohepten-2-ylmethoxy)-7-methoxy-4-(3-methyl-3-triethylsilanyloxy-butylsulfanylmethyl)-chromen-2-one was collected as a pale-yellow oil at 76% yield. ^{1}H NMR (500 MHz, $CDCl_3$) δ 7.42 (d, J = 8.9 Hz, 1H), 7.36 (dd, J = 7.8, 1.3 Hz, 1H), 7.32 (s, 1H), 7.07 (d, J = 7.7 Hz, 1H), 6.89 (d, J = 9.0 Hz, 1H), 6.24 (s, 1H), 5.14 (s, 2H), 4.87 (d, J = 17.0 Hz, 4H), 3.93 (s, 3H), 3.74 (s, 2H), 2.65 – 2.60 (m, 2H), 1.75 – 1.70 (m, 2H), 1.52 (s, 6H), 1.23 (s, 6H), 0.93 (t, J = 7.9 Hz, 9H), 0.56 (q, J = 7.9 Hz, 6H). ^{13}C NMR (126 MHz, $CDCl_3$) δ 160.12, 155.67, 151.55, 148.53, 138.23, 138.08, 135.59, 135.18, 126.79, 126.27, 126.09, 119.93, 112.88, 112.18, 108.12, 102.16, 75.15, 72.81, 64.95, 64.78, 56.34, 44.43, 32.87, 29.83, 27.58, 23.83, 7.09, 6.69. *m/z* calculated for $C_{34}H_{48}O_7SSi$ 629.2963 [M+H]$^+$, found 629.2908.
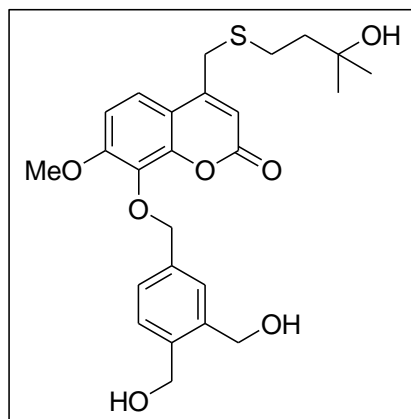
Synthesis of 8-(3,4-Bis-hydroxymethyl-benzyloxy)-4-(3-hydroxy-3-methyl-butylsulfanylmethyl)-7-methoxy-chromen-2-one (11, TM-II-21): MeOH (1 mL) and CSA (3.6 mg, 15.5 µmol) were charged to a glass vial (vial 1) and cooled to 0°C. Compound 10 (33.5 mg, 53.3 µmol) was charged to a separate glass vial (vial 2), and was also cooled to 0°C. Vial 1 was added to vial 2 and was stirred for 4 hours at 0°C. The reaction was neutralized with 20% NH_4Cl solution (pH = 7, 2 mL) and the product was extracted in MTBE (5 mL). The organic layer was collected, dried over $MgSO_4$, filtered, and concentrated to dryness. The crude product was purified by column chromatography using MeOH/DCM (gradient to 10:90 MeOH:DCM). 8-(3,4-Bis-hydroxymethyl-benzyloxy)-4-(3-hydroxy-3-methyl-butylsulfanylmethyl)-7-methoxy-chromen-2-one was collected as a white powder at 49% yield. ^{1}H NMR (500 MHz, DMSO) δ 7.61 (d, J = 9.0 Hz, 1H), 7.55 (s, 1H), 7.41 – 7.36 (m, 2H), 7.14 (d, J = 9.1 Hz, 1H), 6.33 (s, 1H), 5.10 (dt, J = 7.6, 5.5 Hz, 2H), 5.05 (s, 2H), 4.55 (dd, J = 5.3, 3.2 Hz, 4H), 4.27 (s, 1H), 3.94 (s, 3H), 3.92 (s, 2H), 2.55 – 2.52 (m, 2H), 1.64 – 1.58 (m, 2H), 1.07 (s, 6H). ^{13}C NMR (126 MHz, DMSO) δ 160.04, 155.74, 153.02, 148.27, 139.72, 139.70, 135.80, 134.72, 127.16, 127.03, 126.77, 121.49, 112.77, 111.88, 109.26, 75.16, 69.10, 60.80, 60.64, 56.93, 43.36, 31.63, 29.62, 26.90. *m/z* calculated for $C_{25}H_{30}O_7S$ 475.1785 [M+H]$^+$, found 475.1730.

3.4.2 TM-II-72 and intermediate compound characterizations
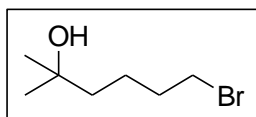
Synthesis of 6-Bromo-2-methyl-hexan-2-ol (12): Methyl 5-bromovalerate (5 mL, 34.9 mmol), dry Et_2O (13 mL), and 3Å sieves were charged to an RBF and cooled to 0°C. MeMgBr, 3.0 M in Et_2O (23.5 mL, 70.5 mmol) was added dropwise to the RBF at 0°C and stirred for 30 min. The ice bath was removed, and the reaction flask was allowed to gradually warm to 25°C over four hours. After complete conversion was seen by TLC, the reaction was quenched with 20% NH_4Cl solution (pH = 7, 10 mL). The product was extracted with Et_2O (40 mL) and washed with water (40 mL). The organic layer was collected, dried over $MgSO_4$, filtered, and concentrated to dryness. 6-Bromo-2-methyl-hexan-2-ol was collected as a yellow oil at 93% yield. No further purification was performed. ^1H NMR (500 MHz, $CDCl_3$) δ 3.31 (t, J = 6.8 Hz, 2H), 2.29 (s, 1H), 1.78 – 1.72 (m, 2H), 1.44 – 1.31 (m, 4H), 1.09 (s, 6H). ^{13}C NMR (126 MHz, $CDCl_3$) δ 70.58, 42.76, 33.76, 33.14, 29.11, 22.95.
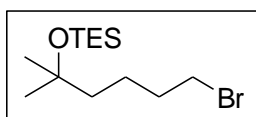
Synthesis of (5-Bromo-1,1-dimethyl-pentyloxy)-triethyl-silane (13): Compound 12 (854 mg, 4.38 mmol) and dry DCM (2.5 mL) were charged to an RBF and cooled to 0°C. TES-Cl (810 µL, 4.82 mmol) was added dropwise at 0°C, followed by 2,6-lutidine (1.1 mL, 9.44 mmol). The ice bath was removed, and the reaction mixture was allowed to gradually reach 25°C overnight. After 18 hours, the reaction was quenched with 20% NH_4Cl solution (pH = 7, 10 mL). The product was extracted in EtOAc (20 mL), washed with 10% $CuSO_4$ solution (50 mL), and brine (20 mL). The organic layer was collected, dried over $MgSO_4$, filtered, and concentrated to dryness. (5-Bromo-1,1-dimethyl-pentyloxy)-triethyl-silane was collected as a yellow oil at 82% yield. ^1H NMR (500 MHz, $CDCl_3$) δ 3.44 (t, J = 6.9 Hz, 2H), 1.91 –

1.84 (m, 2H), 1.55 – 1.49 (m, 2H), 1.47 – 1.42 (m, 2H), 1.22 (s, 6H), 0.97 (t, J = 7.9 Hz, 9H), 0.59

(q, J = 7.9 Hz, 6H). ^{13}C NMR (126 MHz, CDCl$_3$) δ 73.13, 44.10, 33.95, 33.36, 29.83, 23.09, 7.11,

6.78.
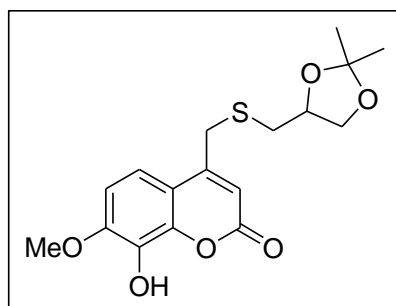
Synthesis of 4-(2,2-Dimethyl-[1,3]dioxolan-4-ylmethylsulfanylmethyl)-8-hydroxy-7-methoxy-chromen-2-one (14): Compound 8 (936 mg, 3.89 mmol) was charged to an RBF and dissolved in dry ACN (10 mL). α-Thioglycerol (360 uL,

4.16 mmol) was added to the RBF in one portion, followed by ground K$_2$CO$_3$ (700 mg, 5.06

mmol). The reaction flask was brought to reflux for 4 hours. After full conversion was visible by

TLC, the reaction was allowed to gradually reach 25°C. The crude product was concentrated to

dryness *in vacuo*, and dry acetone (25 mL) was charged to the RBF. PTSA (1.0 g, 5.26 mmol) was

added to the reaction flask in one portion, and the resulting suspension was stirred for 22 hours

at 25°C. After full conversion by TLC, the reaction flask was poured over 20% NH$_4$Cl solution (pH

= 7, 75 mL) The product was extracted in EtOAc (50 mL) and washed with brine (50 mL). The

organic layers were collected, dried over MgSO$_4$, filtered, and concentrated to dryness. The

product was purified by column chromatography using EtOAc/Hex (gradient to 70:30

EtOAc:Hex). 4-(2,2-Dimethyl-[1,3]dioxolan-4-ylmethylsulfanylmethyl)-8-hydroxy-7-methoxy-

chromen-2-one was collected as a yellow solid in 82% yield. ^{1}H NMR (500 MHz, CDCl$_3$) δ 7.25 (d,

J = 8.9 Hz, 1H), 6.91 (d, J = 8.9 Hz, 1H), 6.32 (s, 1H), 5.81 (s, 1H), 4.33 (p, J = 6.1 Hz, 1H), 4.10 (dd,

J = 8.2, 6.2 Hz, 1H), 4.01 (s, 3H), 3.93 – 3.85 (m, 2H), 3.71 (dd, J = 8.0, 6.9 Hz, 1H), 2.75 – 2.66 (m,

2H), 1.46 (s, 3H), 1.38 (s, 3H). ^{13}C NMR (126 MHz, CDCl$_3$) δ 159.87, 151.50, 149.48, 142.27,

133.14, 115.65, 112.64, 112.58, 109.84, 107.47, 75.91, 68.64, 56.56, 34.66, 32.91, 26.87, 25.50.

m/z calculated for $C_{17}H_{20}O_6S$ 353.1053 [M+H]$^+$, found 353.1049.

Synthesis of 4-(2,2-Dimethyl-[1,3]dioxolan-4-ylmethylsulfanylmethyl)-8-(5-hydroxy-5-methyl-hexyloxy)-7-methoxy-chromen-2-one (15): Compound 14 (313 mg, 888 µmol), compound 13 (550 µL, 1.78 mmol), and dry ACN (5 mL) were charged to an RBF. In one portion, K_2CO_3 (307 mg, 2.22 mmol) was added to the RBF, which was subsequently brought to reflux. The mixture was refluxed for 18 hours before gradually cooling to 25°C. ACN was removed *in vacuo*, and EtOAc (20 mL) was charged to the RBF. The mixture was washed with 20% NH_4Cl solution (pH = 7, 40 mL) and brine (40 mL). The organic layer was collected, dried over $MgSO_4$, filtered, and concentrated to dryness. The resulting product was purified by column chromatography using EtOAc/Hex (gradient to 70:30 EtOAc:Hex). 4-(2,2-Dimethyl-[1,3]dioxolan-4-ylmethylsulfanylmethyl)-8-(5-hydroxy-5-methyl-hexyloxy)-7-methoxy-chromen-2-one was collected as a pale-yellow oil at 52% yield. ^{1}H NMR (500 MHz, CDCl$_3$) δ 7.42 (d, *J* = 8.9 Hz, 1H), 6.92 (d, *J* = 9.0 Hz, 1H), 6.30 (s, 1H), 4.33 (p, *J* = 6.2 Hz, 1H), 4.14 (t, *J* = 6.1 Hz, 2H), 4.10 (dd, *J* = 8.2, 6.2 Hz, 1H), 3.96 (s, 3H), 3.92 – 3.84 (m, 2H), 3.71 (dd, *J* = 8.2, 6.9 Hz, 1H), 2.77 – 2.65 (m, 2H), 1.87 – 1.82 (m, 2H), 1.76 – 1.69 (m, 2H), 1.65 – 1.60 (m, 2H), 1.46 (s, 3H), 1.38 (s, 3H), 1.27 (s, 6H). ^{13}C NMR (126 MHz, CDCl$_3$) δ 160.51, 155.90, 151.32, 148.60, 135.79, 119.69, 112.77, 112.62, 109.85, 108.23, 75.88, 73.82, 70.82, 68.64, 56.36, 43.39, 34.65, 32.95, 30.34, 29.19, 26.87, 25.50, 20.60.
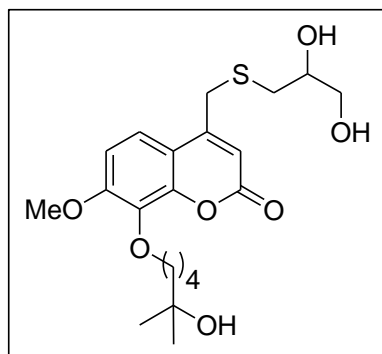
Synthesis of 4-(2,3-Dihydroxy-propylsulfanylmethyl)-8-(5-hydroxy-5-methyl-hexyloxy)-7-methoxy-chromen-2-one (16, TM-II-72): Compound 15 (9.95 mg, 21.3 μmol) was charged to an RBF, followed by the addition of 0.01 M HCl in MeOH (1 mL). The reaction flask stirred for six hours at 25°C. Upon full conversion seen by TLC, the stirring reaction was neutralized with the dropwise addition of saturated KHCO$_3$ solution until CO$_2$ evolution ceased. The crude product was concentrated, redissolved in MeOH, and filtered through an MgSO$_4$ plug. The isolation process was subsequently repeated by concentrating and redissolving the product in CHCl$_3$, filtration through an MgSO$_4$ plug, and concentrating the final product to dryness. 4-(2,3-Dihydroxy-propylsulfanylmethyl)-8-(5-hydroxy-5-methyl-hexyloxy)-7-methoxy-chromen-2-one was isolated as a white powder in 48% yield. ^{1}H NMR (500 MHz, MeOD) δ 7.62 (d, J = 9.0 Hz, 1H), 7.11 (d, J = 9.0 Hz, 1H), 6.35 (s, 1H), 4.11 (t, J = 6.3 Hz, 2H), 3.98 (d, J = 2.4 Hz, 5H), 3.79 (dq, J = 10.5, 5.3 Hz, 1H), 3.57 (dd, J = 5.4, 1.2 Hz, 2H), 3.37 (s, 2H), 2.77 (dd, J = 13.7, 5.0 Hz, 1H), 2.62 (dd, J = 13.7, 7.1 Hz, 1H), 1.83 – 1.76 (m, 2H), 1.70 – 1.61 (m, 2H), 1.59 – 1.54 (m, 2H), 1.23 (s, 6H). ^{13}C NMR (126 MHz, MeOD) δ 161.34, 155.88, 153.42, 148.12, 135.23, 120.39, 112.73, 111.21, 108.42, 73.56, 71.50, 70.12, 64.48, 55.50, 43.09, 34.80, 32.13, 30.36, 27.75, 20.46. *m/z* calculated for C$_{21}$H$_{30}$O$_7$S 449.1604 [M+Na]$^+$, found 449.1574.

3.4.3 TM-II-88 and intermediate compound characterizations
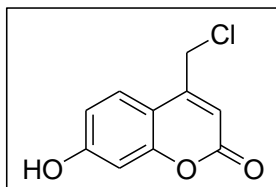
Synthesis of 4-Chloromethyl-7-hydroxy-chromen-2-one (17): Neat H_2SO_4 (40 mL) was charged to an RBF (flask 1) and cooled to 0°C. In a separate RBF (flask 2), resorcinol (3.60 g, 32.7 mmol) and ethyl 4-chloroacetoacetate (4.90 mL, 36.3 mmol) were combined. Flask 2 was added to flask 1 in a dropwise manner at 0°C. H_2SO_4 (20 mL) was used to rinse flask 2, which was subsequently transferred to flask 1. The ice bath was removed, and the reaction gradually warmed up over the course of 4.5 hours. The reaction mixture was then carefully poured over ice water, forming a solid precipitate. The precipitate was filtered and rinsed with water until the filtrate pH was neutral (pH = 6). The crude product was left to dry on the vacuum filter overnight. The crude product was purified by column chromatography using EtOAc/Hex (gradient to 60:40 EtOAc:Hex). 4-Chloromethyl-7-hydroxy-chromen-2-one was collected as a off-white solid in 47% yield. ^{1}H NMR (500 MHz, Acetone) δ 7.74 (d, J = 8.7 Hz, 1H), 6.92 (dd, J = 8.7, 2.4 Hz, 1H), 6.81 (d, J = 2.4 Hz, 1H), 6.42 (s, 1H), 4.93 (d, J = 0.7 Hz, 2H). ^{13}C NMR (126 MHz, Acetone) δ 161.23, 159.89, 155.92, 150.54, 126.32, 112.83, 111.70, 110.10, 102.77, 41.27.

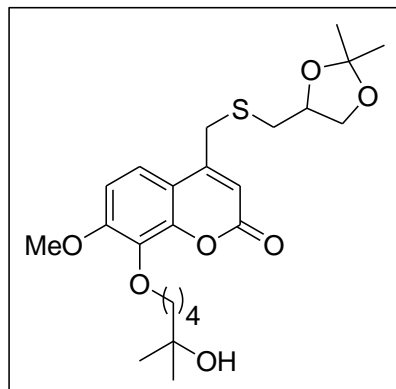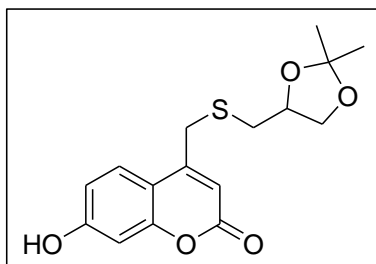**Synthesis of 4-(2,2-Dimethyl-[1,3]dioxolan-4-ylmethylsulfanylmethyl)-7-hydroxy-chromen-2-one (18):** Compound (17) (660 mg, 3.13 mmol) was charged to an RBF and dissolved in dry ACN (8 mL). α-Thioglycerol (291 uL, 3.36 mmol) was added to the RBF, followed by K_2CO_3 (466 mg, 3.37 mmol). The reaction flask was refluxed overnight before allowing to gradually cool to 25°C. Upon full conversion by TLC, removal of

77

ACN was done *in vacuo* and dry acetone (10 mL) was charged to the RBF. PTSA (680 mg, 3.57

mmol) was added to the RBF, and the reaction stirred for 22 hours at 25°C before acetone was

removed *in vacuo*. The crude product was dissolved in EtOAc (20 mL) and washed with 20%

NH_4Cl solution (pH = 7, 40 mL) and brine (40 mL). The organic layer was collected, dried over

$MgSO_4$, filtered, and concentrated to dryness. The product was purified by column

chromatography using EtOAc/Hex (gradient to 70:30 EtOAc:Hex). 4-(2,2-Dimethyl-[1,3]dioxolan-

4-ylmethylsulfanylmethyl)-7-hydroxy-chromen-2-one was collected as a pale-yellow powder in

30% yield (over two steps). ^{1}H NMR (500 MHz, $CDCl_3$) δ 7.73 (s, 1H), 7.62 (d, *J* = 8.8 Hz, 1H), 7.00

(d, *J* = 2.4 Hz, 1H), 6.90 (dd, *J* = 8.8, 2.4 Hz, 1H), 6.30 (s, 1H), 4.36 – 4.30 (m, 1H), 4.10 (dd, *J* =

8.3, 6.1 Hz, 1H), 3.94 – 3.85 (m, 2H), 3.71 (dd, *J* = 8.3, 6.7 Hz, 1H), 2.76 – 2.67 (m, 2H), 1.46 (s,

3H), 1.38 (s, 3H). ^{13}C NMR (126 MHz, MeOD) δ 162.04, 161.64, 155.79, 153.33, 126.44, 112.82,

110.62, 110.19, 109.36, 102.27, 75.97, 68.23, 34.08, 31.93, 25.72, 24.35. *m/z* calculated for

$C_{16}H_{18}O_5S$ 321.0802 [M-H]$^-$, found 321.0775.
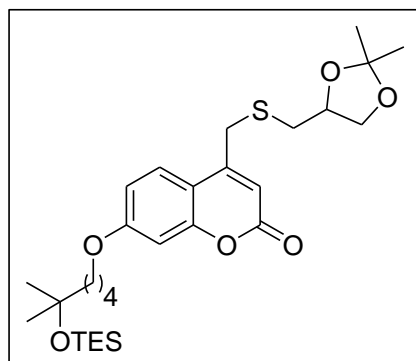
Synthesis of 4-(2,2-Dimethyl-[1,3]dioxolan-4-ylmethylsulfanylmethyl)-7-(5-methyl-5-triethylsilanyloxy-hexyloxy)-chromen-2-one (19): Compound 18 (67.3 mg, 209 μmol), compound 13 (71.0 μL), and dry ACN (3.5 mL) were charged to an RBF. In one portion, K_2CO_3 (72.9 mg, 527 μmol) was added to the RBF, which was subsequently brought to reflux. The mixture was refluxed for

18 hours before gradually cooling to 25°C. ACN was removed *in vacuo*, and EtOAc (15 mL) was

charged to the RBF. The mixture was washed with 20% NH_4Cl solution (pH = 7, 30 mL) and brine

(20 mL). The organic layer was collected, dried over $MgSO_4$, filtered, and concentrated to

dryness. The crude product was purified by column chromatography using EtOAc/Hex (gradient to 50:50 EtOAc:Hex). 4-(2,2-Dimethyl-[1,3]dioxolan-4-ylmethylsulfanylmethyl)-7-(5-methyl-5-triethylsilanyloxy-hexyloxy)-chromen-2-one was collected as a yellow oil at 47% yield. ^{1}H NMR (500 MHz, CDCl$_3$) δ 7.61 (d, J = 8.9 Hz, 1H), 6.88 (dd, J = 8.8, 2.5 Hz, 1H), 6.84 (d, J = 2.4 Hz, 1H), 6.27 (s, 1H), 4.35 – 4.29 (m, 1H), 4.09 (dd, J = 8.3, 6.1 Hz, 1H), 4.05 (t, J = 6.5 Hz, 2H), 3.88 (d, J = 3.4 Hz, 2H), 3.71 (dd, J = 8.3, 6.7 Hz, 1H), 2.70 (qd, J = 13.8, 5.8 Hz, 2H), 1.86 – 1.79 (m, 2H), 1.60 – 1.53 (m, 2H), 1.52 – 1.48 (m, 2H), 1.46 (s, 3H), 1.38 (s, 3H), 1.23 (s, 6H), 0.96 (t, J = 7.9 Hz, 9H), 0.59 (q, J = 7.9 Hz, 6H). ^{13}C NMR (126 MHz, CDCl$_3$) δ 162.42, 161.01, 155.96, 151.20, 125.65, 112.82, 112.03, 111.36, 109.82, 101.64, 75.86, 73.19, 68.65, 68.63, 44.68, 34.57, 32.89, 29.88, 29.48, 26.86, 25.50, 20.77, 7.13, 6.79. m/z calculated for C$_{29}$H$_{46}$O$_6$SSi 551.2857 [M+H]$^+$, found 551.2879.
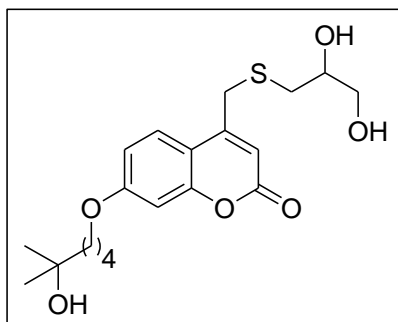
Synthesis of 4-(2,3-Dihydroxy-propylsulfanylmethyl)-7-(5-hydroxy-5-methyl-hexyloxy)-chromen-2-one (20, TM-II-88): Compound 19 (16.6 mg, 30.1 μmol) was charged to an RBF, followed by the addition of 0.05 M HCl in MeOH (3 mL). The reaction flask stirred for eight hours at 25°C and was then neutralized with the dropwise addition 1.0 M NaOH (150 μL). The crude product was concentrated to dryness and purified by reverse-phase column chromatography using MeOH/Water (gradient to 80:20 MeOH:Water). 4-(2,3-Dihydroxy-propylsulfanylmethyl)-7-(5-hydroxy-5-methyl-hexyloxy)-chromen-2-one was isolated as a white crystalline solid in 74% yield. ^{1}H NMR (500 MHz, MeOD) δ 7.81 (d, J = 8.9 Hz, 1H), 6.97 (dd, J = 8.9, 2.5 Hz, 1H), 6.93 (d, J = 2.5 Hz, 1H), 6.32 (s, 1H), 4.12 (t, J = 6.4 Hz, 2H), 3.98 (d, J = 2.1 Hz, 2H), 3.79 (dq, J = 7.0, 5.2

Hz, 1H), 3.56 (dd, *J* = 5.4, 1.7 Hz, 2H), 2.76 (dd, *J* = 13.7, 5.0 Hz, 1H), 2.62 (dd, *J* = 13.7, 7.0 Hz,

1H), 1.88 – 1.80 (m, 2H), 1.63 – 1.53 (m, 4H), 1.22 (s, 6H). ^{13}C NMR (126 MHz, MeOD) δ 162.60,

161.87, 155.74, 153.28, 126.29, 112.49, 111.48, 110.79, 100.97, 71.50, 69.93, 68.32, 64.48,

43.01, 34.72, 32.08, 29.35, 27.76, 20.51. *m/z* calculated for $C_{20}H_{28}O_6S$ 397.1679 [M+H]$^+$, found

397.1669.

3.4.4   TM-III-20 and intermediate compound characterizations
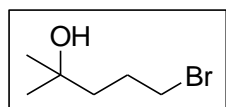
Synthesis of 5-Bromo-2-methyl-pentan-2-ol (21): Methyl 4-bromobutyrate

(5 mL, 39.6 mmol), dry Et$_2$O (13 mL), and 3Å sieves were charged to an RBF

and cooled to 0°C. MeMgBr, 3.0 M in Et$_2$O (26.5 mL, 79.5 mmol) was added dropwise to the RBF

at 0°C and stirred for 30 min. The ice bath was removed, and the reaction flask was allowed to

gradually warm to 25°C over four hours. After complete conversion was seen by TLC, the

reaction was quenched with 20% NH$_4$Cl solution (pH = 7, 10 mL). The product was extracted

with Et$_2$O (40 mL) and washed with water (40 mL). The organic layer was collected, dried over

MgSO$_4$, filtered, and concentrated to dryness. 5-Bromo-2-methyl-pentan-2-ol was collected as a

yellow oil at 88% yield. No further purification was performed. ^{1}H NMR (500 MHz, CDCl$_3$) δ 3.44

(t, *J* = 6.7 Hz, 2H), 3.34 (s, 1H), 2.00 – 1.92 (m, 2H), 1.64 – 1.59 (m, 2H), 1.25 (s, *J* = 8.8 Hz, 6H).

^{13}C NMR (126 MHz, CDCl$_3$) δ 71.33, 42.09, 34.35, 29.21, 27.85.
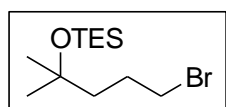
Synthesis of (4-Bromo-1,1-dimethyl-butoxy)-triethyl-silane (22): Compound

21 (1.60 g, 8.84 mmol) and dry DCM (5 mL) were charged to an RBF and

cooled to 0°C. TES-Cl (1.75 mL, 10.4 mmol) was added dropwise at 0°C, followed by 2,6-lutidine

(2.06 mL, 17.7 mmol). The ice bath was removed, and the reaction mixture was allowed to gradually reach 25°C overnight. After 18 hours, the reaction was quenched with 20% NH_4Cl solution (pH = 7, 10 mL). The product was extracted in EtOAc (20 mL), washed with 10% $CuSO_4$ solution (50 mL), and brine (20 mL). The organic layer was collected, dried over $MgSO_4$, filtered, and concentrated to dryness. (4-Bromo-1,1-dimethyl-butoxy)-triethyl-silane was collected as a yellow oil in 86% yield. ^1H NMR (500 MHz, $CDCl_3$) δ 3.43 (t, J = 6.8 Hz, 2H), 2.01 – 1.94 (m, 2H), 1.58 – 1.53 (m, 2H), 1.24 (s, 6H), 0.96 (t, J = 8.0 Hz, 9H), 0.59 (q, J = 7.9 Hz, 6H). ^{13}C NMR (126 MHz, $CDCl_3$) δ 72.81, 43.60, 34.66, 29.89, 28.05, 7.07, 6.75.
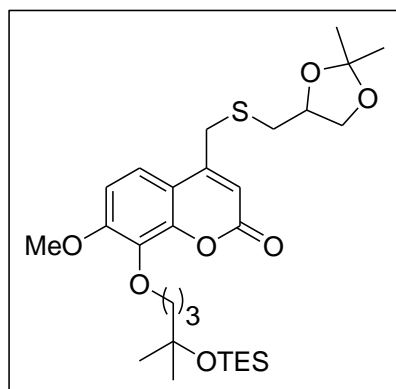
Synthesis of 4-(2,2-Dimethyl-[1,3]dioxolan-4-ylmethylsulfanylmethyl)-7-methoxy-8-(4-methyl-4-triethylsilanyloxy-pentyloxy)-chromen-2-one (23):

Compound 14 (57.5 mg, 163 µmol), compound 22 (60 µL), and dry ACN (5 mL) were charged to an RBF. In one portion, K_2CO_3 (40 mg, 289 µmol) was added to the RBF, which was subsequently brought to reflux. The mixture was refluxed for 18 hours before gradually cooling to 25°C. ACN was removed *in vacuo*, and EtOAc (15 mL) was charged to the RBF. The mixture was washed with 20% NH_4Cl solution (pH = 7, 30 mL) and brine (20 mL). The organic layer was collected, dried over $MgSO_4$, filtered, and concentrated to dryness. The product was purified by column chromatography using EtOAc/Hex (gradient to 70:30 EtOAc:Hex). 4-(2,2-Dimethyl-[1,3]dioxolan-4-ylmethylsulfanylmethyl)-7-methoxy-8-(4-methyl-4-triethylsilanyloxy-pentyloxy)-chromen-2-one was collected as a pale-yellow oil at 70% yield. ^1H NMR (500 MHz, $CDCl_3$) δ 7.40 (d, J = 8.9 Hz, 1H), 6.91 (d, J = 9.0 Hz, 1H), 6.29 (s, 1H), 4.35 – 4.29 (m, 1H), 4.14 (t, J = 6.8 Hz, 2H), 4.10 (dd, J =

8.3, 6.1 Hz, 1H), 3.96 (s, 3H), 3.88 (d, J = 2.3 Hz, 2H), 3.71 (dd, J = 8.2, 6.8 Hz, 1H), 2.76 – 2.65 (m, 2H), 1.96 – 1.86 (m, 2H), 1.68 – 1.61 (m, 2H), 1.46 (s, 3H), 1.38 (s, 3H), 1.26 (s, 6H), 0.95 (t, J = 7.9 Hz, 9H), 0.58 (q, J = 7.9 Hz, 6H). ^{13}C NMR (126 MHz, CDCl$_3$) δ 160.26, 155.78, 151.06, 148.58, 135.85, 119.47, 112.74, 112.66, 109.82, 108.15, 75.86, 74.99, 73.18, 68.64, 56.32, 41.05, 34.65, 32.96, 29.93, 26.87, 25.50, 25.26, 7.12, 6.76. m/z calculated for C$_{29}$H$_{46}$O$_7$SSi 567.2806 [M+H]$^+$, found 567.2834.
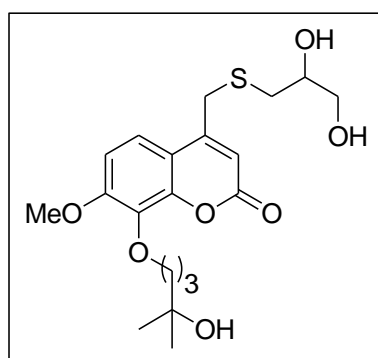
Synthesis of 4-(2,3-Dihydroxy-propylsulfanylmethyl)-8-(4-hydroxy-4-methyl-pentyloxy)-7-methoxy-chromen-2-one (24, TM-III-20): Compound 23 (32.6 mg, 57.5 μmol) was charged to an RBF, followed by the addition of 0.05 M HCl in MeOH (4 mL). The reaction flask stirred for four hours at 25°C. After full conversion was seen by TLC, the reaction was neutralized with the dropwise addition 1.0 M NaOH (200 μL) and concentrated to dryness. The crude product was purified by reverse-phase column chromatography using MeOH/Water (gradient to 70:30 MeOH:Water). 4-(2,3-Dihydroxy-propylsulfanylmethyl)-8-(4-hydroxy-4-methyl-pentyloxy)-7-methoxy-chromen-2-one was collected in 90% yield. ^{1}H NMR (500 MHz, MeOD) δ 7.60 (d, J = 9.0 Hz, 1H), 7.08 (d, J = 9.0 Hz, 1H), 6.33 (s, 1H), 4.08 (t, J = 6.4 Hz, 2H), 3.96 (d, J = 2.5 Hz, 5H), 3.77 (dq, J = 6.9, 5.2 Hz, 1H), 3.54 (dd, J = 5.4, 1.4 Hz, 2H), 2.74 (dd, J = 13.7, 5.0 Hz, 1H), 2.60 (dd, J = 13.7, 7.0 Hz, 1H), 1.87 – 1.82 (m, 2H), 1.73 – 1.69 (m, 2H), 1.22 (s, 6H). ^{13}C NMR (126 MHz, MeOD) δ 162.77, 157.30, 154.85, 149.57, 136.64, 121.84, 114.18, 112.67, 109.87, 75.74, 72.96, 71.30, 65.93, 56.93, 40.96, 36.25, 33.58, 29.26, 26.32. m/z calculated for C$_{20}$H$_{28}$O$_7$S 411.1483 [M-H]$^-$, found 411.1496.

3.4.5 TM-III-31 and intermediate compound characterizations
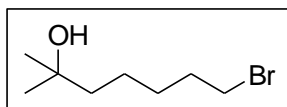
Synthesis of 7-Bromo-2-methyl-heptan-2-ol (25): Methyl 6-bromohexanoate (1.09 g, 5.21 mmol), dry Et_2O (5 mL), and 3Å sieves were charged to an RBF and cooled to 0°C. MeMgBr, 3.0 M in Et_2O (3.6 mL, 10.8 mmol) was added dropwise to the RBF at 0°C and stirred for 30 min. The ice bath was removed, and the reaction flask was allowed to gradually warm to 25°C over four hours. After complete conversion was seen by TLC, the reaction was quenched with 20% NH_4Cl solution (pH = 7, 10 mL). The product was extracted with Et_2O (20 mL) and washed with water (20 mL). The organic layer was collected, dried over $MgSO_4$, filtered, and concentrated to dryness. 7-Bromo-2-methyl-heptan-2-ol was collected as a pale-yellow oil at 96% yield. No further purification was performed. ^{1}H NMR (500 MHz, $CDCl_3$) δ 3.42 (t, J = 6.8 Hz, 2H), 1.89 (p, 2H), 1.48 – 1.37 (m, 6H), 1.21 (s, 6H). ^{13}C NMR (126 MHz, $CDCl_3$) δ 70.89, 43.67, 33.87, 32.77, 29.26, 28.67, 23.51.
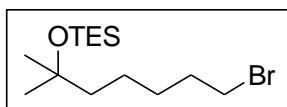
Synthesis of (6-Bromo-1,1-dimethyl-hexyloxy)-triethyl-silane (26): Compound 25 (1.05 g, 5.02 mmol) and dry DCM (5 mL) were charged to an RBF and cooled to 0°C. TES-Cl (1.7 mL, 10.1 mmol) was added dropwise at 0°C, followed by 2,6-lutidine (900 μL, 7.73 mmol). The ice bath was removed, and the reaction mixture was allowed to gradually reach 25°C overnight. After 18 hours, the reaction was quenched with 20% NH_4Cl solution (pH = 7, 10 mL). The product was extracted in EtOAc (20 mL), washed with 10% $CuSO_4$ solution (50 mL), and brine (20 mL). The organic layer was collected, dried over $MgSO_4$, filtered, and concentrated to dryness. (6-Bromo-1,1-dimethyl-hexyloxy)-triethyl-silane was collected as a pale-yellow oil at 60% yield. ^{1}H NMR (500 MHz, $CDCl_3$) δ 3.43 (t, J = 6.9 Hz, 2H),

1.93 – 1.85 (m, 2H), 1.48 – 1.38 (m, 6H), 1.21 (s, 6H), 0.96 (t, *J* = 7.9 Hz, 9H), 0.58 (q, *J* = 7.9 Hz,

6H). ^{13}C NMR (126 MHz, CDCl$_3$) δ 73.22, 44.86, 33.93, 32.91, 29.85, 28.74, 23.51, 7.11, 6.79.
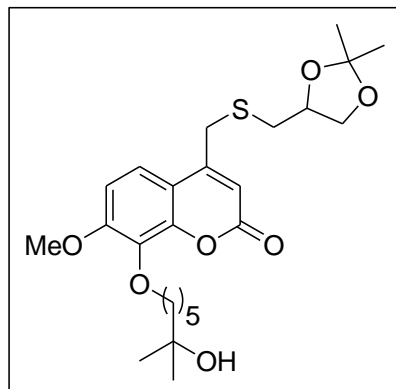
Synthesis of 4-(2,2-Dimethyl-[1,3]dioxolan-4-ylmethylsulfanylmethyl)-8-(6-hydroxy-6-methyl-heptyloxy)-7-methoxy-chromen-2-one (27): Compound 14 (44.5 mg, 126 µmol), compound 26 (47 µL), and dry ACN (5 mL) were charged to an RBF. In one portion, K$_2$CO$_3$ (39.5 mg, 286 µmol) was added to the RBF, which was subsequently brought to reflux.

The mixture was refluxed for five hours before gradually cooling to 25°C. ACN was removed *in vacuo*, and CHCl$_3$ (15 mL) was charged to the RBF. The mixture was washed with 20% NH$_4$Cl solution (pH = 7, 30 mL) and brine (20 mL). The organic layer was collected, dried over MgSO$_4$, filtered, and concentrated to dryness. The product was purified by column chromatography using EtOAc/Hex (gradient to 100% EtOAc). 4-(2,2-Dimethyl-[1,3]dioxolan-4-ylmethylsulfanylmethyl)-8-(6-hydroxy-6-methyl-heptyloxy)-7-methoxy-chromen-2-one was collected as a pale-yellow oil at 84% yield. ^{1}H NMR (500 MHz, CDCl$_3$) δ 7.41 (d, *J* = 8.9 Hz, 1H), 6.91 (d, *J* = 9.0 Hz, 1H), 6.29 (s, 1H), 4.32 (p, *J* = 6.1 Hz, 1H), 4.13 (t, *J* = 6.5 Hz, 2H), 4.09 (dd, *J* = 8.3, 6.2 Hz, 1H), 3.96 (s, 3H), 3.91 – 3.84 (m, 2H), 3.71 (dd, *J* = 8.2, 6.8 Hz, 1H), 2.75 – 2.65 (m, 2H), 1.90 – 1.83 (m, 2H), 1.62 – 1.48 (m, 6H), 1.46 (s, 3H), 1.38 (s, 3H), 1.24 (s, 6H). ^{13}C NMR (126 MHz, CDCl$_3$) δ 160.41, 155.82, 151.22, 148.57, 135.80, 119.60, 112.75, 112.63, 109.82, 108.21, 75.86, 73.80, 70.86, 68.63, 56.36, 43.94, 34.63, 32.93, 29.95, 29.26, 26.87, 26.19, 25.50, 23.79.
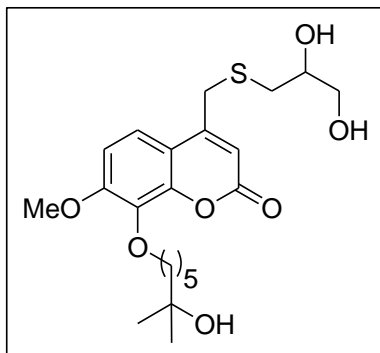
Synthesis of 4-(2,3-Dihydroxy-propylsulfanylmethyl)-8-(6-hydroxy-6-methyl-heptyloxy)-7-methoxy-chromen-2-one (28, TM-III-31): Compound 27 (41.5 mg, 86.3 µmol) was charged to an RBF, followed by the addition of 0.01 M HCl in MeOH (3 mL). The reaction flask stirred for eight hours at 25°C. After conversion was observed by TLC, the reaction was neutralized with the dropwise addition 1.0 M NaOH (30 µL) and concentrated to dryness. The crude product was purified by reverse-phase column chromatography using MeOH/Water (gradient to 70:30 MeOH:Water). 4-(2,3-Dihydroxy-propylsulfanylmethyl)-8-(6-hydroxy-6-methyl-heptyloxy)-7-methoxy-chromen-2-one was isolated in 91% yield. ^{1}H NMR (500 MHz, MeOD) δ 7.62 (d, J = 9.0 Hz, 1H), 7.10 (d, J = 9.0 Hz, 1H), 6.35 (s, 1H), 4.10 (t, J = 6.4 Hz, 2H), 3.98 (s, 5H), 3.79 (dq, J = 6.9, 5.2 Hz, 1H), 3.57 (dd, J = 5.4, 1.4 Hz, 2H), 2.77 (dd, J = 13.7, 5.0 Hz, 1H), 2.62 (dd, J = 13.7, 7.1 Hz, 1H), 1.86 – 1.78 (m, 2H), 1.61 – 1.44 (m, 6H), 1.20 (s, 6H). ^{13}C NMR (126 MHz, MeOD) δ 161.33, 155.86, 153.40, 148.11, 135.21, 120.38, 112.72, 111.21, 108.43, 73.62, 71.49, 70.08, 64.48, 55.51, 43.39, 34.81, 32.13, 29.75, 27.77, 26.20, 23.74. *m/z* calculated for $C_{22}H_{32}O_7S$ 439.1796 [M-H]$^-$, found 439.1819.

3.4.6 TM-III-90, TM-III-91, and intermediate compound characterizations
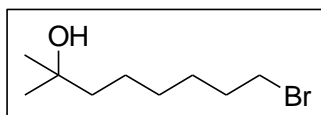
Synthesis of 8-Bromo-2-methyl-octan-2-ol (29): Ethyl 7-bromoheptanoate (5 mL, 25.7 mmol), dry Et$_2$O (15 mL), and 3Å sieves were charged to an RBF and cooled to 0°C. MeMgBr, 3.0 M in Et$_2$O (19.5 mL, 58.5 mmol)

was added dropwise to the RBF at 0°C and stirred for 30 min. The ice bath was removed, and the reaction flask was allowed to gradually warm to 25°C over four hours. After complete conversion was seen by TLC, the reaction was quenched with 20% NH_4Cl solution (pH = 7, 10 mL). The product was extracted with Et_2O (40 mL) and washed with water (40 mL). The organic layer was collected, dried over $MgSO_4$, filtered, and concentrated to dryness. The crude product was purified by column chromatography using EtOAc/Hex (gradient to 30:70 EtOAc:Hex). 8-Bromo-2-methyl-octan-2-ol was collected as a pale-yellow oil in 99% yield. ^{1}H NMR (500 MHz, CDCl$_3$) δ 3.42 (t, J = 6.8 Hz, 2H), 1.91 − 1.84 (m, 2H), 1.50 − 1.44 (m, 4H), 1.41 − 1.34 (m, 4H), 1.22 (s, 6H). ^{13}C NMR (126 MHz, CDCl$_3$) δ 70.97, 43.80, 33.95, 32.75, 29.29, 29.25, 28.15, 24.16.
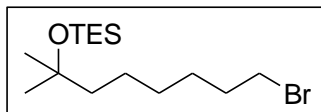
Synthesis of (7-Bromo-1,1-dimethyl-heptyloxy)-triethyl-silane (30): Compound 29 (2.27 g, 9.57 mmol) and dry DCM (3.8 mL) were charged to an RBF and cooled to -78°C. TES-OTf (2.60 mL, 11.5 mmol) was added dropwise at -78°C, followed by 2,6-lutidine (2.23 mL, 19.1 mmol). The dry ice/acetone bath was removed and the reaction mixture was allowed to gradually reach 25°C overnight. After 18 hours, the reaction was quenched with 20% NH_4Cl solution (pH = 7, 20 mL). The product was extracted in EtOAc (30 mL), washed with 10% $CuSO_4$ solution (50 mL), and brine (20 mL). The organic layer was collected, dried over $MgSO_4$, filtered, and concentrated to dryness. (7-Bromo-1,1-dimethyl-heptyloxy)-triethyl-silane was collected as a yellow oil at 87% yield. ^{1}H NMR (500 MHz, CDCl$_3$) δ 3.43 (t, J = 6.9 Hz, 2H), 1.93 − 1.84 (m, 2H), 1.50 − 1.28 (m, 8H), 1.21 (s, J = 5.3 Hz, 6H), 0.97 (t, J = 7.9 Hz, 9H), 0.58 (q, J = 7.9 Hz, 6H). ^{13}C NMR (126 MHz, CDCl$_3$) δ 73.31, 44.99, 34.01, 32.83, 29.85, 29.35, 28.24, 24.17, 7.12, 6.80.
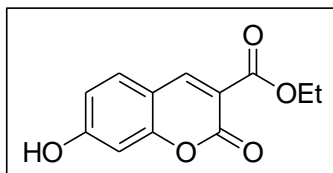
Synthesis of 7-Hydroxy-2-oxo-2*H*-chromene-3-carboxylic acid ethyl ester (31): 2,4-Dihydroxybenzaldehyde (3.5 g, 25.3 mmol) and diethyl malonate (3.9 mL, 25.3 mmol) were charged to an RBF and vigorously stirred at 25°C. Piperidine (2.5 mL, 25.3 mmol) was added dropwise to the reaction flask and the mixture was stirred for one hour at 25°C. After full conversion was seen by TLC, the reaction mixture was slowly poured over 1.0 M HCl and ice. The resulting slurry was stirred for 15 minutes before filtering the precipitate, which was subsequently washed with water until the filtrate ran clear and the pH was neutral (pH = 6). The solid product was left to dry on the vacuum filter overnight. Recrystallization of the product was achieved in anhydrous EtOH. 7-Hydroxy-2-oxo-2*H*-chromene-3-carboxylic acid ethyl ester was collected as white crystals at 51% yield. ^{1}H NMR (500 MHz, CDCl$_3$) δ 8.55 (s, 1H), 7.53 (d, *J* = 8.5 Hz, 1H), 6.93 (s, 1H), 6.90 (dd, *J* = 8.5, 2.3 Hz, 1H), 6.46 (s, 1H), 4.43 (q, *J* = 7.1 Hz, 2H), 1.43 (t, *J* = 7.1 Hz, 3H). ^{13}C NMR (126 MHz, CDCl$_3$) δ 163.41, 161.99, 157.52, 157.32, 149.22, 131.30, 114.15, 113.98, 111.81, 103.09, 61.81, 14.29. *m/z* calculated for C$_{12}$H$_{10}$O$_5$ 233.0455 [M-H]$^-$, found 233.0455.
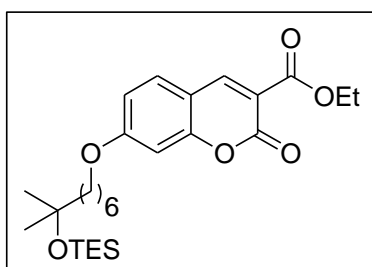
Synthesis of 7-(7-Methyl-7-triethylsilanyloxy-octyloxy)-2-oxo-2*H*-chromene-3-carboxylic acid ethyl ester (32): Compound 31 (118 mg, 504 µmol) and K$_2$CO$_3$ (150 mg, 1.09 mmol) were charged to an RBF and dissolved in dry ACN (5 mL). Compound 30 (339 µL, 1.00 mmol) was added to the reaction flask in one portion, and the reaction was subsequently brought to reflux. The reaction was held at reflux for 72 hours and was then allowed to return to 25°C. The ACN was removed in vacuo, and the solids were resuspended in Et$_2$O (20 mL). The organic layer was washed with 20% NH$_4$Cl solution (pH = 7, 20 mL) and water

(15 mL). The organic layers were collected, dried over MgSO₄, filtered, and concentrated to dryness. The crude product was purified by column chromatography using EtOAc/Hex (gradient to 50:50 EtOAc:Hex). 7-(7-Methyl-7-triethylsilanyloxy-octyloxy)-2-oxo-2*H*-chromene-3-carboxylic acid ethyl ester was collected as a white powder in 54% yield. ^{1}H NMR (500 MHz, CDCl₃) δ 8.52 (s, 1H), 7.51 (d, *J* = 8.7 Hz, 1H), 6.90 (dd, *J* = 8.7, 2.4 Hz, 1H), 6.82 (d, *J* = 2.3 Hz, 1H), 4.42 (q, *J* = 7.1 Hz, 2H), 4.06 (t, *J* = 6.5 Hz, 2H), 1.88 – 1.81 (m, 2H), 1.54 – 1.37 (m, 11H), 1.21 (s, 6H), 0.96 (t, *J* = 7.9 Hz, 9H), 0.58 (q, *J* = 7.9 Hz, 6H). ^{13}C NMR (126 MHz, CDCl₃) δ 164.78, 163.53, 157.62, 157.23, 149.02, 130.63, 114.03, 113.90, 111.46, 100.79, 73.32, 68.98, 61.68, 45.01, 29.86, 28.86, 25.97, 24.24, 14.30, 7.13, 6.80. *m/z* calculated for $C_{27}H_{42}O_6Si$ 513.2643 [M+Na]⁺, found 513.2672.
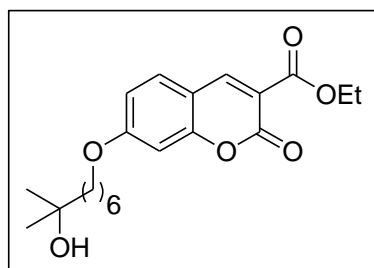
Synthesis of 7-(7-Hydroxy-7-methyl-octyloxy)-2-oxo-2*H*-chromene-3-carboxylic acid ethyl ester (33, TM-III-90):

Compound 32 (52.1 mg, 106 µmol) was charged to a glass vial, followed by the addition of 0.015 M HCl in EtOH (1.5 mL) and THF (500 µL). The reaction was stirred for three hours at 25°C. After full conversion was seen by TLC, the reaction was neutralized with 0.1 M LiOH (225 µL). The crude product was concentrated to dryness and purified by column chromatography using EtOAc/Hex (gradient to 60:40 EtOAc:Hex). 7-(7-Hydroxy-7-methyl-octyloxy)-2-oxo-2*H*-chromene-3-carboxylic acid ethyl ester was collected as a white crystalline solid in 91% yield. ^{1}H NMR (500 MHz, CDCl₃) δ 8.52 (s, 1H), 7.51 (d, *J* = 8.7 Hz, 1H), 6.89 (dd, *J* = 8.7, 2.4 Hz, 1H), 6.82 (d, *J* = 2.3 Hz, 1H), 4.42 (q, *J* = 7.1 Hz, 2H), 4.06 (t, *J* = 6.5 Hz, 2H), 1.89 – 1.81 (m, 2H), 1.56 – 1.38 (m, 11H), 1.24 (s, 6H). ^{13}C NMR (126 MHz, CDCl₃) δ 164.72, 163.51, 157.60, 157.22, 149.02, 130.66, 114.02, 113.92, 111.48,

100.78, 70.99, 68.90, 61.69, 43.81, 29.82, 29.29, 28.83, 25.93, 24.22, 14.30; *m/z* calculated for

$C_{21}H_{28}O_6$ 377.1959 [M+H]$^+$, found 377.1955.
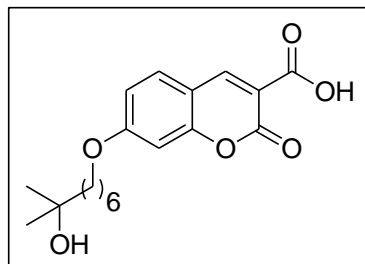
Synthesis of 7-(7-Hydroxy-7-methyl-octyloxy)-2-oxo-2*H*-chromene-3-carboxylic acid (34, TM-III-91): TM-III-90 (27.1 mg, 72.0 μmol) was charged to a glass vial and was dissolved in THF (2 mL). The resulting solution was stirred vigorously while 0.1 M LiOH (3 mL) was added dropwise to the vial. The reaction was stirred at 25°C for one hour. After full conversion was observed by TLC, the reaction was neutralized with 1.0 M HCl (300 μL). The flask was concentrated to dryness and attempted purification by reverse-phase column chromatography using MeOH/Water (gradient to 80:20 MeOH:Water). Further purification was achieved through acid-base extraction on the mixed column fractions. Following concentration of the crude product, 0.01 M LiOH (1 mL) was added to the product. Remaining TM-III-90 was extracted in DCM (2 mL), and the basic aqueous layer was collected and acidified using 0.01 M HCl (2 mL). The product was extracted using CHCl₃ (5 mL) and concentrated to dryness. 7-(7-Hydroxy-7-methyl-octyloxy)-2-oxo-2*H*-chromene-3-carboxylic acid was collected as a white solid in 45% yield. ¹H NMR (500 MHz, MeOD) δ 8.77 (s, 1H), 7.75 (d, *J* = 8.7 Hz, 1H), 7.03 (dd, *J* = 8.7, 2.3 Hz, 1H), 7.00 (d, *J* = 2.3 Hz, 1H), 4.16 (t, *J* = 6.4 Hz, 2H), 1.90 – 1.83 (m, 2H), 1.58 – 1.39 (m, 8H), 1.19 (s, 6H). ¹³C NMR (126 MHz, CDCl₃) δ 165.87, 164.60, 163.15, 157.11, 151.23, 131.66, 115.48, 112.18, 110.72, 101.18, 70.98, 69.32, 43.77, 29.80, 29.31, 28.77, 25.91, 24.21. *m/z* calculated for $C_{19}H_{24}O_6$ 347.1500 [M-H]$^-$, found 347.1478.

3.4.7   TM-IV-6, TM-IV-18, and intermediate compound characterizations
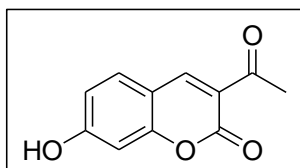
Synthesis of 3-Acetyl-7-hydroxy-chromen-2-one (35): 2,4-Dihydroxybenzaldehyde (1.0 g, 7.24 mmol) and ethyl acetoacetate (920 µL, 7.27 mmol) were charged to an RBF and vigorously stirred at 25°C. Piperidine (720 µL, 7.29 mmol) was added dropwise to the reaction flask and the mixture was stirred for one hour at 25°C. After full conversion was seen by TLC, the reaction mixture was slowly poured over 1.0 M HCl and ice. The resulting slurry was stirred for 15 minutes before filtering the precipitate, which was subsequently washed with water until the filtrate ran clear and the pH was neutral (pH = 6). The solid product was left to dry on the vacuum filter overnight. Recrystallization of the product was achieved in anhydrous EtOH. 3-Acetyl-7-hydroxy-chromen-2-one was collected as light, golden-yellow crystals at 57% yield. ^{1}H NMR (500 MHz, MeOD) δ 8.58 (s, 1H), 7.67 (d, J = 8.6 Hz, 1H), 6.87 (dd, J = 8.6, 2.3 Hz, 1H), 6.75 (d, J = 2.2 Hz, 1H), 2.63 (s, 3H). ^{13}C NMR (126 MHz, MeOD) δ 195.72, 164.73, 160.09, 157.84, 148.21, 132.15, 119.26, 114.12, 111.18, 101.63, 28.91. *m/z* calculated for $C_{11}H_8O_4$ 203.0350 [M-H]$^-$, found 203.0362.
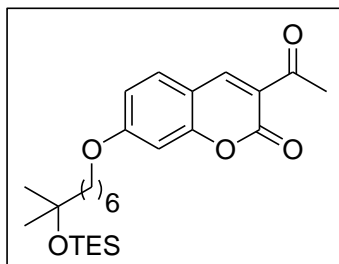
Synthesis of 3-Acetyl-7-(7-methyl-7-triethylsilanyloxy-octyloxy)-chromen-2-one (36): Compound (35) (19.8 mg, 97.0 µmol) and compound (30) (65.4 µL) were charged to an RBF and stirred in dry ACN (2.5 mL). In one portion, K_2CO_3 (31.4 mg, 227 µmol) was added to the RBF and the reaction was brought to reflux overnight. After full conversion by TLC, removal of ACN was done *in vacuo*. The crude mixture was resuspended in EtOAc (20 mL) and

washed with 20% NH$_4$Cl solution (pH = 7, 30 mL) and brine (20 mL). The organic layer was

collected, dried over MgSO$_4$, filtered, and concentrated to dryness. The crude product was

purified by column chromatography using EtOAc/Hex (gradient to 30:70 EtOAc:Hex). 3-Acetyl-7-

(7-methyl-7-triethylsilanyloxy-octyloxy)-chromen-2-one was collected as a white powder in 42%

yield. ^{1}H NMR (500 MHz, CDCl$_3$) δ 8.51 (s, 1H), 7.55 (d, J = 8.7 Hz, 1H), 6.91 (dd, J = 8.7, 2.3 Hz,

1H), 6.83 (d, J = 2.2 Hz, 1H), 4.07 (t, J = 6.5 Hz, 2H), 2.73 (s, 3H), 1.90 – 1.81 (m, 2H), 1.55 – 1.47

(m, 2H), 1.46 – 1.35 (m, 6H), 1.21 (s, 6H), 0.96 (t, J = 7.9 Hz, 9H), 0.58 (q, J = 7.9 Hz, 6H). ^{13}C NMR

(126 MHz, CDCl$_3$) δ 195.55, 164.92, 159.83, 157.84, 147.84, 131.44, 120.44, 114.25, 111.86,

100.71, 73.31, 69.03, 45.01, 30.60, 29.86, 28.85, 25.96, 24.24, 7.13, 6.80. *m/z* calculated for

C$_{26}$H$_{40}$O$_5$Si 483.2537 [M+Na]$^+$, found 483.2533.
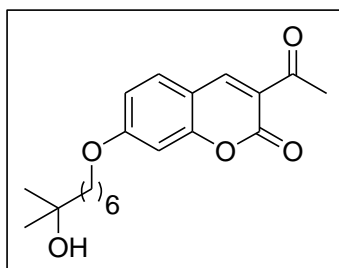
Synthesis of 3-Acetyl-7-(7-hydroxy-7-methyl-octyloxy)-chromen-2-one (37, TM-IV-6): Compound (36) (14.2 mg, 30.8 µmol) was charged to a glass vial, followed by the addition of 0.01 M HCl in MeOH (800 µL) and THF (200 µL). The reaction vial stirred

vigorously for one hour at 25°C. Upon full conversion seen by TLC, the stirring reaction was

neutralized with the dropwise addition of 0.01 M LiOH in water (800 µL). The crude product

was concentrated to dryness and purified by column chromatography using EtOAc/Hex

(gradient to 50:50 EtOAc:Hex). 3-Acetyl-7-(7-hydroxy-7-methyl-octyloxy)-chromen-2-one was

collected as a white powder in 78% yield. ^{1}H NMR (500 MHz, CDCl$_3$) δ 8.52 (s, 1H), 7.55 (d, J =

8.7 Hz, 1H), 6.91 (dd, J = 8.7, 2.3 Hz, 1H), 6.83 (d, J = 2.2 Hz, 1H), 4.08 (t, J = 6.5 Hz, 2H), 2.73 (s,

3H), 1.90 – 1.82 (m, 2H), 1.56 – 1.48 (m, 4H), 1.45 – 1.39 (m, 4H), 1.24 (s, 6H). ^{13}C NMR (126

MHz, CDCl$_3$) δ 195.56, 164.87, 159.83, 157.83, 147.85, 131.46, 120.47, 114.25, 111.89, 100.71,

71.00, 68.96, 43.81, 30.61, 29.82, 29.30, 28.83, 25.94, 24.23. *m/z* calculated for $C_{20}H_{26}O_5$

347.1853 [M+H]$^+$, found 347.1842.
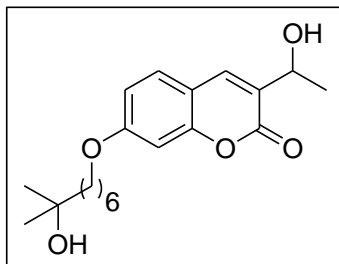
Synthesis of 3-(1-Hydroxy-ethyl)-7-(7-hydroxy-7-methyl-octyloxy)-chromen-2-one (38, TM-IV-18): TM-IV-6 (31.0 mg, 89.5 µmol) and CeCl$_3$ (24.6 mg, 99.8 µmol) were charged to an RBF, followed by THF (2 mL) and MeOH (2 mL). The reaction flask was cooled to 0°C

and NaBH$_4$ (5.6 mg, 148 µmol) was added in one portion. After 1.5 hours, the reaction was

quenched with 20% NH$_4$Cl solution (pH = 7, 1 mL). The flask was concentrated to dryness and

purified by column chromatography using EtOAc/Hex (gradient to 70:30 EtOAc:Hex). 3-(1-

Hydroxy-ethyl)-7-(7-hydroxy-7-methyl-octyloxy)-chromen-2-one was collected as a white

crystalline solid in 63% yield. ^{1}H NMR (500 MHz, MeOD) δ 7.92 (s, 1H), 7.55 (d, *J* = 8.6 Hz, 1H),

6.93 (dd, *J* = 8.6, 2.4 Hz, 1H), 6.90 (d, *J* = 2.3 Hz, 1H), 4.84 (td, *J* = 6.3, 0.8 Hz, 1H), 4.08 (t, *J* = 6.4

Hz, 2H), 1.88 – 1.79 (m, 2H), 1.57 – 1.47 (m, 4H), 1.46 – 1.39 (m, 7H), 1.19 (s, 6H). ^{13}C NMR (126

MHz, MeOD) δ 162.16, 161.40, 154.70, 137.42, 129.15, 128.83, 112.79, 112.75, 100.38, 70.00,

68.32, 64.32, 43.33, 29.69, 28.73, 27.76, 25.68, 23.92, 21.52.

3.4.8   TM-IV-16 and intermediate compound characterizations
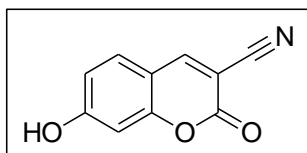
Synthesis of 7-Hydroxy-2-oxo-2*H*-chromene-3-carbonitrile (39):

Malononitrile (375 mg, 5.68 mmol) was transferred in water (10 mL)

to an RBF containing 2,4-dihydroxybenzaldehyde (507 mg, 3.67 mmol). Ammonium acetate

(423 mg, 5.49 mmol) was added in one portion to the stirring reaction flask, and the sides of the

RBF were rinsed with water (5 mL). The reaction mixture stirred at 25°C for 4 hours. The solid

precipitate was filtered, rinsed with water (15 mL), and left to dry on the vacuum filter

overnight. The crude solid was transferred back to the RBF, which was subsequently charged

with 3.0 M HCl (10 mL). The reaction flask was brought to 75°C and stirred for one hour, upon

which, full conversion was visible by TLC. The resulting solid was filtered, rinsed with water (40

mL), and dried on the vacuum filter overnight. The product was further purified by

recrystallization in EtOH, yielding 7-hydroxy-2-oxo-2H-chromene-3-carbonitrile as a red-orange

solid at 44% yield. ^{1}H NMR (500 MHz, Acetone) δ 8.62 (s, 1H), 7.72 (d, J = 8.6 Hz, 1H), 6.99 (d, J =

8.6 Hz, 1H), 6.85 (s, 1H). ^{13}C NMR (126 MHz, Acetone) δ 164.46, 157.18, 157.16, 152.59, 131.69,

114.58, 114.47, 110.89, 102.76, 97.56.
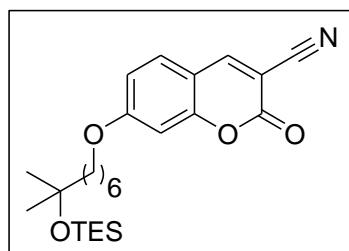
Synthesis of 7-(7-Methyl-7-triethylsilanyloxy-octyloxy)-2-oxo-2H-chromene-3-carbonitrile (40): Compound (39) (48.5 mg, 259 µmol) and compound (30) (175 µL) were charged to an RBF and stirred in dry ACN (5 mL). In one portion, K_2CO_3 (84.8 mg, 614 µmol) was

added to the RBF and the reaction was brought to reflux overnight. After full conversion by TLC,

removal of ACN was done *in vacuo*. The crude mixture was resuspended in EtOAc (15 mL) and

washed with 20% NH_4Cl solution (pH = 7, 30 mL) and brine (20 mL). The organic layer was

collected, dried over $MgSO_4$, filtered, and concentrated to dryness. The crude product was

purified by column chromatography using EtOAc/Hex (gradient to 40:60 EtOAc:Hex). 7-(7-

Methyl-7-triethylsilanyloxy-octyloxy)-2-oxo-2H-chromene-3-carbonitrile was collected as a

white powder in 68% yield. ^{1}H NMR (500 MHz, CDCl$_3$) δ 8.19 (s, 1H), 7.50 (d, J = 8.8 Hz, 1H), 6.95

(dd, J = 8.7, 2.3 Hz, 1H), 6.84 (d, J = 2.3 Hz, 1H), 4.09 (t, J = 6.5 Hz, 2H), 1.89 – 1.82 (m, 2H), 1.52

– 1.35 (m, 8H), 1.20 (s, 6H), 0.95 (t, *J* = 7.9 Hz, 9H), 0.57 (q, *J* = 7.9 Hz, 6H). ^{13}C NMR (126 MHz,

CDCl₃) δ 165.62, 157.22, 157.09, 151.51, 130.47, 114.73, 114.24, 110.85, 101.52, 98.47, 73.30,

69.31, 44.99, 29.86, 29.83, 28.79, 25.92, 24.21, 7.12, 6.80.
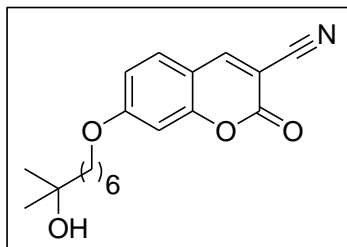
Synthesis of 7-(7-Hydroxy-7-methyl-octyloxy)-2-oxo-2*H*-chromene-3-carbonitrile (41, TM-IV-16): Compound (40) (31.5 mg, 71.0 µmol) was charged to a glass vial, followed by the addition of 0.01 M HCl in MeOH (1.8 mL) and THF (400 µL). The reaction vial

stirred vigorously for one hour at 25°C. Upon full conversion seen by TLC, the stirring reaction

was neutralized with the dropwise addition of 0.1 M LiOH in water (180 µL). The crude product

was concentrated to dryness and purified by column chromatography using EtOAc/Hex

(gradient to 80:20 EtOAc:Hex). 7-(7-Hydroxy-7-methyl-octyloxy)-2-oxo-2*H*-chromene-3-

carbonitrile was collected as a white powder in 99% yield. ^{1}H NMR (500 MHz, CDCl₃) δ 8.18 (s,

1H), 7.49 (d, *J* = 8.8 Hz, 1H), 6.95 (dd, *J* = 8.7, 2.4 Hz, 1H), 6.85 (d, *J* = 2.3 Hz, 1H), 4.09 (t, *J* = 6.5

Hz, 2H), 1.90 – 1.83 (m, 2H), 1.56 – 1.47 (m, 4H), 1.46 – 1.39 (m, 4H), 1.24 (s, 6H). ^{13}C NMR (126

MHz, CDCl₃) δ 165.55, 157.15, 157.11, 151.40, 130.39, 114.74, 114.17, 110.85, 101.50, 98.62,

70.97, 69.23, 43.78, 29.79, 29.31, 28.77, 25.90, 24.21.

References

1.   Coster, M. J.; De Voss, J. J., Medium Ring Ethers by Ring Expansion–Ring Contraction: Synthesis of Lauthisan. *Organic letters* **2002,** *4* (18), 3047-3050.

2.   Crossland, R.; Wells, W.; Shiner Jr, V., Sulfonate leaving groups, structure and reactivity. 2,2,2-Trifluoroethanesulfonate. *Journal of the American Chemical Society* **1971,** *93* (17), 4217-4219.

3.   Lepore, S. D.; Mondal, D., Recent advances in heterolytic nucleofugal leaving groups. *Tetrahedron* **2007,** *63* (24), 5103.

4.   Jefford, C.; Kirkpatrick, D.; Delay, F., Reductive dehalogenation of alkyl halides with lithium aluminum hydride. Reappraisal of the scope of the reaction. *Journal of the American Chemical Society* **1972,** *94* (25), 8905-8907.

5.   Kathiresan, M.; Walder, L.; Ye, F.; Reuter, H., Viologen-based benzylic dendrimers: selective synthesis of 3,5-bis (hydroxymethyl) benzylbromide and conformational analysis of the corresponding viologen dendrimer subunit. *Tetrahedron Letters* **2010,** *51* (16), 2188-2192.

6.   Cao, D.; Liu, Z.; Verwilst, P.; Koo, S.; Jangjili, P.; Kim, J. S.; Lin, W., Coumarin-based small-molecule fluorescent chemosensors. *Chemical reviews* **2019,** *119* (18), 10403-10519.

7.   Jeon, J. Y.; Park, S.; Han, J.; Maurya, S.; Mohanty, A. D.; Tian, D.; Saikia, N.; Hickner, M. A.; Ryu, C. Y.; Tuckerman, M. E., Synthesis of aromatic anion exchange membranes by Friedel–Crafts bromoalkylation and cross-linking of polystyrene block copolymers. *Macromolecules* **2019,** *52* (5), 2139-2147.

8.   Sahai, N., Is silica really an anomalous oxide? Surface acidity and aqueous hydrolysis revisited. *Environmental science & technology* **2002,** *36* (3), 445-452.

9.   Brahmachari, G., Room temperature one-pot green synthesis of coumarin-3-carboxylic acids in water: a practical method for the large-scale synthesis. *ACS Sustainable Chemistry & Engineering* **2015,** *3* (9), 2350-2358.

10.   Alvim Jr, J.; Dias, R. L.; Castilho, M. S.; Oliva, G.; Corrêa, A. G., Preparation and evaluation of a coumarin library towards the inhibitory activity of the enzyme gGAPDH from Trypanosoma cruzi. *Journal of the Brazilian Chemical Society* **2005,** *16* (4), 763-773.

11.   Luche, J.-L.; Rodriguez-Hahn, L.; Crabbé, P., Reduction of natural enones in the presence of cerium trichloride. *Journal of the Chemical Society, Chemical Communications* **1978,** (14), 601-602.

12.   Gemal, A. L.; Luche, J. L., Lanthanoids in organic synthesis. 6. Reduction of. alpha.-enones by sodium borohydride in the presence of lanthanoid chlorides: synthetic and mechanistic aspects. *Journal of the American Chemical Society* **1981,** *103* (18), 5454-5459.

13.   Ho, T.-L., Hard soft acids bases (HSAB) principle and organic chemistry. *Chemical Reviews* **1975,** *75* (1), 1-20.

14.   Wang, P.; Xia, Y. L.; Zou, L. W.; Qian, X. K.; Dou, T. Y.; Jin, Q.; Li, S. Y.; Yu, Y.; Wang, D. D.; Luo, Q., An Optimized Two-Photon Fluorescent Probe for Biological Sensing and Imaging of Catechol-O-Methyltransferase. *Chemistry–A European Journal* **2017,** *23* (45), 10800-10807.

Chapter Four: Spectral analysis of novel VDR ligands

4.1   Excitation and emission of fluorophores

Fluorescence results as a means of electromagnetic energy dissipation from an excited

molecule. It is the observable result of a photon being released from a compound during the

transition from an excited singlet state to the ground state.[1] This process occurs in conjugated

π-systems, when a photon from a UV or visible light source that matches the π/π* energy gap is

absorbed by the compound. Promotion of a π-electron from the highest occupied molecular

orbital (HOMO) to the anti-bonding (π*) lowest unoccupied molecular orbital (LUMO) places

the compound into an excited state.[2] A favorable thermodynamic transition of the excited

electron back to the ground state is encouraged by the lowered energy of the ground state.

This transition occurs in two successive steps.[3] First, the processes of vibrational relaxation and

internal conversion occur by dissipating energy to the surrounding environment. Vibrational

relaxation is the electronic transition between vibrational states of the same spin state,

whereas internal conversion is electronic transition between energy states of the same spin

state. The second step in returning an excited molecule to the ground state includes multiple

competitive processes. Collisional energy transfer with the surrounding solvent or nearby

molecules, photochemical reactions, release as thermal energy, or as re-emission as radiative

energy (fluorescence or phosphorescence) are all potential pathways for an excited state molecule to disperse energy when transitioning back to the ground state.[3-4]

During fluorescence, the excited molecule will re-emit a photon at a lower energy than it was absorbed. The energy of a re-emitted photon is always less than the energy in which a photon is absorbed by a molecule, due to the vibrational relaxation and internal conversion that occurs during the first step of energy dissipation.[5] (Figure 42) Collisions
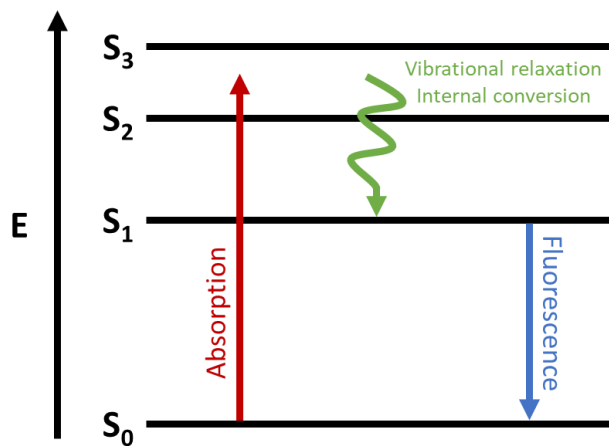
Figure 42. Simplified Jablonski diagram of molecular excitation and emission.

between the excited molecule and the surrounding environment occur very quickly. These non-radiative processes transfer vibrational and rotational energy away from the excited electron on the timescale of 10^{-14} to 10^{-12} seconds.[4] This rapid method of energy dissipation in the higher energy states occurs faster than the transition from the first energy state to the ground state. Fluorescence only occurs during this deexcitation from the first excited state back to the ground state, and thus is a lengthier process occurring on the timescale of 10^{-9} to 10^{-8} seconds.[4] As previously mentioned, many compounds do not fluoresce due to the other competitive processes in play during this timeframe.

According to the Planck-Einstein relation, $E = hc/\lambda$, there is an inverse relationship between photon energy and wavelength. Since the emitted photon during fluorescence has a lower energy than the energy in which the photon was absorbed, the observed emission will occur at a longer wavelength. A fluorescence spectrum plots the fluorescence intensity as a function of

the wavelength.[3] Each fluorophore has unique spectral properties that can often be altered through various substituent additions. These substituents can influence the wavelength, fluorescence intensity, and lifetime of the fluorophore.[3, 5] Coumarins, for example, have been observed to emit in the blue-green region of the visible light spectrum when properly substituted.[6] (See chapter 2) Additionally, compound fluorescence is often sensitive to the surrounding environment. The dipole orientation of the fluorophore changes as the compound enters an excited state and develops unstable interactions with the neighboring solvent. Reorientation of the solvent dipole leads to increased stability. Each solvent will reorient differently and influence the spectral observations made by the fluorophore.[3]

4.2   Synthetic compound analysis

The ten final ligands synthesized to target VDR underwent spectral analysis to determine their photophysical properties. Analysis of the excitation and emission wavelengths showed sufficient signal separation characterized by the Stokes shift. Signal separation is necessary in order to avoid interference from the entering excitation light on the emission intensity.[2] Additionally, for effective use as a biological probe, the ligands need to minimally possess an emission wavelength in the visible spectral region (400-700 nm). Below the visible light range, biological cellular components are able to strongly interfere with the absorption of light.[7]

Absorbance and emission were evaluated in both methanol and water for each ligand, in order to show the effect solvent polarity has on the molecule. The first compound, TM-II-21, was
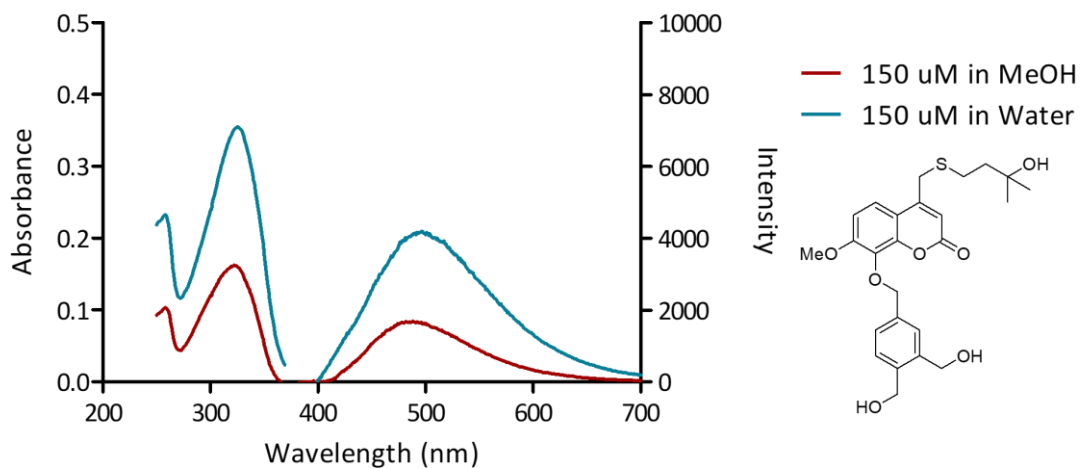
Figure 43. Spectral properties of TM-II-21 in methanol and water.

observed to have a maximal absorbance at 322 nm and 325 nm in methanol and water,

respectively. Emission was seen at a maximum of 488 nm in methanol and 497 nm in water.

Hence, the Stokes shift was determined to be 166 nm in methanol and 172 nm in water. A

higher signal intensity was also observed for both the excitation and emission signals in the

aqueous solvent. (Figure 43) This indicates that fluorescence signal suppression is likely to be

observed upon binding of TM-II-21 to the VDR-LBD due to the highly hydrophobic nature of the

binding pocket in contrast from the aqueous, surrounding cellular environment.

Similar results were observed during spectral analysis of TM-II-72. The comparable substitution

pattern on the coumarin ring-structure for the initial two ligands supports this observation. A

maximal absorbance at 323 nm and 325 nm was observed in methanol and water, respectively.

Emission maxima occur at 489 nm in methanol and 509 nm in water, thus producing a Stokes

shift of 166 nm in methanol and 184 nm in water. Higher signal intensity occurred in the

aqueous solvent for both the excitation and emission signals. (Figure 44)
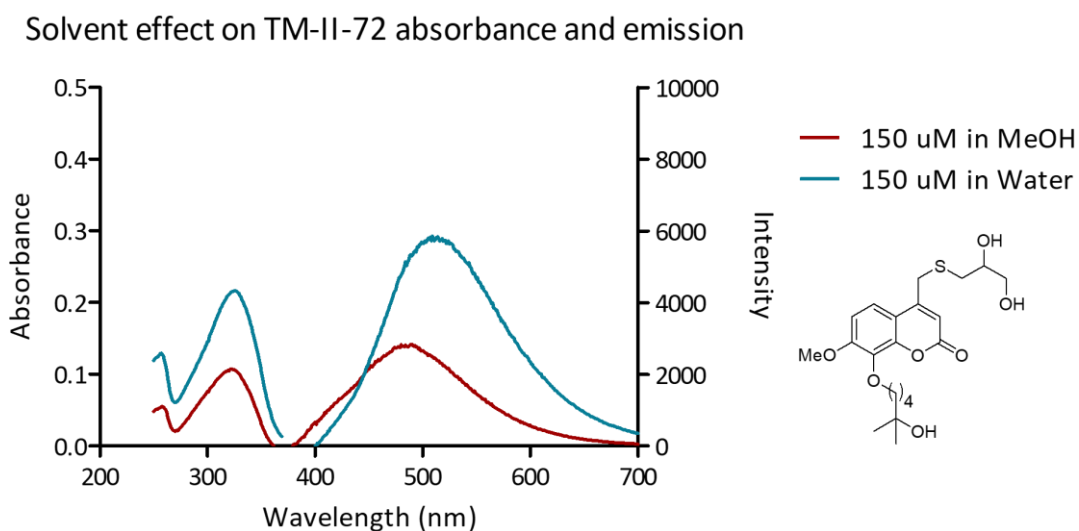
Figure 44. Spectral properties of TM-II-72 in methanol and water.

A substantial impact on emission wavelength was seen for compound TM-II-88, which bears a different substitution pattern than TM-II-21 and TM-II-72. Considerable blue-shifting of the emission signal in water was observed, with the maximum observed at 402 nm. Absorbance in the aqueous solvent was seen at 329 nm, resulting in a Stokes shift of 73 nm. Due to this decreased Stokes shift, significant interference by the excitation signal affected the clarity of the emission curve. The available instrumentation did not allow for this interference to be avoided, despite attempts to change instrument parameters, decrease sample concentration, and excite at non-maximal wavelengths. Absorbance of TM-II-88 in methanol occurred at 327 nm; however, the emission signal could not be detected due to significant signal suppression in the organic solvent. Additionally, a larger emission signal intensity was observed for this compound. The instrument gain needed to be decreased to 50 so as not to max out the detector. TM-II-88 was consistent with the former compounds, in that a larger signal intensity was observed for both the excitation and emission signals in water. (Figure 45)
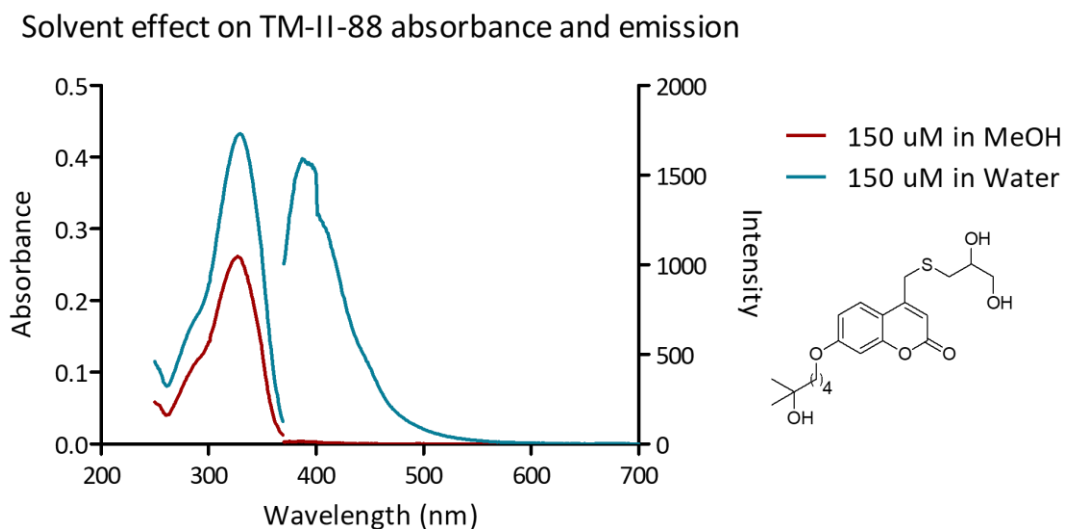
Figure 45. Spectral properties of TM-II-88 in methanol and water.

Compounds TM-III-20 and TM-III-31 are structurally similar to compound TM-II-72, differing

only in the length of the aliphatic carbon chain that bears the tertiary alcohol functionality.

Compound TM-III-20, the shorter derivative of TM-II-72, showed a maximal absorbance at 322

nm and 325 nm in methanol and water, respectively. Emission was seen at a maximum of 492

nm in methanol and 514 nm in water. Thus, the Stokes shift for TM-III-20 was 170 nm in

methanol and 189 nm in water. The signal intensity was heightened for both the excitation and

emission curves when performed in water. (Figure 46)
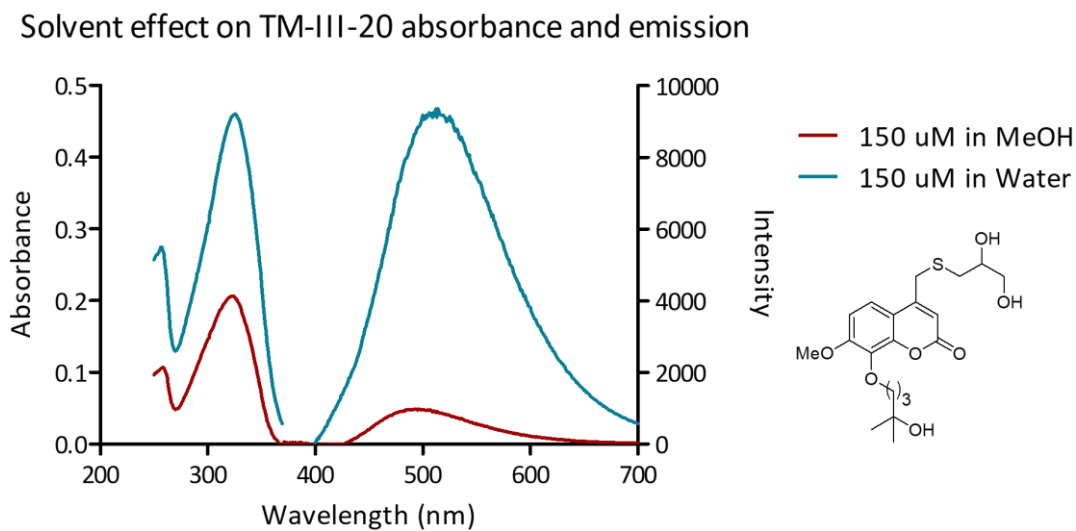
Figure 46. Spectral properties of TM-III-20 in methanol and water.

The derivative of TM-II-72 with a longer carbon chain, compound TM-III-31, showed a maximal

absorbance at 322 nm in methanol and 325 nm in water. Emission occurred at a maximum of

497 nm and 506 nm in methanol and water, respectively. In methanol, this compound

displayed a Stokes shift of 175 nm, while in water a Stokes shift of 181 nm was observed. As

expected, a higher signal intensity for both the excitation and emission signals occurred in the

aqueous solvent. (Figure 47)
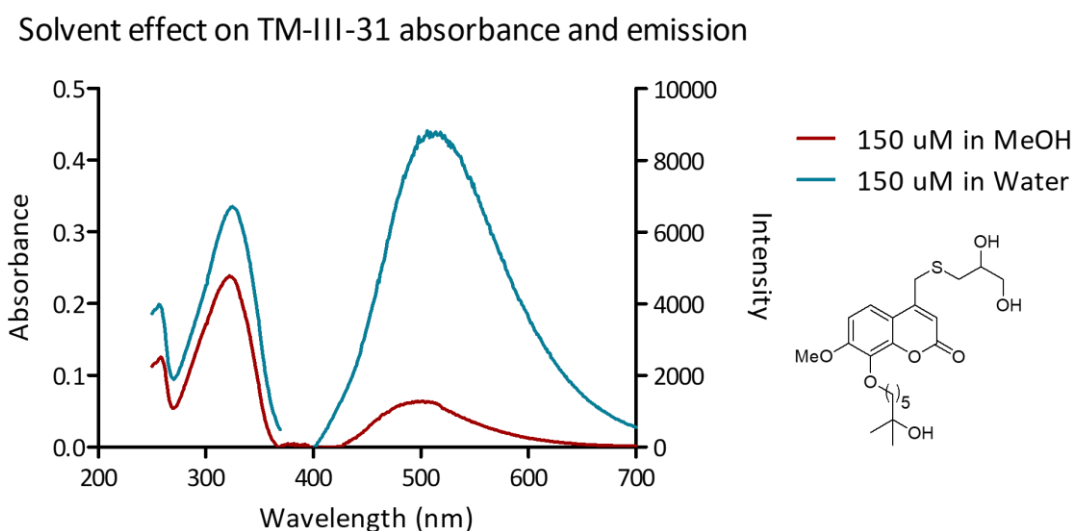
Figure 47. Spectral properties of TM-III-31 in methanol and water.

The first Series D compound to be evaluated was TM-III-90. Series D compounds are substituted in positions 3 and 7 on the coumarin ring. Similar to compound TM-II-88, which is substituted in positions 4 and 7, the maximum emission wavelength observed for TM-III-90 was blue-shifted relative to the ligands substituted in positions 4, 7, and 8. This observation supports the idea that increased electron-donating substitution results in a red-shifted emission wavelength. TM-III-90 had maximal emission at 404 nm in both methanol and water, however, interference from the excitation signal was observed due to a relatively small Stokes shift. Maximum excitation occurred at 350 nm and 353 nm in methanol and water, respectively, occurring at a longer wavelength than what was observed by the previously synthesized ligands. Consequently, the Stokes shifts for TM-III-90 were 54 nm in methanol and 51 nm in water. Excitation and emission intensity were both higher when in the aqueous solvent. (Figure 48)
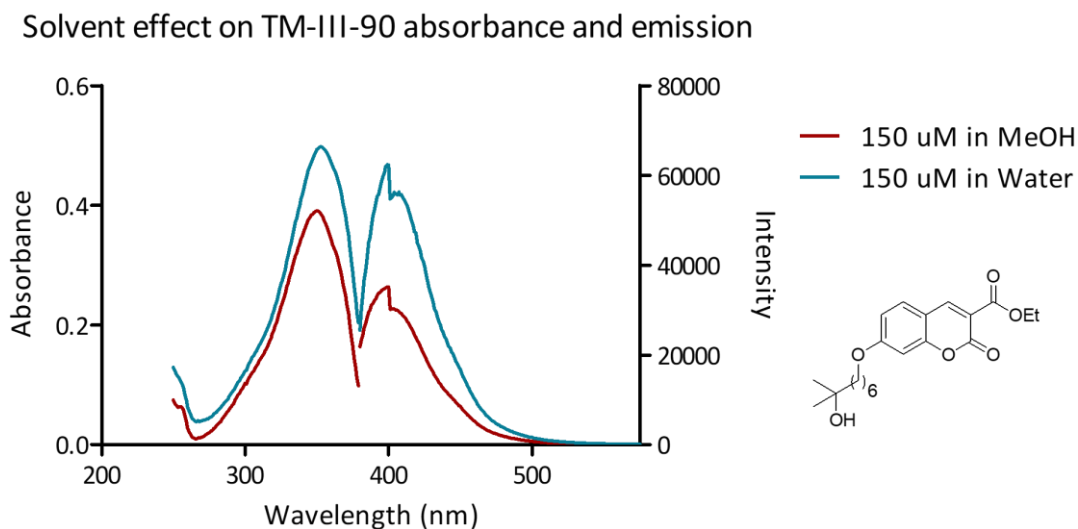
Figure 48. Spectral properties of TM-III-90 in methanol and water.

Due to the presence of the carboxylic acid functionality in position 3, compound TM-III-91

spectral data at different pH levels were obtained. Carboxylic acids have approximate pKa

values of 4-5, thus under physiological conditions (pH = 7), it is expected that the deprotonated

carboxylate takes primary form. Under neutral conditions, TM-III-91 is observed to have a

maximal absorbance at 342 nm and 340 nm in methanol and water, respectively. Emission was

observed at a maximum of 402 nm in methanol and 401 nm in water, though slight interference

from the excitation signal is observed around 400 nm. Therefore, the Stokes shift for TM-III-91

under neutral conditions is 60 nm in methanol and 61 nm in water. The absorbance signal is

more intense in water, but the emission signal was greater in methanol. (Figure 49) This is likely

due to the more acidic pH of 5.0 that was measured in the organic solvent. A higher intensity

was consistently observed in the emission signals of acidic solutions. (Figures 50 and 51)
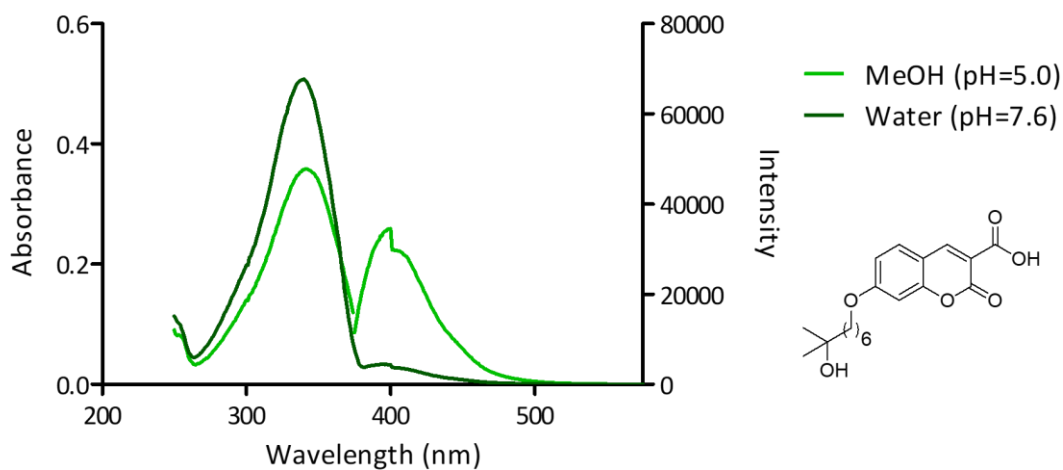
Figure 49. Spectral properties of TM-III-91 in methanol and water, at a neutral pH.

To determine whether a change of pH would shift the wavelength emission, spectral data for TM-III-91 was observed under acidic and basic conditions. The carboxylic acid functionality in position 3 on the coumarin ring would be protonated below pH = 3. A 150 µM solution of TM-III-91 was prepared following the sample preparation described in the absorbance and emission procedures, though the dilution solvent for the acidic trials were substituted for 0.01 M HCl in methanol and 0.01 M HCl in water. The solvent for the basic trials were substituted for 0.01 M LiOH in methanol and 0.01 M LiOH in water.

There was minimal to no shifting of the emission wavelength for TM-III-91 under acidic or basic conditions. At a low pH, TM-III-91 was observed to have a maximal absorbance at 351 nm and 353 nm in methanol and water, respectively. Emission was seen at a maximum of 404 nm in methanol and 408 nm in water, equating to a Stokes shift of 53 nm in methanol and 55 nm in water. The emission intensity signal increased for TM-III-91 at a decreased pH, with the organic solvent producing a more intense absorption and emission curve. (Figure 50)
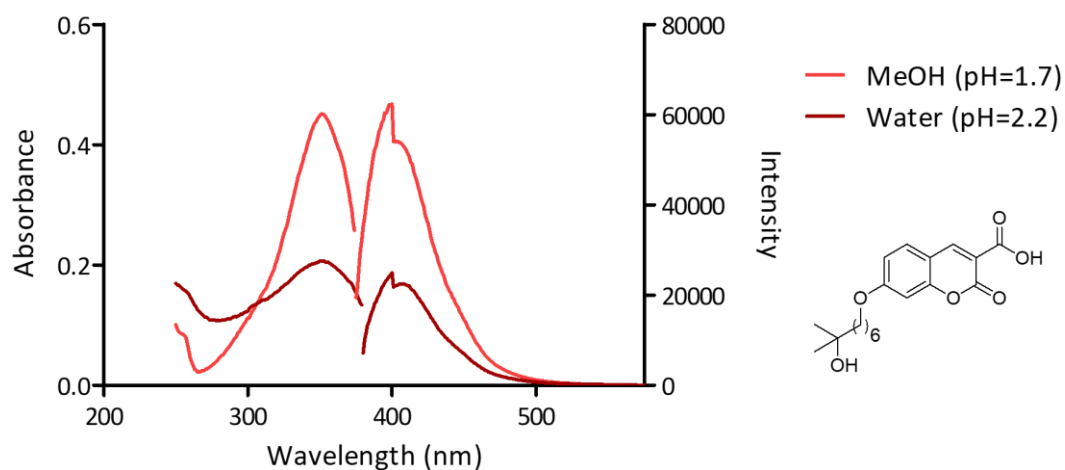
Figure 50. Spectral properties of TM-III-91 in 0.01 M HCl in methanol and 0.01 M HCl in water.

A maximal absorbance at 336 nm in methanol and 339 nm in water was observed at the increased pH. Emission occurred at approximately 402 nm for both methanol and water, however the signal was sufficiently suppressed at the basic pH to make observation of the signal difficult. Nonetheless, the Stokes shift at the increased pH remains at approximately 60 nm. (Figure 51)
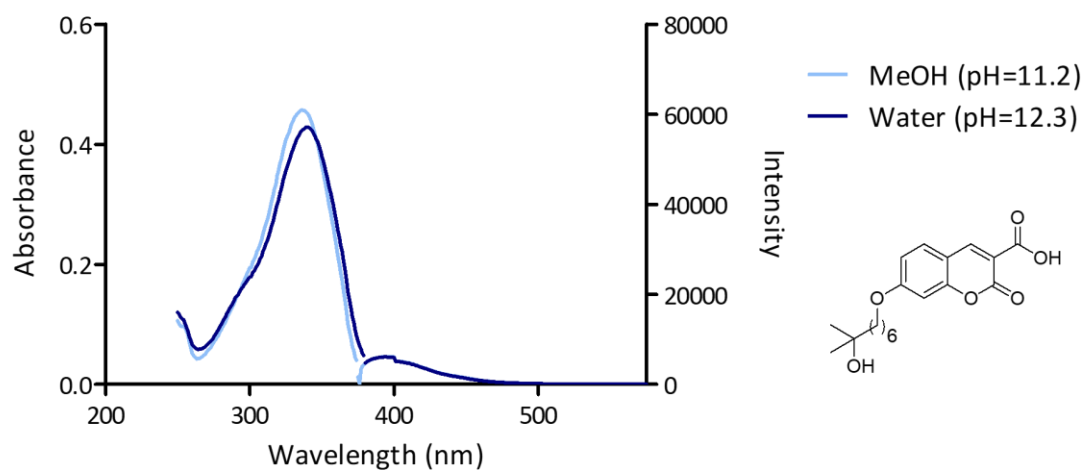
Figure 51. Spectral properties of TM-III-91 in 0.01 M LiOH in methanol and 0.01 M LiOH in water.
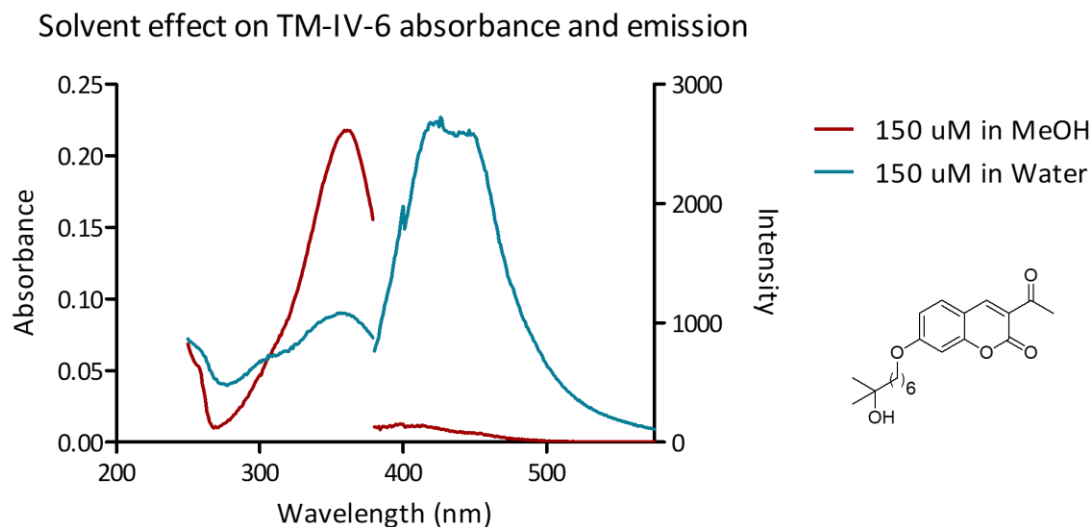
Figure 52. Spectral properties of TM-IV-6 in methanol and water.

A maximal absorbance at 361 nm in methanol and 356 nm in water was observed for TM-IV-6, which has a 3-acetyl substituent. Emission occurred at a maximum of 413 nm and 426 nm in methanol and water, respectively. In methanol, this compound displayed a Stokes shift of 52 nm, while in water a Stokes shift of 70 nm was observed. A higher absorbance was observed in methanol, though emission was drastically quenched in the organic solvent. (Figure 52)

The nitrile substituent in position 3 followed a similar spectral pattern to TM-IV-6 in that the absorbance signal was higher in methanol, while the emission intensity was higher in water. The maximal absorbance detected in methanol and water was 354 nm and 355 nm, respectively. Maximal emissions occurred at 405 nm in methanol and 410 nm in water. Therefore, the Stokes shifts for TM-IV-16 were 51 nm in methanol and 55 nm in water. (Figure 53)

Solvent effect on TM-IV-16 absorbance and emission
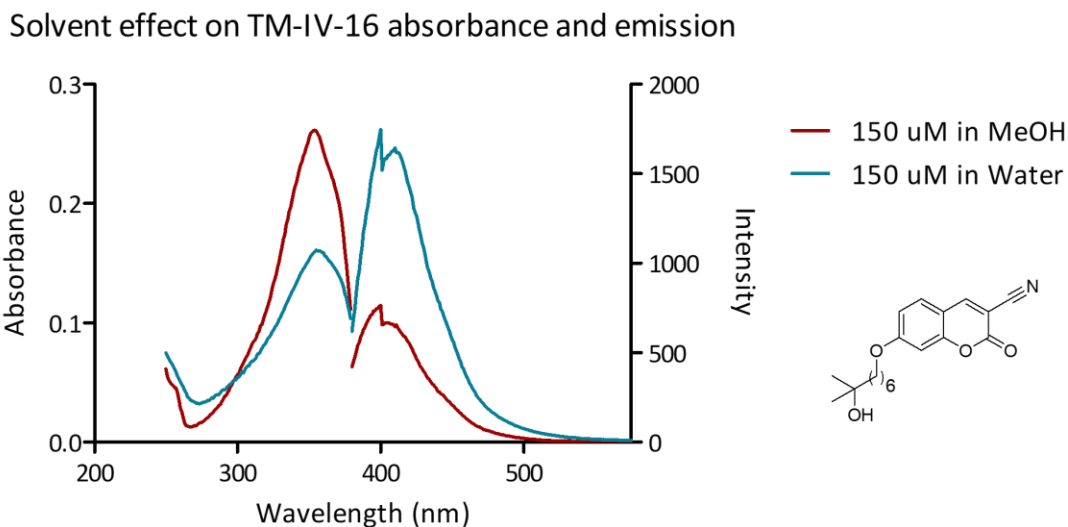
Figure 54. Spectral properties of TM-IV-16 in methanol and water.

Higher absorbance and emission signals occurred in water for TM-IV-18. Moreover, reduction

to the secondary alcohol substantially increased the emission intensity signal relative to the

ketone precursor. Maximal absorbance occurred at 325 nm in both methanol and water. The

maximal emission was unable to be determined in either solvent due to interference from the

absorbance signal, however, an approximation places the emission signal at 400 nm. Therefore,

the Stokes shifts for TM-IV-18 in methanol and water would be about 75 nm. (Figure 54)

Solvent effect on TM-IV-18 absorbance and emission
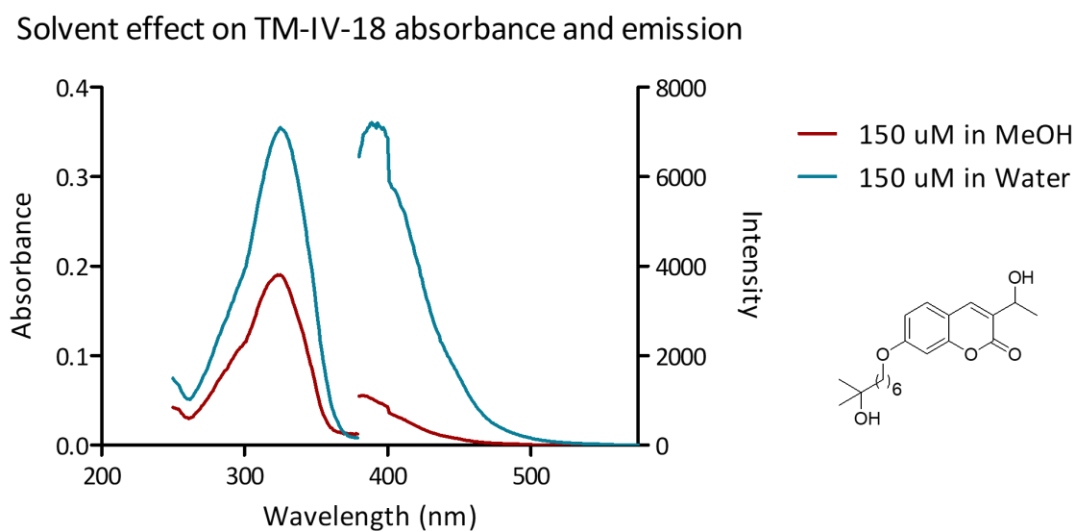
Figure 53. Spectral properties of TM-IV-18 in methanol and water.

Discussion

Small-molecule fluorophores are frequently used for biological imaging because of their generally low toxicity, well-defined excretion mechanisms, and ability to target specific binding sites.[8] The spectral properties for ten fluorescent VDR ligands were evaluated in both methanol and water. For compound TM-III-91, which contains a carboxylic acid functionality, spectral data was also evaluated in acidic (0.01 M HCl) and basic (0.01 M LiOH) organic and aqueous solutions. It was generally observed that the absorption and emission intensity for these fluorescent ligands is higher in an aqueous solvent, though absorption for TM-IV-6 and TM-IV-16 was higher in methanol. Presence of electron donating functional groups in positions 7- and 8- on the coumarin ring were observed to significantly red-shift the emission wavelength relative to the compounds substituted in solely the 7- position. Despite literature reports describing a red-shift in the emission wavelength when creating a "push-pull" system throughout the coumarin core[6], electron-withdrawing groups present in the 3- position did not noticeably increase the emission wavelength in regard to developing a sufficient biological probe. The spectral properties of coumarins are sensitive to differing substitution patterns on the ring-system. Aligning with the spectral observations of the synthesized VDR ligands, an increase in the Stokes shift has been observed for attaching a bulky substituent at the 4- position relative to the 3- position.[9] The geometric changes to the molecule upon excitation are generally smaller for 3- substituted coumarins; thus, the larger Stokes shifts of 4- substituted coumarins are rationalized through the amount of torsional work done during relaxation.[9] This justification alongside the increased electron-donating substitution occurring in compound Series A and B explains the more desirable spectral properties for these compounds. The Stokes

shift in the Series C and D compounds was relatively small (<75 nm), which often allowed the excitation signal to interfere with the emission signal analysis for these compounds. Additionally, these molecules emit at just over 400 nm, which is not ideal for a biological probe. Cellular autofluorescence remains a challenge during diagnostic imaging.[10] Fluorophores that emit with a lower wavelength in the visible region are highly likely to face fluorescent interference from other biological components. Observation of these initial scaffolds provides a foundation for further optimization on developing a fluorescent VDR ligand.

General absorbance procedure: Samples were prepared from 30 mM compound in DMSO stock solutions, which were further diluted to 150 μM in either methanol or water. In a 384-well UV-STAR® transparent plate (Greiner Bio-One, 781801), 150 μM compound in methanol (20 μL), 150 μM compound in water (20 μL), pure methanol (20 μL), and pure water (20 μL) were added to separate wells. Two replicates of each solvent blank were plated and recorded. Absorbance was measured using a Tecan Infinite M1000 plate reader. Absorbance curves were generated after subtracting the average blank solvent values from the corresponding compound solution values.

General fluorescence emission procedure: Samples were prepared from 30 mM compound in DMSO stock solutions, which were further diluted to 150 μM in either methanol or water. In a 384-well black polystyrene microplate (Thermo Fisher Scientific, 262260), 150 μM compound in methanol (20 μL), 150 μM compound in water (20 μL), pure methanol (20 μL), and pure water

(20 μL) were added to separate wells. Two replicates of each solvent blank were plated and

recorded. Fluorescence emission was measured using a Tecan Infinite M1000 plate reader. The

instrument bandwidth (emission and excitation) was set to 20 nm and the gain was manually

set to 100, unless otherwise noted. The Z-position was automatically calculated by the Tecan

Infinite M1000 plate reader from the 384-well containing the aqueous compound solution.

References

1.   Guilbault, G. G., *Practical Fluorescence, Second Edition*. CRC Press: 2020.
2.   Fu, Y.; Finney, N. S., Small-molecule fluorescent probes and their design. *RSC advances* **2018,** *8* (51), 29051-29061.
3.   Albani, J. R., *Principles and applications of fluorescence spectroscopy*. John Wiley & Sons: 2008.
4.   Jaffé, H. H.; Miller, A. L., The fates of electronic excitation energy. *Journal of chemical education* **1966,** *43* (9), 469.
5.   Ramanujam, N., Fluorescence spectroscopy in vivo. *Encyclopedia of Analytical Chemistry: Applications, Theory and Instrumentation* **2006**.
6.   Cao, D.; Liu, Z.; Verwilst, P.; Koo, S.; Jangjili, P.; Kim, J. S.; Lin, W., Coumarin-based small-molecule fluorescent chemosensors. *Chemical reviews* **2019,** *119* (18), 10403-10519.
7.   Shen, Q.; Wang, S.; Yang, N.-D.; Zhang, C.; Wu, Q.; Yu, C., Recent development of small-molecule organic fluorophores for multifunctional bioimaging in the second near-infrared window. *Journal of Luminescence* **2020**, 117338.
8.   Schnermann, M. J., Organic dyes for deep bioimaging. *Nature* **2017,** *551* (7679), 176-177.
9.   Liu, X.; Xu, Z.; Cole, J. M., Molecular design of uv–vis absorption and emission properties in organic fluorophores: toward larger bathochromic shifts, enhanced molar extinction coefficients, and greater stokes shifts. *The Journal of Physical Chemistry C* **2013,** *117* (32), 16584-16595.
10.   Owens, E. A.; Lee, S.; Choi, J.; Henary, M.; Choi, H. S., NIR fluorescent small molecules for intraoperative imaging. *Wiley Interdisciplinary Reviews: Nanomedicine and Nanobiotechnology* **2015,** *7* (6), 828-838.

Chapter Five: Biological evaluation of novel VDR ligands

5.1   Cell-based assay screening

A total of ten synthetic ligands were evaluated *in vitro* for the biological responses they produced when introduced in various concentrations to the cellular environment. The fundamental purpose in developing a fluorescent ligand for VDR was to utilize the ligand to create a new *in vitro* binding assay that targets the VDR-LBD, as well as an *in vivo* diagnostic tool to observe the distribution and localization of VDR. While cell-free assays that utilize isolated proteins are available as fast and convenient screening methods for potential receptor ligands[1], the ability to monitor VDR activity in the cellular environment with fluorescence offers further clarity to the behavior of our ligands. Cell-based assays offer real-time visualization of cellular responses while providing the capacity to differentiate between agonistic and antagonistic activity of screened ligands.[2] In certain cases, the likelihood of false-positive results arising from nonspecific interactions can be reduced cell-based assays.[3] As a primary screening method, a cell-based transcription assay was used to assess the usefulness of our novel compounds.

A luciferase-based transcription assay was conducted to determine agonist and/or antagonistic properties of the synthetic VDR ligands, as well as their cellular toxicity. The transcription assay functions by transfecting HEK293 cells with cytomegalovirus-VDR (CMV-VDR) plasmid and CYP24A1-luciferase plasmid, which is a known VDR target gene.[4-5] Overexpressed VDR is dosed
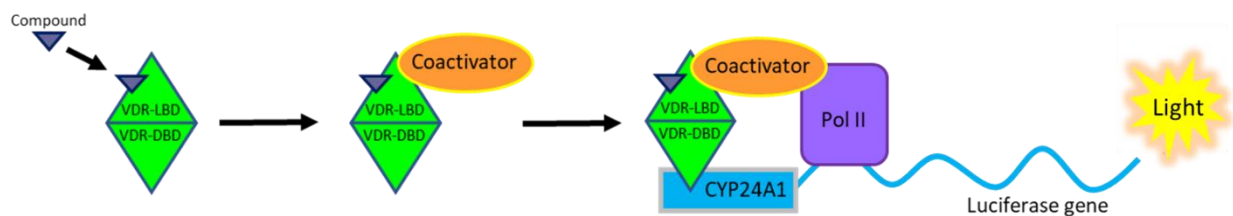
Scheme 11. General process of the luciferase transcription assay for VDR.

with varying concentrations of ligand, either in the presence or absence of a known agonist. In the presence of an agonist, VDR will undergo a conformational change that triggers dissociation of corepressors and promotes coactivator binding.[6] Activation of VDR induces recognition of the vitamin D response element on the CYP24A1 promoter, and recruitment of RNA polymerase occurs to transcribe the luciferase reporter gene. (Scheme 11) Transcription of the luciferase gene occurs proportionally to the amount of activated VDR; therefore, quantification of luciferase can be used to report the efficacy of ligand-activated VDR.

Bright-Glo™ reagent (Promega, E2620) is used to quantify the amount of luciferase enzyme created by generating a bioluminescent signal. The luminescent signal is a byproduct of the enzymatic reaction that converts luciferin to oxyluciferin in the presence of ATP, Mg^{2+}, and O_2. (Scheme 12) A directly proportional correlation between the intensity of the resulting bioluminescent signal and the amount of expressed luciferase indicates the degree to which the transcription occurred by ligand-activated VDR. As a result, a highly potent agonist would yield a strong luminescent signal at low concentration. Conversely, an antagonist of VDR would compete with an agonist and stimulate a conformational change that prevents receptor-coactivator binding. The lack of transcriptional activity on the luciferase gene causes a diminished luminescence signal in the presence of an agonist.

Transfected HEK293 cell viability was evaluated in the presence of various concentrations of the

synthetic ligands in tandem to the transcription assay. Quantification of cellular ATP is achieved

using the CellTiter-Glo® reagent (Promega, G7572). CellTiter-Glo® lyses the cellular membrane

and releases cytoplasmic ATP from viable cells, which is in turn promotes the conversion of

luciferin to oxyluciferin. (Scheme 12) Natural production of ATP supports cellular metabolism,

therefore decreased amounts of ATP in the cell viability assay is an indicator of cell death.[7]

Scheme 12. Enzymatic reaction converting luciferin to oxyluciferin.

5.2   Cellular response to synthetic compounds

Activation of VDR with calcitriol stimulates a strong recognition of the CYP24A1 promoter and

substantial gene transcription. Our transcription assays confirm that 100 nM calcitriol strongly

induced CYP24A1 binding and luciferase transcription, unlike 500 nM of compound 31b (toxic

control), a known irreversible inhibitor of VDR.[8] The first synthetic ligand, TM-II-21, did not

induce CY24A1 binding, as seen by the unaffected luminescence signal. (Figure 55A) A reduction

in luminescence was observed as increasing concentrations of TM-II-21 were introduced to the

cellular environment containing 100 nM calcitriol, however. The IC_{50} of TM-II-21 was observed

at 17.87 μM (Log IC_{50} = 1.252 uM, R^2 = 0.9787). (Figure 55A) A decrease in the viability of the

HEK293 cells under transfected conditions was observed with increasing concentrations of TM-

II-21. The highest concentration of TM-II-21 (150 µM) left 29.8% of the HEK293 cells viable.

(Figure 55B)

Figure 55. A) Results of TM-II-21 agonistic (blue) and antagonistic (red) effects on VDR, relative to 100 nM calcitriol and 500 nM 31b (toxic control). B) HEK293 cell viability while in the presence of increasing TM-II-21 concentrations.

The second ligand, which contains the series B scaffold, displayed similar transcription results to series A compound, TM-II-21. Recognition of the CYP24A1 promoter was not observed when evaluating TM-II-72 for agonistic activity toward VDR, as displayed by the unaffected luminescence signal. (Figure 56A) A reduction in luciferase transcription was detected with increasing concentrations of TM-II-72 while in the presence of 100 nM calcitriol. The IC_{50} of TM-II-72 was observed at 52.87 μM (Log IC_{50} = 1.723 uM, R^2 = 0.8979). (Figure 56A) A substantial improvement on cell viability was observed with TM-II-72 over TM-II-21. The highest concentration of TM-II-72 tested (150 μM) left 89.5% of the transfected HEK293 cells viable. (Figure 56B)

A

HEK293 cellular response to TM-II-72

IC$_{50}$ = 52.87 uM

Legend:
- TM-II-72
- TM-II-72 + 100 nM Calcitriol
- ◆ DMSO + 100 nM Calcitriol
- ◆ Toxic Control

B

HEK293 cell viability in the presence of TM-II-72

%Viable = 89.5%

Legend:
- 5 minutes
- 15 minutes
- 30 minutes
- 1 hour
- 2 hours
- ◆ DMSO (30 min)
- ◆ Toxic Control

Figure 56. A) Results of TM-II-72 agonistic (blue) and antagonistic (red) effects on VDR, relative to 100 nM calcitriol and 500 nM 31b (toxic control). B) HEK293 cell viability while in the presence of increasing TM-II-72 concentrations.

118

TM-II-88, having a series C scaffold, did not trigger VDR to recognize the CYP24A1 promotor.

Transcription of the luciferase gene did not occur, as displayed by the unchanging luminescence

signal with increasing concentrations of TM-II-88 in the absence of calcitriol. (Figure 57A) With

100 nM calcitriol present in the cellular environment, a reduction in the transcription of

luciferase was observed with increasing concentrations of TM-II-88, though to a lesser extent

than the inhibition by TM-II-21 or TM-II-72. The IC_{50} of TM-II-88 was observed to be 138.8 μM

(Log IC_{50} = 2.142 uM, R^2 = 0.7693). (Figure 57A) Minimal impact to the viability of the

transfected HEK293 cells was observed with concentrations of TM-II-88 up to 150 uM. At the

highest concentration of TM-II-88 (150 μM), 92.5% of the HEK293 cells remained viable. (Figure

57B)

Figure 57. A) Results of TM-II-88 agonistic (blue) and antagonistic (red) effects on VDR, relative to 100 nM calcitriol and 500 nM 31b (toxic control). B) HEK293 cell viability while in the presence of increasing TM-II-88 concentrations.

Containing the series B scaffold, TM-III-20 displays comparable transcription results to TM-II-72. A lack of CYP24A1 recognition and luciferase transcription is demonstrated through an unchanging luminescence signal when utilizing TM-III-20 as an agonist. (Figure 58A) A reduction of luciferase transcription was observed as the luminescent signal decreased with increasing concentrations of TM-III-20 while in the presence of 100 nM calcitriol. The IC_{50} of TM-III-20 was observed at 73.78 µM (Log IC_{50} = 1.868 uM, R^2 = 0.9083). (Figure 58A) The viability of the transfected HEK293 cells lessened in the presence of TM-III-20, relative to TM-II-72. The highest concentration of TM-III-20 tested (150 µM) left 77.5% of the HEK293 cells viable. (Figure 58B)
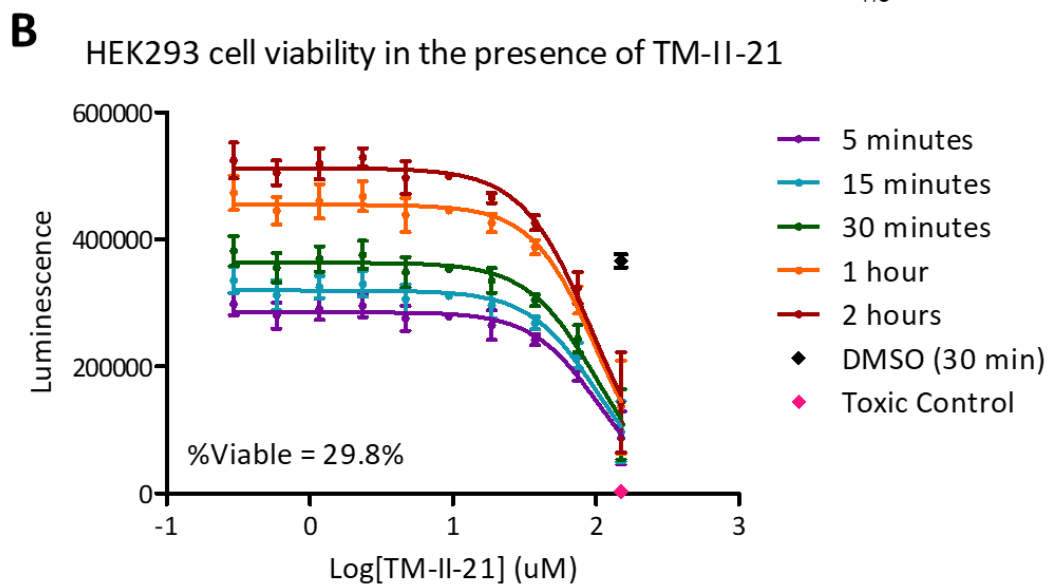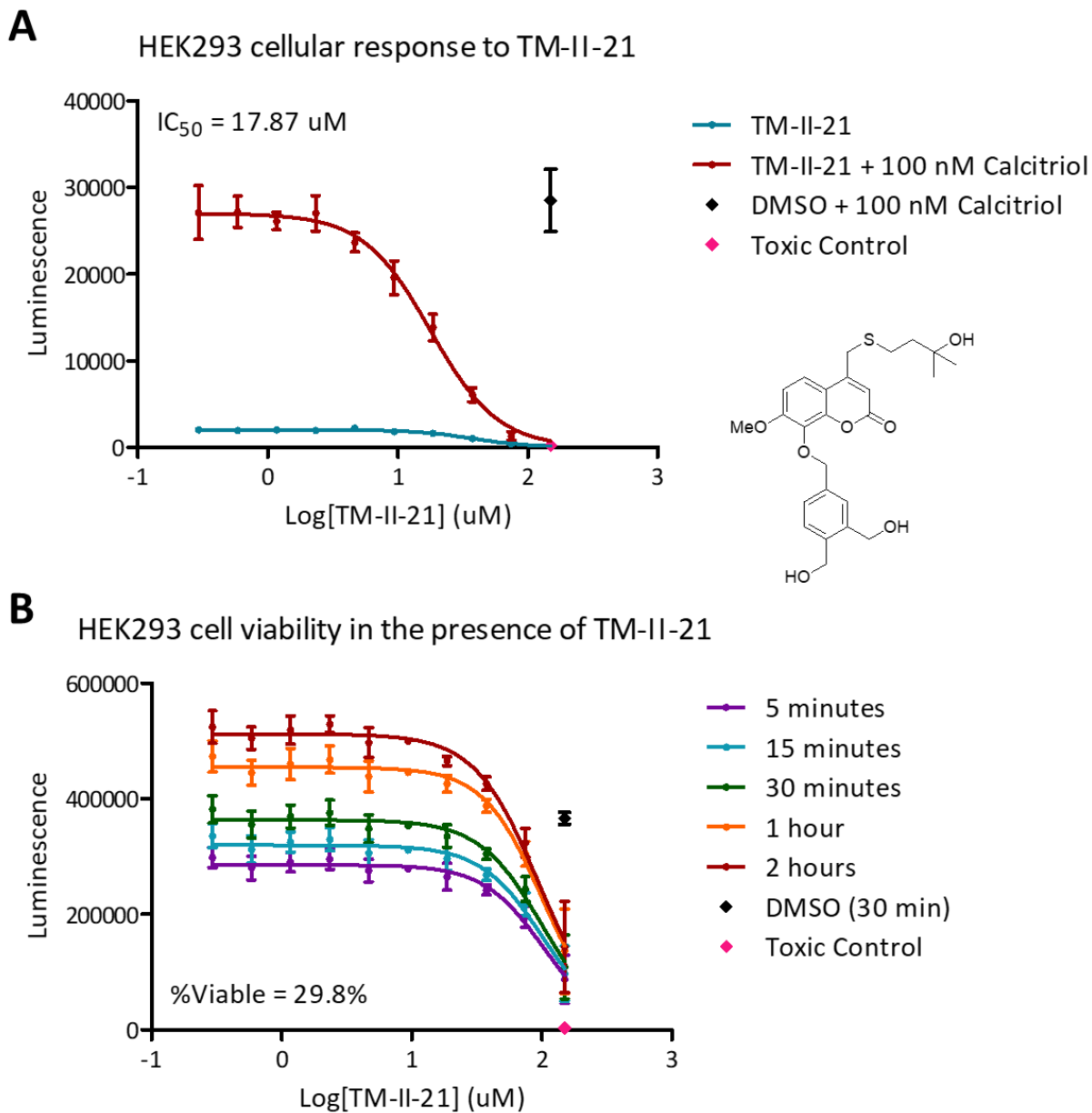
Figure 58. A) Results of TM-III-20 agonistic (blue) and antagonistic (red) effects on VDR, relative to 100 nM calcitriol and 500 nM 31b (toxic control). B) HEK293 cell viability while in the presence of increasing TM-III-20 concentrations.

TM-III-31 followed suit in transcriptional activity to the other series B compounds. CYP24A1

recognition did not occur when in the presence of TM-III-31, as displayed by the unaffected

luminescence signal. (Figure 59A) Reduction of the luminescent signal was observed with

increasing concentrations of TM-III-31 while in the presence of 100 nM calcitriol, indicating an

inhibition of luciferase transcription. The IC_{50} of TM-III-31 was observed at 21.84 µM (Log IC_{50} =

1.339 uM, R^2 = 0.9595). (Figure 59A) Transfected HEK293 cell viability was impacted with

increasing concentrations of TM-III-31. At 150 µM TM-III-31, 60.2% of the HEK293 cells
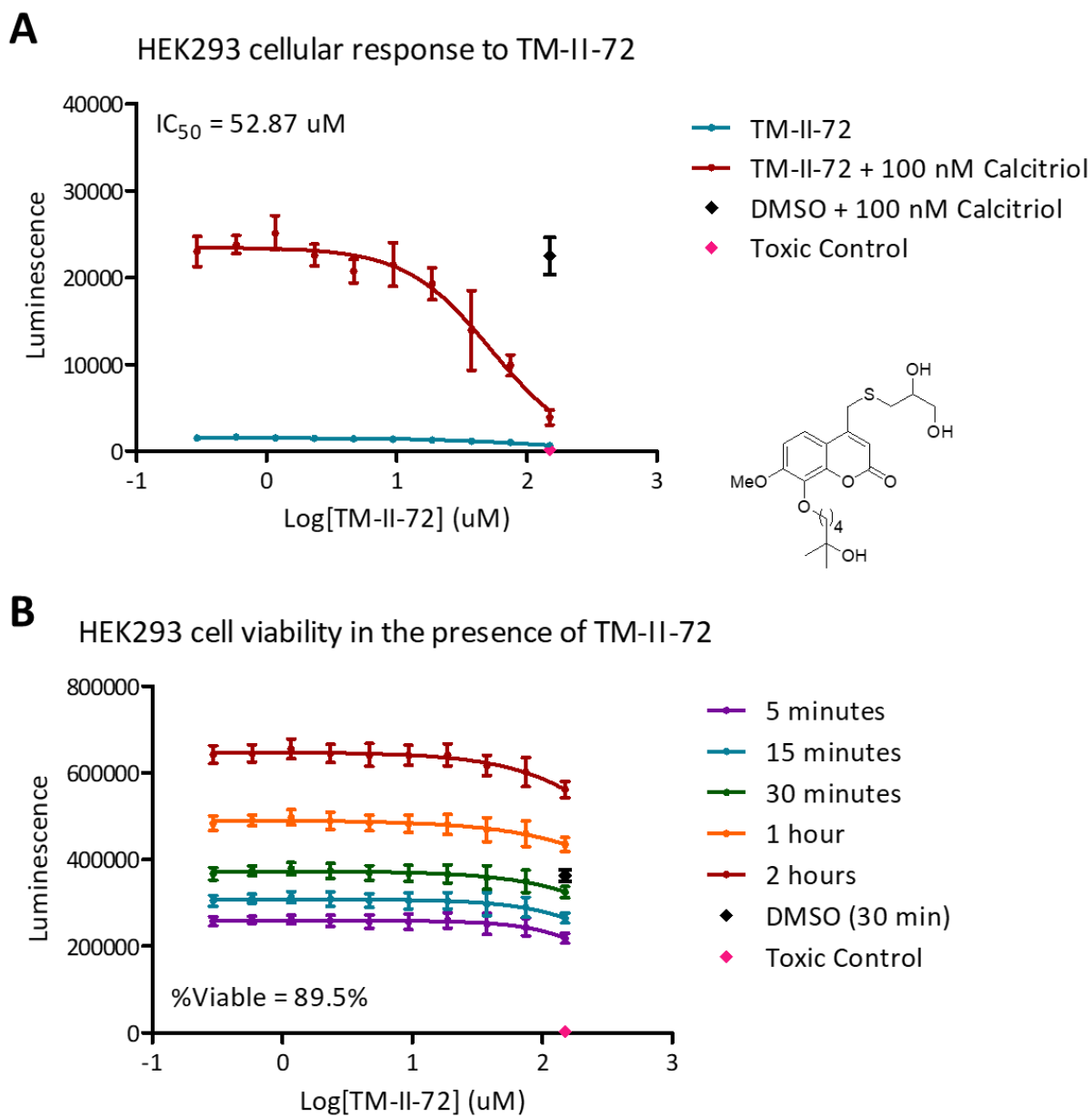
remained viable. (Figure 59B)

Figure 59. A) Results of TM-III-31 agonistic (blue) and antagonistic (red) effects on VDR, relative to 100 nM calcitriol and 500 nM 31b (toxic control). B) HEK293 cell viability while in the presence of increasing TM-III-31 concentrations.

TM-III-90 was the first compound to be analyzed *in vitro* that contained the linear series D

scaffold. No CYP24A1 recognition was observed when using TM-III-90 to activate VDR, as seen

through the unchanging luminescent signal. (Figure 60A) Interference of luciferase transcription

was displayed as the concentration of TM-III-90 increased while in the presence of 100 nM

calcitriol. The IC_{50} of TM-III-90 was observed to be 18.47 µM (Log IC_{50} = 1.266 uM, R^2 = 0.9700).

(Figure 60A) The viability of the transfected HEK293 was greatly impacted with increasing

concentrations of TM-III-90. The highest concentration of TM-III-90 tested (171 µM) left 3.9% of

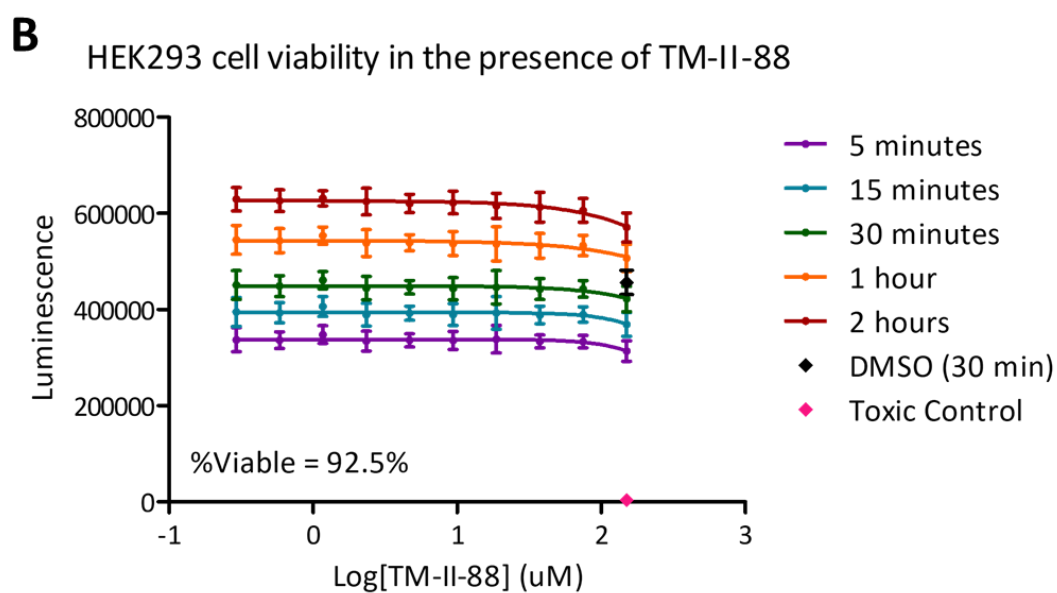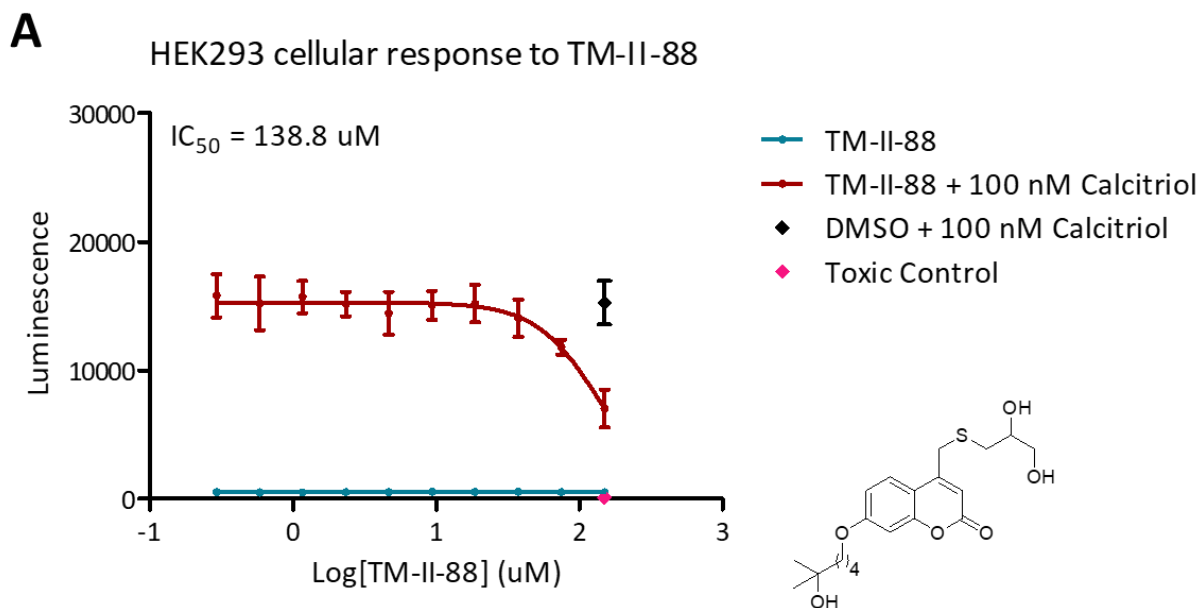the HEK293 cells viable. (Figure 60B)

Figure 60. A) Results of TM-III-90 agonistic (blue) and antagonistic (red) effects on VDR, relative to 100 nM calcitriol and 500 nM 31b (toxic control). B) HEK293 cell viability while in the presence of increasing TM-III-90 concentrations.

Compound TM-III-91, the hydrolysis product of TM-III-90, did not act as an agonist toward VDR

to induce luciferase transcription, and thus did not alter the luminescent signal. (Figure 61A)

Differing from the prior compounds discussed, TM-III-91 did not inhibit luciferase transcription

while in the presence of 100 nM calcitriol. (Figure 61A) The inhibition of gene transcription

displayed by TM-III-90 indicates that the series D scaffold is able to interfere with the VDR-

calcitriol interaction. TM-III-91 contains a polar carboxylate group that is presumed to prevent

the compound from passing through the nuclear membrane. Gene transcription would

therefore be unaffected if the compound remains in the cytoplasm. The viability of the

transfected HEK293 cells was minimally impacted by increasing concentrations of TM-III-91. The

highest concentration of TM-III-91 tested (171 µM) left 93.1% of the HEK293 cells viable. (Figure
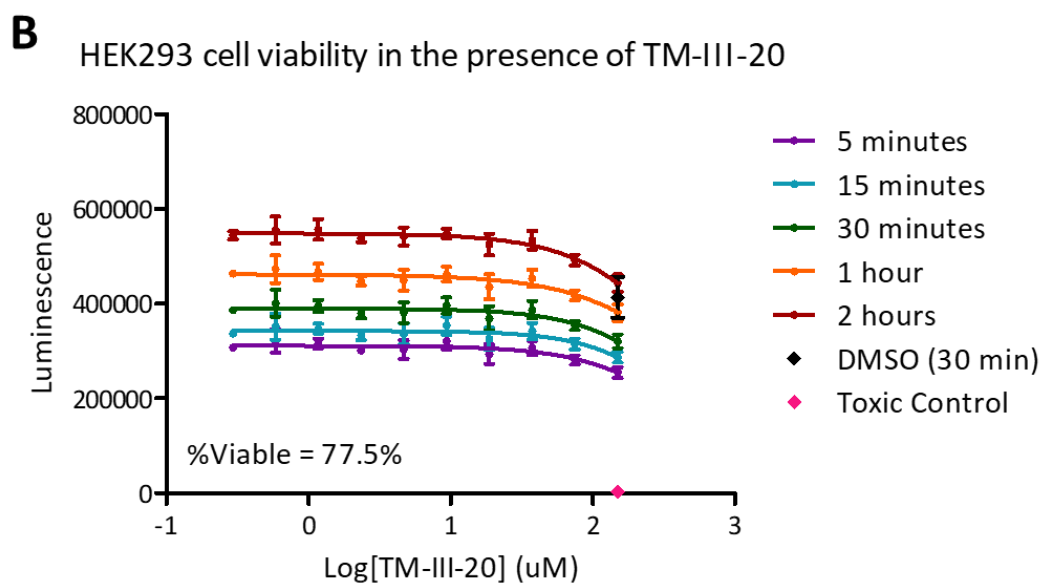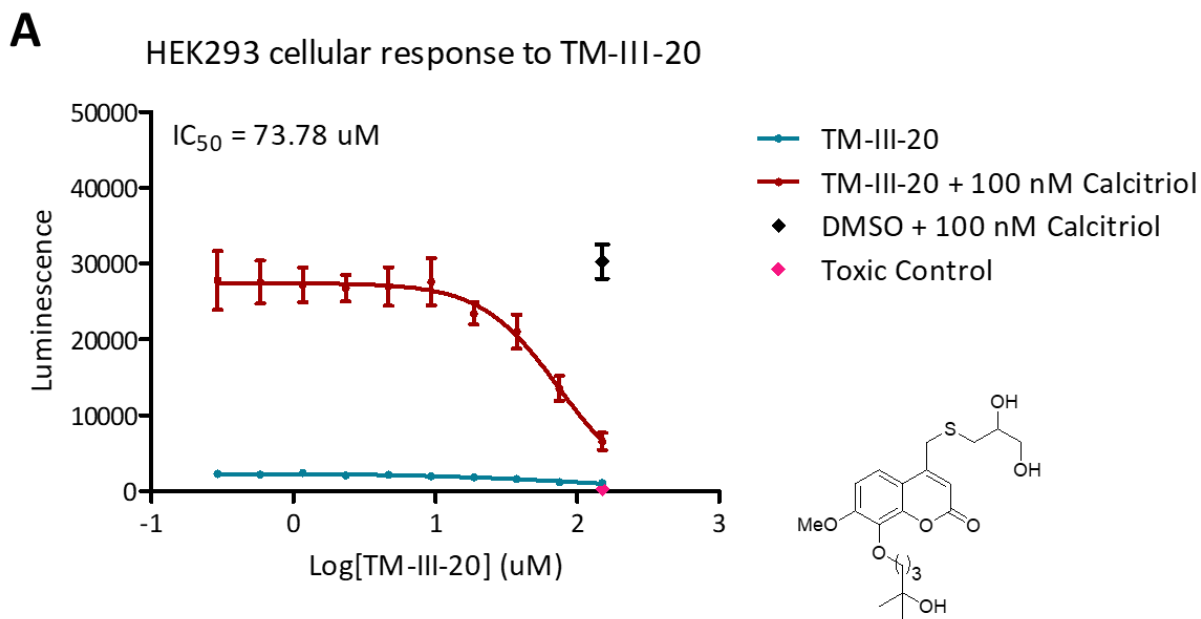
61B)

Figure 61. A) Results of TM-III-91 agonistic (blue) and antagonistic (red) effects on VDR, relative to 100 nM calcitriol and 500 nM 31b (toxic control). B) HEK293 cell viability while in the presence of increasing TM-III-91 concentrations.

TM-IV-6 did not induce CYP24A1 recognition during the transcription assay, leaving the luminescent signal unphased. (Figure 62A) When in the presence of 100 nM calcitriol, inhibition of luciferase transcription and reduction of the luminescent signal was displayed with increasing concentrations of TM-IV-6, however. The IC_{50} of TM-IV-6 was observed at 33.43 μM (Log IC_{50} = 1.524 uM, R^2 = 0.9749). (Figure 62A) Toxicity on the transfected HEK293 cells is associated with increasing concentrations of TM-IV-6. The highest concentration of TM-IV-6 evaluated (171 μM) left only 36.7% of the HEK293 cells viable. (Figure 62B)

Figure 62. A) Results of TM-IV-6 agonistic (blue) and antagonistic (red) effects on VDR, relative to 100 nM calcitriol and 500 nM 31b (toxic control). B) HEK293 cell viability while in the presence of increasing TM-IV-6 concentrations.

Compound TM-IV-16 did not induce luciferase transcription, leaving the luminescent signal

unphased as the concentration of TM-IV-16 increased. (Figure 63A) In the presence of 100 nM

calcitriol, inhibition of CYP24A1 recognition and reduction of luminescence occurred with

increasing concentrations of TM-IV-16. The IC_{50} of TM-IV-16 was seen at 60.19 μM (Log IC_{50} =

1.780 uM, R^2 = 0.9458). (Figure 63A) The viability of HEK293 cells decreased with increasing

concentrations of TM-IV-16 under the transfected conditions. The highest concentration of TM-

IV-16 evaluated (171 μM) left 59.5% of the HEK293 cells viable. (Figure 63B)
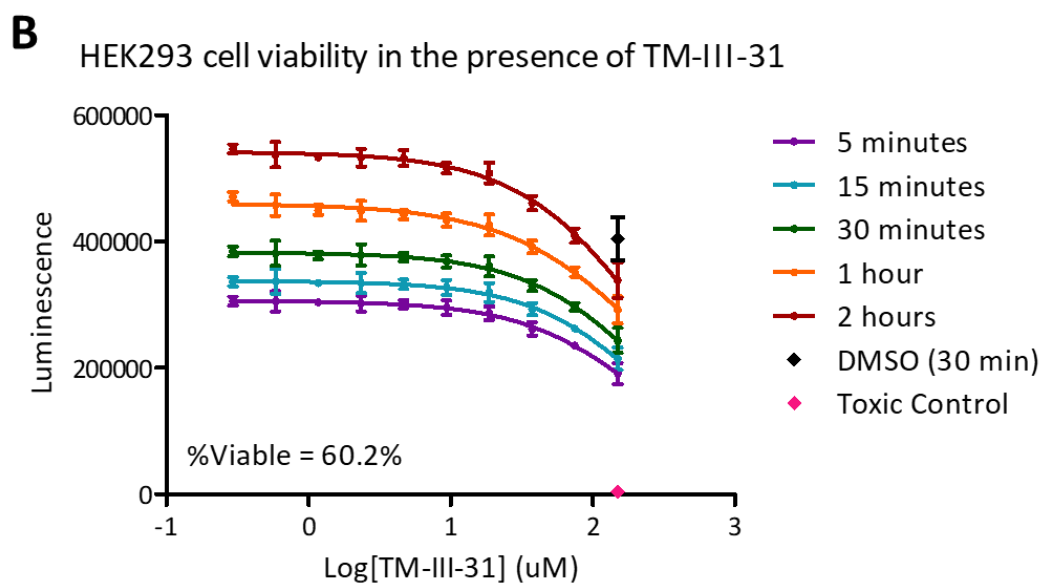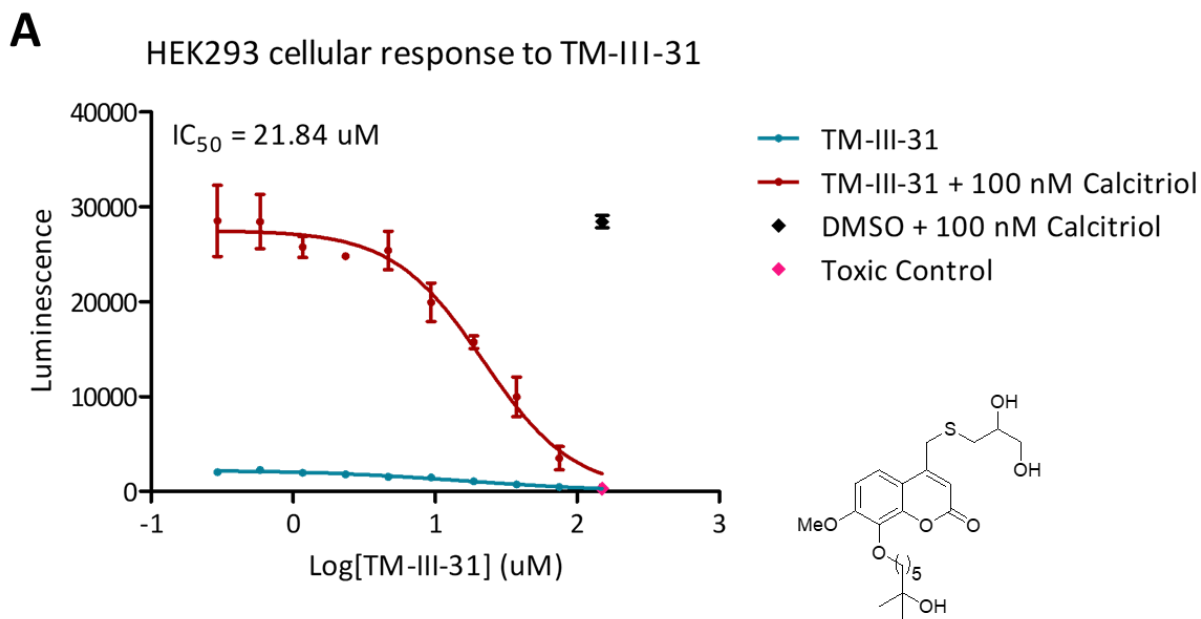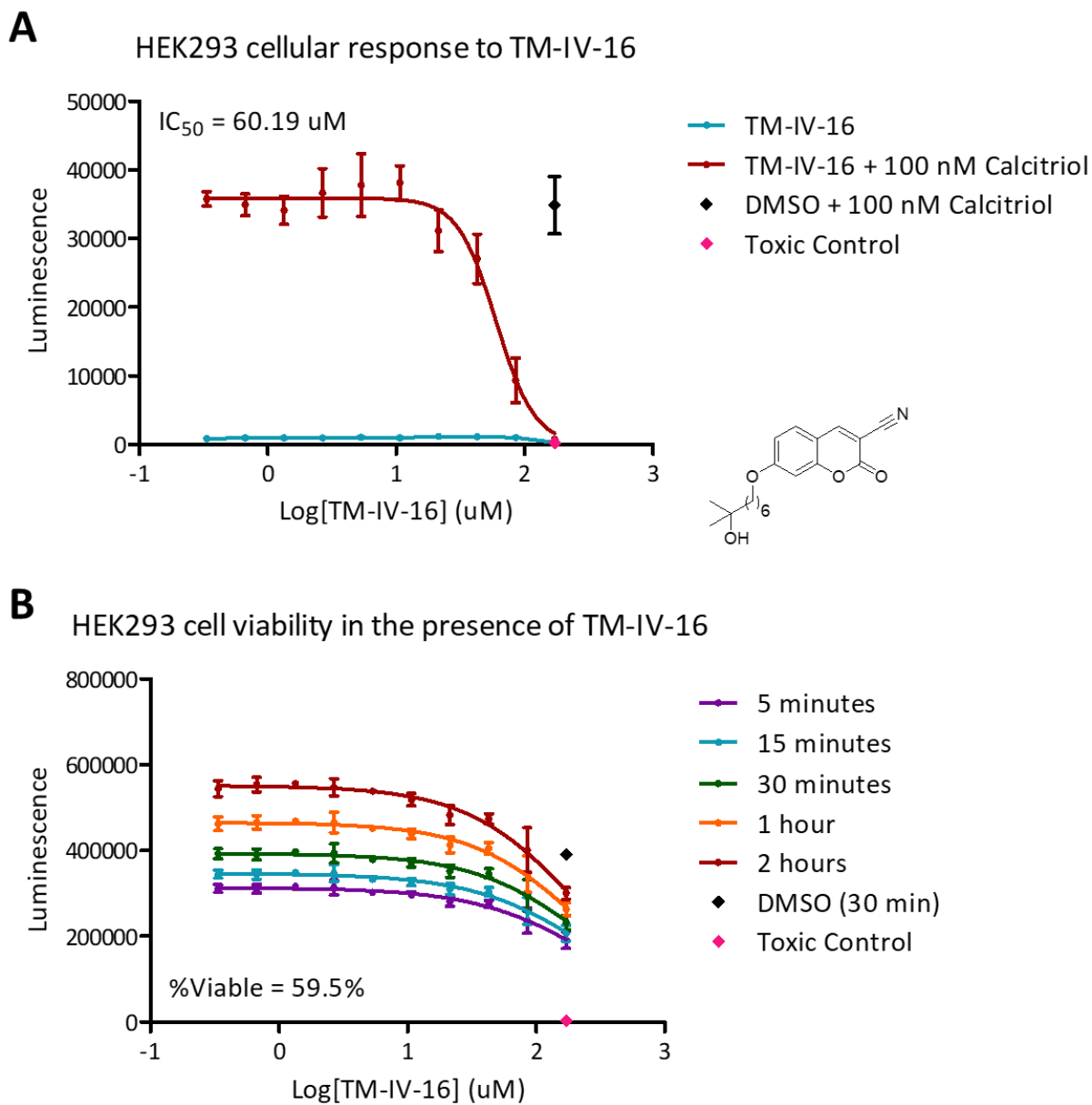
Figure 63. A) Results of TM-IV-16 agonistic (blue) and antagonistic (red) effects on VDR, relative to 100 nM calcitriol and 500 nM 31b (toxic control). B) HEK293 cell viability while in the presence of increasing TM-IV-16 concentrations.

The final compound evaluated, TM-IV-18, contains a chiral secondary alcohol that resulted from the ketone reduction of compound TM-IV-6. When in the presence of 100 nM calcitriol, inhibition of CYP24A1 recognition and reduction of luminescence occurs with increasing concentrations of TM-IV-18. The IC_{50} of TM-IV-18 is observed at 26.95 µM (Log IC_{50} = 1.431 uM, R^2 = 0.9742). (Figure 64A) While TM-IV-18 does not activate VDR as effectively as calcitriol, a small increase in the agonist curve hints toward some luciferase transcription by TM-IV-18. (Figure 64A) Significant toxicity of the transfected HEK293 cells was exhibited with increasing concentrations of TM-IV-18. The highest concentration of TM-IV-18 tested (171 µM) left only 1.3% of the HEK293 cells viable. (Figure 64B) The strong cellular toxicity associated with TM-IV-18 is thought to be interfering with potential agonistic activity by the compound at higher concentrations. A slight increase in luminescence is observed at 2.68 µM TM-IV-18 relative to the DMSO control, which supports the speculation of minimal agonistic activity by TM-IV-18. (Figure 65)
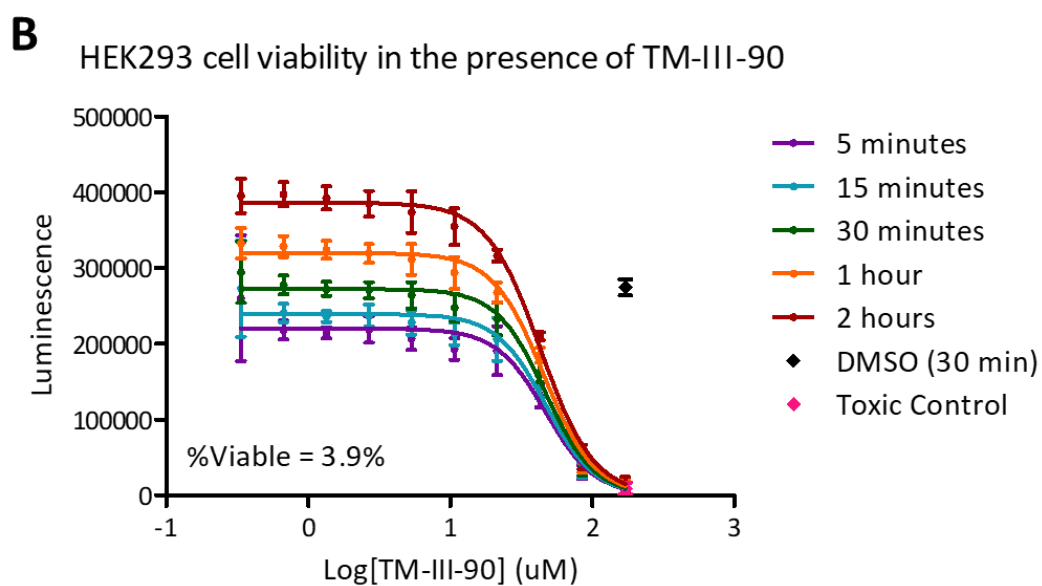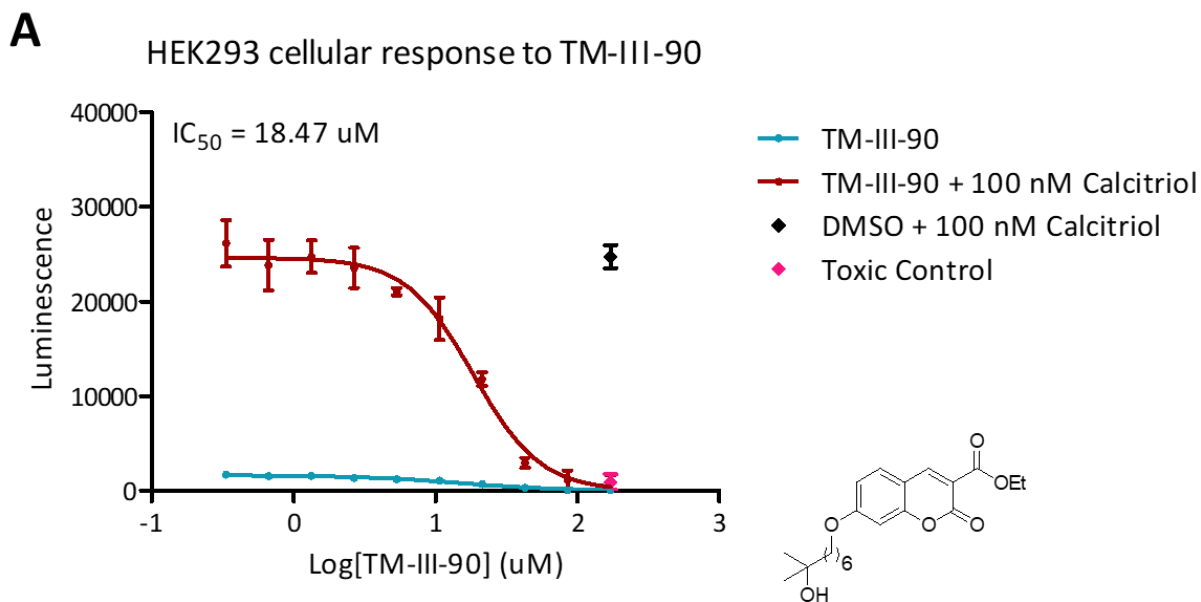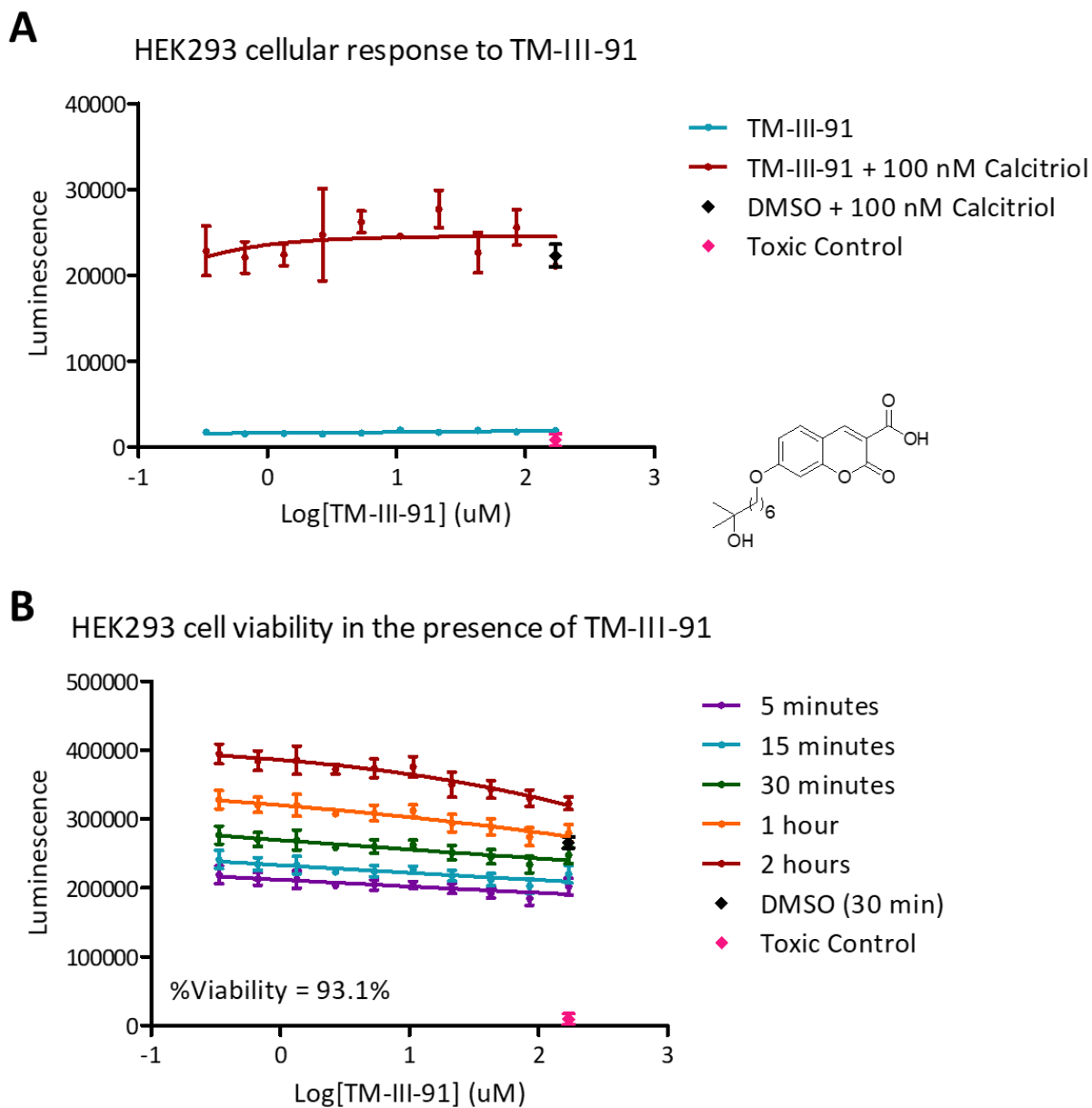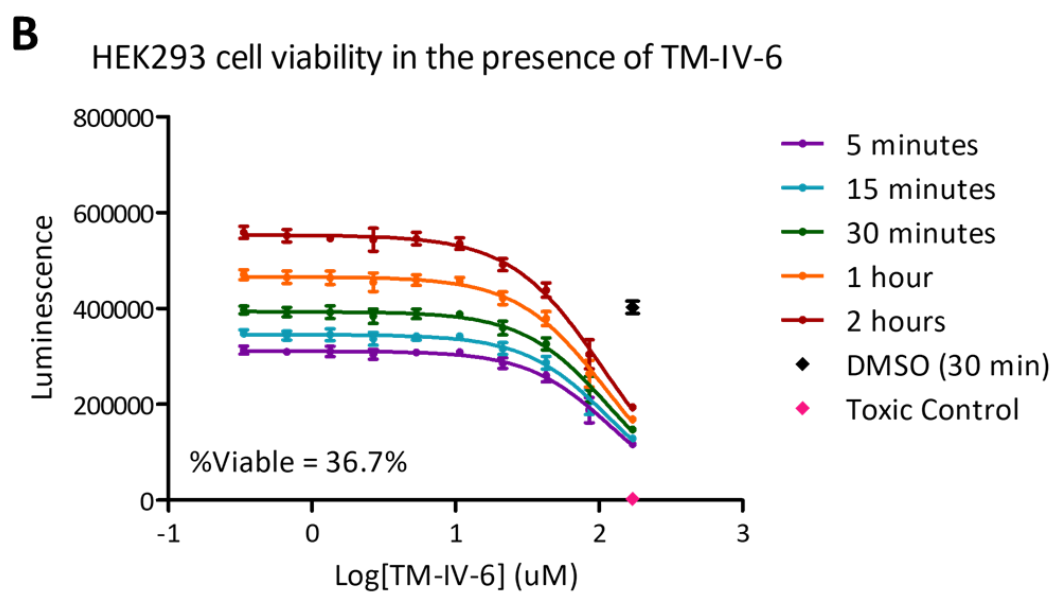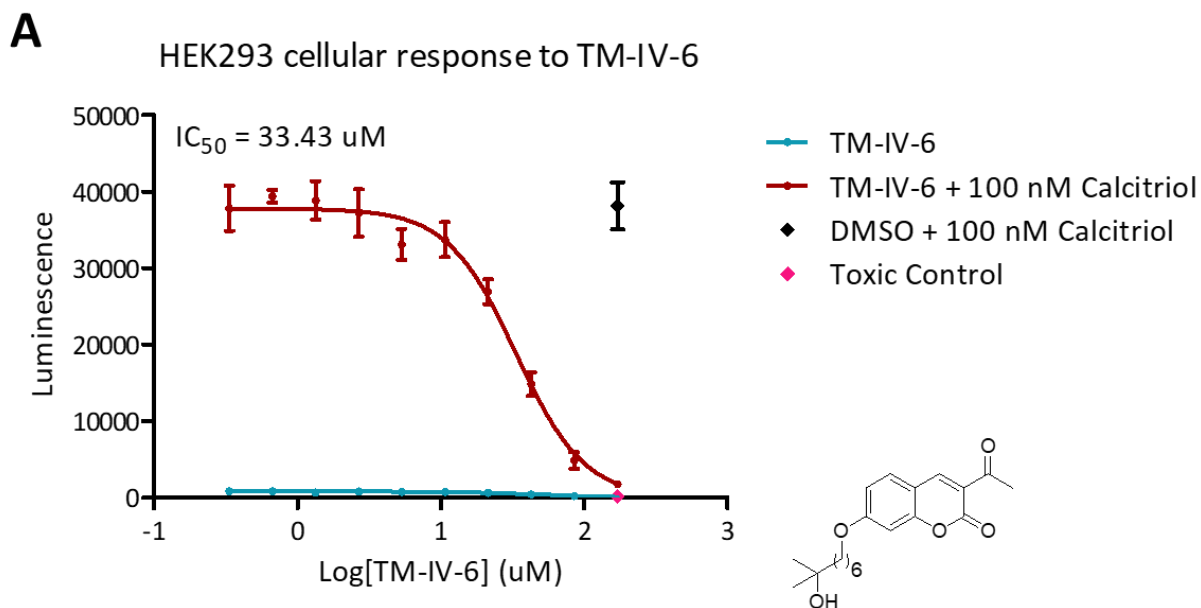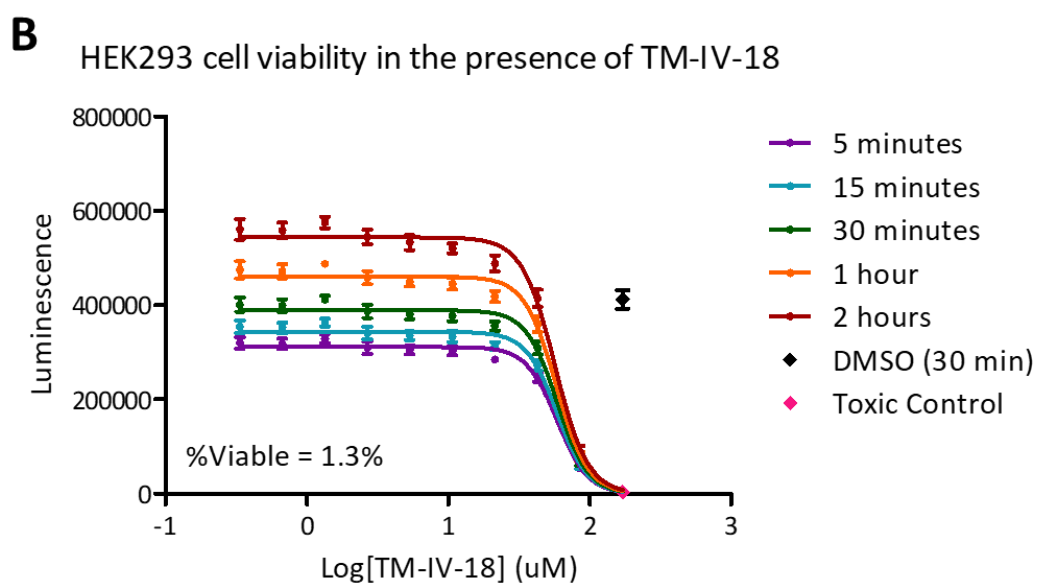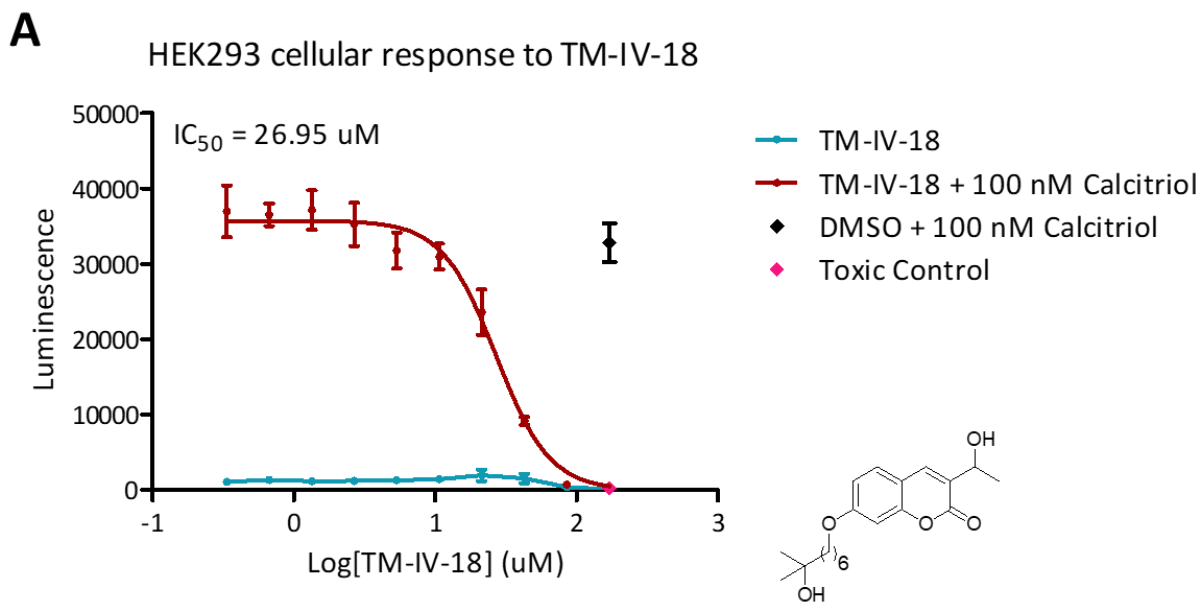
Figure 64. A) Results of TM-IV-18 agonistic (blue) and antagonistic (red) effects on VDR, relative to 100 nM calcitriol and 500 nM 31b (toxic control). HEK293 cell viability while in the presence of increasing TM-IV-18 concentrations.

Figure 65. Enhanced view of TM-IV-18 agonistic activity relative to DMSO and toxic controls.

Discussion

Ten synthetic ligands were evaluated in the transcription assay to determine their respective agonist and antagonistic properties towards VDR. Series A, B, and C compounds were not able to induce CYP24A1 recognition and luciferase transcription, as displayed through a consistent baseline luminescent signal. Series D compounds also lacked the agonistic activity to induce luciferase transcription, although compound TM-IV-18 is speculated to potentially activate VDR at concentrations ranging from 10 to 20 μM. All of the compounds were able to disrupt the calcitriol-VDR interaction to varying extents at high concentrations, with the exception of TM-III-91 which was likely unable to cross the nuclear membrane. Compound TM-II-21 antagonized VDR most effectively, with an IC_{50} value of 17.87 μM, while compound TM-II-88 was the weakest antagonist, with an IC_{50} value of 138.8 μM. Additionally, viability of the transfected HEK293 cells was evaluated while in the presence of each synthetic ligand. Overall, compound TM-II-72 displayed the least toxicity coupled with the highest antagonistic activity (IC_{50} = 52.87 μM) toward VDR. At a concentration of 150 uM, 89.5% of the transfected HEK293 cells remained viable while in the presence of TM-II-72. Compound TM-III-91 minimally impacted the cellular environment, retaining 93.1% cell viability at a concentration of 171 uM. Similarly, TM-II-88 also displayed minimal toxicity with 92.5% of the HEK293 cells remaining viable while in the presence of 150 μM TM-II-88. Both TM-IV-18 and TM-III-90 were toxic. A concentration of 171 μM TM-IV-18 left only 1.3% of the HEK293 cells viable, while 171 μM TM-III-90 left 3.9% of the HEK293 cells viable. The toxicity of TM-IV-18 at increasing concentrations would cover any potential agonistic activity exhibited by the compound at high concentrations. The racemic ratio of the chiral secondary alcohol in TM-IV-18 is assumed to be 1:1 but has not been determined.

136

Synthesis of the individual enantiomers may uncover further insight toward the behavior of TM-IV-18 as a potential agonist of VDR. The transcription results of TM-IV-18 further support the understanding that an alcohol functionality to hydrogen-bond with the polar residues near the opening of the VDR-LBD is crucial for agonistic activity. Secondary binding assays may be worth exploring with TM-IV-18, as well as for future structural improvements. The fluorescence polarization (FP) assay is a commonly used binding assay for VDR, which is able to interrogate protein-peptide interactions.[9-10] Agonistic and antagonistic results from the luciferase transcription assay can be supported through the binding data available by the FP assay. Surface plasmon resonance (SPR) is another technique that can be utilized for determining the association and dissociation kinetics of potential ligands. Previous studies have utilized SPR to evaluate vitamin D, vitamin D metabolites, and vitamin D analogues with vitamin D binding protein[11], as well as observe the SRC2-3 interaction with VDR in the presence of agonist, partial agonist, and antagonists.[12] These secondary assays are able to provide valuable insights towards ligand-protein interaction that supplement the transcription assay results.

Designing a ligand to satisfy chemical, optical, and biological requirements is a challenging task. The ten fluorescent ligands that emit in the visible light range were developed for VDR and have provided a basis for future development for an appropriate agonist with desirable spectral properties. Development of this unique assay premise will offer a simple means of high-throughput screening to efficiently remove unsuitable drug candidates from consideration when focusing on VDR as a pharmaceutical target.

Transcription assay protocol: Human embryonic kidney (HEK293) cells were cultured in

DMEM/High Glucose (Hyclone™, SH3024301) with 10% heat-inactivated fetal bovine serum

(Fisherbrand™, FB12999102)**,** 1% non-essential amino acids (Hyclone™, SH30238.01), 1% 10

mM HEPES buffer (Hyclone™, SH302237.01), and 1% penicillin and streptomycin (Hyclone™,

SV30010) additives. Using 3 wells of a sterile 6-well plate, 1.5 million HEK293 cells were added

to each well and incubated in DMEM/High Glucose (3 mL/well) for 3 hours. In a sterile 5 mL

conical vial, 990 µL of SFM4Transfx-293 media (Hyclone™, SH30860.02), 0.78 µg of VDR-CMV

plasmid, 7.9 µg of a CYP24A1-luciferase reporter gene, and 12.5 µL of PLUS™ reagent were

combined and incubated at room temperature for 5 minutes. Following, 37.5 µL

Lipofectamine™ LTX (Life Technologies, 15338020) or ViaFect™ Transfection Reagent

(Promega™, E4981) were added to the conical vial and incubated for 30 minutes, before adding

350 µL of the resulting solution to each of the cell-containing wells in the 6-well plate. After 18

hours of incubation at 37 °C with 5% CO_2, the cells were harvested with 300 µL of 0.05% trypsin

(Hyclone™, SH3023601) and added to three separate conical vials in 5 mL of DMEM/High

Glucose. The three conical vials were centrifuged, underwent media exchange, and

resuspended to result in 400,000 cell/mL suspensions. To one conical vial, calcitriol (50 µM in

DMSO) was added to create a 100 nM calcitriol concentration. The suspensions were plated (40

uL/well) in sterile optical-bottom 384-well plates that had been treated with 0.25% Matrigel

solution. The plates were centrifuged for two minutes at 1000 RPM. After two hours, plated

cells were treated with 200 nL of compound, 31b (100 µM in DMSO), or DMSO using an EVO

liquid handling system with a 100 nL pin tool (V&P Scientific, Inc.). After 18 hours of incubation

at 37 °C with 5% CO_2, 20 µL of Bright-Glo™ (Promega™, E2620) reagent was added and

luminescence was detected with a Tecan Infinite M1000 reader. The assay was carried out in quadruplicate trials. Non-linear regression was used to calculate IC_{50} values.

Viability assay protocol: HEK293 cells were treated following the protocol for the transcription assay. After 18 hours of incubation at 37 °C with 5% CO_2, 20 μL of CellTiter-Glo® (Promega, G7572) reagent was added and luminescence was detected with a Tecan Infinite M1000 reader. The assay was carried out in quadruplicate trials. Percent viability was calculated based on the average luminescence of the compound treated wells (highest concentration) relative to the average luminescence of the DMSO control wells.

References

1.   Ishigami-Yuasa, M.; Kagechika, H., Chemical Screening of Nuclear Receptor Modulators. *International Journal of Molecular Sciences* **2020,** *21* (15), 5512.
2.   Weissman, A.; Keefer, J.; Miagkov, A.; Sathyamoorthy, M.; Perschke, S.; Wang, F., Cell-based screening assays. In *Comprehensive Medicinal Chemistry II*, Taylor, J. B.; Triggle, D. J., Eds. Elsevier: 2007; Vol. 3, pp 617-646.
3.   Lea, W. A.; Simeonov, A., Fluorescence polarization assays in small molecule screening. *Expert opinion on drug discovery* **2011,** *6* (1), 17-32.
4.   Anderson, M. G.; Nakane, M.; Ruan, X.; Kroeger, P. E.; Wu-Wong, J. R., Expression of VDR and CYP24A1 mRNA in human tumors. *Cancer chemotherapy and pharmacology* **2006,** *57* (2), 234-240.
5.   Lou, Y.-R.; Molnár, F.; Peräkylä, M.; Qiao, S.; Kalueff, A. V.; St-Arnaud, R.; Carlberg, C.; Tuohimaa, P., 25-Hydroxyvitamin D_3 is an agonistic vitamin D receptor ligand. *The Journal of steroid biochemistry and molecular biology* **2010,** *118* (3), 162-170.
6.   Carlberg, C., Ligand-mediated conformational changes of the VDR are required for gene transactivation. *The Journal of steroid biochemistry and molecular biology* **2004,** *89*, 227-232.
7.   Crouch, S.; Kozlowski, R.; Slater, K.; Fletcher, J., The use of ATP bioluminescence as a measure of cell proliferation and cytotoxicity. *Journal of immunological methods* **1993,** *160* (1), 81-88.

8.   Nandhikonda, P.; Lynt, W. Z.; McCallum, M. M.; Ara, T.; Baranowski, A. M.; Yuan, N. Y.; Pearson, D.; Bikle, D. D.; Guy, R. K.; Arnold, L. A., Discovery of the first irreversible small molecule inhibitors of the interaction between the vitamin D receptor and coactivators. *Journal of medicinal chemistry* **2012,** *55* (10), 4640-4651.

9.   Hall, M. D.; Yasgar, A.; Peryea, T.; Braisted, J. C.; Jadhav, A.; Simeonov, A.; Coussens, N. P., Fluorescence polarization assays in high-throughput screening and drug discovery: a review. *Methods and applications in fluorescence* **2016,** *4* (2), 022001.

10.   Sundberg, S. A., High-throughput and ultra-high-throughput screening: solution-and cell-based approaches. *Current opinion in biotechnology* **2000,** *11* (1), 47-53.

11.   Canoa, P.; Rivadulla, M. L.; Popplewell, J.; van Oosten, R.; Gómez, G.; Fall, Y., Use of surface plasmon resonance in the binding study of vitamin D, metabolites and analogues with vitamin D binding protein. *Analytical and bioanalytical chemistry* **2017,** *409* (10), 2547-2558.

12.   Egawa, D.; Itoh, T.; Kato, A.; Kataoka, S.; Anami, Y.; Yamamoto, K., SRC2-3 binds to vitamin D receptor with high sensitivity and strong affinity. *Bioorganic & medicinal chemistry* **2017,** *25* (2), 568-574.

PART II: DEVELOPMENT OF A SCALABLE MANUFACTURING PROCESS FOR ORCEIN DYE

Chapter Six: Manufacturing of orcein dye

6.1 The history and use of orcein dye

Orcein dye was commonly used as a cheap, alternative means to dye silk and wool various

shades of purple during the Middle Ages.[1] It was nicknamed "poor person's purple", regularly

being compared to Tyrian purple, which was known to be an extremely precious and expensive

dye.[2] Today, orcein is known and commercially available as Natural Red 28.[3] *Roccella*, *Lecanora*,

and *Varialaria* lichens have historically been the natural source to obtain the red-violet dye.

Orsellinic acid depside components from the lichens undergo hydrolysis, decarboxylation, and

treatment with either urine or ammonia and air to produce orcein dye.[1] (Scheme 13) In present

day, direct production from synthetic orcinol is more common.[4]
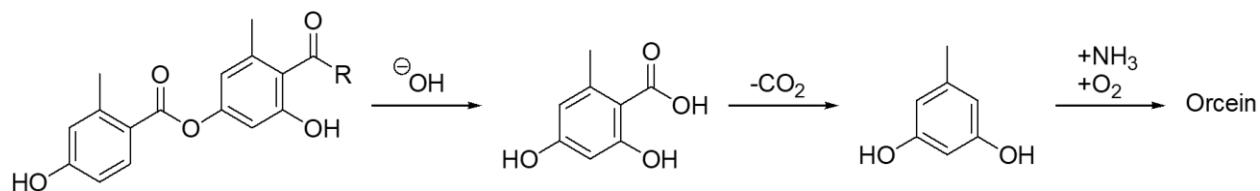
Scheme 13. Extraction of orcein dye from lichen depsides.

The composition of orcein dye was determined when partition chromatography became an

available technique in the 1940s.[5] Shortly thereafter, between 1955-1957, eight major and six

minor components of orcein dye were isolated.[6-7] (Figure 66) The eight major structural

components include α, β, and γ-derivatives of both hydroxy and amino orcein, as well as β and

γ-amino orceimin. The α-derivatives have a singular orcinol substituent at position 6, whereas

the beta and gamma derivatives contain orcinol substituents at both positions 3 and 6. Steric

hindrance, caused by the presence of methyl functional groups in positions 4 and 5 on the

parent structure, prevents free rotation of the orcinol substituents around the linkage axes at

room temperature. The β and γ-derivatives are therefore *cis-trans*-isomeric compounds. The

trans-racemate has previously been labeled as the β-derivative, whereas the *cis*-racemate has

been labeled as the γ-derivative.[1]
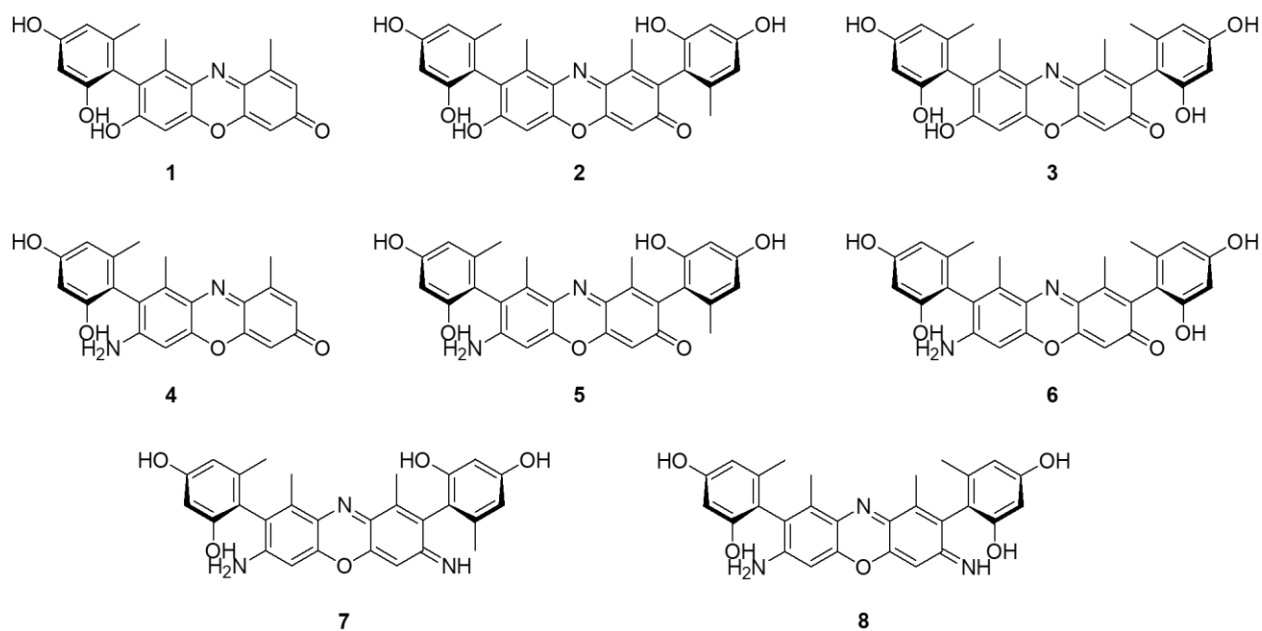
Figure 66. Major components of orcein dye: 1) α-hydroxy orcein 2) β-hydroxy orcein 3) γ-hydroxy orcein 4) α-amino orcein 5) β-amino orcein 6) γ-amino orcein 7) β-amino orceimin 8) γ-amino orceimin

Orcein dye is not frequently used to color fabrics anymore but has since been adopted for

histochemical staining. German Professor of Dermatology, Paul Unna, first reported the staining

of elastic fibers in skin a red-brown color in 1890, thus starting the use of orcein as a

histochemical stain.[8-9] Histochemistry is an important and widely used technique for

visualization of colorless cellular components and biological tissues. Exploiting the interaction

of stains with cellular components allow for simple visualization of contrasted components

under a microscope. Orcein has been a favorable dye due to its simple preparation procedure, ease of use, versatile nature, and ability to be combined with counterstains, which can optimize the visibility of various structures.[10] A typical solution of orcein can be prepared by combining 0.1-1% orcein and 1% HCl in 70% ethanol.[10] Variations in preparation and application can be done to visualize different biological components that include, but are not limited to, altered stromal material, elastic and connective tissues, collagen, basement membrane, chromosomes, hepatitis B surface antigens, copper-associated protein, and hepatocellular carcinoma.[11]

6.2   Synthetic approach towards α-hydroxy orcein

The current process towards orcein dye manufacturing continues to utilize the exposure of orcinol to ammonia gas in the presence of oxygen. Since this process is known to yield eight major and six minor chemical structures, batch to batch differences can vary greatly, even when produced by the same manufacturer.[4, 12] Although the chemical components have been isolated, it is currently unclear which compounds or combination thereof are responsible for staining the various structures in tissue sections. Isolated synthesis of the specific chemical components within orcein dye will allow for the determination of the structures responsible for optimal staining. Furthermore, consistency with the synthesis of orcein dye would diminish the variation currently observed between stain batches.

The initial synthetic route towards α-hydroxy orcein was conceived as a five-step process starting from commercially available orcinol. (Scheme 14) Step one began with the protection of both phenolic positions of orcinol as methoxy groups, which has been reported with quantitative yields.[13] Following this reaction, electrophilic aromatic bromination using NBS has been reported to yield the 2-substituted aryl bromide in high yield.[13-14] Production of the aryl bromide allows for a variety of potential cross-coupling mechanisms to yield the biphenyl scaffold. The Suzuki-Miyaura cross-coupling reaction is an appealing mechanism to use, as this reaction is successful with a variety of aryl substrates while tolerating a wide range of functional groups.[15] Additionally, it has been shown to be a successful reaction in the cross-coupling of hindered substates.[16-17] The scalability of the Suzuki-Miyaura reaction is beneficial when developing a process for industrial-sized batches, as reagents used are typically non-toxic and air stable in respect to boronic acid.[15] In order to minimize the number of steps of the synthetic route, *in situ* generation of the aryl boronate ester would precede the cross-coupling with a second equivalent of the aryl bromide to yield the biaryl product. Demethylation to form the
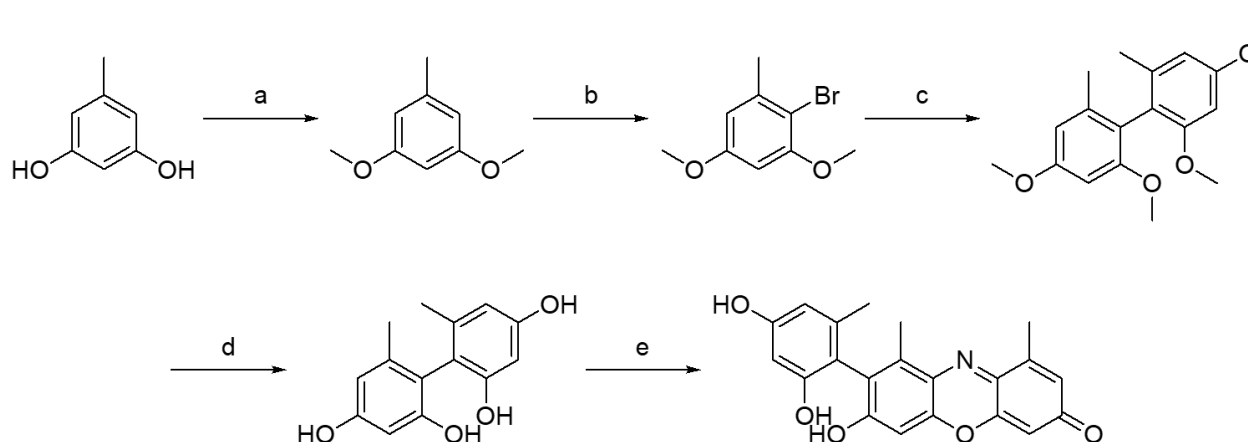
Scheme 14. Initial synthetic route towards α-hydroxy orcein: a) MeI, K$_2$CO$_3$, Acetone b) NBS, DCM c) 1. *n*-BuLi, B(OMe)$_3$ 2. Pd(PPh$_3$)$_4$, 2-Bromo-3,5-dimethoxytoluene, K$_2$CO$_3$ d) BBr$_3$, DCM e) 5-Methyl-4-nitroso-benzene-1,3-diol, H$_2$SO$_4$, Water.

deprotected tetrol has been reported in the presence of boron tribromide[18], a common reagent

used to demethylate ethers. To yield the final compound, α-hydroxy orcein, cyclization

between the 4 or 4'-phenol on the biaryl with the appropriately substituted aryl nitroso could

be accomplished under acidic conditions. Reacting isopentyl nitrite with orcinol in the presence

of potassium hydroxide, water, and ethanol has proven to be a simple means for obtaining 5-

methyl-4-nitrosobenzene-1,3-diol in good yield on industrial scale. The final cyclization step

using the nitroso compound was reported by Musso in 1957, where the final compound was

formed in low yield.[19] We anticipate that further optimization of the cyclization might increase

the yield of this reaction.

6.2.1   Completed reaction steps

The methylation of orcinol was a straightforward reaction in which K_2CO_3 was used to

deprotonate both phenolic hydrogens, and the phenolates subsequently behave as

nucleophiles to substitute iodide on iodomethane. Theoretically the

reaction requires two equivalents of K_2CO_3 and two equivalents of

iodomethane for each equivalent of orcinol, in order to obtain the

dimethylated product. The first run of the compound took five days

to complete while refluxing between 55-60°C in acetone, utilizing

3.5 equivalents of K_2CO_3 and 4.5 equivalents of iodomethane.

Iodomethane appeared to escape the system too quickly at this

temperature, as its boiling point is 42°C. The second reaction batch
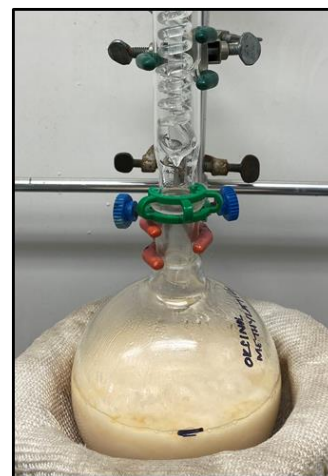
Figure 67. Methylation of orcinol (at reflux).

refluxed between 40-45°C for a total of three days before complete conversion to the

dimethylated product was observed. (Figure 67) Furthermore, this batch only used three

equivalents K_2CO_3 and three equivalents of iodomethane for each equivalent of orcinol on a 67-

gram scale.

Bromination of the aromatic ring began by screening different solvents for reaction

compatibility. Electrophilic aromatic bromination is commonly performed in chlorinated

solvents such as CCl_4 or DCM.[20] Due to environmental concerns with chlorinated solvents that

become increasingly prominent on the industrial scale, a screening was done to find an

environmentally friendly and reaction-compatible solvent to perform the reaction. Solvents

that were tested included DCM, DMF, toluene, dioxane, Et_2O, MTBE, and THF. (Figure 68)
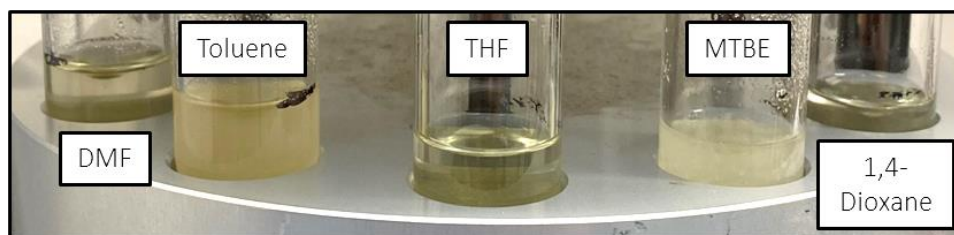
Figure 68. Aromatic bromination solvent screening, after NBS addition.

All of the solvents that were screened appeared to be compatible with the reaction and formed

the same major product by TLC after one hour. Promising trials for ease of product isolation

included the reactions performed in toluene and DMF. Succinimide, a known byproduct of the

reaction, is marginally soluble in toluene and enables removal by filtration. On the other hand,

DMF is water miscible, which enables precipitated the desired product as a white powder.

(Figure 69) Either of these solvents and methods had potential to become convenient processes

for the industrial scale. Emphasis was given to minimization of equipment transfers allowing for

less product loss and ultimately providing higher yields. Ultimately, DMF was chosen as the

147

reaction solvent for this process due to a slightly cleaner crude product. Repeating this reaction on a larger scale revealed heat formation that occurs during the NBS addition when using DMF as a solvent.[21] This went unnoticed when performing the reaction on the milligram scale. Further optimization on this process in regard to solvent use and reaction compatibility will need to be addressed prior to synthesis with kilogram-scale batches.

Figure 69. Slurry formation after cold water addition to the DMF trial.

The envisioned *in situ* reaction in which an aryl boronate intermediate is cross-coupled with a second equivalent of aryl bromide was a complex process and did not initially form the biaryl dimer under the original conditions. (Scheme 15) To confirm successful borylation of the aryl bromide, isolation of the aryl boronic acid intermediate was achieved to negate possibility of issues arising from the first step of this reaction.
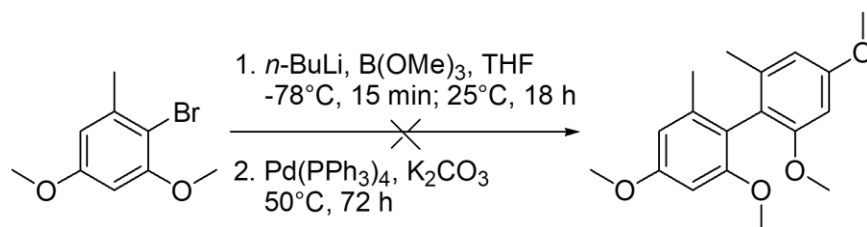
Scheme 15. Attempted in situ aryl borylation and Suzuki-Miyaura cross-coupling conditions.

The aryl boronic acid was formed through halogen-lithium exchange using *n*-BuLi in a mixture of Et$_2$O and THF. After stirring for one hour at -65°C, trimethyl borate was added over an additional two hours to form the aryl boronic ester. Conversion observed by TLC prompted the addition of 3 M HCl in water at -65°C. The reaction gradually warmed up to room temperature, causing the aryl boronic acid to slowly crash out of solution. The product was isolated by filtration; however, a higher yield was obtained when Et$_2$O was used to extract additional

product from the aqueous layer. Further washing of the crude material was done by stirring in hexanes and filtering. Optimizing the percentage of THF used during the lithium-halogen exchange would likely negate the need to perform a work-up on the aqueous layer during product isolation.

6.2.2   Biaryl cross-coupling attempts

Formation of the desired biaryl dimer turned out to be a very challenging task. There is steric hindrance to overcome when forming a tetra-*ortho*-substituted structure. Furthermore, oxidative addition becomes increasingly less favorable when working with electron-rich aryl halides during palladium cross-coupling.[15, 22-23] The Suzuki-Miyaura cross-coupling attempt using Pd(PPh$_3$)$_4$ and K$_2$CO$_3$ was the first attempt at forming the biaryl after separately isolating the aryl boronic acid. The solvent was switched to DMF from THF, which was used during the previously described *in situ* trial. The reflux temperature of THF is 66°C, therefore DMF was used in hopes that a higher reflux temperature would aid in overcoming the energy barrier associated with the particular reaction. A similar procedure was reported tri-*ortho*-substituted products in 78% yield.[14] Unfortunately, biaryl dimer formation was not observed under these conditions. (Scheme 16)
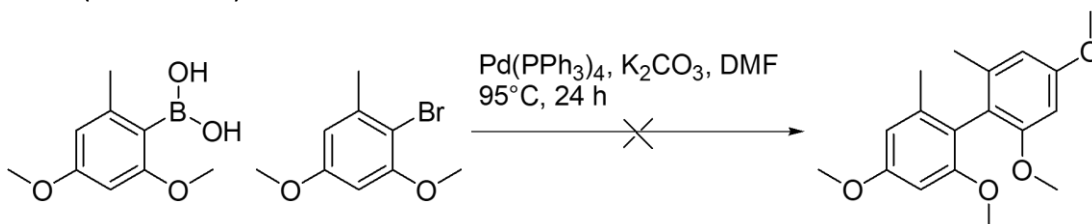
Scheme 16. Attempted conditions for the Suzuki-Miyaura cross-coupling after boronic acid isolation.

149

To investigate, whether oxidative addition or ligand exchange is responsible for the absence of

product, replacement of the synthesized aryl bromide with phenyl bromide was attempted.

Successful synthesis of this moiety would confirm steric hindrance as the problematic step in

catalytic cycle of the cross-coupling reaction. Beyond using DMF as the solvent, mixtures of

DMF/H_2O, DME/H_2O, ACN/H_2O, THF/H_2O, and toluene/H_2O were also screened as potential

solvent systems. Furthermore, Cs_2CO_3 was used as the base in the dry DMF, as K_2CO_3 was not

fully soluble in this solvent. The reactions were carried out in parallel at 75°C (in an attempt to

not overly exceed the boiling point of THF); however, after 18 hours there was no indication of

$C(sp^2)$-$C(sp^2)$ cross coupling by ^{13}C NMR. The reaction was heated to 100°C for an additional 20

hours, but no biaryl dimer formation was observed following the temperature increase.

(Scheme 17)
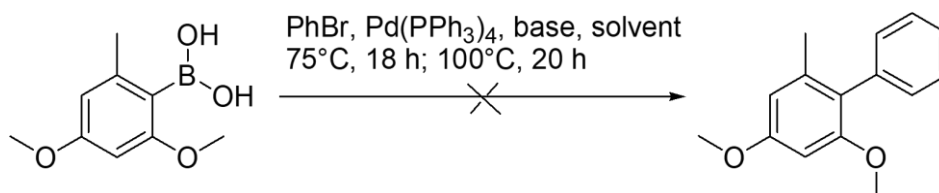
Scheme 17. Suzuki-Miyaura test reaction with phenyl bromide.

At this time, a change of palladium catalyst was thought to be necessary for successful

synthesis of the desired biaryl dimer. Reactions using $Pd_2(dba)_3$ and SPhos had been shown to

successfully synthesize tetra-*ortho*-substituted products by following the Suzuki-Miyaura

reaction mechanism[16] so similar conditions were applied in our cross-coupling attempts.

Potassium phosphate was substituted by K_2CO_3. Comparable conditions otherwise were

followed in that two equivalents of aryl boronic acid and four equivalents of K_2CO_3 were used

for each equivalent of aryl bromide. Additionally, 3 mol% of $Pd_2(dba)_3$ and 10 mol% of SPhos

were added to the reaction. The reaction mixture was stirred in dry and degassed toluene for

18 hours at 100°C. A small peak at 118.48 ppm in the ^{13}C NMR hints at a minor amount of C(sp^2)-C(sp^2) cross-coupling hat occurred; however, significant dehalogenation of the aryl bromide forming 3,5-dimethoxytoluene rendered this reaction inadequate for the industrial scale. (Scheme 18)
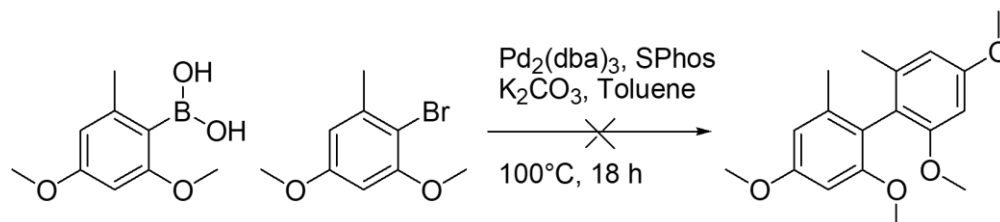
Scheme 18. Attempted Suzuki-Miyaura cross-coupling with alternative catalyst conditions.

The lack of success observed for this particular application of the Suzuki-Miyaura cross-coupling caused us to investigate the application of Negishi cross-coupling conditions. High temperatures that are necessary during the Suzuki-Miyaura reaction may have been a contributing factor for dehalogenation. Thus, employing a different cross coupling at low temperature could potentially provide the biaryl dimer while side-stepping the unwanted dehalogenated product. Additionally, successful application of the Negishi cross-coupling would no longer require the synthesis of the boronic acid intermediate, eliminating a synthetic step from the total synthesis.
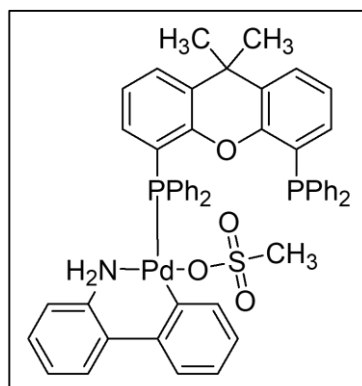
Figure 70. Chemical structure of XantPhos Pd G3.

The Negishi cross-coupling reaction includes a lithium-halogen exchange, followed by formation of an organozinc species. The unstable intermediate is subsequently coupled to a second equivalent of the aryl bromide by palladium catalysis. Initially we explored the use of XantPhos Pd G3 (Figure 70) as a catalyst that was effectively used in an alternative protocol at MilliporeSigma. XantPhos Pd G3 has been used for large-scale synthesis, thus a

suitable catalyst for scale-up chemistry.[24] For each equivalent of aryl bromide, 1.1 equivalents

of *n*-BuLi and 1.2 equivalents of $ZnCl_2$ were used to form the organozinc compound in THF. The

cross-coupling employed 10 mol% of XantPhos Pd G3 and 0.67 equivalents additional aryl

bromide. Unfortunately, after 18 hours at room temperature, a mixture of aryl bromide starting

material and the undesired, dehalogenated product were detected by TLC and confirmed by

NMR. (Scheme 19)
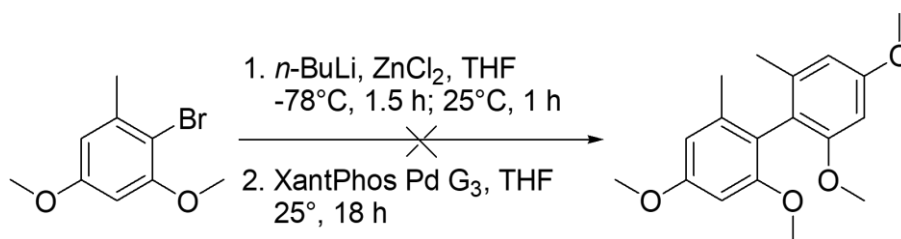
Scheme 19. Attempted Negishi cross-coupling conditions using XantPhos
Pd G3.

The Negishi cross-coupling reaction has been used to generate hindered biaryls when catalyzed

with $Pd_2(dba)_3$ in combination with RuPhos or other ligands.[25] While RuPhos would have been

the preferred ligand to attempt this reaction, it was not readily available to us during this

project. Since SPhos and XPhos (Figure 71) were present in the laboratory and have previously

been successful to a lesser extent, I decided to test these ligands with $Pd_2(dba)_3$ in the Negishi

cross-coupling reaction as well. (Scheme 20)

This process followed the same initial procedure as described

earlier to form the organozinc species. Relative to one

equivalent of the initial aryl bromide, 5 mol% $Pd_2(dba)_3$ and

10 mol% of the respective ligand (SPhos or XPhos) were

applied as the catalyst system. An additional 0.67 equivalents
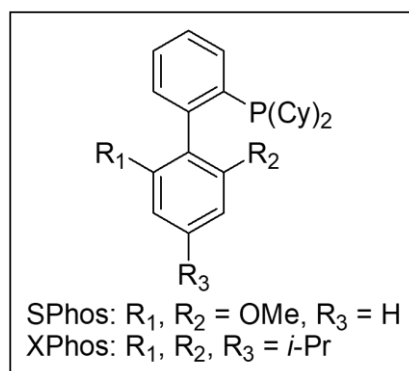
Figure 71. Chemical structures of
SPhos and XPhos.

of aryl bromide were introduced after formation of the organozinc, and NMP was charged as a

co-solvent into the reaction. NMP has been shown to improve reaction yields for certain

coupling products.[25] To our dismay, similar results to the XantPhos Pd G3 trial were observed.
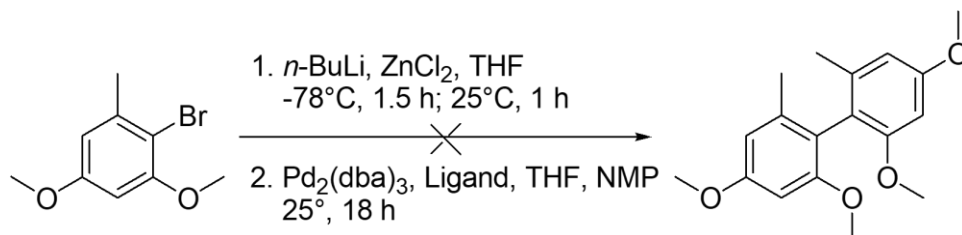
Scheme 20. Attempted Negishi cross-coupling conditions using Pd$_2$(dba)$_3$ and SPhos or XPhos.

Discussion

Three steps towards α-hydroxy orcein were successfully conducted and products were

characterized by NMR analysis. The methylation of orcinol was performed on a multigram-scale

(upwards of 65 grams) while maintaining near quantitative yields. The electrophilic aromatic

bromination and following borylation of the aromatic ring were successfully completed in 1-10

gram amounts. The product yield over the first three steps was 51%, although future

modifications to the precipitation/isolation procedures might allow further increase of the

overall yield. While the procedures attempted for biaryl cross-coupling were unsuccessful, a

promising route utilizing Pd-PEPPSI-IPent as the catalyst has yet to be explored for our

application in developing a scalable synthesis. Bulky tetra-*ortho*-substituted biaryls have proved

to be synthesized in good yields under mild reaction conditions with this catalyst.[26] Pd-PEPPSI-

IPent is bench-stable and compatible with both Suzuki-Miyaura and Negishi mechanisms[27],

among other mechanistic routes. In fact, Pd-PEPPSI-IPent has successfully catalyzed the

153

formation of our desired biaryl dimer following direct lithium-halogen exchange in 75% yield.[28]

Demethylation to form the tetraol-dimer and following cyclization with the synthesized nitroso

aryl compound has yet to be attempted to complete the synthesis towards a scalable

manufacturing process for orcein dye.

6.3   Characterization of α-hydroxy orcein intermediates

All reactions were performed under a nitrogen atmosphere. Reaction temperatures refer to the

surrounding bath temperatures, or an oil bath held under the same reaction conditions in the

case of reactions run in tandem on the carousel. Reactions were monitored by TLC using

POLYGRAM SIL G UV254 plates (Macherey-Nagel, 805023). Visualization was performed with

UV light and cerium molybdate general stain followed by heating. NMR spectra were recorded

on a Bruker Advance 500 MHz instrument with compounds dissolved in the specified

deuterated solvent. HPLC purity analysis was completed on the Shimadzu 2020 LC-MS (single

quadrupole) instrument.

General procedure for HPLC purity analysis: Samples were prepared at 0.5 mg/mL in ACN and

5 μL was separated by a Kinetex 1.7 um XB-C18 100 Å, LC Column (100 x 2.1 mm) with a flow

rate of 0.4 mL/min. The mobile phase consisted of ACN and 0.1% formic acid in water. A

gradient of 5% ACN to 100% ACN in 5 minutes, followed by 100% ACN for 1 minute was used

for separation followed by column equilibrated from 100% ACN to 5% ACN over 1 min and isocratic 5% ACN for 1 minute. Compound purities were determined at 275 nm.
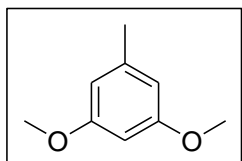
Synthesis of 3,5-dimethoxytoluene: Orcinol (10.1 g, 81.4 mmol) and K_2CO_3 (27.9 g, 202 mmol) were charged to an RBF equipped with a reflux condenser. The system was evacuated and backflushed with nitrogen (3x). Dry acetone (100 mL) was added to the RBF and the solution was stirred for 10 minutes. MeI (11.0 mL, 177 mmol) was added to the RBF and the reaction was subsequently heated to 55-60°C. Additional MeI (11.5 mL, 185 mmol) and K_2CO_3 (11.0 g, 79.6 mmol) were added to the RBF after 72 hours, as complete conversion was not yet observed by TLC. The reaction continued to reflux for an additional 48 hours, at which time complete conversion was observed by TLC. (Note that the reaction time was decreased to a total of 72 hours, utilizing 3 equivalents of both K_2CO_3 and MeI, when the reflux temperature was decreased to 40-45°C.) The reaction was then allowed to cool to room temperature. Acetone and excess MeI were removed *in vacuo*, and Et_2O (150 mL) was charged to the reaction flask. The crude suspension was filtered and rinsed with Et_2O (3 x 50 mL). The filtrate was collected and concentrated to dryness to provide the product as a red to yellow oil at 100% yield. No further purification was performed. Product purity was determined as 88.4% pure by HPLC analysis. ^{1}H NMR (500 MHz, CDCl$_3$) δ 6.39 (d, J = 1.8 Hz, 2H), 6.34 (d, J = 2.0 Hz, 1H), 3.82 (s, 6H), 2.36 (s, 3H). ^{13}C NMR (126 MHz, CDCl$_3$) δ 160.74, 140.21, 107.10, 97.54, 55.21, 21.83.
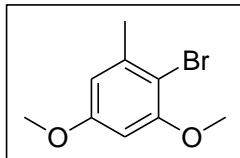
Synthesis of 2-bromo-3,5-dimethoxytoluene: 3,5-Dimethoxytoluene (6.16 g, 40.5 mmol) was charged to an RBF and the system was evacuated and backflushed with nitrogen (3x). Dry DMF (21 mL) was added to the RBF and NBS (7.20 g, 40.5 mmol) was added in portions while stirring. The reaction proceeded at 25°C for 2.5 hours or until complete conversion was observed by TLC. Chilled water (11 mL) was added dropwise to the reaction flask, causing the product to precipitate out of solution. The resulting slurry was stirred in an ice water bath for 20 minutes before filtering. The precipitate was left to dry on the vacuum filter overnight. The solid product was collected as a white powder at 88% yield. Product purity was determined as 92.4% pure by HPLC analysis. ^{1}H NMR (500 MHz, CDCl$_3$) δ 6.45 (d, J = 2.7 Hz, 1H), 6.37 (d, J = 2.7 Hz, 1H), 3.88 (s, 3H), 3.81 (s, J = 4.8 Hz, 3H), 2.42 (s, 3H). ^{13}C NMR (126 MHz, CDCl$_3$) δ 159.30, 156.63, 139.82, 107.21, 105.12, 97.24, 56.28, 55.47, 23.59.
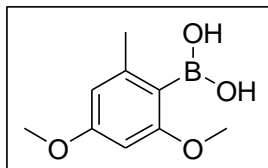
Synthesis of 2,4-dimethoxy-6-methylphenylboronic acid: 2-Bromo-3,5-dimethoxytoluene (2.51 g, 10.9 mmol) was charged to an RBF (Flask 1) and the system was evacuated and backflushed with nitrogen (3x) before charging dry THF (4 mL). Dry Et$_2$O (12.5 mL) was charged to a secondary nitrogen-flushed RBF (Flask 2) and cooled to -65°C. In a dropwise manner, n-BuLi solution (2.5 M in hexanes) (4.6 mL, 11.5 mmol) was added to Flask 2 at -65°C. Flask 1 was transferred by syringe to Flask 2 in a dropwise manner over the course of 20 minutes. Flask 1 was rinsed with dry THF (3.4 mL), and the rinse was syringe transferred to Flask 2. The reaction was stirred for one hour at -65°C before B(OMe)$_3$ (1.3 mL, 11.7 mmol) was added dropwise to the RBF. The reaction was stirred for two hours at -65°C at which time conversion was observed by TLC. While stirring at -65°C, 3

M HCl in water (0.1 eq) was added to the RBF. The solution was then allowed to gradually warm

to 25°C. Water (20 mL) was added to the crude solution, and the product was extracted with

Et_2O (3 x 20 mL). The organic layers were collected and concentrated to dryness. Hexanes (20

mL) were added to the concentrated product, and the resulting slurry was stirred for 15

minutes before filtering. The product was left to dry on the vacuum filter overnight. The solid

product was collected as a white powder at 58% yield. Product purity was determined as 92.3%

pure by HPLC analysis. ^{1}H NMR (500 MHz, MeOD) δ 6.38 (d, J = 1.7 Hz, 1H), 6.34 (d, J = 1.8 Hz,

1H), 3.79 (s, 3H), 3.77 (s, 3H), 2.22 (s, 3H). ^{13}C NMR (126 MHz, MeOD) δ 162.59, 161.72, 141.70,

106.60, 106.16, 94.28, 54.25, 54.18, 20.56.

6.4   Suzuki-Miyaura and Negishi cross-coupling procedures

Borylation and Suzuki-Miyaura cross-coupling *in situ* procedure: 2-Bromo-3,5-

dimethoxytoluene (193 mg, 835 μmol) was charged to an RBF (flask 1) and the system was

evacuated and backflushed with nitrogen (3x) before charging dry THF (5 mL). The reaction flask

was cooled to -78°C, after which n-BuLi (2.5 M in Hex) (350 μL, 875 μmol) was added dropwise

to the RBF. The reaction was stirred for 50 minutes at -78°C before B(OMe)$_3$ (120 μl, 1.08 mmol)

was added dropwise to the RBF. After the addition was complete, the dry ice/acetone bath was

removed, and the reaction was allowed to gradually reach 25°C. The reaction stirred overnight

at 25°C. After 18 hours, a separate RBF (flask 2) was charged with 2-Bromo-3,5-

dimethoxytoluene (68.8 mg, 298 μmol) and dry THF (3 mL). K_2CO_3 (232 mg, 1.68 mmol) was

added to flask 2 in one portion, followed by Pd(PPh$_3$)$_4$ (98.4 mg, 85.2 μmol). The mixture in flask

2 was transferred by syringe needle to flask 1 in a dropwise manner. Subsequently, dry THF (3

mL) was used to rinse flask 1 and was transferred to flask 2 under an inert atmosphere. The

reaction flask stirred for two hours at room temperature, after which it was heated to 50°C for

an additional 72 hours while monitoring the progress by TLC. The reaction was allowed to

gradually cool to 25°C before quenching the reaction with MeOH (2 mL). The mixture was

concentrated *in vacuo*, before 20% NH_4Cl solution (pH = 7, 5 mL) and EtOAc (10 mL) were

charged to the RBF. The organic layer was washed with brine (15 mL) and was collected. The

organic layer was then dried over $MgSO_4$, filtered, and concentrated to dryness prior to

analysis.

Suzuki-Miyaura cross-coupling procedure 1 – Pd(PPh₃)₄ catalyst in DMF: 2,4-Dimethoxy-6-

methylphenylboronic acid (105 mg, 536 µmol), 2-bromo-3,5-dimethoxytoluene (41.2 mg, 178

µmol), K_2CO_3 (49.3 mg, 357 µmol), and Pd(PPh₃)₄ (20.6 mg, 17.8 µmol) were charged to an RBF.

The system was evacuated and backflushed with nitrogen (3x) before charging dry, degassed

DMF (3 mL) to the RBF. The reaction flask was heated to 95°C for 24 hours, after which it was

allowed to gradually reach 25°C overnight. The reaction was concentrated *in vacuo* and Et_2O (3

mL) was subsequently charged to the RBF. The organic product was filtered through celite 545

prior to analysis.

Suzuki-Miyaura cross-coupling procedure 2 – Phenyl bromide test: 2,4-Dimethoxy-6-

methylphenylboronic acid (100 mg, 510 µmol) and phenyl bromide (26.9 µL, 255 µmol) were

charged to a reaction vial. The system was evacuated and backflushed with nitrogen (3x) before

charging the respective, degassed solvent (5 mL). Degassed water (400 µL) was added to

specified reaction trials. Pd(PPh₃)₄ (29.5 mg, 25.5 µmol) was then charged to the reaction vial in

one portion, followed by the respective base (3 eq). The reaction was heated to 75°C for 18 hours before increasing the temperature to 100°C for an additional 20 hours. The reaction was allowed to gradually cool to 25°C, after which it was concentrated to dryness. The organic product was dissolved in Et_2O and filtered through celite 545 prior to analysis.

Suzuki-Miyaura cross-coupling procedure 3 – $Pd_2(dba)_3$ catalyst, SPhos ligand: 2,4-Dimethoxy-6-methylphenylboronic acid (100 mg, 510 µmol), 2-bromo-3,5-dimethoxytoluene (58.9 mg, 255 µmol), K_2CO_3 (141 mg, 1.02 mmol), SPhos (6.30 mg, 15.3 µmol), and $Pd_2(dba)_3$ (7.00 mg, 7.64 µmol) were charged to an RBF. The system was evacuated and backflushed with nitrogen (3x) before charging dry, degassed toluene (1 mL) to the RBF. The reaction flask was heated to 100°C for 18 hours, after which it was allowed to gradually reach 25°C overnight. The reaction was concentrated *in vacuo* and Et_2O (1 mL) was subsequently charged to the RBF. The organic product was filtered through celite 545 prior to analysis.

Negishi cross-coupling procedure 1 – XantPhos Pd G3 catalyst: 2-Bromo-3,5-dimethoxytoluene (100.7 mg, 435.8 µmol) was charged to an RBF (flask 1) and the system was evacuated and backflushed with nitrogen (3x). Dry, degassed THF (2 mL) was subsequently charged to flask 1, and the solution was cooled to -78°C. *n*-BuLi solution (2.5 M in Hex, 0.19 mL, 476 µmol) was added dropwise to the reaction and stirred for 1 hour at -78°C. $ZnCl_2$ solution (1.9 M in MeTHF, 0.27 mL, 519 µmol) was then added dropwise at -78°C and stirred for 30 minutes before gradually warming up to 25°C. The reaction stirred for 1 hour at 25°C. In a separate RBF (flask 2), XantPhos Pd G3 (44.0 mg, 46.4 µmol) was added to a solution of 2-bromo-3,5-dimethoxytoluene (67.9 mg, 294 µmol) in dry, degassed THF (1 mL). Flask 2 was transferred to flask 1 in a dropwise manner, and flask 2 was rinsed with THF (1 mL). The reaction mixture

stirred at 25°C for 18 hours. An aliquot from the reaction flask was quenched in MeOH and concentrated prior to analysis.

Negishi cross-coupling procedure 2 – Pd$_2$(dba)$_3$ catalyst, SPhos/XPhos ligand: 2-Bromo-3,5-dimethoxytoluene (100 mg, 433 µmol) was charged to an RBF (flask 1) and the system was evacuated and backflushed with nitrogen (3x). Dry, degassed THF (2 mL) was subsequently charged to flask 1, and the solution was cooled to -78°C. *n*-BuLi solution (2.5 M in Hex, 0.19 mL, 476 µmol) was added dropwise to the reaction and stirred for 1 hour at -78°C. ZnCl$_2$ solution (1.9 M in MeTHF, 0.27 mL, 519 µmol) was then added dropwise at -78°C and stirred for 30 minutes before gradually warming up to 25°C. The reaction stirred for 1 hour at 25°C. In a separate RBF (flask 2), Pd$_2$(dba)$_3$ (19.8 mg, 21.6 µmol) and the respective ligand (10 mol%) were stirred in dry, degassed THF (1 mL) for 2 hours at 25°C. Following, 2-bromo-3,5-dimethoxytoluene (68.0 mg, 294 µmol) in dry, degassed THF (1 mL) was charged to flask 2. Flask 2 was subsequently transferred to flask 1 in a dropwise manner, and flask 2 was rinsed with NMP (2 mL). The reaction mixture was heated to 100°C for 18 hours, after which it was allowed to gradually reach room temperature. An aliquot from the reaction flask was quenched in MeOH and concentrated prior to analysis.

References

1. Beecken, H.; Gottschalk, E.; v Gizycki, U.; Krämer, H.; Maassen, D.; Matthies, H.; Musso, H.; Rathjen, C.; Zdhorszky, U., Orcein and litmus. *Biotechnic & histochemistry* **2003,** *78* (6), 289-302.
2. Clementi, C.; Carlotti, B.; Burattini, C.; Pellegrino, R.; Romani, A.; Elisei, F., Effect of hydrogen bonding interaction on the photophysics of α-amino-orcein. *Spectrochimica Acta Part A: Molecular and Biomolecular Spectroscopy* **2019,** *214*, 522-530.

3.   Sabnis, R. W., *Handbook of biological dyes and stains: synthesis and industrial applications*. John Wiley & Sons: 2010.

4.   Kirkpatrick, P., Use of orcein in detecting hepatitis B antigen in paraffin sections of liver. *Journal of clinical pathology* **1982,** *35* (4), 430-433.

5.   Ettre, L. S., Development of chromatography. *Analytical Chemistry* **1971,** *43* (14), 20A-31a.

6.   Musso, H., Die Trennung des Orceins in seine Komponenten (II Mitteil. Über Orceinfarbstoffe). *Chemische Berichte* **1956,** *89* (7), 1659-1673.

7.   Musso, H.; Beecken, H., Über Orceinfarbstoffe, VI. Die Konstitution von α-,β-und γ-Amino-Orcein. *Chemische Berichte* **1957,** *90* (10), 2190-2196.

8.   Cook, H., Origins of... tinctorial methods in histology. *Journal of clinical pathology* **1997,** *50* (9), 716.

9.   Lillie, R., Exploration of Dye Chemistry in Taenzer Unna Orcein Type Elastin Staining. *Histochemie* **1969,** *19* (1), 1-12.

10.   Henwood, A., The Orcein Stain—A Versatile Stain for Histopathology. *Journal of histotechnology* **2002,** *25* (1), 29-31.

11.   Henwood, A., Current applications of orcein in histochemistry. A brief review with some new observations concerning influence of dye batch variation and aging of dye solutions on staining. *Biotechnic & histochemistry* **2003,** *78* (6), 303-308.

12.   Kerr, R.; Hall, P., An evaluation of orcein methods for demonstrating hepatitis B surface antigen and copper-associated protein in human liver. *Stain Technology* **1986,** *61* (4), 243-247.

13.   Mondal, M.; Puranik, V. G.; Argade, N. P., A facile phenol-driven intramolecular diastereoselective thermal/base-catalyzed dipolar [2+2] annulation reactions: An easy access to complex bioactive natural and unnatural benzopyran congeners. *The Journal of Organic Chemistry* **2007,** *72* (6), 2068-2076.

14.   Koch, K.; Podlech, J.; Pfeiffer, E.; Metzler, M., Total synthesis of alternariol. *The Journal of Organic Chemistry* **2005,** *70* (8), 3275-3276.

15.   Blakemore, D., Chapter 1 Suzuki–Miyaura Coupling. In *Synthetic Methods in Drug Discovery: Volume 1*, The Royal Society of Chemistry: 2016; Vol. 1, pp 1-69.

16.   Walker, S. D.; Barder, T. E.; Martinelli, J. R.; Buchwald, S. L., A rationally designed universal catalyst for Suzuki–Miyaura coupling processes. *Angewandte Chemie* **2004,** *116* (14), 1907-1912.

17.   Barder, T. E.; Walker, S. D.; Martinelli, J. R.; Buchwald, S. L., Catalysts for Suzuki–Miyaura coupling processes: scope and studies of the effect of ligand structure. *Journal of the American Chemical Society* **2005,** *127* (13), 4685-4696.

18.   Bringmann, G.; Hinrichs, J.; Henschel, P.; Kraus, J.; Peters, K.; Peters, E. M., Atropo-Enantioselective Synthesis of the Natural Bicoumarin (+)-Isokotanin A via a Configurationally Stable Biaryl Lactone. *European Journal of Organic Chemistry* **2002,** *2002* (6), 1096-1106.

19.   Ulrich, H., One Oxygen and One Nitrogen or Phosphorus Atom. *ChemInform* **2005,** *36* (18), 55-115.

20.   Mitchell, R. H.; Lai, Y.-H.; Williams, R. V., *N*-Bromosuccinimide-dimethylformamide: a mild, selective nuclear monobromination reagent for reactive aromatic compounds. *The Journal of Organic Chemistry* **1979,** *44* (25), 4733-4735.

21.   Shimizu, S.; Imamura, Y.; Ueki, T., Incompatibilities between *N*-bromosuccinimide and solvents. ACS Publications: 2014.

22.   Ashfield, L.; Barnard, C. F., Reductive carbonylation–an efficient and practical catalytic route for the conversion of aryl halides to aldehydes. *Organic process research & development* **2007,** *11* (1), 39-43.

23.   Denmark, S. E.; Smith, R. C.; Chang, W.-T. T.; Muhuhi, J. M., Cross-coupling reactions of aromatic and heteroaromatic silanolates with aromatic and heteroaromatic halides. *Journal of the American Chemical Society* **2009,** *131* (8), 3104-3118.

24.   Cherney, A. H.; Hedley, S. J.; Mennen, S. M.; Tedrow, J. S., Xantphos as a Branch-Selective Ligand for the Acyclic *sec*-Alkyl Negishi Cross-Coupling of Heteroaryl Halides. *Organometallics* **2018,** *38* (1), 97-102.

25.   Milne, J. E.; Buchwald, S. L., An extremely active catalyst for the Negishi cross-coupling reaction. *Journal of the American Chemical Society* **2004,** *126* (40), 13028-13032.

26.   Organ, M. G.; Calimsiz, S.; Sayah, M.; Hoi, K. H.; Lough, A. J., Pd-PEPPSI-IPent: An Active, Sterically Demanding Cross-Coupling Catalyst and Its Application in the Synthesis of Tetra-Ortho-Substituted Biaryls. *Angewandte Chemie International Edition* **2009,** *48* (13), 2383-2387.

27.   Çalimsiz, S.; Sayah, M.; Mallik, D.; Organ, M. G., Pd-PEPPSI-IPent: Low-Temperature Negishi Cross-Coupling for the Preparation of Highly Functionalized, Tetra-*ortho*-Substituted Biaryls. *Angewandte Chemie* **2010,** *122* (11), 2058-2061.

28.   Buter, J.; Heijnen, D.; Vila, C.; Hornillos, V.; Otten, E.; Giannerini, M.; Minnaard, A. J.; Feringa, B. L., Palladium-Catalyzed, *tert*-Butyllithium-Mediated Dimerization of Aryl Halides and Its Application in the Atropselective Total Synthesis of Mastigophorene A. *Angewandte Chemie* **2016,** *128* (11), 3684-3688.

CURRICULUM VITAE

TANIA ROSEANN MUTCHIE

EDUCATION

Ph.D. in Chemistry   **August 2016 – May 2021**
University of Wisconsin – Milwaukee   Milwaukee, WI
Dissertation: "Part I: Development of small-molecule-based probes for the vitamin D receptor
Part II: Development of a scalable manufacturing process for orcein dye"

B.S. in Chemistry   **August 2011 – May 2015**
Drake University   Des Moines, IA
Biology Minor, Biophysics Concentration

EMPLOYMENT EXPERIENCE

Research & Teaching Assistant   **August 2016 – May 2021**
University of Wisconsin – Milwaukee   Milwaukee, WI

- Rationally designed novel ligands for the vitamin D receptor using MOE molecular modeling software
- Developed multi-step synthetic routes resulting in the formation of complex organic molecules
- Fully characterized compounds by utilizing NMR, LCMS, and HRMS analysis
- Performed in vitro biochemical assays targeting the vitamin D receptor (binding, transcription, and toxicity)
- Aided in the creation of a laboratory-specific chemical hygiene plan and chemical SOPs
- Trained and supervised undergraduate students in research and teaching laboratories

Graduate Student Intern   **June 2020 – August 2020**
MilliporeSigma   Sheboygan Falls, WI

- Involved in the development of a scalable manufacturing process for orcein dye
- Optimized multiple organic reactions for the industrial scale by successfully avoiding chromatographic purification
- Determined purity of reaction products by HPLC

Process Chemist I   **June 2015 – August 2016**
Alcami Corporation   Germantown, WI

- Carried out chemical reactions on a gram to multi-kilogram scale
- Manufactured active pharmaceutical ingredients (APIs) through a variety of organic reaction mechanisms
- Isolated and purified products and intermediates using standard laboratory techniques
- Followed proper cGMP practices and documentation

AWARDS

- UWM Graduate Student Excellence Fellowship (GSEF) Award (2020)
- MilliporeSigma Summer Graduate Research Fellowship (2020)
- Sosnovsky Award for Excellence in Graduate Research (2020)
- UWM Department of Chemistry & Biochemistry Discussion Teaching Assistant Award (2018-2019)
- Drake University College of Arts & Sciences President's List (2015)
- Drake University College of Arts & Sciences Dean's List (2014-2015)
- Drake University Presidential Scholarship (2011-2015)

PUBLICATIONS

- **Mutchie, T.R.**, Webb, D.A., Di Milo, E.S., Arnold, L.A. Ligand Design for the Vitamin D Receptor. Nuclear Receptors, Badr M.Z. Ed. 2020 in press.
- Yu, O. B.; **Mutchie, T. R.**; Di Milo, E. S.; Arnold, L. A., Synthesis and biological evaluation of calcioic acid. *Steroids* 2020, 154, 108536.
- **Mutchie, T. R.**; Yu, O. B.; Di Milo, E. S.; Arnold, L. A., Alternative binding sites at the vitamin D receptor and their ligands. *Molecular and cellular endocrinology* 2019, 485, 1-8.

PRESENTATIONS

- Mutchie, T. R., *et al*. Development of small-molecule-based probes for the vitamin D receptor. Poster presentation at the ACS National Meeting & Expo, Virtual Conference. (March 2020, August 2020)
- Mutchie, T. R., *et al.* Synthesis of novel compounds to study expression and localization of the vitamin D receptor. Poster presentation at the UWM Department of Chemistry & Biochemistry Research Symposium, Milwaukee, WI. (May 2017, May 2018, April 2019)
- Mutchie, T. R., *et al*. Synthesis of novel compounds to study expression and localization of the vitamin D receptor. Poster presentation at the Milwaukee Analytical Chemistry Conference, Milwaukee, WI. (January 2019)
- Mutchie, T. R. The Ritter Reaction. Oral presentation at the UWM Department of Chemistry & Biochemistry Graduate Seminar, Milwaukee, WI. (February 2018)